2007

The Role of Pot1 in Telomere Protection and Maintenance

Dirk Hockemeyer

THE ROLE OF POT1 IN TELOMERE PROTECTION AND MAINTENANCE

A Thesis Presented to the Faculty of

The Rockefeller University

in Partial Fulfillment of the Requirements for

the degree of Doctor of Philosophy

by

Dirk Hockemeyer

June 2007

THE ROLE OF POT1 IN TELOMERE PROTECTION AND MAINTENANCE

Dirk Hockemeyer, Ph.D.

The Rockefeller University 2007

POT1 is a single stranded telomeric DNA binding protein implicated in telomere length regulation in human cells. To address the role of POT1 in telomere protection we used RNAi in human cells. We confirmed that POT1 acts as a negative regulator of telomerase and showed that POT1 is required to protect telomeres. Reduced levels of POT1 elicited a strong telomere DNA damage response and a growth arrest in primary cells; the 3' telomeric overhang shortened and the sequence of the 5' terminus changed from its precise sequence (ATC-5') to a randomized ending.

In order to determine the phenotype of complete POT1 loss, we used conditional gene deletion in the mouse. Unexpectedly, we identified two POT1 orthologs in the mouse and rat genomes, whereas other mammals have one. As both proteins (POT1a and POT1b) localized to telomeres based on IF and ChIP, we targeted both genes for Cre-mediated deletion. POT1a/b double-knockout (DKO) cells exhibited a telomeric DNA damage signal and senescence. DKO cells also displayed a novel telomere dysfunction phenotype, extensive endoreduplication. However, POT1a/b were largely dispensable for repression of telomere fusions, which is a prominent outcome of inhibition of another telomere binding protein, TRF2. Previous structural analysis of POT1 and its binding partner TPP1 predict that they act interdependently. Consistent with this, we found that TPP1 is essential for the telomeric function of both mouse POT1 proteins.

Single knockouts and complementation experiments revealed that POT1a and POT1b have distinct functions. POT1a was found to be primarily responsible for repression of the DNA damage signal at telomeres, while POT1b had a unique role in repressing an activity that creates extended telomeric overhangs. POT1b KO cells showed accelerated telomere shortening indicating that POT1b controls exonucleolytic degradation of the C-rich strand. The enhanced telomere shortening of POT1b KO cells explains our finding that POT1b KO mice display aging phenotypes reminiscent of late generation telomerase knockout mice.

My results argue that a gene duplication event gave rise to two functionally distinct POT1 proteins in rodents. Such a divergence is unprecedented in chromosome biology and has implications for modeling telomere biology and telomere-related disease states in the mouse.

Meinen Eltern
Barbara und Friedrich Hockemeyer
in Liebe gewidmet

Acknowledgements

Foremost I would like to thank Titia de Lange for her excellent mentorship. Thank you for taking so much of your time to teach me how to ask scientific questions and how to design good experiments to answer these questions. Thanks for encouraging me but also for challenging me when it was necessary. I am eternally grateful for the knowledge and skills gained in your laboratory, and I know there are many more things I could learn from you. You are a fantastic role model as a scientist and teacher.

A special thanks goes to Dr. Diego Loayza, who was my benchmate for so many years. Thanks for taking so much of your time to give advice, share reagents, explain results and have scientific discussions.

I would also like to thank Hiro Takai, Jeffrey Ye, Diego Loayza, and Jan Karlseder for their invaluable guidance, experimental training, and friendship.

Only through the immense help of Devon White was I able to keep organized and focused during the POT1 mouse project. Thanks to your admirable care and your dedication to animal work, I always remained confident that our mice were very well taken care of and that our mouse projects were justified and worth the effort. I am grateful to have you as my coworker and friend.

I would also like to acknowledge the contributions of Jan-Peter Daniels, Wilhelm Palm and Kaori Takai to the POT1 project. Your help and companionship made a great impact. I would like to recognize Agnel Sfeir for performing the telorette assays on human POT1 knockdown cells.

I would like to thank Nadya Dimitrova, Kristina Hoke, Jill Donigian, Eros Lazzerini-Denchi and Sean Rooney for their stimulating discussions and for helping me

on many occasions. I appreciate and honor your scientific judgment and am thankful for the ideas that were inspired by you.

I am especially grateful to Nadya, Kristina and Helen Bateup for helping me with the task of writing and editing my thesis. I would not have accomplished this without your patient help.

I had the privilege to work with many other highly gifted members of the laboratory. Thanks to Diana Argibay, Stewart Barnes, Eliana Forero, Yi Gong, Akimitsu Konishi, Megan van Overbeek, Sara Buonomo and Rita Rodney, our workspace was not only professional, but also a pleasant.

I would also like to thank Stephanie Blackwood for making things run so smoothly in the lab. Thanks for helping me so many times; I always knew I could rely on you.

Importantly, I would like to thank Dr. Robert Roeder and Dr. Paul Nurse for serving on my thesis committee. I am grateful to them for their advice and interest in my work. Their helpful suggestions, constructive criticism and their rigorous scientific standards, supported and encouraged me in my endeavor to become a scientist. I would also like to thank Dr. Joachim Lingner who examined my thesis as an external reviewer. Thank you for taking the time to come all the way to New York, and for your insightful questions and comments.

I would also like to acknowledge two of my fellow graduate students, Valentin Piech and Chad Euler for their support throughout my PhD, giving both helpful scientific advice as well as much needed social diversion.

Very special thanks go to Helen Bateup, for her support and encouragement during the crucial time of my thesis. Thank you for being there for me and making it so much easier and enjoyable.

Lastly and most importantly, I would like to thank my parents and my sisters Imke and Anke and my brother Cord for their unconditional care and help and for supporting me in my decision to come to New York for my studies. Thank you for being there for me!

Table of Contents

List of Figures

1. Introduction

Telomeres

Maintenance of genomic information is vital to the preservation of all organisms. During the evolution of multi-cellular organisms, the packaging of hereditary information into linear chromosomes proved to be a successful strategy. Nevertheless, the fact that linear chromosomes have "ends" presents an important problem, demanding a specialized machinery to protect and stabilize the chromosome ends. Telomeres are the DNA-protein complex at the end of linear chromosomes, which provide this specialized function. Understanding of the telomere is important, as research over the past decades has shown that telomeres are vital in maintaining genomic integrity and preserving proper function of the cell and organism. Telomere dysfunction results in a wide array of cellular problems and ultimately can cause human disease [1-3].

Telomere function relies on several proteins that specifically recognize DNA sequences at the chromosome end [4,5]. Recent studies have determined the role of many of these proteins in telomere function. In this work, I will study in detail one of the most recently discovered telomere binding proteins, POT1, whose function had not yet been fully characterized. The study of POT1 requires an understanding of the overall function of the telomere as well as the composition of the telomeric complex. In my introduction I will discuss first the essential cellular functions of telomeres telomere, then I will introduce the individual components of the telomeric complex, and finally describe how these components regulate telomere length and protection.

Maintenance of genomic integrity by telomeres

First described by Barabara McClintock and Herman Muller [6,7], the telomere has distinct properties, which allow the cell to distinguish between natural chromosome ends and internal DNA breaks [4]. Telomeres are not recognized by the DNA damage surveillance machinery and therefore cause neither the activation of DNA damage checkpoints nor the induction of DNA repair. When the protective function of telomeres is compromised, cells arrest due to a DNA damage signal and can enter senescence or apoptosis. Cells with deprotected telomeres can accumulate telomere-telomere fusions, telomere recombination events, or degradation of telomeric DNA, each due to inappropriate DNA repair reactions.

The end replication problem

The ends of linear chromosomes also present a difficulty during DNA replication [8,9]. This so-called "end-replication-problem" originates from the properties of DNA polymerases. DNA polymerases use RNA primers to initiate DNA synthesis and these primers are degraded and replaced by DNA by 5' to 3' DNA polymerases. On the lagging strand, the terminal RNA primer cannot be replaced by DNA, as the DNA polymerases lack a 3'OH to prime replacement. This process, if not counteracted, leads to a terminal sequence loss of linear chromosomes in every round of DNA replication. Noncoding telomeric repeats at the end of chromosomes serve as a reservoir of DNA that can be lost over consecutive rounds of replication without immediate loss of genomic information. In order to maintain long-term genomic integrity, telomeric DNA has to be replenished. This function is fulfilled in almost all organisms by an enzyme called telomerase (see below) [10,11]. In human cells the expression of telomerase is limited to germ cells and highly

proliferative tissues. Therefore, telomeres shorten over time in somatic human cells that are telomerase deficient [12-16]. This telomere shortening limits the replicative lifespan of somatic cells [17]. After a limited number of divisions, telomeres of somatic cells become critically short and loose their protective function. These cells enter a permanent growth arrest termed replicative senescence. This proliferation barrier, known as the Hayflick limit [18], is thought to be a tumor suppressor mechanism. Germline cells and tumor cells express telomerase and evade this arrest by maintaining a stable telomere length [13,19]. Expression of telomerase, which is reactivated in 94% of all tumors [13,20,21], is sufficient for primary cells to overcome telomere-induced senescence [19,22].

Telomeric DNA

Although telomeric DNA differs in sequence and length among different species, telomeric DNA is usually composed of double stranded tandem repeats. Human telomeres contain double stranded TTAGGG arrays and their length ranges from about 4 to 20 kilobases (kb) [23,24]. Telomeres of *Mus musculus* share the human telomeric sequence TTAGGG, but are longer, ranging from 20 kb to 150 kb [25]. Telomeres are heterogeneous in length. Telomere length can differ on individual chromosome ends within one cell and can also differ according to cell type and age of the organism.

The telomeric double stranded repeats end in a single stranded 3'overhang that is about 150 to 300 bases long [26,27]. The length of the telomeric overhang is largely independent from the length of the double stranded part of the telomere and also independent of cell type and age of the organism. The 5' end of human and mouse telomeres ends predominantly on the sequence ATC-5' and therefore the transition from

double stranded to single stranded telomeric DNA is defined precisely [28]. In human telomerase positive cells, the 3' end of the telomeric overhang shows a preference for the sequence TAG-3', while it appears to be almost random in telomerase negative cells [28]. Internal to the telomere are sequences known as subtelomeric sequences or telomere-associated sequences (TAS) [29]. These sequences are highly polymorphic repetitive sequences, can be extensively methylated, and are organized as heterochromatin. TAS can be megabases long and some classes contain telomeric TTAGGG repeats. In humans and mice, TAS are not essential for proper telomere function and there are no known proteins that bind specifically to the subtelomeric regions.

Telomeric DNA, like other sequences containing arrays of guanidine residues, can fold into four-stranded conformations composed of structural elements called G-quartets [30]. G-quartets can form intra- and intermolecularly and are stabilized through hydrogen bonding between four guanidines. G-quartets can stack to form a four-stranded structure, called G4 DNA, which is stabilized by monovalent cations such as Na^+ and K^+ that bind in the middle of the planar G-quartets. Once formed, G-quartets are thermodynamically and kinetically stable. G-quartets have only been studied *in vitro* and it is not established whether G4-DNA occurs *in vivo*. Although the relevance of G-quartets is still poorly understood, they have been suggested to affect binding of telomeric binding proteins and may impede telomere replication [31-33].

Telomeres of many species are organized in a tertiary structure called the t-loop (Griffith et al., 1999). Electron microscopic analysis of telomeric DNA isolated from *Homo sapiens*, *Mus musculus*, *Trypsosoma brucei*, *Oxytricha fallax*, and *Pisum sativum* (garden pea) [34-36] shows that the chromosomes end in a loop structure. Initial experiments

were performed after fixation with psoralen, which introduces inter-strand cross-links at A-T steps. As these cross linking events enhanced the number of loops seen in electron micrographs, it has been proposed that t-loops are formed by the invasion of the telomeric overhang into the double stranded part of the telomere. This strand invasion event displaces the G-rich strand of the double stranded part of the telomere. The displaced strand then forms a structure known as the displacement loop (D-loop). The presence of a D-loop is consistent with the finding that *Escherichia coli* single stranded binding protein (SSB) can coat the base of isolated t-loops [35]. Studies by Woodcock demonstrated that t-loops could be isolated without cross-linking if mild extraction conditions were used [37]. The size of the t-loop is variable for individual telomeres and also varies between organisms. T-loops found in *Pisum sativum* can consist of up to 50 kb [34] whereas t-loops of *Trypsosoma brucei* are on average 1 kb long [36]. It is also not clear if the t-loop is the only structural conformation of the telomere. It has been proposed that telomeres can acquire an open conformation that allows telomere extension and modifications and that the closed t-loop structure represents the protected configuration of chromosome ends. Although little is known about the formation and dynamics of the t-loop, it has been suggested that one of the telomeric binding proteins is necessary for its establishment (reviewed in) [4].

Telomere replication and maintenance of telomeric DNA

In most eukaryotic cells, the enzymatic activity of telomerase is necessary to synthesize *de novo* telomeric DNA at the end of linear chromosomes. Telomerase was first purified from *Euplotes aediculatus* and shown to be a reverse transcriptase [14,15,38]. Telomerase has an RNA component and uses this as a template to add repeats to the ends of telomeres

[10,11]. The catalytic activity of telomerase is characteristic for Non-LTR retro transposon reverse transcriptases [39]. This is because telomerase extends a 3' DNA end directly as opposed to using an RNA primer like other transcriptases [40]. Comparison of telomerase template RNA (TRs) sequences from divergent organisms reveals the rapid evolution of this RNA [15]. TRs are of heterogeneous length ranging from 1200 bases in yeast, to 450 nucleotides in mammals to 150-200 bases in ciliates. Although TRs are divergent in sequence and length, distinct structural elements are conserved. Among these elements is the single stranded template region in the catalytic center of the enzyme, which allows telomerase to anneal to the overhang and add nucleotides to the chromosome end [41,42]. Telomerase is a processive enzyme *in vitro*. Repeated reverse transcription of the template leads to the repetitive nature of the telomeric sequence. In order for telomerase to add multiple repeats without dissociating from its substrate, the protein translocates processively after each repeat addition to the 3' end of the newly formed DNA. In yeast, telomerase reverse transcriptase (est2) and the telomerase RNA (tlc) component are sufficient for the detectable telomerase activity in cell extracts [43,Lingner et al., 1997, Proc Natl Acad Sci U S A, 94, 11190-5]. Similarly, telomerase activity can be generated *in vitro* with human hTert and hTR. However, human telomerase is a multiprotein complex of about 1.5 MDa. In addition to hTert and hTR, it contains Est1a and b which are homologues of the yeast Est1 gene, and the telomerase RNA interacts with the Ku protein [44-46]. Telomerase RNA is also associated with several ribonucleoproteins (RNPs) that are necessary for telomerase maturation and stability. One of these factors, dyskerin, is discussed below in detail because of its clinical relevance [47]. The *in vivo* mechanism of telomere elongation by telomerase is still poorly understood. Telomerase has been found to be present in cells

as a dimer [48-50], but the significance of telomerase dimerization for its catalytic activity has not been defined.

Telomerase is only capable of synthesizing the G-rich strand of telomeric DNA. C-strand synthesis is likely achieved by the conventional DNA replication machinery coupled to telomerase activity [51-53]. In humans, telomeres are replicated throughout S-phase [54], but the mechanism that coordinates this event with telomerase activity is unclear. Under conditions where telomerase is forced to add telomeric repeats and telomeres elongate with a rate of 300 bp per population doubling (PD), no strong increase in telomere overhang length can be detected [55]. This result suggests that the elongation of the overhang by telomerase is translated rapidly into double stranded telomeric DNA and provides evidence that telomere elongation in human cells is coupled to DNA replication. Several major questions regarding telomere replication have yet to be addressed. Does telomerase act before or after telomere replication? How can telomerase act on the leading strand if it is blunt after replication, and therefore a poor substrate for elongation?

It is important to note that two telomerase-independent mechanisms can maintain telomere length. One is used in *Drosophila melanogaster*, which lack telomerase and where the telomere DNA consists of long retrotransposable elements. In this case endogenous retrotransposons sporadically transpose to the end of the chromosome and thereby counteract terminal sequence loss [56-58]. Another telomerase-independent method of telomere elongation has been observed in *S. cereviasiae*. In strains lacking telomerase activity, telomeres shorten and the culture arrests and undergoes senescence. Two types of survivors overcome this arrest by activating a recombination pathway. In Type I survivors, subtelomeric DNA is amplified, while in Type II survivors telomeric repeats

are amplified at the chromosome end. Both survivor types are dependent on the recombination gene Rad52.

In human cells telomeres can also be maintained through recombination in a telomerase independent manner. This pathway termed Alternative Lengthening of Telomere (ALT) allows short telomeres to be elongated by recombination mediated DNA synthesis. Using this pathway cells can be propagated indefinitely without telomerase. It has been proposed that the ALT recombination mechanism can either use two telomeres, the t-loop structure, or the extra chromosomal telomeric DNA found in ALT cells as a recombination template (reviewed in) [59,60].

Overhang generation

Although telomerase uses the telomeric overhang to elongate telomeres, generation of the overhang is telomerase independent [61]. The process that creates the overhang is not understood in detail, but it has been suggested that in human cells, the overhang is generated by nucleolytic degradation of telomeric DNA [27]. This hypothesis is based on the fact the telomeric overhangs can be found on both chromosome ends. As leading strand synthesis is predicted to result in blunt ends, overhang generation requires the resection of the telomeric C-strands. This theory is further supported by the rate of telomere shortening in telomerase negative cells. In many organisms, telomeres in cells deficient for telomerase shorten with only a few nucleotides per cell division, the rate predicted form the end replication problem [62-66]. In contrast, in human and mouse cells that are deficient for telomerase, telomeres shorten at a rate of about 50-150 bp/PD [17,67,68]. This fast shortening rate suggests additional telomere sequence loss by degradation of telomeric DNA through nucleases. Furthermore the telomeric overhang in mammals is

significantly longer than in other organisms [27,69,70]. These results indicate that a yet unidentified nuclease may be responsible for generating the overhang in mammalian cells.

Interestingly, it has been shown that the overhang on telomeres generated by lagging strand synthesis is longer than the leading strand counterpart. In the presence of telomerase, the leading strand overhang becomes slightly elongated and thereby the preference for a longer lagging strand overhang is diminished [71]. These findings suggest that leading and lagging strands are generated differently.

Shelterin

The protein complex bound to telomeric DNA is called shelterin. Shelterin is characterized by its selective localization to chromosome ends, its presence at the telomere throughout the cell cycle, and its exclusive telomeric function. Shelterin determines telomere structure and function. It is implicated in the formation of t-loops, is necessary to determine the telomere terminus, and regulates the addition of telomeric repeats by telomerase (reviewed in) [72].

The shelterin complex consists of six proteins that are found exclusively at the end of mammalian chromosomes (Figure1.1). Three members of shelterin are DNA binding proteins. TRF1 and TRF2, bind double stranded telomeric DNA [73-76], while POT1 has binding activity for single stranded telomeric DNA. POT1 is connected to the other shelterin components through a protein-protein interaction. This interaction is thought to be the main mechanism of POT1 recruitment to the telomere, despite its ability to bind ss telomeric DNA *in vitro*. DNA. The other three proteins, TIN2, TPP1 and

RAP1, are tethered to the telomere exclusively through protein-protein interactions with the DNA-binding proteins (Figure1.1).

Shelterin is a stable complex that can be isolated in absence of telomeric DNA [77,78]. Shelterin is abundant on telomeric DNA and more than 100 copies are thought to be associated with the duplex telomeric repeats of each chromosome end. Very little is known however, about the spatial distribution of shelterin on telomeric DNA.

Recruitment of shelterin to telomeres is correlated with telomere length. Long telomeres recruit more shelterin than short telomeres [55,79]. These characteristics allow shelterin to "measure" telomere length and a counting model was proposed to explain how shelterin mediates telomere length homeostasis in mammalian cells (see section about telomere length regulation).

Shelterin also regulates the telomere terminus by protecting the integrity of telomeric DNA. It has been shown that shelterin loss can lead to nucleolytic degradation of the 3' end of the telomere resulting in the loss of the telomeric overhang [76,80,81]. Shelterin also protects telomeric DNA from covalent telomere-to-telomere fusions, which are the product of non-homologous end joining (NHEJ) (see section about telomere protection). It has been proposed that these functions of shelterin result to some extent from the ability of shelterin components to promote t-loop formation.

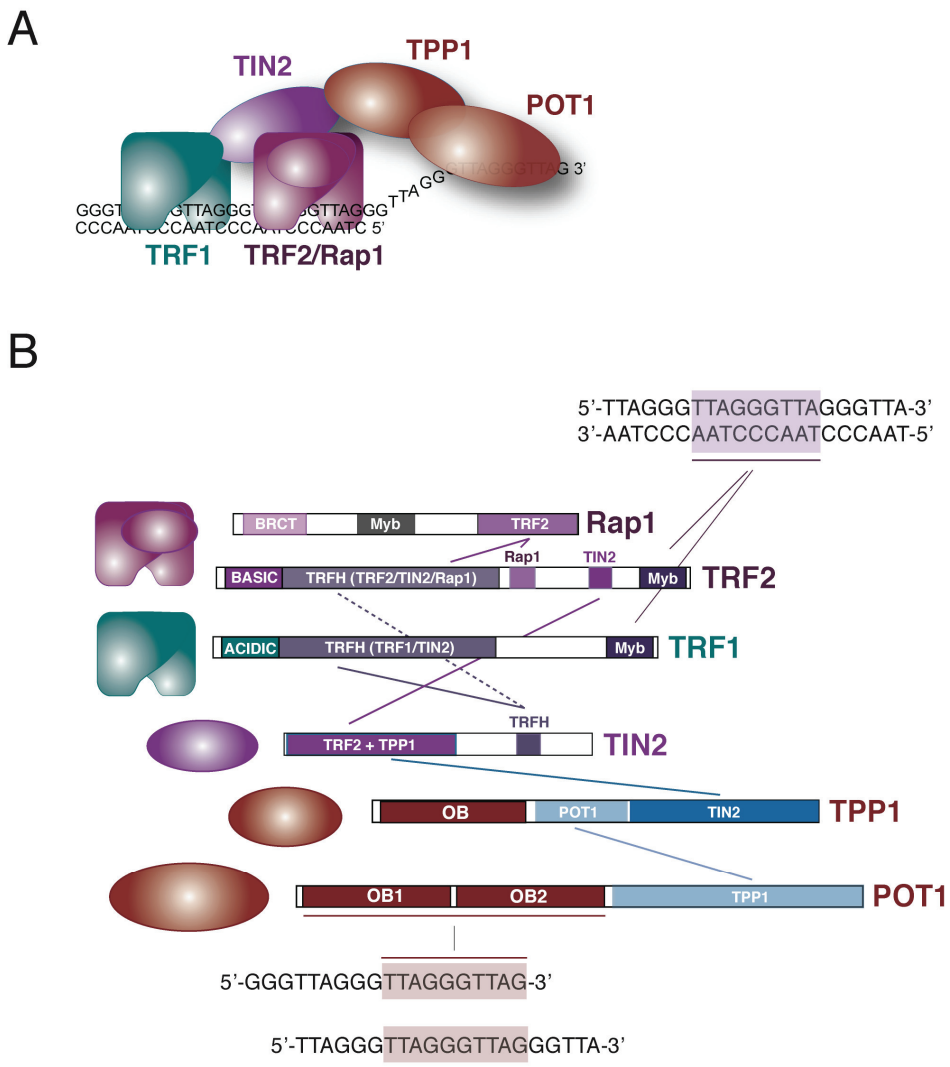

Figure 1.1 Shelterin the protein complex at mammalian telomeres

(A) Schematic overview of shelterin bound to the telomere (B) Diagram of the binding domains between shelterin proteins and between shelterin proteins and telomeric DNA

TRF1

TRF1 (Telomere repeat binding factor 1) was the first member of shelterin to be isolated. TRF1 was purified as a protein with specific binding affinity for telomeric double stranded DNA [82,83]. Human TRF1 is a 439 aa protein that is ubiquitously expressed and

present at all telomeres throughout the cell cycle. TRF1 consists of an N-terminal acidic domain, a central protein-protein interaction domain, and a C-terminal MYB-domain. The central domain allows TRF1 to homodimerize and recruit TIN2 to the telomere, while the MYB-domain enables TRF1 to bind telomeric DNA [73,82,84]. Homodimerization of TRF1 is necessary for efficient DNA binding to two TRF1 5'-YTAGGGTTR-3' half sites [74,85]. TRF1 binding *in vitro* has been shown to be very flexible, allowing TRF1 to bend and pair telomeric DNA [74]. Depletion of TRF1 from cells using RNAi techniques not only results in the loss of its binding partner TIN2 from the telomere but also depletes telomeres of TRF2 and RAP1 [78]. These findings point to a central role of TRF1 in assembling and stabilizing shelterin. Although the specific function of TRF1 is not very well understood, TRF1 is known to be essential, as targeted deletion of TRF1 results in early embryonic lethality in the mouse [86,87].

TRF2 and RAP1

TRF2 (Telomere repeat binding factor 2) was the second telomeric repeat binding factor to be characterized [88,89]. It is a small ubiquitously expressed protein that localizes to telomeres throughout the cell cycle. TRF2 consists of an N-terminal basic domain, a central protein-protein interaction domain, and a C-terminal MYB-domain. Similar to TRF1, the central domain allows TRF2 to homodimerize and to interact with TIN2. TRF2 homodimerizes and binds DNA using its C-terminal MYB-domain. TRF2 does not form heterodimers with TRF1 and appears to be approximately 10-fold more abundant than TRF1. Although TRF2 dimerization is sufficient for DNA binding *in vitro*, TRF2

can form higher order oligomers. The *in vivo* relevance of oligomerization of TRF2 is not understood [75,90].

RAP1 (Repressor activator protein1) is a constitutive binding partner of TRF2 and they from a 1:1 stoichiometric complex [91,92]. RAP1 contains a MYB-like DNA binding domain and a BRCT protein-protein interaction domain in its N-terminus. RAP1 does not bind DNA on its own and has no known interacting partners other than TRF2 [91]. RAP1 protein stability is dependent on TRF2 and as a result cells that are deficient for TRF2 also loose RAP1 protein [80].

POT1

POT1 (Protection Of Telomeres) is the single stranded binding protein found at telomeres. Pot1 was first identified in *S. pombe* and shown to protect telomeres by preventing telomere degradation [93]. [93] The protein structure of spPOT1 shows that it binds the telomeric overhang using a structurally conserved oligonucleotide/oligosaccharide binding fold (OB-fold). Sequence homology in this OB-fold with an OB-fold in the Telomere End Binding Protein (TEBP) of *oxytricha nova* served to identify spPot1.

TEBP, a protein complex consisting of two subunits TEBPα and TEBPβ, binds the 16 nucleotide long telomeric overhang of *oxytricha nova* telomeres. TEBPα can bind telomeric DNA alone, but this binding affinity is greatly enhanced upon binding to TEBPβ. As a heterodimer this complex binds ss telomeric DNA with high affinity and specificity, forming a very stable ternary complex. In this complex the 3' end of the telomere is hidden in a hydrophobic pocket, which has several contacts to the last

guanidine residue containing the 3' end. It has been proposed that this mode of binding to the 3' end of the overhang functions as a physical cap protecting the telomere.

Human POT1 is a 632 aa protein and immunofluorescence as well as chromatin immunoprecipitation of telomeric DNA shows that POT1 is a telomere associated protein and a member of the shelterin complex. POT1 contains three OB-folds. The first of these OB-folds served to identify human POT1 through its homology to SpPot1 and to relate human POT1 to the telomere end binding protein α (TEBPα) [93,94]. POT1 uses its two N-terminal OB-folds to recognize the minimal binding site 5'-TAGGGTTAG-3' [94,95]. POT1 has two binding modes in which it recognizes this sequence. POT1 can either bind directly to the 3' end or to an internal site of the overhang [96]. Although POT1 can bind directly to the 3' end of telomeres, structural analysis suggests that POT1 does not function like TEBP by capping the chromosome end. This is mostly because direct 3'-binding requires that the overhang ends in GGTTAG-3', a sequence that is found only on a subset of telomeres [28].

POT1 is ubiquitously expressed and localizes to the telomere throughout the cell cycle [55,97]. The human POT1 gene is differentially spliced resulting in five different mRNA of POT1. Variant form 1 of POT1 (V1) is the message used to make the full-length protein, while the variants V2, V3 and V5 are predicted to result in C-terminal truncated deletions of POT1. V4 variant of POT1, which skips exon 8, was predicted to result in an unstable, 5 kD long N-terminal fragment of POT1.

POT1 interacts via its C-terminus with TPP1 [98,99]. This interaction with TPP1 is thought to be essential for the recruitment of POT1 to telomeres [55], as a truncated form of POT1, POT1ΔOB, which lacks its DNA binding affinity, can still be targeted to the

telomere by its interaction with TPP1. The expression of POT1ΔOB leads to strong telomere elongation possibly by suppressing the endogenous levels of POT1 [95].

TIN2

TIN2 (TRF1-interacting nuclear protein 2) is a ubiquitously expressed protein found to directly interact with TRF1, TRF2 and TPP1 [78,84,100,101]. TIN2 makes contact at its N-terminal domain to the C-terminus of TPP1 and TRF2, while a central peptide of TIN2 is thought to bind the homodimerization domain of TRF1. The interaction of TIN2 with TRF2 appears to be significantly weaker than its interaction with TRF1 based on quantitative yeast two-hybrid analysis and has been shown to be salt sensitive. As a result of its protein interactions, TIN2 resides in the center of shelterin and mutation analysis reveals its crucial role in shelterin assembly. Overexpression of an N-terminal truncated form of TIN2, which still interacts with TRF1 but not TRF2 or TPP1, leads to the loss of TRF2 from telomeres. Similarly, depletion of TIN2 in cells using RNAi results in reduced levels of telomeric TRF2. The finding that over-expression of a C-terminal fragment of TIN2, which still interacts *in vitro* with TRF2 and TPP1 but not TRF1, leads to a reduction of both TRF1 and TRF2 telomere binding could indicate that TIN2 is necessary to allow the cooperative DNA binding of shelterin through TRF1 and TRF2.

TPP1

TPP1, formerly known as PIP1, PTOP, TINT1 and acd, was the last member of shelterin to be identified [98-100,102]. Like POT1, TPP1 has recently been shown to be an OB-fold containing protein [103]. This OB-fold has strong structural similarity to the one found in

the β-subunit of the telomere end binding protein of *oxytricha nova* (TEBP). This similarity led to the proposal that the POT1/TPP1 complex is the homologue of TEBPα/β complex. TPP1 interacts at its central domain with POT1, while its C-terminal domain interacts with TIN2. Through these two protein interactions, TPP1 bridges the double stranded telomere-binding proteins and the single stranded binding protein POT1 [98,99]. Biochemical analysis of TPP1's role in shelterin assembly suggests that TPP1 has the ability to enhance the binding of TIN2 to TRF2 and weaken the association of TRF1 with the TRF2 complex. TPP1 uses its OB-fold to interact with telomerase. In one study this interaction was proposed to be necessary for telomerase recruitment and in a second study it was implied to enhance telomerase processivity [103,104].

Recently, a splicing mutation within the mouse TPP1 gene was reported to cause a developmental defect in the acd mouse strain (adrenocortical dysplasia) [102]. This mutation, which arose spontaneously in the Jackson laboratories, leads to adrenocortical dysplasia and defects in organs derived form the urogenital ridge. Acd mice grow to adulthood but are infertile. The finding that acd mice are viable was at first somewhat surprising because null mutations for all other shelterin components were shown to be lethal early during mouse development. As discussed later in the results section, the acd mutation does not lead to the complete loss of TPP1 function, but to a hypomorphic allele of TPP1.

Telomere length regulation

Although the size of an individual telomere is variable, the average telomere length of cells that express telomerase is maintained within a confined and species-specific range.

This finding suggests that the addition of telomeric repeats by telomerase is a regulated process, which establishes equilibrium between telomere attrition and elongation by telomerase. This hypothesis is further supported by the observation that chromosome ends that lack telomeric DNA can be stabilized through telomere repeat addition by telomerase. In these so-called "chromosome-healing events" the newly formed telomere is elongated to and then maintained at a length appropriate for the host cell. Additionally, in tumor cells lines the activation of telomerase counteracts telomeres attrition and individual tumor cell lines maintain a constant average telomere length. These observations suggest that the length of individual telomeres regulates repeat addition by telomerase in cis. Experiments in human tumor cells established that this cis-regulation is mediated through a counting model in which the amount of double stranded repeats are "measured" by telomere binding proteins which then restrict telomere elongation by telomerase.

This counting model was first established in human cells for the shelterin protein TRF1 [105]. Overexpression of TRF1 in a telomerase positive fibrosarcoma cell line (HTC75) caused gradual telomere shortening, while overexpression of a dominant negative form of TRF1 induced telomere elongation. These experiments show that TRF1 is a negative regulator of telomere length. Telomere length regulation by TRF1 is telomerase dependent, as telomere length is not altered by TRF1 changes in telomerase negative cells. TRF1 acts in cis and does not influence the overall enzymatic activity of telomerase, as TRF1 specifically targeted to one telomere by Gal4 binding sites changes only the length of this modified telomere [12].

Several experiments show that TRF2 is involved in telomere length regulation in a similar manner. Overexpression of TRF2, like TRF1, leads to telomere shortening in HTC75 telomerase positive cells [79]. A role of TRF2 in telomere length homeostasis is also supported by the finding that cells depleted for TRF2 using RNAi show rapid telomere elongation (Takai and de Lange unpublished). The telomere length regulation functions of the other components of shelterin have been confirmed in a similar fashion. Depletion of TIN2, TPP1 and POT1[55,84,98-100] (see also chapter 2) using RNAi techniques results in telomerase dependent telomere elongation in HTC75 cells.

These experiments established that shelterin acts as negative regulator of telomere length and led to the current model of telomere length regulation. Long telomeres recruit more shelterin, which through a cis-acting mechanism reduces the likelihood for the telomere to be elongated by telomerase. On a short telomere the reduced binding of shelterin releases suppression and telomerase will elongate this telomere preferentially. Telomere length homeostasis is reached in cells when telomere shortening and telomerase elongation reach equilibrium, depending on the amount of shelterin that is bound.

Recently a mechanism was proposed by which the amount of shelterin bound to the double stranded part of the telomere can be translated into the regulation of telomerase activity on the single stranded overhang. The finding that a mutant form of POT1, lacking the first OB-fold of its DNA binding domain, causes telomere elongation, led to the proposal that POT1 acts as the terminal transducer of telomere length information from the double stranded part of the telomere to the overhang [55]. Since long telomeres recruit more POT1 through shelterin than short telomeres, there is an increased

chance on long telomeres that POT1 will associate with the telomeric overhang and inhibit telomerase. The finding that cells depleted for TRF1, TRF2 or TPP1 ([55] and shown in the result section) recruit less POT1 to telomeres supports this model.

Direct competition for the 3' end of the single stranded overhang between POT1 and telomerase has been suggested to account for the ability of POT1 to inhibit telomerase. *In vitro* data shows that POT1 bound to the 3' end of the overhang can block telomerase access [96,106]. Interestingly, these studies also found that POT1 can bind in two positions on the telomeric overhang. In one conformation POT1 is bound at the 3' end and blocks telomerase; in the other POT1 is bound internal to the overhang, which allows telomerase access. In the latter position POT1 appears to promote telomerase activity on the 3' end [96]. This *in vitro* data suggests that POT1 may have a dual role in telomere length regulation. A dual role is not unprecedented, as it has also been suggested for Cdc13, the single-strand telomeric DNA protein of *S. cerevisiae*.

Another way in which POT1 could stimulate telomerase activity is by changing the telomeric overhang into a conformation that is favored as a substrate by telomerase. This hypothesis is supported by data showing that POT1 can eliminate G-quartets from single stranded telomeric DNA. Oligos that are able to form G-quartets are known to be a poor substrate for telomerase elongation *in vitro*, but become a better substrate for telomerase upon internal binding of POT1 [33]. An additional line of evidence for a positive role of POT1 in telomere length regulation emerged form the finding that TPP1, the protein that brings POT1 to the telomere, can stimulate telomerase activity and might even directly interact with telomerase. As TPP1 has no intrinsic affinity for DNA, it seems possible that TPP1 in complex with POT1 could positively regulate the access of

telomerase to the overhang [103,104]. In the results section I will present data confirming the role of POT1 as a negative regulator of telomere length, while leaving open the possibility for an additional function of POT1 in telomerase recruitment.

Telomere protection and the function of TRF2

In addition to regulating telomere length, shelterin is essential for the protective function of telomeres. Telomeres become deprotected either if they become critically short or if shelterin function is impaired. The consequences of both forms of telomere deprotection have been studied intensively and have been found to result in similar outcomes. As my studies on POT1 are mostly concerned with telomere deprotection as a result of loss of shelterin function, I will first discuss the cellular consequences of shelterin loss. I will discuss the consequences of telomere shortening in a later section in the context the telomerase mouse knockout. As most of our knowledge about telomere protection came from experiments that focus on the function of TRF2, I will illustrate the paradigms of telomere protection by describing the phenotypes arising from the loss or overexpression of TRF2.

Cellular responses to telomere dysfunction

The first insight into the role of TRF2 in telomere protection came from experiments in which a dominant negative form of TRF2 was expressed in human cells. This dominant negative form of TRF2, called TRF2ΔBΔM, lacks the MYB-DNA binding and basic domain of TRF2 but retains its dimerization domain. TRF2ΔBΔM has the ability to form heterodimers with endogenous TRF2, but this heterodimer cannot bind DNA as is lacks

one of the two necessary MYB-DNA binding domains. Therefore, overexpression of TRF2ΔBΔM strips the endogenous TRF2 molecules from the telomere and acts as a dominant negative allele [76]. Cells expressing TRF2ΔBΔM exhibit cell cycle arrest and undergo premature senescence or apoptosis, indicating the essential role of TRF2 for cellular viability [76,107]. Several lines of evidence indicate that these outcomes are the result of telomeres being sensed as double stranded breaks. Loss of TRF2 results in the activation of the DNA damage checkpoint kinase ATM (Ataxia-Telangiectasia Mutated). Activation of ATM by double stranded breaks leads to the rapid autophosphorylation of ATM at serine residue 1981 [108]. ATM then phosphorylates the chk2 kinase, which actives p53. Depending on the cell type, p53 up-regulation induces either a cell cycle arrest through the Cdk2 inhibitor p21, or apoptosis.

Cytological studies confirmed the finding that telomeres depleted for TRF2 are recognized as double stranded DNA breaks. When telomeres become deprotected due to the expression of TRF2ΔBΔM, DNA damage factors including 53BP1, γ-H2AX, Rad17, ATM, and Mre11 localize to telomeres in large aggregates [109]. These foci were termed Telomere Dysfunction-Induced Foci (TIFs) and can also be found in cells that have reduced TIN2, TPP1 and POT1 levels and in cells that have entered replicative senescence [78,101,104,110-112] (see also chapter 3). Thus, the DNA damage machinery recognizes deprotected telomeres induced both by gradual telomere shortening and by interference with shelterin.

Telomere fusions as a result of telomere dysfunction

In parallel with these signaling events, telomeres that are deficient for TRF2 are subject to processing by the DNA repair machinery. When TRF2 function in cells becomes impaired, telomeres fuse to each other. Theses fusion events are covalent links between two telomeres and are mediated by the Non-Homologous-End-Joining (NHEJ) pathway. Cells that are deficient for DNA Ligase IV, the ligase that rejoins broken ends after DNA breaks, show a marked reduction of telomere fusions after the inhibition of TRF2 [81]. A conditional TRF2 mouse knockout model recently confirmed the findings that were derived from studies of TRF2ΔBΔM expression. After deletion of TRF2, mouse cells stop proliferating and almost all telomeres become fused [80].

Telomere end-to-end fusions are a prominent outcome of telomere deprotection and can be found not only after the deprotection of TRF2 but also once telomeres become critically short. If telomeres fuse before S phase, the result will be a chromosome-type dicentric chromosome whereas fusions that happen after DNA synthesis result in chromatid-type dicentric chromosomes in which only one chromatid of a chromosome participates in the fusion event. A third form of telomere fusions, is generated by the union of sister telomeres. Dicentric chromosomes can lead to anaphase bridges and bridge-fusion-breakage (BFB) cycles. BFB cycles can cause chromosome nondisjunction, translocations, and changes in chromosome number. These karyotypic changes are seen in cells entering crisis and can explain the genome instability of tumor cells that overcome crisis (reviewed in) [113,114].

Overhang processing of deprotected telomeres

In addition to telomere fusions, TRF2 loss compromises the integrity of the telomeric overhang. Whereas the double-stranded part of the telomere remains intact after the expression of TRF2ΔBΔM, the telomeric overhang is partially lost [76]. Mouse cells deficient for TRF2 completely lose the overhang [80]. This loss of overhang can be partially attributed to the fact that overhang processing precedes covalent telomere-to-telomere fusions, but it is also the result of nucleolytic degradation of overhang DNA independent of telomere fusions. After the inhibition of TRF2, the telomeric overhang becomes a substrate for the ERCC1/XPF nuclease complex [115]. While human cells that express TRF2ΔBΔM show a 50% reduction of the telomeric overhang, cells that are also deficient for XPF retain normal overhangs. Interestingly, cells that are deficient for the NHEJ pathway also do not show overhang loss as a consequence of TRF2 deficiency, although these cells present TIFs at almost all telomeres indicating that they are sites of DNA damage [80]. This finding shows that overhang degradation is not a prerequisite for recognition of unprotected telomeres, and also provides evidence for a coupling between overhang processing by ERCC1/XPF and the NHEJ pathway.

The dual role of DNA-damage response proteins for telomere function

Although the recognition of telomeres by the DNA damage machinery presents an imminent threat to telomeres, some DNA damage and repair proteins paradoxically localize to unperturbed and functional telomeres. A small fraction of the cellular Mre11/NBS1/ RAD50 (MRN) complex, which is involved in sensing DNA double stranded breaks, localizes to intact telomeres [92]. This finding might imply that the DNA-damage machinery serves additional functions on mammalian telomeres. Experiments

that address the function of these proteins put forward the idea that they are involved in telomere processing steps occurring after the replication of the telomeres [92,116-118].

Similarly, the Ku protein, which is necessary for efficient NHEJ can be found at normal telomeres. Ku seems to have a dual role in telomere biology [119,120]: on the one hand it is necessary for the efficient fusion of deprotected telomeres, on the other hand it is involved in the suppression of a telomere recombination pathway [119]. Cells that are double deficient for TRF2 and Ku show a ten fold increase in rare recombination events called sister telomere exchanges (STE) [119], which are the result of homologous recombination between the telomeres of two sister chromatids.

Another protein that is necessary to maintain the integrity of telomeres, but has additional nontelomeric functions, is the Werner protein (Wrn). Wrn is a helicase, implicated in the resolution of abnormal DNA structures (reviewed in) [121]. During S phase Wrn localizes to telomeres and this is likely mediated through a direct interaction with TRF2 [122-124]. Human cells deficient for Wrn display sporadic loss of telomeric DNA. Analysis of metaphase chromosomes shows that this loss is restricted to lagging strand telomeres, suggesting that Wrn is necessary to resolve aberrant DNA structure during replication of lagging-strand telomeres. It has been proposed that these observations explain the symptoms of patients with mutations in Wrn [122].

Several other proteins with additional nontelomeric functions have be found at telomeres of unperturbed cells, including Tankyrase 1 and 2, Apollo, Rad51D the 9-1-1 complex, the BLM helicase, and XPF/ERCC1 [115,125-131].

Suppression of the telomeric DNA damage response by TRF2

In addition to experiments addressing loss of TRF2 function, overexpression of TRF2 revealed important aspects of telomere function. Overexpression of TRF2 is capable of blunting an irradiation induced ATM DNA damage response by directly inhibiting ATM kinase activity [132]. Interestingly, it has been shown that TRF2 binds directly to ATM This interaction occurs within the region where activated ATM auto-phosphorylates itself [108]. It has been suggested that due to this interaction and the high local concentration of TRF2, ATM activity at telomeres is blocked by TRF2. This model provides molecular insight into how TRF2 could function in telomere protection [132].

Homologous recombination of telomeres and t-loop formation

T-loops are thought to be formed by the invasion of the telomeric overhang into the double stranded part of the telomere. The resulting D-loop structure at the base of the t-loop is reminiscent of Holiday-junctions (HJ) formed during homologous recombination. During DNA repair by homologous recombination these HJs are resolved releasing the two recombined DNA strands. However, resolution of the t-loop HJ is predicted to lead to loss of telomeric DNA. This process, called t-loop homologous recombination (t-loop HR), can be detected in unperturbed cells and might contribute to telomere shortening in primary human cells. It has been proposed that t-loop HR is regulated by shelterin. This hypothesis is based on the finding that overexpression of TRF2 or an allele of TRF2 lacking the basic domain (TRF2ΔB) induces these intramolecular telomere homologous recombination events [133]. As TRF2 can promote the deletion of t-loops through t-loop HR and conversely is known to promote t-loop formation *in vitro*, the amount of TRF2 appears to be critical for regulation of t-loop formation [35,75,90,133]. Additionally, these

observations could explain how overexpression of TRF2 can lead to accelerated telomere shortening in telomerase negative cells.

Telomerase function in human disease

The replicative capacity of normal human cells is limited and as a result cultured cells eventually enter a terminal growth arrest called senescence [17]. Most human tumors have reactivated telomerase suggesting that counteracting telomeres shortening is a requirement for indefinite proliferation [13,20,21]. Direct evidence for this hypothesis came from the demonstration that ectopically expressed telomerase allows human fibroblasts to overcome senescence and become immortal [19,22]. Although it has not been established that normal telomere attrition affects human health, recent data has corroborated the potential contribution of telomerase loss to human disease. Patients with the rare genetic disorder dyskeratosis congenita (DC), also known as Zinsser-Cole-Engman-syndrome were found to have two types of mutations that affect telomerase (reviewed in)[134,135]. Patients with the autosomal dominant form of DC have mutations in the telomerase RNA (hTR) [3], and patients with the X-linked form of DC have mutations in the dyskerin gene [47]. Dyskerin is a protein in the telomerase complex that is thought to associate with and stabilize telomerase. These mutations in the telomerase complex can account for 50% of DC cases. Cells from DC patients have reduced levels of hTR, low levels of telomerase activity, and short telomeres [47]. DC is associated with an increase in tumor incidence, but most patients die of bone marrow failure and immunodeficiency. Other symptoms of DC are cutaneous pigmentation, nail dystrophy, anemia, mucosal leukoplakia, and in most cases testicular atrophy. Affected tissues in DC are generally highly proliferative, which is consistent with accelerated telomere erosion. The progressive telomere shortening also

explains the generational anticipation of the DC symptoms found in families carrying a DC allele.

The telomerase knockout mouse

The consequence of telomerase loss and telomere shortening were studied extensively using mice deficient for the telomerase RNA component (mTR). Later studies showed that mice, in which the mouse telomerase protein (mTert) was knocked out, display essentially the same phenotypes as the deletion of mTR [136]. Telomeres of telomerase knockout (KO) mice shorten by approximately 80-100 bp/PD, a rate consistent with the attrition rate in telomerase negative human cells [67]. This telomere shortening does not result in a phenotype in early mouse generations, but consecutive intercrosses of mice deficient for telomerase lead to critically short telomeres and telomere dysfunction [67]. The genetic anticipation of these phenotypes in later generations can be explained by the long telomeres of *Mus musculus*, which need to be shortened over several consecutive generations before the phenotype is manifested. Progressive telomere shortening also occurs in mice heterozygous for mTR showing that like the human autosomal dominant DC disease, telomerase is haplo-insufficient in mice [137-139].

Late generation telomerase KO mice display a stem cell depletion phenotype and symptoms of premature aging [140,141]. In particular these mice suffer from infertility, hair loss, decreased wound healing, reduced lymphocyte counts, bone marrow failure and an overall reduced lifespan. Histological analysis of these mice revealed that highly proliferative tissues such as testis and intestines show an increase in apoptosis [140,141]. This increase in apoptosis is caused by the accumulation of critically short telomeres, telomere fusions, anaphase bridges and genomic instability [141-143].

As expected from the tumor suppressing capacities of telomere shortening, late generation telomerase KO mice have a lower tumor frequency in tumor promoting mouse models such as the INK4a KO [144]. However, when telomerase KO mice with short telomeres are crossed into a background that abrogates the p53 DNA damage pathway, the tumor incidences increases. This difference has been attributed to ability of p53 to induce a growth arrest in response to dysfunctional telomeres. While cells that maintain a functional p53 pathway can sense short telomeres, p53 deficiency renders cells resistant telomere dysfunction signals. These cells will continue to proliferate and can accumulate secondary mutations through the genomic instability arising from dysfunctional telomeres [142,145].

2. Identification of POT1-55 and the role of POT1 in telomere length regulation

Introduction

Shortly after the initial study by Baumann et al. [93], on the discovery of human POT1, two studies implicated POT1 in telomere length regulation. The first study determined the length of telomeres in a clonal cell population overexpressing transfected POT1 and found that ectopic expression of full-length or POT1V2, a C-terminal truncation leads to telomere elongation [146]. The authors of this study concluded that POT1 is a positive regulator of telomere length. In contrast, experiments conducted in the de Lange lab showed that the overexpression of POT1ΔOB, a form of POT1 lacking its DNA binding domain, leads to telomere elongation, indicating that POT1 is a negative regulator of telomere length [55]. In this study telomere length did not change after the retroviral transduction of a pool of cells with full-length POT1.

To further investigate the role of POT1 in telomere length control, I determined the protein levels of the putative POT1 protein variants and then studied their role in telomere length regulation using an RNAi based approach. Some data and text presented below was published and were used for this section [99,147].

Results

Two forms of human POT1 generated by alternative splicing

In order to study the phenotypes of POT1 depletion induced by RNAi, we first assessed the protein products generated by the human POT1 gene. Based on the structure of five alternatively spliced transcripts (variants V1–5), five potential polypeptides were predicted [97]. Antibodies raised against a peptide present in all putative variants of POT1 reacted with the 71 kDa POT1 expressed from V1 mRNA, but the polypeptides predicted to be encoded by mRNA V2, V3, and V5 were not detectable [55] (Figure 2.1A). Instead, a POT1 polypeptide with an MW of 55 kDa (Figure 2.1A), referred to as POT1–55, was detected. Although POT1–55 was not a predicted product [97], we noticed that the V4 mRNA, lacking exon 8, could encode a 55 kDa protein starting with an inframe ATG in exon 9 (Figure 2.1A). Consistent with this, POT1– 55 migrated closely to POT1ΔOB, an N-terminal truncation mutant that starts five amino acids upstream of POT1–55 [55] (Figure 2.5). Retroviral expression of V4 mRNA led to the overexpression of a protein that comigrated with the putative 55 kDa POT1 species (Figure 2.1A).

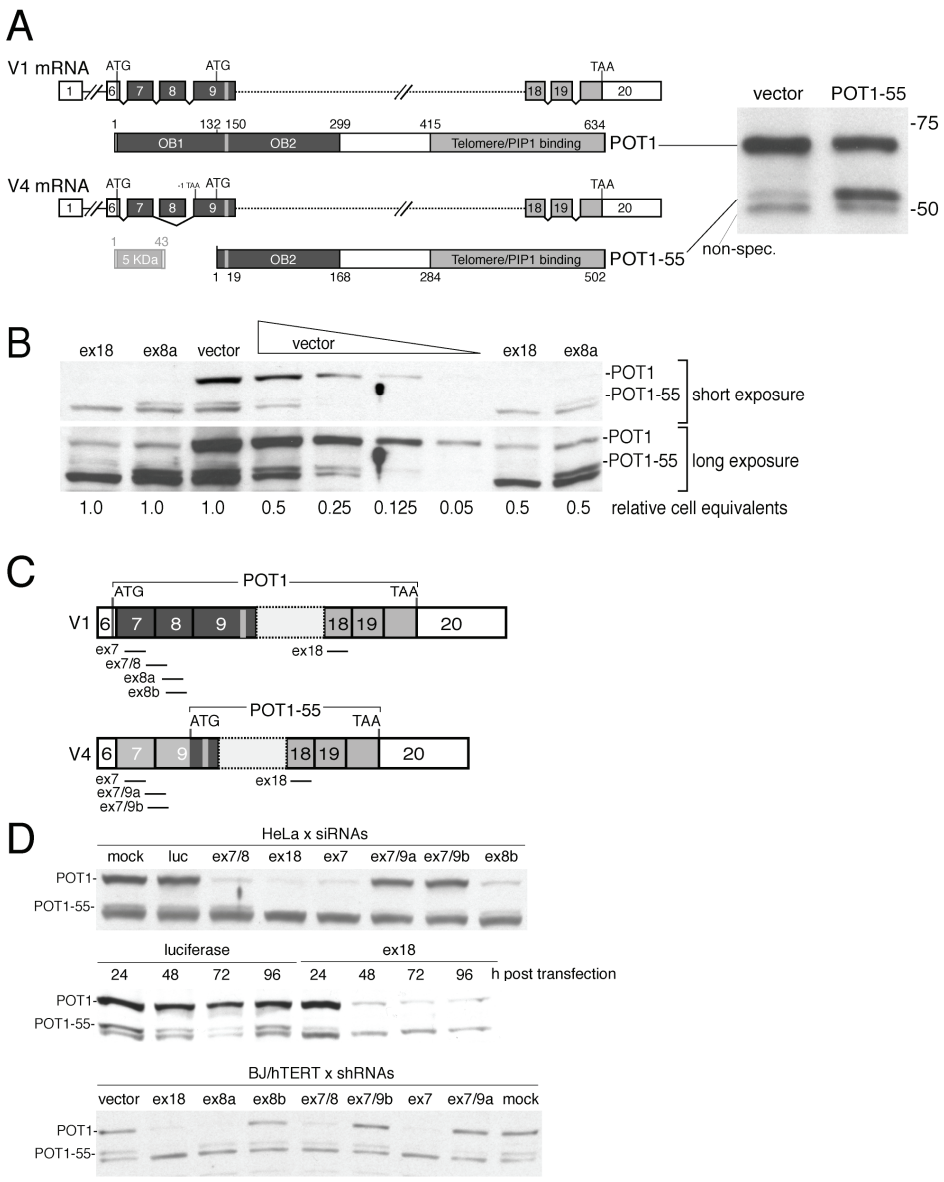

Figure 2.1 POT1 and POT1–55 and their depletion with RNAi

(A) Schematic of two POT1 mRNAs and the proteins they encode. The immunoblot to the right shows HTC75 cells infected with the pLPC vector or the same vector expressing POT1–55 from the V4 mRNA. Dark fill: OB-folds. Light fill: TPP1 interacting domain. (B) Quantitative immunoblot to determine the level of POT1 knockdown in HelaS3 cells. Serial dilutions of vector protein extract were compared to the indicated relative cell equivalents of ex18 and ex8a knockdown cell extracts. (C) Schematic of POT1 mRNAs variant 1 and 4 and the si/shRNAs target sites used in this study. (D) Immunoblot of HeLa cells transfected with the indicated siRNAs and BJ/hTERT cells infected with the indicated shRNA vectors. HeLa cells were analyzed 2 days (top panel) or at the indicated time points (middle panel) after transfection. BJ/hTERT cells were analyzed 5 days after infection and selection

In order to verify that POT1–55 was derived from V4 mRNA, we used RNAi target sites in exons shared by V1 and V4 mRNAs (exons 7 and 18), target sites in exon 8 (absent from V4), the junctions of exons 7/9 (only found in V4), and the junction of exons 7/8 (present in all POT1 mRNAs but V4) (Figure 2.1B and 2.1C). The results established that the human POT1 gene encodes two main products, the 71 kDa POT1 and the smaller POT1–55 encoded by an mRNA lacking exon 8 (Figure 2.1 A and D). Using an antibody raised against a peptide present in both forms of POT1, we estimate that POT1 is approximately 10-fold more abundant than POT1–55 (Figure 2.1B). POT1-55 is present in all cell types investigated, including tumor cells, primary cells and primary cells immortalized with telomerase.

Telomere elongation in cells with reduced POT1 levels

To investigate the role of POT1 and POT1-55 in telomere length control, we used RNAi to diminish the expression of POT1 in HTC75 cells, a subclone of the telomerase positive fibrosarcoma cell line HT1080, widely used for telomere length regulation studies [105]. Three retrovirally-expressed shRNAs directed against POT1 resulted in a significant reduction of POT1 or POT1-55 expression compared with the vector control. There was no detectable change in the growth rate of cells infected with POT1 shRNAs, indicating that HTC75 cells tolerate the reduced levels of POT1. Consistent with this, POT1 levels remained stably reduced for >50 population doublings. Telomere length analysis showed significant telomere elongation in cells that have reduced levels of full-length POT1 (Figure 2.2). This telomere elongation is also seen in cells with simultaneous reductions of full-length POT1 and POT1-55. As these results clearly showed that full-length POT1

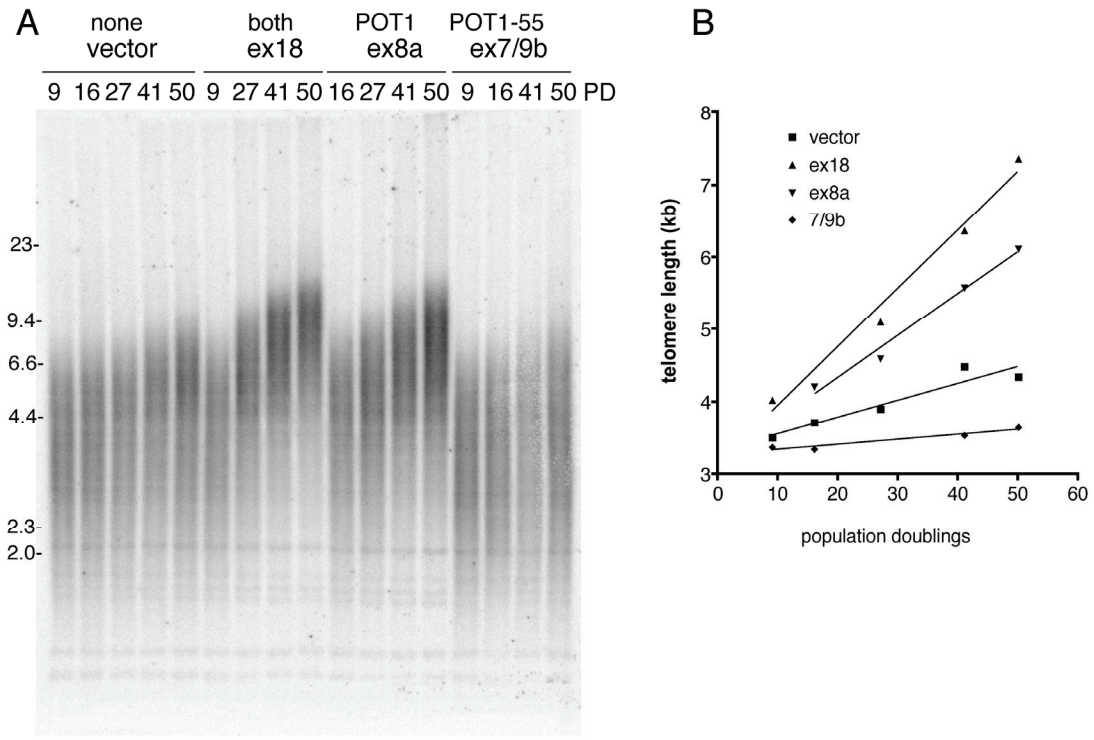

Figure 2.2 Telomere elongation induced by RNAi-mediated reduction of POT1

(A) Telomeric restriction fragment blot of HTC75 cells expressing the indicated shRNAs (vector control represents cells infected with the empty virus) at the indicated population doublings (PDs). The molecular mass in kilobases of HindIII-digested DNA fragments is shown on the left. (B) Graph of the mean telomeric restriction fragment length of the indicated cell lines plotted versus PD. Elongation rates of the telomeres are indicated.

can function as a negative regulator of telomere length, we next focused on investigating the role of POT1-55 in telomere length regulation.

Cells that had reduced levels of POT1-55, due to the expression of an shRNA targeting the exon 7/9 junction, showed a slower telomere elongation rate than cells infected with a vector control (Figure 2.2). This finding could indicate that reduced levels of POT1-55 lead to telomere shortening. In order to confirm these results we decided to reduce POT1-55 levels in a different cell type. HTC75 cells have relatively short telomeres of an average length of about 4-5 kb. We reasoned that the telomere shortening

effects caused by reduced levels of POT1-55 might be better detectable in cells that maintain longer telomeres. Therefore, we targeted POT1 in Hela 1.2.11 cells, which have an average telomere length of approximately 12 kb (Figure 2.3). As expected from the findings in HTC75 cells, reduction of full-length POT1 in Hela1.2.11 cells results in telomere elongation regardless of the levels of POT1-55. The reduction of POT1-55 alone in Hela1.2.11 cells resulted in a modest telomere shortening compared to vector control cells (Figure 2.3).

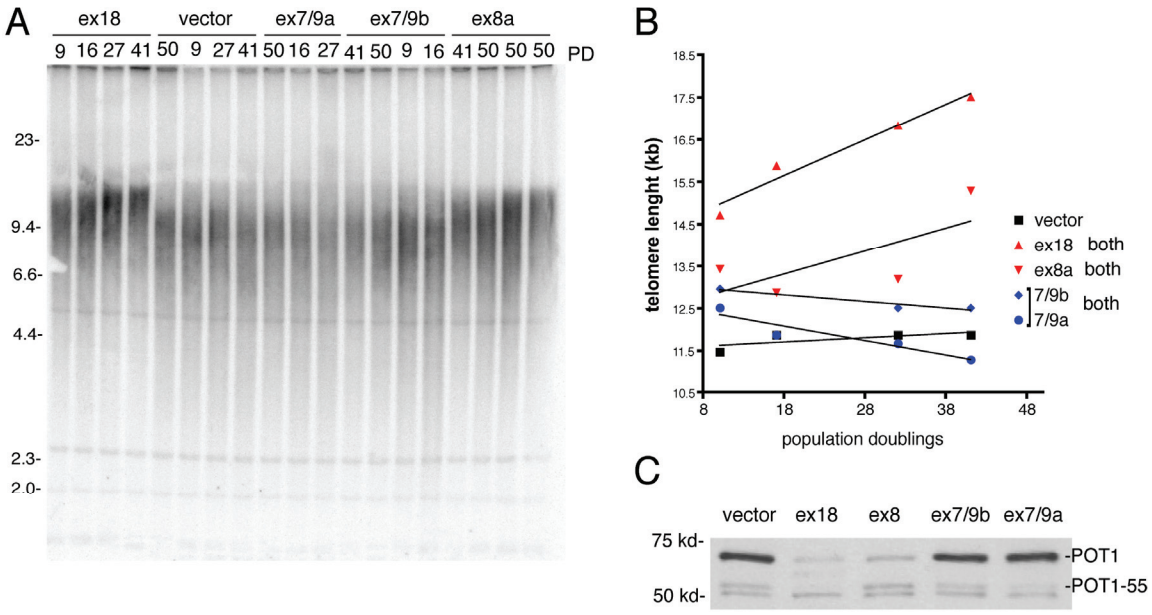

Figure 2.3 Telomere elongation induced by RNAi-mediated reduction of POT1

(A) Telomeric restriction fragment blot of Hela 1.2.11 cells expressing the indicated shRNAs (vector control represents cells infected with the empty virus) at the indicated population doublings (PDs). The molecular mass in kilobases of HindIII-digested l-DNA fragments is shown on the left. (B) Graph of the mean telomeric restriction fragment length of the indicated cell lines plotted versus PD. Elongation rates of the telomeres are indicated. (C) Immunoblot of Hela 1.2.11 cells expressing the indicated shRNAs (vector control represents cells infected with the empty virus) at PD50 post selection. POT1 was detected with Ab 978.

The RNAi target sites in the 7-9 exon junction resulted only in a mild knockdown of POT1-55. We reasoned that a better knockdown of POT1-55 could result in stronger telomere length changes. As the specific knockdown of POT1-55 is limited to the 7/9 exon junction we decided to deplete POT1-55 through an alternative approach. We retroviraly transduced cells with a full-length POT1 cDNA carrying a silent mutation in the targeting site of the exon 18 shRNA and thereby rendering this cDNA resistant to the ex18 shRNA. Then we depleted endogenous POT1 and POT1-55 proteins using the ex18 shRNA (Figure 2.4C). We expected that this approach would result in the selective depletion of POT1-55 from the cells, as full-length POT1 was expressed exogenously from the shRNA resistant cDNA. Surprisingly, we detected by western blot analysis the presence of an additional band with a size similar to POT1-55 in cells expressing mutated full-length POT1 (Figure 2.4A). This additional band was previously not seen in cells expressing full-length POT1 and we could only detect this POT1 product when POT1 was expressed using the pBabe retroviral vector in HTC75 cells. In order to address whether this protein is POT1-55 made from the exogenous POT1 cDNA, we mutated the ATG in exon 9 that is used as the translational start of POT1-55 in the V4 variant (Figure 2.4C). As mutation of this ATG did not abrogate the presence of the additional band (Figure 2.4B), we conclude that this band is not POT1-55. Nevertheless, we could not exclude that this band represents an additional POT1-fragment, which could retain some function of POT1. We therefore assumed that studying telomere length control by POT1-55 using this approach would not yield interpretable data. Further experiments and a different experimental approach will be necessary to address the telomere length phenotype of POT1-55 depletion.

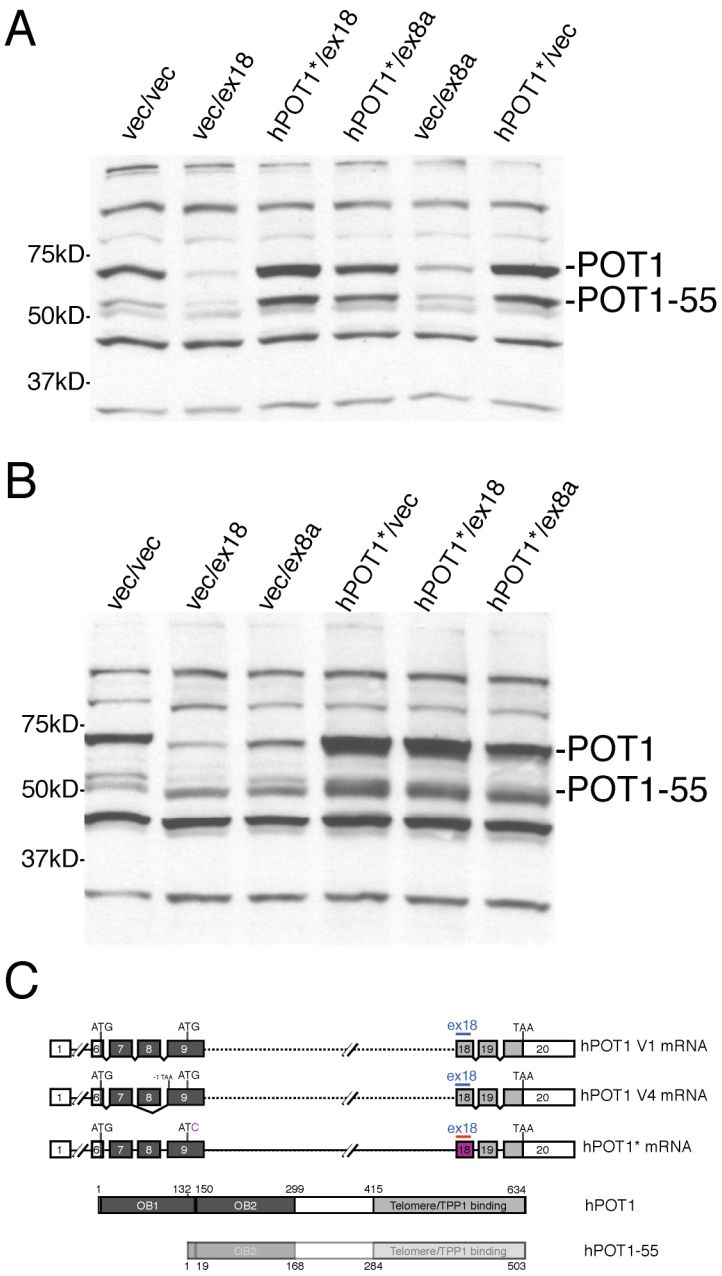

Figure 2.4 Knockdown of POT1-55 using the non degradable POT1* and ex18

(A) Immunoblot of HTC75 cells infected with human POT1 carrying a silent mutation in exon 18 rendering it resistant to POT1siRNAs. Cells were additionally infected with the indicated shRNAs to deplete cells for endogenous POT1 and POT1-55. (B) As in panel (A); In addition to the silent mutation in the shRNA target site the POT1 cDNA contained a mutation in the ATG encoding for the methionine of POT1-55. (C) Schematic of POT1 mRNAs variant 1 and 4 and the exogenous mRNA mutated in the ex18 target site and in the ATG encoding the POT1-55 starting methionine.

In order to further investigate the function of POT1-55 we determined the telomere length changes in HTC75 cells overexpressing POT1-55. Although expression of POT1-55 from the V4 splice variant1 was mild, it partially suppressed the endogenous full length POT1 protein (Figure 2.1A) and resulted in telomere elongation, as expected from its similarity to POT1ΔOB (Figure 2.5)

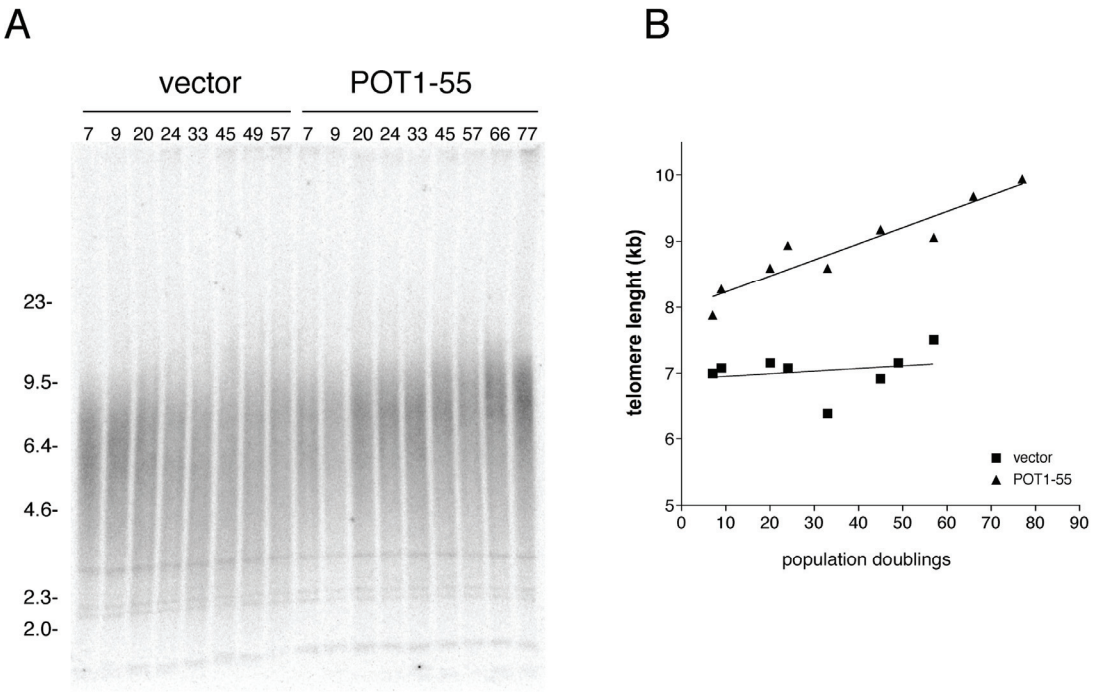

Figure 2.5 Telomere elongation induced by expression POT1-55 form the V4 mRNA

(A) Telomeric restriction fragment blot of HTC75 cells expressing vector of POT1-55 from the V4 mRNA (Δexon8) at the indicated population doublings (PDs). The molecular mass in kilobases of HindIII-digested DNA fragments is shown on the left. (B) Graph of the mean telomeric restriction fragment length of the indicated cell lines plotted versus PD. Elongation rates of the telomeres are indicated.

The fact that telomere elongation resulting from the overexpression of POT1-55 was less severe than in cells expressing POT1ΔOB may be explained by the lower expression of POT1-55 compared to POT1ΔOB. This hypothesis is supported by experiments performed by Diego Loayza. When POT1-55 is translated from a strong

Kozak starting directly with the ATG in exon 9, POT1-55 levels are similar to the levels of POT1ΔOB. Under these conditions POT1-55 overexpression causes telomere elongation with rates equal to POT1ΔOB overexpression (Diego Loayza, personal communication).

Regulation of POT1

Western blot analysis shows POT1ΔOB overexpression results in the suppression of endogenous POT1 [55]. The finding that both POT1ΔOB expression and POT1 knockdown, result in telomere elongation, supports the proposed model that POT1ΔOB acts mainly as a dominant negative protein by suppressing levels of endogenous POT1 protein. How this suppression works is still unclear, but several observations shed light on the mechanism. Down regulation of endogenous POT1, as in the case of POT1ΔOB overexpression, is also seen after the overexpression of MYC-tagged full-length POT1 [55] (Figure 2.7 and 2.8). However, a remarkable difference in the level of overexpression between full-length POT1 and POT1ΔOB can is observed, when both are expressed from the same promoter and Kozak sequence (Figure 2.7). Whereas POT1ΔOB is over expressed about 30-fold compared to endogenous POT1 levels, overexpression of full-length POT1 results only in a three-fold increase of POT1 levels [55]. This finding suggests that the N-terminus of POT1 inhibits its cellular accumulation and that the endogenous protein levels of POT1 are tightly regulated.

In order to determine the mechanism by which POT1ΔOB reduces full-length POT1 levels, we determined the mRNA levels of endogenous POT1 in the presence of POT1ΔOB. Using semi-quantitative RT-PCR we found that POT1 mRNA levels remain

unchanged upon the expression of POT1ΔOB or full-length POT1 compared to control cells (Figure 2.6). This result indicated that POT1ΔOB does not regulate endogenous POT1 on the transcriptional level.

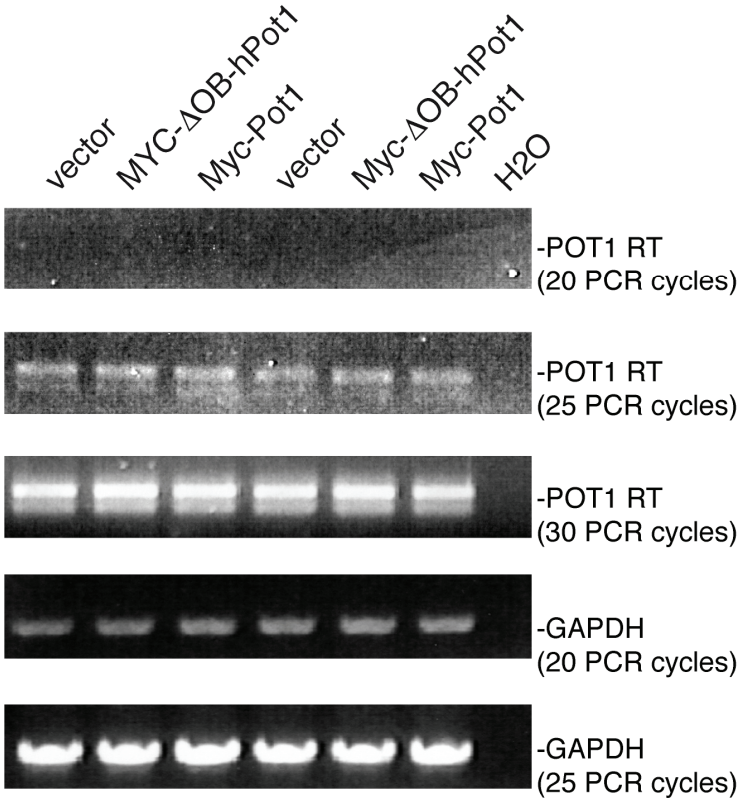

Figure 2.6 POT1 mRNA levels in POT1ΔOB expressing cells

Ethidium-bromide staining of semi-quantitative RT-PCR analysis of POT1 mRNA isolated from HTC75 cells expressing either vector controls, MYC-POT1 or MYC-POT1ΔOB. To show the approximate linearity of the PCR amplification, PCRs were performed with increasing numbers of cycles. As an internal control for the cDNA synthesis, GAPDH was amplified using standard primers. RNA extractions and RT reactions were preformed in duplicates. The amplification of the correct PCR product was confirmed by restriction digest and RT reactions without reverse transcriptase did not result in product amplification.

We next tested whether POT1ΔOB overexpression changes the stability of endogenous POT1 protein. Using cyclohexamide to inhibit *de novo* protein synthesis we determined the protein half live of POT1 and POT1-55 after the overexpression of either

POT1ΔOB or full-length POT1. In control cells POT1 levels were relatively stable with an approximate half-life of 6-8 hours, while the half-life of POT1-55 was somewhat shorter (about 4 hours). As expected, cells that overexpressed POT1ΔOB were depleted for endogenous full-length POT1 and interestingly, overexpression of full-length POT1 reduced the abundance of POT1-55 (Figure 2.7).

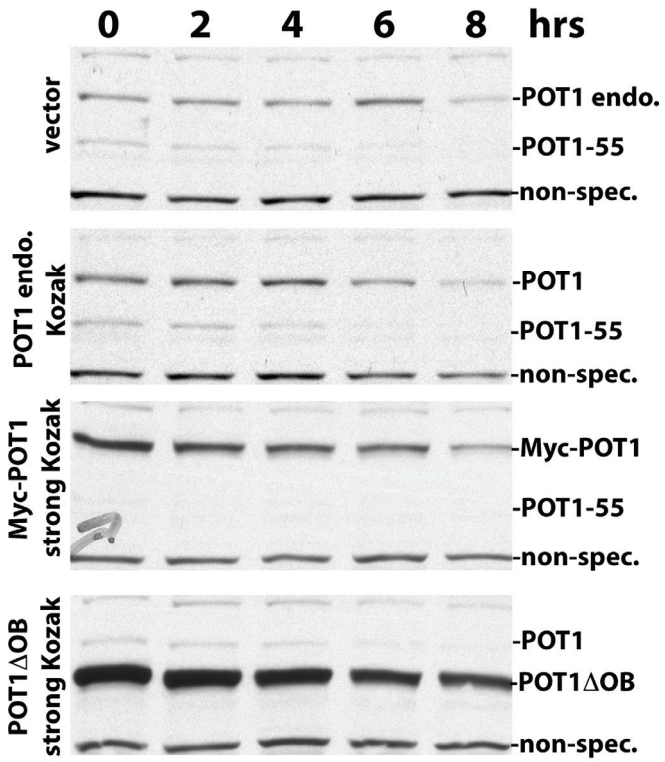

Figure 2.7 The stability of POT1 variants

Immunoblot analysis of HTC75 cells expressing the indicated POT1 constructs or a vector control. POT1 translation was either driven from a strong Kozak consensus sequence or from its endogenous Kozak as indicated. Cells expressing these constructs were treated with cyclohexamide and proteins lysates were prepared after the time indicated above the lanes. POT1 and POT1-55 were detected with Ab 978.

In these cells, both POT1ΔOB and overexpressed full-length POT1 were found to have also a slightly reduced half-life of approximately four hours (Figure 2.7). This result could indicate that excessive amounts of full length POT1 are subjected to an increased turnover rate.

Next, we asked whether proteasome-mediated degradation is responsible for the shorter half-lives of POT1ΔOB, POT1-55 and over expressed full length POT1 (Figure 2.8).

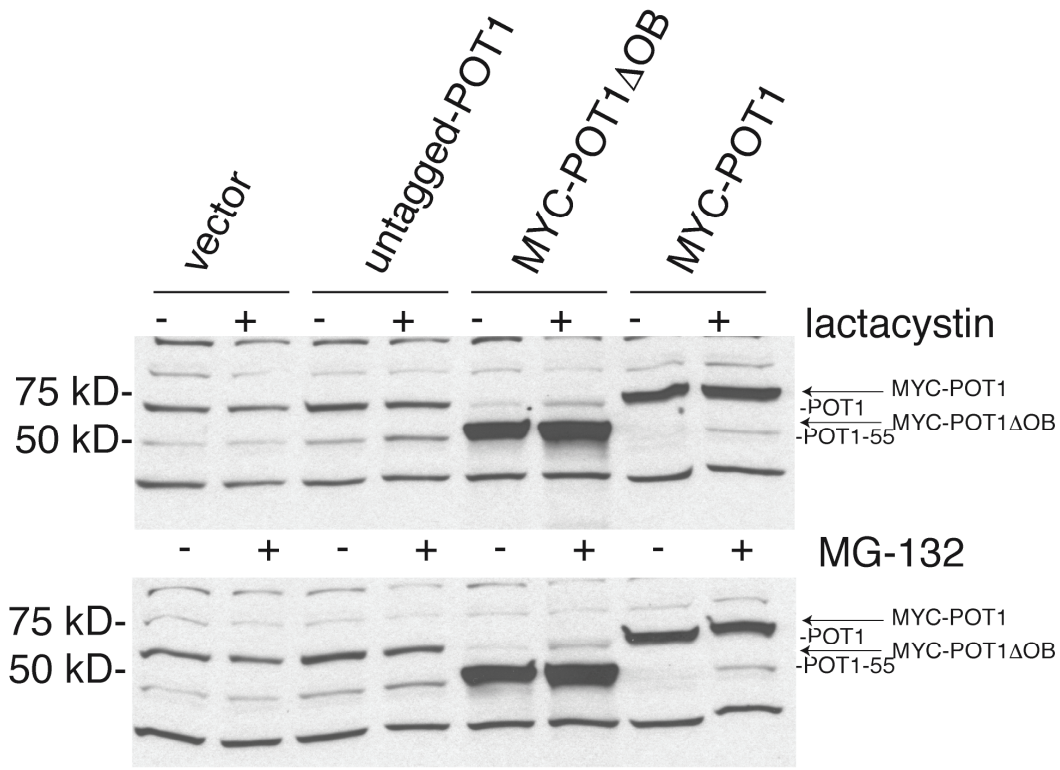

Figure 2.8 Degradation of POT1 protein variants by the proteasome

Immunoblot analysis of HTC75 cells expressing the indicated POT1 constructs or a vector control. POT1 translation was either driven from a strong Kozak consensus sequence (MYC-POT1 and MYC-POT1ΔOB) or from its endogenous Kozak as indicated. Cells expressing these constructs were treated with lactostatine or MG132 (+) or DMSO vehicle (-) for 3.5 hours. POT1 and POT1-55 were detected with Ab 978. The DNA vector constructs used in this experiment were generated by Diego Loayza.

While inhibition of the proteasome with MG-132 or lactacystin leads only to a small increase of full-length endogenous POT1 in unperturbed cells, a greater accumulation of POT1 is detectable in cells that overexpress POT1ΔOB. Furthermore, in cells overexpressing full-length POT1 stabilization of POT1-55 can be detected after inhibition of the proteasome (Figure 2.8). Together these results could indicate that POT1 is regulated on the protein level and that POT1ΔOB increases the amount of POT1 that is targeted for degradation by the proteasome.

Discussion

Telomere length regulation by POT1

The finding that depletion of POT1 by RNAi leads to telomere elongation confirms that full-length POT1 is a negative regulator of telomere length and suggests that POT1ΔOB acts in telomere length regulation by displacing the endogenous POT1 protein. Our results indicate that displaced POT1 protein becomes unstable and is degraded. The model that POT1 is degraded when it is not bound to chromatin is consistent with the finding that cellular POT1 levels correlate strictly with telomere length. These results confirm that POT1 negatively regulates telomere length and allow us to elaborate the current model of telomere length regulation by POT1. In this model endogenous POT1 is targeted to the telomere by its interaction with shelterin and is thus protected against protein degradation. POT1 when not bound to telomeres seems to be actively degraded, and thereby unable to affect telomere length. As a consequence, all cellular POT1 is telomere bound and its abundance on individual telomeres is tightly correlated with the individual telomere length. Long telomeres bind more POT1 than shorter telomeres and through the ability to inhibit telomerase, POT1 renders these long telomeres less likely to be elongated. Thus, POT1 transduces the information about the length of the telomere to the telomere terminus and establishes telomere length homeostasis. The ability of POT1 to inhibit telomerase is dependent on its DNA binding domain, as POT1ΔOB fails to repress telomerase after displacing endogenous POT1 from the telomere.

One main characteristic of this model is the inhibition of telomerase in cis. Cis-inhibition has formally only been shown for TRF1 and TRF2, but not for POT1. But, as

TRF1 and TRF2 recruit POT1 to telomeres through TPP1, a cis-acting mechanism has been implied also for POT1. It is possible that inhibition of telomerase by POT1 in cis is partially a consequence of its active degradation when it is not bound to telomeres. If POT1 were stable in a telomere non-bound form, POT1 might be able to accumulate in the nucleus resulting in an increased local concentration of POT1 around telomeres. If POT1 were able to bind under these conditions directly to the overhang and inhibit telomerase, cis-regulation by shelterin would be circumvented. The hypothesis that POT1 degradation is necessary to establish its cis-inhibition predicts that overexpression of an undegradable form of POT1 would lead to the permanent inhibition of telomerase on all telomeres.

Although the presented experiments clearly identify the negative role of POT1 in telomere length regulation, they do not exclude that POT1 can also act as a positive regulator. In both experimental approaches, shRNA knockdown of POT1 and overexpression of POT1ΔOB, some residual POT1 remains on the telomere [95]. It is possible that this residual POT1 is sufficient to positively regulate telomere length. The recent finding that TPP1, the interacting protein of POT1, is the ortholog of oxytricha nova TEBPβ and is able to stimulate telomerase activity supports this hypothesis [103,104]. As TPP1 and POT1 are predicted to form TEBP like complex on the telomeric overhang, it will be interesting to determine whether POT contributes to telomerase activation and recruitment.

The role of POT1-55

In addition to the full-length form of POT1, cells express POT1-55, which is an N-terminally truncated splice variant of POT1. As POT1–55 is virtually identical to POT1ΔOB, it is expected to have the same properties: association with telomeres through protein–protein interaction, lack of DNA-binding activity *in vitro*, and the capacity to block the negative regulation of telomerase when over expressed [55]. The finding that the specific knockdown of POT1-55 leads to mild telomere shortening and its overexpression to telomere elongation supports this claim. It suggests that POT1-55 could have a positive role in regulating telomere length by a mechanism similar to POT1ΔOB. As the knockdown of full length POT leads to telomere elongation regardless of the presence of POT1-55, POT1-55 is probably not essential for telomerase elongation. However, it is not proven that POT1-55 or POT1ΔOB influence telomere length exclusively through competition with full-length POT1. It is not ruled out that POT1ΔOB partially acts as a gain of function mutation that mimics a stimulating role of POT1-55 on telomere length regulation. As POT1-55 is thought to be able to interact with TPP1, and as TPP1 appears to be able to stimulate telomerase activity, it appears prudent to investigate POT1-55 in the context of the function of TPP1.

3. POT1 protects telomeres from a transient DNA damage response and determines how human chromosomes end

Introduction

The mechanism by which the telomeric complex protects chromosome ends from being recognized as sites of DNA damage is not understood in detail. As interference with members of the shelterin complex leads to the activation of DNA-damage pathways, it is generally assumed that shelterin functions to protect natural chromosome ends (reviewed in)[72]. In particular the shelterin protein TRF2 has been found to be a key player in the suppression of telomere dysfunction. Most insights into the signaling pathways that are repressed at natural chromosome ends come from studies addressing the events at dysfunctional telomeres induced by the loss of TRF2. These studies have revealed that chromosome ends are threatened by the nonhomologous end-joining (NHEJ) pathway [76,80,81]. NHEJ-mediated chromosome end fusions are a prominent consequence of TRF2 inhibition and can also occur when telomeres become critically short. In addition, dysfunctional telomeres can induce the ATM kinase and become associated with DNA damage response factors such as 53BP1, γ-H2AX, and the Mre11 complex [109,110]. When these DNA damage response factors localize to the telomere they form detectable cytological structures called Telomere dysfunction Induced Foci (TIF). Concurrent with these signaling events, the loss of TRF2 function leads to partial degradation of the telomeric overhang by the XPF/ERCC1 nuclease [76,115].

How does shelterin suppress these events? How does TRF2, which binds along the double stranded part of the telomere, prevent the processing of the telomeric

overhang? One mechanism that has been proposed for how TRF2 protects the chromosome terminus is by facilitating t-loop formation. T-loops are large duplex DNA lariats and formed through the invasion of the telomeric overhang into the double stranded part of the telomere [35]. Although the t-loop could be a protective configuration, the t-loop in its proposed form still contains DNA structures, such as the single stranded D-loop and the 3' and 5' DNA ends, that might activate a DNA damage response. Furthermore, during replication the t-loops might be resolved into a linear structure with an accessible telomeric overhang. As POT1 has the ability to bind the telomeric overhang *in vitro* and can potentially recognize structures generated by the t-loop is seems possible that POT1 binding can contribute to telomere protection [94,95]. The finding that loss of the single stranded binding proteins in other organisms leads to telomere deprotection supports this notion [93,148,149]. The crystal structure of the POT1 OB-folds in complex with their DNA-recognition site suggests that POT1 might physically protect TTAGGGTTAG-3' ends [94]. However, only a fraction of the telomeres in primary human cells end on this sequence [28], arguing that physical capping by POT1 is not the main mode of telomere protection. In order to study the protective role of POT1 in telomere protection, POT1 levels were reduced by RNAi induced knock down of POT1 in human cells. I will summarize my finding on POT1 protection below. Part of the text and data in this chapter is published [147].

Results

TIFs without telomere fusions

The effects of lowered POT1 and POT1–55 levels on telomere protection were determined using retroviral delivery of shRNAs into primary human fibroblasts (IMR90 and BJ), fibroblasts immortalized with hTERT (BJ/hTERT), and telomerase- positive tumor cell lines (HeLa, cervical carcinoma, HTC75 fibrosarcoma, and HCT116, colon carcinoma). The RNAi reagents were named for the exons or exon junctions they target (e.g. ex18 targets exon 18; see Figure 2.1). Both forms of POT1 were targeted with ex7 and ex18; ex7/8 and ex8a and b affected POT1 but not POT1–55, and ex7/9a and b partially depleted POT1–55 without affecting POT1 (Figure 2.1). Quantitative immunoblotting showed that the residual POT1 levels in HeLaS3 cells were about 5–10% for shRNAs ex18 and ex8a (Figure 2.1B). Similar knockdown effects were observed in BJ fibroblasts and HCT116 cells, RNAi for POT1 was less efficient in HTC75 and HT1080 cells (Figures 2.1, 3.6, 3.7). Western blotting analysis of synchronized HeLa cells indicated that the knockdown of POT1 was stable through the cell cycle. Telomeric ChIP confirmed that HeLa cells expressing shRNA ex18 (targeting both forms) or ex8a (specific for POT1) had reduced levels of POT1 at telomeres (Figure 3.1). The average reduction of telomeric DNA recovered in the POT1 ChIP was 6.7-fold (n=3; SD +/– 1.5-fold). There was no loss of the duplex telomeric repeats and other components of the telomeric protein complex (TRF1, TRF2, RAP1, and TIN2) remained associated with telomeric DNA (Figure 3.1). Thus, RNAi can remove more than 90% of POT1 from the telomeric complex.

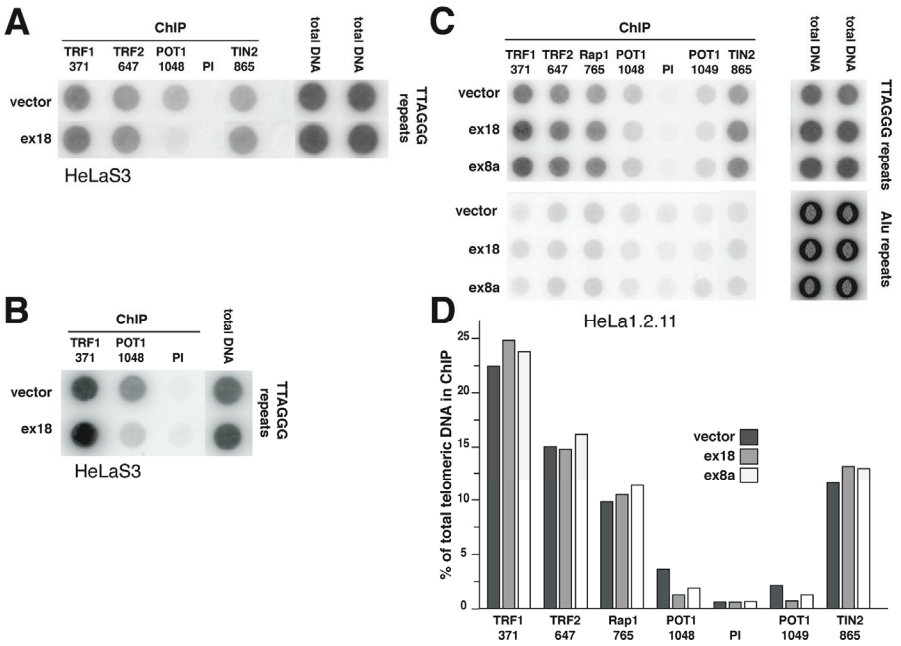

Figure 3.1 Diminished telomeric accumulation of POT1, but not other telomeric proteins upon POT1 knockdown

(A-C) ChIPs with the indicated antibodies using HeLa cells expressing the indicated POT1 shRNAs. DNA in the IPs was dot-blotted and hybridized with a probe for telomeric DNA (from pSP73.Sty11) or Alu repeats. Total DNAs and precipitated telomeric DNA (TTAGGGn) samples were blotted in parallel. Antibodies are indicated above each row. PI is pre-immuno sera from the rabbit that generated serum 1048. (D) Bargraph of quantification of the data in (C). The reduction of POT1 at telomeres in panels (C) is less than in the other two experiments. The average reductions is ~7-fold (see text). There was no significant reduction of the accumulation of other telomeric proteins.

RNAi knockdown experiments have obvious limitations, since there is residual POT1 expression and localization. Nevertheless, RNAi depletion of POT1 is still informative not only because it allows analysis of human cells but also because partial inhibition of other human telomeric proteins has identified important hallmarks of telomere dysfunction in previous studies [76]. As telomere fusions are a pervasive signature of telomere dysfunction, metaphase chromosomes were examined for this defect. In HTC75 and HeLa cells, the frequency of chromosome end fusions after stable POT1 knockdown was increased less than two-fold compared to the control cultures (Figure

3.2A and B), resulting in approximately one telomere fusion event in 25 cells. A similar result was obtained when cells were examined after transient transfection with siRNAs directed to POT1 or when chromosome fusions were evaluated without telomeric FISH. Others also recently reported this frequency of chromosome end fusions for cells with similar or milder POT1 knockdown levels [111,112]. The significance of this phenotype was evaluated by comparing it to partial inhibition of TRF2 using the dominant-negative allele (TRF2ΔBΔM). Expression of this allele of TRF2 increased the frequency of telomere fusions by 10–100-fold, and fusions are observed in 50% of the cells (Figure 3.2 A and B; [76]). Thus, in comparison to partial inhibition of TRF2, the telomere fusion phenotype of POT1 depletion is marginal.

The absence of significant telomere fusions could indicate that normal POT1 levels are not required for this aspect of telomere protection. Alternatively, POT1 could be necessary for both telomere protection and for the processing of telomeres by NHEJ. While counterintuitive, this situation is not unprecedented, as the Ku heterodimer is required for both the protection of chromosome ends and their fusion by NHEJ [Bailey et al., 1999, Proc Natl Acad Sci U S A, 96, 14899-904.,119]. As a consequence, Ku-deficient cells have a very low number of telomere fusions even when TRF2 is absent [119]. In order to test whether this scenario pertains to POT1, we asked whether POT1 shRNA lowered the frequency of telomere fusions in cells expressing TRF2ΔBΔM, the dominant-negative allele of TRF2. The results showed that POT1 depletion does not inhibit telomere fusions in this context (Figure 3.2B). On the contrary, POT1 depletion slightly increased the incidence of telomere fusions after TRF2 inhibition. The significance of this increase remains to be determined.

A

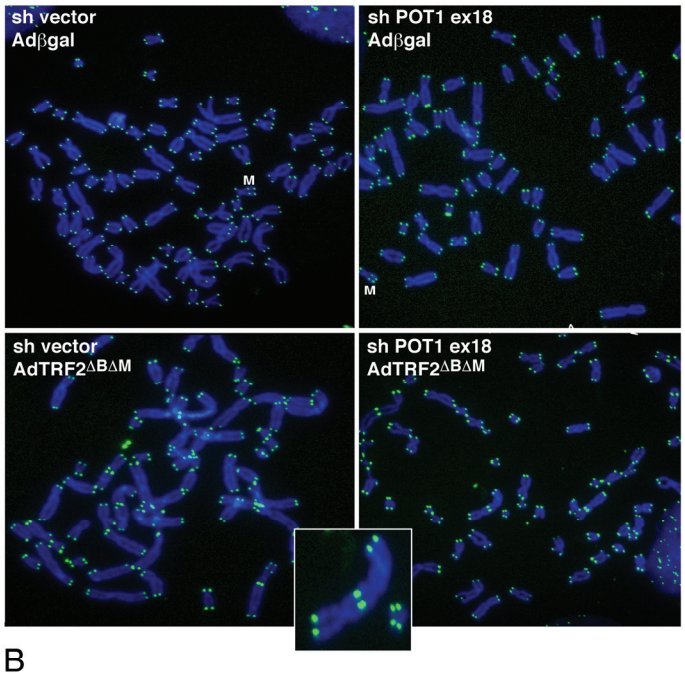

B

Cell line and viruses	number of metaphases	% metaphases with fusions	fusions per metaphase	fusions per chromosome
HTC75				
vector	75	1.3	0.013	0.0003
ex18	75	2.7	0.027	0.0006
HeLa				
vector	50	2.0	0.020	0.0003
ex18	155	3.2	0.032	0.0005
vector + AdTRF2$^{\Delta B\Delta M}$	16	50	3.6	0.07
ex18 + AdTRF2$^{\Delta B\Delta M}$	16	70	7.1	0.10
ex8a + AdTRF2$^{\Delta B\Delta M}$	16	68	6.1	0.11

Figure 3.2 POT1 depletion does not induce significant levels of chromosome end fusions

(A) Metaphase spreads of the indicated HeLa cells with telomeric DNA detected by FISH (green). HeLa cells stably expressing the indicated shRNAs were infected with adenovirus expressing the TRF2 dominant-negative allele (AdTRF2ΔBΔM) or a control adenovirus (Adβgal), and processed for chromosome analysis after 2 days. M indicates a marker chromosome with internal TTAGGG repeats. The inset shows an enlarged image of one chromosome-type fusion from the AdTRF2ΔBΔM/POT1 shRNA panel. (B) Summary of the frequency of chromosome fusions in HeLa cells and HCT75 cells stably expressing POT1 shRNA and treated with the AdTRF2ΔBΔM adenovirus to inhibit TRF2. Chromosomes were analyzed 2 days after introduction of AdTRF2ΔBΔM and 15 days after knockdown of POT1.

As a second index for telomere dysfunction, we analyzed the formation of TIFs in POT1 knockdown cells. Cells treated with shRNA to POT1 ex18 had significant levels of TIFs, as shown by the colocalization of 53BP1 and γ-H2AX with TRF1 (Figure 3.3). In asynchronous populations of BJ fibroblasts and HeLa cells, up to 40% of the cells had more than 10 TIFs and, in these TIF-positive cells, the majority of the TRF1 signals coincided with 53BP1 (Figure 3.3B and C). Telomerase expression did not affect this phenotype (Figure 3.3C; Wilcoxon test on the distribution of TIF frequencies in BJ and BJ/hTERT cells indicated that the difference is not statistically significant, P=0.3). Synchronization of HeLa cells by double-thymidine block (Figure 3.3D and E) or elutriation showed that TIFs were particularly prominent in G1, but rare or undetectable in S and G2 cells. POT1 knockdown resulted in TIF formation in ATM deficient cells and ATR deficient Seckel cells suggesting that redundancies in the pathways the sense telomeres after POT1 deprotection.

In order to verify that this cell cycle dependent occurrence of TIFs is not due to a cell cycle variation in POT1 knockdown, we analyzed residual POT1 levels in POT1 knockdown cells. ChIP analysis and immunoblotting in different stages of the cell cycle separated by elutriation showed that the residual levels of POT1 were the same in G1, S, and G2/M (Figure 3.4). Therefore, the transient telomere damage response indicated that normal POT1 levels were required to repress a DNA damage signal at telomeres in G1, but not in S and G2. This phenotype is different from that of TRF2 inhibition, as conditional deletion of mouse TRF2 generates TIFs in all interphase cells [80] and expression of a dominant-negative allele of TRF2 in HeLa cells can generate TIFs in S and G2 phase [109].

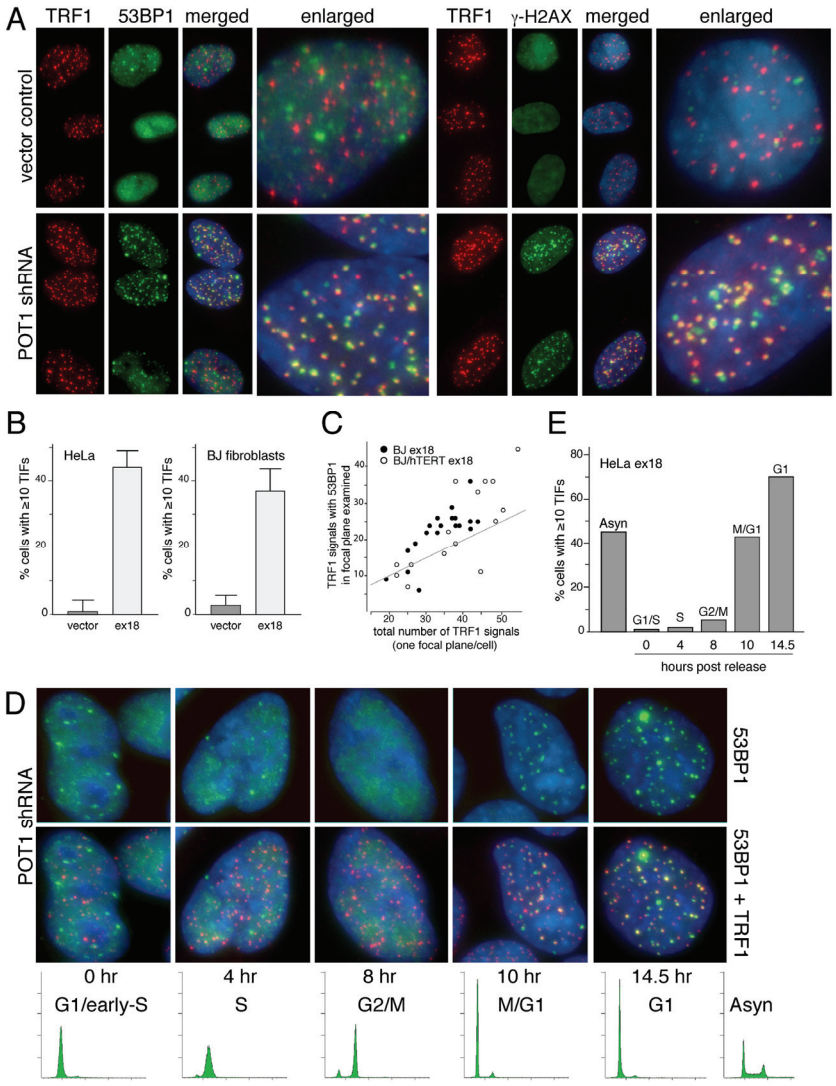

Figure 3.3 Transient telomere damage response upon POT1 depletion

(A) TIFs induced by POT1 shRNA ex18. BJ/hTERT cells were processed for TIF analysis 8 days after infection and selection of the ex18 vector or the vector control by IF for TRF1 (red) and 53BP1 (green) or γ-H2AX (green). Merged images are shown with DAPI. (B) Quantification of the induction of TIFs by POT1 ex18 shRNA. IF for TRF1 and 53BP1 (see (A)) was used and randomly selected groups of cells were evaluated for the number of TRF1 signals per cell that contained a 53BP1 signal. The bars show the percentage of cells containing 10 or more TIFs. (C) The majority of the telomeres in TIF-positive cells colocalize with 53BP1. TIF positive BJ and BJ/hTERT cells were selected and imaged using deconvolution software. Each point in the graph represents one TIF positive cell and shows the number of TRF1 signals plotted versus the number of TRF1 signals containing 53BP1. Points above the line represent cells in which more than 50% of the TRF1 signals contained 53BP1. (D) Transient TIFs in G1. HeLa cells expressing POT1 shRNA ex18 or vector control were released from double-thymidine block and processed for IF at the indicated time points. FACS profiles are shown below the IF images. Top: 53BP1 signal (green) merged with DAPI (blue). Bottom: 53BP1, TRF1 (red), and DAPI signals merged. (E) Quantification of cell cycle dependence of TIF-positive cells. Quantification as in (B), using the cells shown in (D).

ChIP analysis also revealed that the amount of telomere associated Mre11 protein was increased throughout the cell cycle in cells that were depleted for POT1 compared to control cells (Figure 3.4). In contrast, ChIP analysis of other DNA-damage proteins like 53BP1 failed to precipitate detectable amounts of telomeric DNA (Figure 3.4). Mre11 has a dual role in telomere biology, it binds to functional telomeres through its interaction with TRF2 [92], and also localizes to dysfunctional telomere after telomere deprotection [109]. Therefore, enhanced Mre11 association with telomeres after POT1 knockdown is of potential interest.

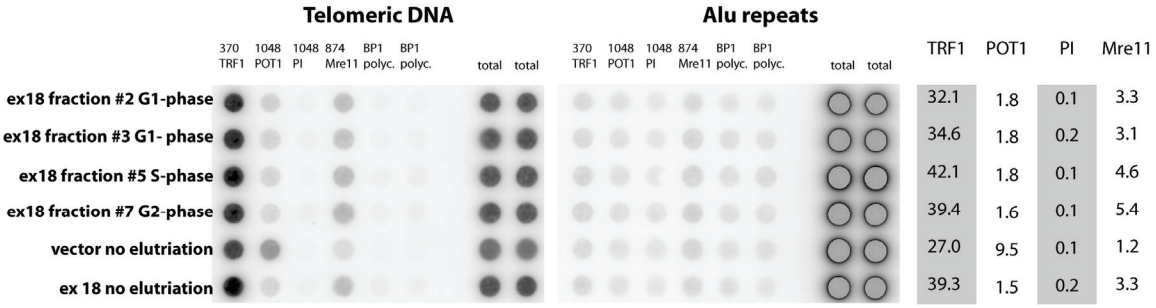

Figure 3.4 Lack of cell cycle variation of POT1 knockdown

ChIP with the indicated antibodies using HeLa cells at different stages of the cell cycle separated by elutriation after POT1 knockdown or asynchronous vector control cells. DNA in the IPs was dot-blotted and hybridized with a probe for telomeric DNA (from pSP73.Sty11) or Alu repeats. Total DNAs and precipitated telomeric DNA (TTAGGGn) samples were blotted in parallel. Antibodies are indicated above each row. PI is pre-immuno sera from the rabbit that generated serum 1048. The table to the right indicated % of telomeric DNA recovered in the IP compared to total telomeric DNA. The FACS analysis of POT1 knockdown cells after elutriation is shown in Figure 3.7 C.

Impaired proliferation of primary, but not transformed, cells

Despite the occurrence of frequent TIFs in G1, HeLa cells did not show significant growth defects after knockdown of POT1 (Figure 3.5A). Consistent with their

unimpaired proliferation, synchronized cells did not reveal an obvious delay in the cell cycle, and the FACS profile of POT1 shRNA cells was indistinguishable for vector control cells (Figure 3.5B). We considered that the lack of a cell cycle arrest might be due to selection of a subpopulation of cells that can tolerate low POT1 levels. To address this, we examined the proliferation of HeLa cells treated with siRNA, allowing the detection of immediate effects occurring in the first few days after POT1 depletion. Also, in this setting, the HeLa cells treated with POT1 siRNA behaved identically to cells treated with a control (luciferase) siRNA (Figure 3.5C; see for Western analysis Figure 2.1). Furthermore, no growth defect was observed in HTC75 and HCT116 cells. We conclude that the depletion of POT1 does not significantly affect the proliferation of these tumor cell lines, despite the presence of telomere damage detectable by the TIF assay. In contrast to tumor cell lines, primary human fibroblasts responded to POT1 depletion with strongly reduced proliferation and induction of a senescent phenotype in a subset of the cells (Figure 3.5D and E). This phenotype was largely rescued by overexpression of a POT1 cDNA with a silent mutation in the shRNA ex18 target site (Figure 3.5E), arguing that it is due to lack of full-length POT1 rather than reflecting a function of POT1–55. Induction of senescence was also observed for BJ fibroblasts and telomerase-positive BJ/hTERT cells, indicating that telomerase status does not determine how cells respond to POT1 depletion. In contrast, abrogation of the p53 and p16/Rb pathways with SV40 large T improved the proliferation of cells with diminished POT1 levels (Figure 3.5F). However, SV40LT-expressing cells still had a slightly diminished growth rate when POT1 was inhibited (Figure 3.5F).

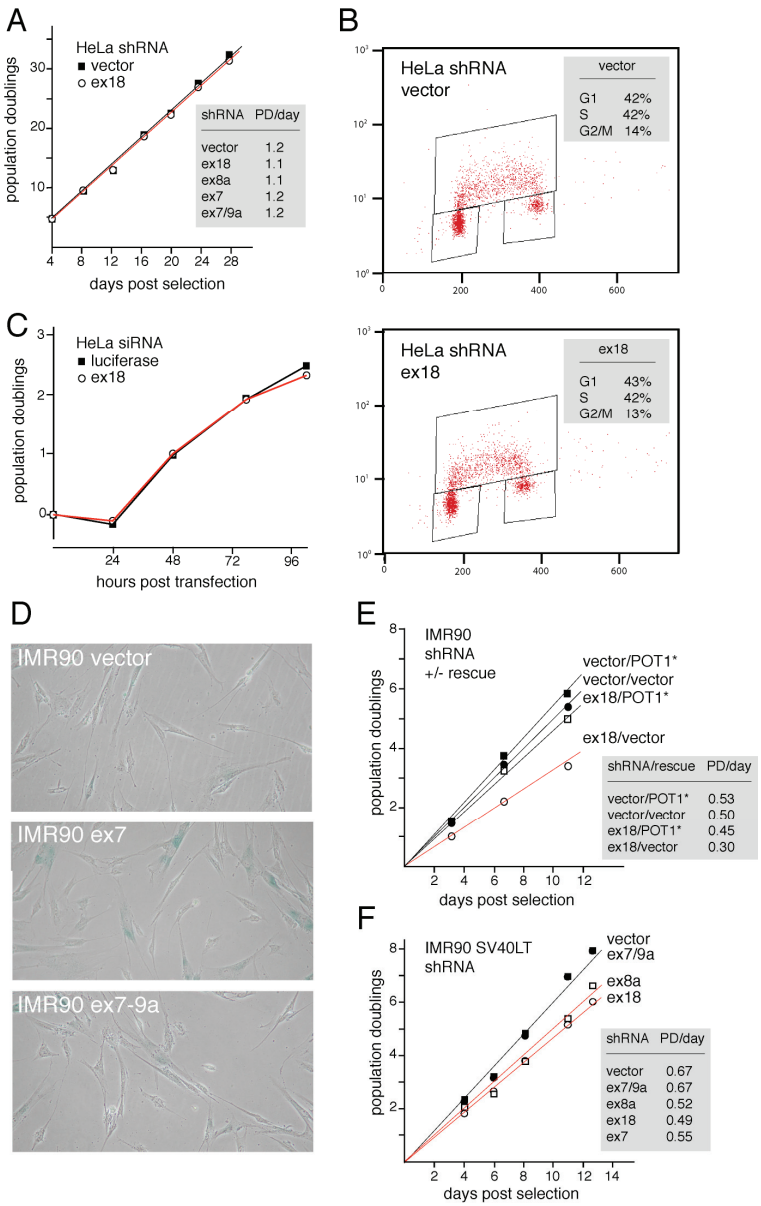

Figure 3.5 Differential effect of POT1 shRNA on proliferation of primary and transformed cells

(A) Graph showing growth curves of HeLa cells with and without POT1 shRNA. The inset shows the growth rate (PD/day) of these and additional HeLa cells with lowered POT1 level. (B) Graph showing proliferation of HeLa cells transfected with POT1 siRNA or control siRNA. (C) FACS profiles of BrdU-labeled HeLa cells infected with the indicated shRNA viruses. Insets show the % cells in G1, S, and G2/M. (D) Phase-contrast microscopic images of IMR90 cells 7 days after infection and selection with the indicated shRNA viruses stained for SA-β-galactosidase activity (Dimri et al, 1995) for 10 h. (E) Graph showing the effect of POT1 shRNA ex18 on the proliferation of IMR90 cells. The inset shows the growth rates (PD/day) in cells infected with the indicated shRNAs and a vector expressing a POT1 cDNA resistant to ex18 shRNA (POT1*). (F) Graph showing the effect of POT1 shRNAs on IMR90 cells transformed by introduction of SV40 large T antigen (pBabeNeoLT). The inset lists the growth rate of the cells.

Protection of telomeric overhangs by POT1, but not POT1–55

Whereas fission yeast that lack POT1 undergo an immediate loss of all telomeric DNA [93], the duplex part of human telomeres persisted after depletion of POT1 (Figure 3.6). However, a quantitative assay for the amount of ss TTAGGG repeat DNA showed that POT1 inhibition affected the maintenance of the 3' telomeric overhang (Figure 3.6). The ratio of ss to ds TTAGGG repeats of IMR90 telomeres (measured by an in-gel hybridization assay [150]) was reduced by 30–40% within a week after introduction of three different shRNAs (Figure 3.6A and B). Similar reduction of the overhang signal was observed upon POT1 knockdown in BJ and BJ/hTERT cells, showing that the effect is not counteracted by telomerase (Figure 3.6C–H).

The loss of overhang signal was also observed in HeLa and HCT116 tumor cell lines. In these settings, overhang reduction was a stable phenotype that persisted for at least 40 PD (Figure 3.7D). Ex7/9 shRNAs, which did not affect POT1 and only mildly reduced POT1–55, did not alter the ss TTAGGG signal (Figure 3.6C–H). The overhang phenotype could be rescued by coexpression of a version of POT1 resistant to shRNA ex18 (Figure 3.7A-C). Since the rescuing construct did not express POT1–55, POT1 was sufficient to protect the overhangs. Furthermore, one of the shRNAs (ex8a) that resulted in overhang loss did not affect POT1–55 (Figure 3.6A), consistent with the phenotype being due to diminished full-length POT1. Nevertheless, it cannot be excluded that POT1–55 also plays a role in the regulation of telomere overhang formation or overhang protection.

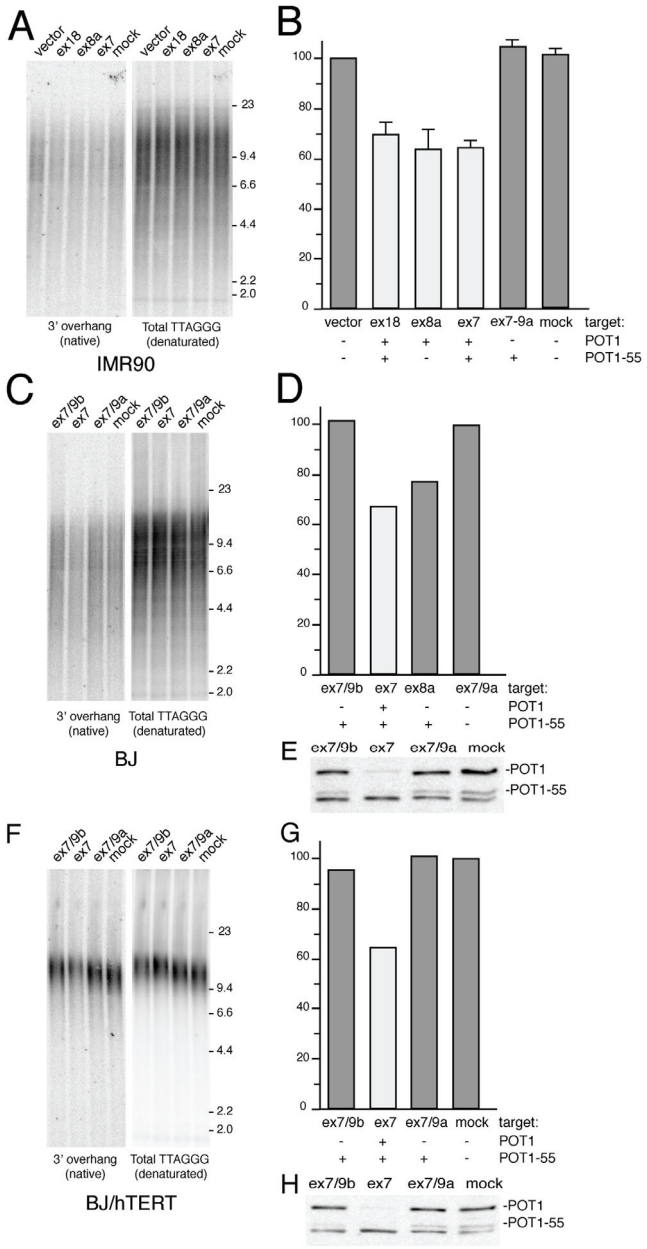

Figure 3.6 POT1 is required for the maintenance of the 3' overhang

(A, C, F) In-gel assay for ss TTAGGG repeats with the indicated cell lines expressing the indicated shRNAs. DNA was isolated 7–10 days post-infection, cut with MboI and AluI and processed by in-gel hybridization to a $(CCCTAA)_4$ probe to detect ss TTAGGG repeats (left panels). The DNA was subsequently denatured in situ and rehybridized to the probe to detect the total TTAGGG repeat signal (right panels). (B, D, G) Bar graphs representing quantified overhang signals. Overhang signals in each lane were normalized to the total TTAGGG signal. The values are expressed relative to the value obtained with mock or vector (B) infected cells. The values in (B) represent averages of three experiments (SDs indicated). Below the bargraph, + and - indicate whether the shRNA targets POT1 and/or POT1–55. (E, H) Immunoblots of POT1 and POT1–55 levels in BJ (E) and BJ/hTERT (H) cells infected with retroviruses expressing the indicated shRNAs.

Telomeres shorten in telomerase deficient human cells due to the end replication problem and due of the nucleolytic degradation of telomeric DNA during overhang generation [8,9,27]. Accordingly, the shortening rate of telomeres is thought to be correlated with overhang length.

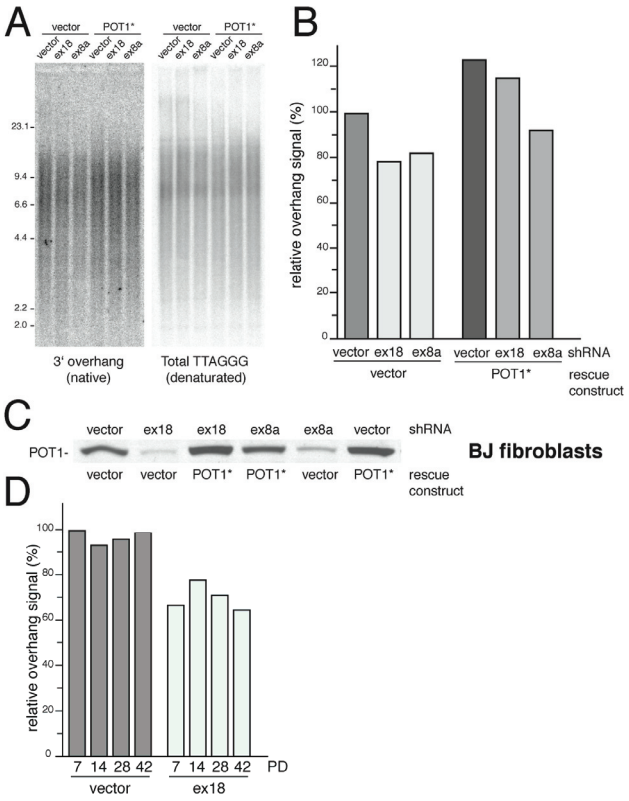

Figure 3.7 Loss of overhang signal can be rescued by expression of full length POT1 and persists during long-term culturing

(A) Autoradiographs of G-strand overhang assay on BJ fibroblast expressing the indicated shRNAs in combination with a version of POT1 (POT1*) that is resistant to shRNA ex18 or the empty retroviral vector. Cells were analyzed at 5 PDs after introduction of the shRNA. (B) Bargraph representing quantified data from (A). (C) Immunoblot of POT1 levels in the cell lines used in (A) using antibody #978. (D) Bargraph of G-strand show the relative overhang signal in long-term cultures of HeLa cells expressing the indicated shRNAs. Methods are described in (A) and (B).

Therefore, we speculated that the reduced overhang length in POT1 knockdown cells could lead to slower telomere shortening rate in telomerase negative cells. In order to test this hypothesis, we determined the telomere shorting rate of telomerase negative SV40 transformed IMR90 cells with reduced POT1 levels. These experiments revealed that telomeres in cells depleted for POT1 shortened slightly slower than telomeres in vector

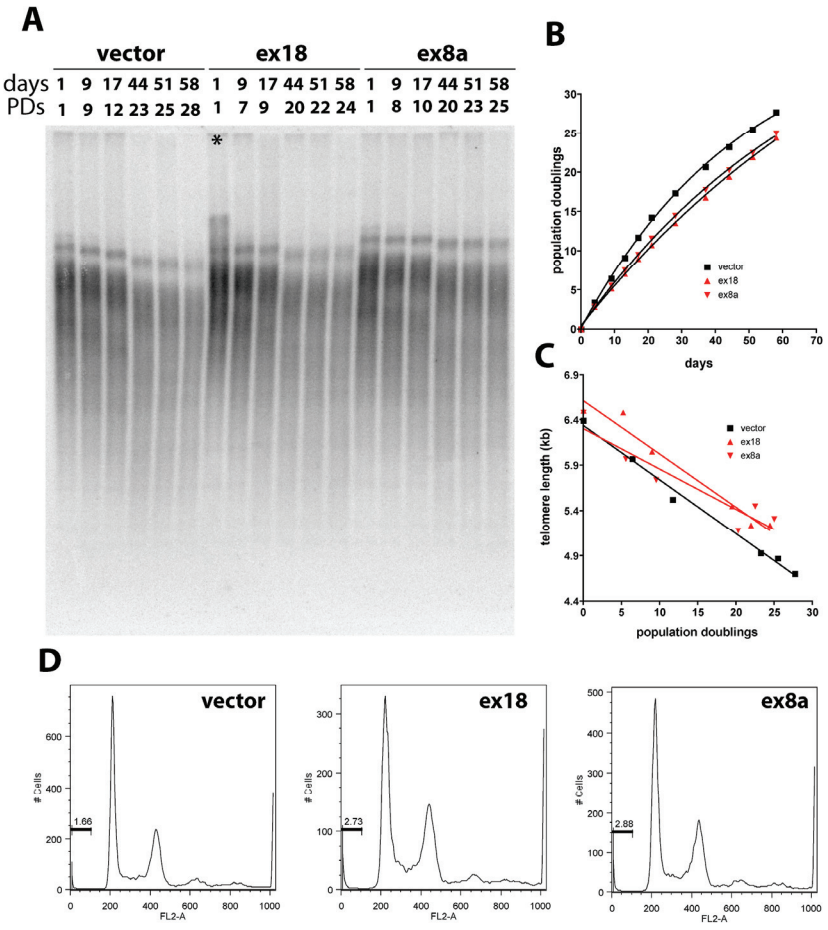

Figure 3.8 Telomere shortening rates in SV40 transformed IMR90 cells after the knockdown of POT1

(A) Autoradiographs of telomere length analysis of IMR90 cells infected with the indicated shRNAs or vector control at the indicated population doublings (PD) and days after selection. The * indicates a lane were the genomic DNA was not completely digested. This data point was therefore excluded from the analysis. (B) Growth curve of cells shown in panel (A). (C) Quantification of telomere shortening shown in panel (A). (D) FACS analysis of cells shown in panel (A) and (B) at PD 30. Numbers to the left of the G1-peak indicate the % of cells with a sub-G1 DNA content, which is indicative of cells undergoing apoptosis.

control cells (Figure 3.8A and C).

However, in the process of this experiment it became apparent that, although SV40 transformation abrogates most of the growth phenotype of primary cells after POT1 knockdown, a slight growth arrest remains (Figure 3.8B). This slight growth disadvantage of cells with reduced POT1 levels results in lower accumulative cell numbers over time (Figure 3.8A). This difference makes the presented result of a slower telomere shortening rate difficult to interpret as the number of cell divisions that POT1 knockdown cells underwent can not be precisely determined. If the lower cumulative cell number of POT1 deficient cells is the result of an increased cell death it is likely that the surviving cells underwent the same amount of cell division as control cell. But, if the lower numbers are caused by a cell cycle delay, without an increase of cell death, cells with POT1 knock down underwent less cell divisions. Although, FACS analysis and frequency of BrdU incorporation does not indicate a cell cycle arrest in these cells (Figure 3.8D), it can not be excluded that over the length of the experiment a minor difference in the cell cycle profile, not detected by this analysis, would be sufficient to lead to this growth difference. Therefore, the presented data is only suggestive and has to be confirmed with a different experimental approach that circumvents the inherent problem of altered proliferation in primary cells after POT1 knockdown.

The observations that SV40 transformed IMR90 cells respond to reduced levels of POT1 with a growth disadvantage, while Hela cells do not, suggests that reduced levels of POT1 affect a p53 and Rb independent pathway. IMR90 cells and Hela cells differ significantly in their chromosome number, while IMR90 cells are diploid, Hela cells are genomically unstable and aneuploid. In cells that are depleted for POT1 using shRNAs

we find a significant increase in extranuclear chromosomes. These exrtranuclear chromosomes, which are most likely the product of chromosome miss-segregation events, become apparent as DAPI staining material of inter phase nuclei staining for four telomeres in telomeric FISH. This increase of chromosome miss-segregation events can explain why SV40 IMR90 respond with diminished growth after POT1 knockdown.

Reduced telomere overhang length is also seen in cells that overexpress a dominant negative from of TRF2 (TRF2ΔBΔM), and it has been shown that this overhang loss is dependent on the XPF nuclease [115]. In order to address if loss of overhang signal after knockdown of POT1 is also mediated by this nuclease, POT1 levels were reduced in XPF deficient cells and overhang length was measured by in-gel-hybridization. While XPF proficient cells show a mild reduction of telomeric overhang after the knockdown of POT1, no significant decrease of overhang length is detectable in XPF deficient cells (Figure 3.9 A and B). This suggests that, similarly to the expression of TRF2ΔBΔM, the telomeric overhang becomes a substrate for the XPF nuclease after POT1 knockdown. It has to be mentioned that XPF deficient cells grow very slowly (doubling time >42 hours) compared to isogenic XPF proficient cells (doubling time ~24 hours). For this reason control cells underwent more cellular divisions than XPF deficient cells after the knock down of POT1. If cell cycle progression is a prerequisite for the induction of overhang loss, the lack of overhang processing in XPF cells could simply be caused by their slow growth. Although this seems unlikely, because the same cells were used to establish the role of XPF after TRF2 dysfunction [115], further experiments will be necessary to establish the involvement of ERCC1/XPF in overhang processing after POT1 loss.

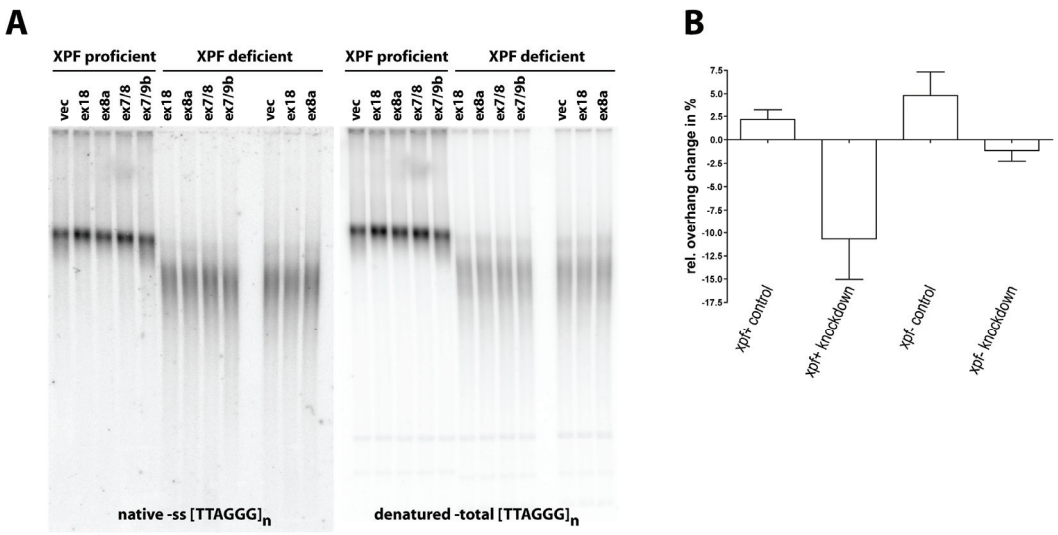

Figure 3.9 Overhang changes after POT1 knockdown in XPF deficient cells

(A) Autoradiographs of G-strand overhang assay on XPF proficient and XPF deficient cells [115]. Cells were analyzed at 10 days after introduction of the shRNA. (B) Bargraph representing quantified data from (A).

POT1 reduction leads to a DNA damage response and the induction of TIFs predominantly in G1 of the cell cycle. In order to determine if changes in overhang length are triggering this cell cycle dependent TIF formation, we monitored overhang length at different stages of the cell cycle. Hela cells depleted for POT1 and cells infected with a vector control were separated by elutriation and their overhang length was determined by in-gel hybridization. As cells were in culture for more than 3 weeks before sufficient cells could be collected to perform the elutriation protocol, the long-term depletion of POT1 resulted as expected in a detectable telomere elongation. Consequently, POT1 knockdown cells contained more double stranded telomeric DNA than control cells. This increase of total telomeric DNA is detectable in the in-gel hybridization under denaturing conditions by the increase of the total signal in each lane (Figure 3.10). Therefore, overhang signals from control cells and POT1 knockdown cells had to be normalized

separately and only relative changes in the overhang profile between POT1 depleted and control cells were compared. This comparison shows that the overhang cell cycle profile of POT1 depleted cells and vector control cells are similar (Figure 3.10). In both cases a slight increase in single stranded telomeric DNA can be detected in cells that are in S-phase, compared to cells that are in G1 and G2 (Figure 3.10). A similar cell cycle profile of overhang length was found in experiments performed by Jeffrey Ye in unperturbed cells (personal communication).

As the in-gel overhang assay determines the amount of single stranded telomeric DNA, it is possible that the increase of single stranded DNA reflects replication intermediates during S-phase rather than longer overhangs. Furthermore, the in-gel

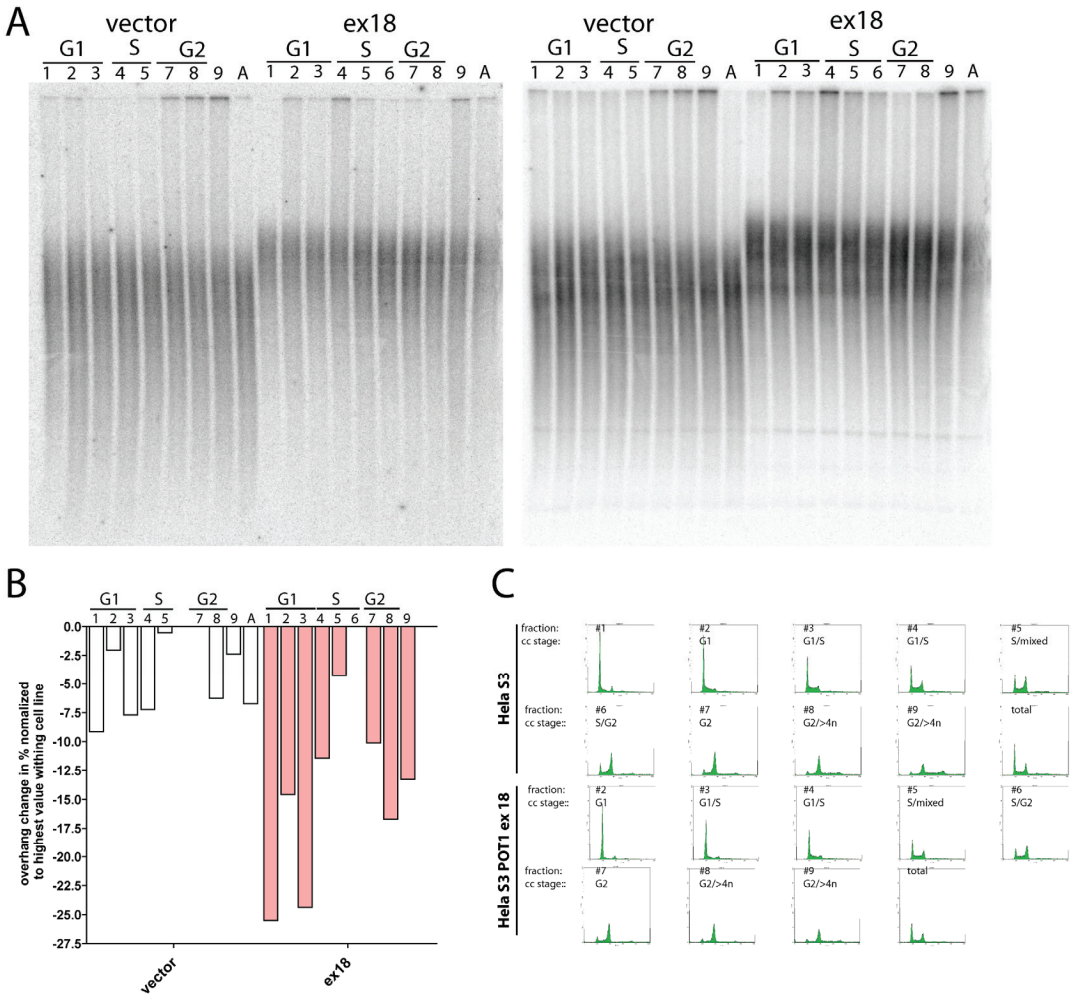

Figure 3.10 Cell cycle variation of single-stranded telomeric DNA after POT1 knockdown

(A) Autoradiographs of G-strand overhang assay on Hela cells infected either with a control vector of sh18 after elutriation. The numbers above the graph indicate the faction collected by elutriation. (B) Bargraph representing quantified data from (A). (C) FACS analysis of the factions collected after elutriation and used for overhang analysis in panel (A).

overhang assay determines the average overhang length of a cell population. Therefore, the assay does not allow the detection of very small overhang length changes (<5%), and does not discriminate for example between leading and lagging strand overhangs. Because of these limitations, the presented results do not rule out that cell cycle

dependent changes of the overhang length or its structure are causing the induction of TIFs. In order to test this possible relationship it will be necessary to develop molecular tools that allow simultaneous analysis of overhang integrity and protective state of individual telomere over the cell cycle.

POT1 determines the last nucleotide of human chromosomes

The 5' end of human chromosomes is remarkably specific, ending more than 80% of the time with the sequence ATC-5' [28]. To test whether POT1 is required to define this precise ending, we used the recently developed ligation-mediated PCR assay. In this assay, oligonucleotides (5' telorettes) representing the six different phases within the 3'-AATCCC-5' telomeric repeat sequence are ligated to the 5' end of the chromosome, using the telomeric overhang as an annealing platform (Figure 3.11A). The product is amplified with two nontelomeric primers, one that anneals to a sequence common to the 5' telorettes and the other that anneals to a subtelomeric site in the pseudo-autosomal region of the X and Y chromosomes. Prior to amplification, the DNA is diluted to the point where individual molecules are amplified to give discrete bands, so that the number of bands is proportional to the number of ligated telomeres. This assay previously established that both ends (the lagging and the leading end) of each human chromosome have the same 5' terminal sequence and that this sequence is not influenced by telomerase activity [28]. The 5' telorette assay showed the expected predominance of the sequence ATC-5' in vector control HeLa cells (Figure 3.11B). Depletion of POT1 with two different shRNAs had a striking effect, leading to nearly random ends representing

all six possible terminal nt (Figure 3.11C and D). Similarly, BJ cells lost their prevalence for ATC-5’ ends upon

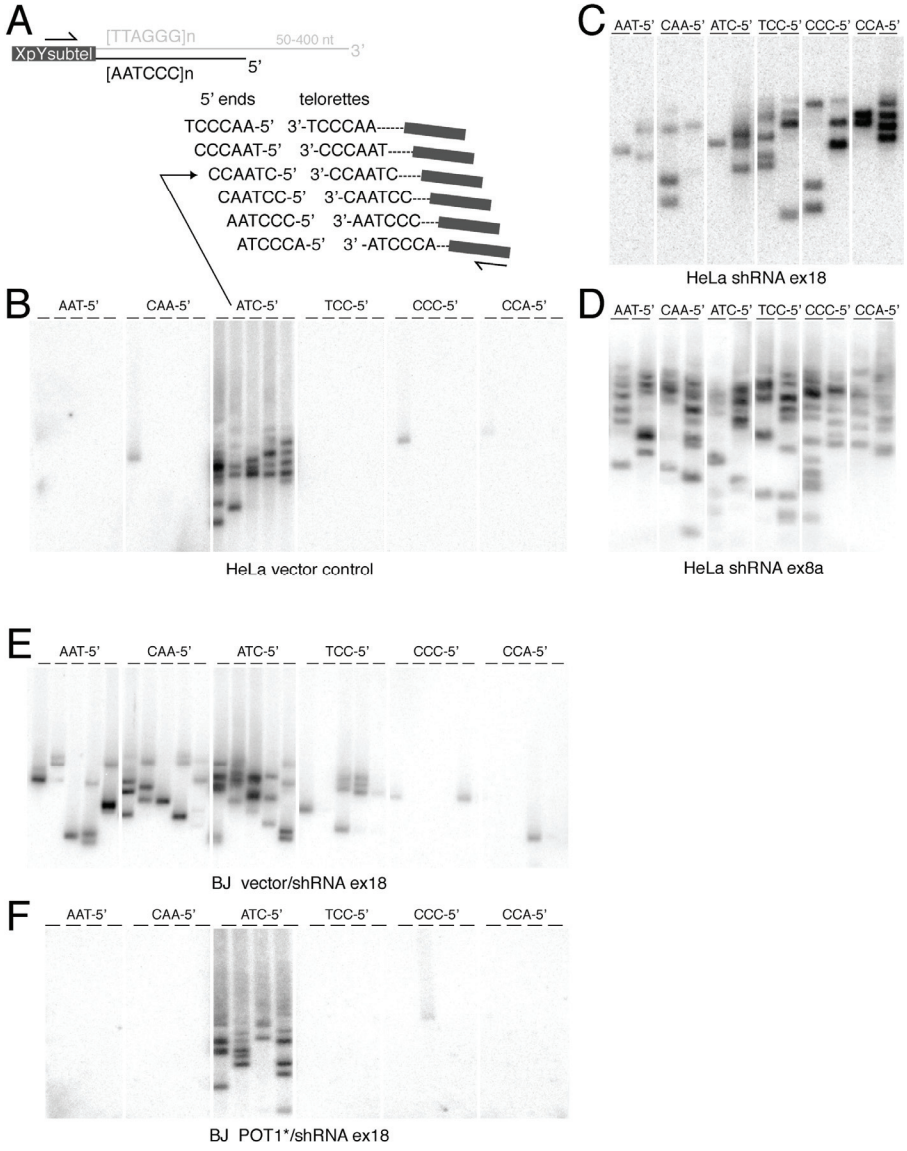

Figure 3.11 POT1 determines the sequence at the 5’ end of human chromosomes

(A) Schematic of the ends of human chromosomes and the 5’ telorette assay. The six telorettes and the 5’ ends to which they can ligate are shown. PCR primers used for amplification are shown schematically. (B–F) Products of the 50 telorette assay using the indicated cell lines. Each telorette was used for 2–5 independent assays and the products were run in separate lanes. The sequences of the 5’ end detected with each telorette is shown above the groups of lanes. POT1* is a vector expressing full-length POT1 mutated to create resistance to the ex18 target site. The MWs of the detected products range from 1 to 8 kb. The assays were performed by Agnel Sfeir.

knockdown of POT1 (Figure 3.11E). BJ fibroblasts showed some residual predominance of ATC-5' ends, most likely because they were analyzed within a week after POT1 depletion. A POT1 cDNA mutated to create resistance to the shRNA reverted the structure of the 5' end to its normal ATC-5' setting (Figure 3.11F), indicating that POT1 alone, in the absence of POT1–55, is sufficient to restore the 5' end sequence. We conclude that POT1 is required for the precise determination of the sequence at the 5' ends of human chromosomes.

Discussion

As anticipated from the function of fungal POT1-like proteins, human POT1 is required for telomere integrity. RNAi to human POT1 leads to an aberrant structure of the telomere terminus and the induction of TIFs. Unexpectedly, POT1 inhibition did not result in telomere fusions and cells with prominent TIFs continued to proliferate unimpeded. When TRF2 is inhibited, telomeres not only have altered telomere termini and TIFs, but also undergo fusions in G1 and G2 and induce cell cycle arrest. Therefore, the deprotected telomeres resulting from POT1 inhibition are distinct from those lacking sufficient TRF2. The difference is not due to fewer telomeres being affected by POT1 RNAi, because the structural and functional defects occurred at many more telomeres; yet, cells proliferated normally and chromosome ends remained protected from the NHEJ pathway. We conclude therefore that telomeres can escape NHEJ despite having an aberrant structure that elicits the DNA damage response. In addition, the POT1 RNAi data indicate that TIFs are not necessarily harbingers of impending cell cycle arrest. The analysis of synchronized cells showed that these TIFs are present every time a cell exits mitosis. This is a stable phenotype in HeLa cells, arguing against the detrimental effects of TIFs on cell proliferation, and there is no indication that the TIFs induce a cell cycle arrest in G1. One possibility is that the type of telomere damage induced by lowered POT1 levels is repaired in G1 before a cell cycle arrest is induced. Unraveling these distinct aspects of telomere protection illuminated by inhibition of TRF2 and POT1 is pertinent to the question of how telomere attrition induces senescence in primary human cells. Although the reduced presence of TRF2 on short telomeres can explain many aspects of critically shortened telomeres, concomitant reduction in POT1 may well

contribute to the behavior of cells as they approach the end of their replicative lifespan. In this regard, the partial inhibition of POT1 achieved with RNAi may be more informative than the null phenotype.

Definition of the 5'- end

Our data show that normal POT1 levels determine the ultimate 5'-end of human chromosomes. When POT1 is diminished, the 5'-ends terminate at all positions in the 3'-AATCCC-5' repeat strand; when POT1 is fully functional, human chromosomes end with ATC-5'. How does POT1 set the end? Two general models can be envisaged. In one, POT1 recruits a nuclease that specifically cleaves the C-strand at the 3'-AATC^CC-5' position. Nuclease trimming of the C-strand has been invoked to explain the formation of 3' overhangs and the high shortening rate of human telomeres [27]. Perhaps the diminished recruitment of a C-strand nuclease in cells with diminished POT1 results in incomplete processing of telomeres that have just been replicated. This could explain both the lack of specific C-strand ends and the diminished amount of ss TTAGGG repeats seen upon POT1 shRNA. In a variation of this model, POT1 does not recruit the nuclease, but stimulates it. POT1 could act similarly to another OB-fold ss DNA-binding protein, RPA, which directs the nuclease ERCC1/XPF in NER [151]. A second possibility is that POT1 protects the sequence ATC-5', but not other ends, from nucleolytic attack. In this model, the nuclease that generates telomeric overhangs need not be specific for the sequence ATC-5' and degradation would continue until an end is generated that POT1 can protect. The ATC end is very close to the first POT1 recognition site (5'-(T)TAGGGTTAG-3') in the 3' overhang, perhaps allowing protection. The tethering of

POT1 to the TRF1(2)/ TIN2/TPP1 complex, lodged on its nearby duplex 5'-YTAGGGTTR-3' half-sites [74], could also contribute to the protection of the 5' end. Biochemical and structural studies may be able to clarify these issues. The idea that human POT1 acts to protect the end from further nuclease attack is attractive because budding yeast Cdc13, a telomeric protein of substantially similar structure, protects the C-rich strand of yeast telomeres from degradation [148]. Furthermore, in pot1- fission yeast, all telomeric DNA, including the C-rich strand, disappears rapidly [93]. Although human cells treated with POT1 shRNA does not show a similar dramatic loss of the C-rich strand, it will be interesting to determine whether more extensive degradation of the C-rich strand will take place in POT1 null cells.

A transient postmitotic telomere damage signal

Cells with diminished POT1 accumulate γ-H2AX and 53BP1 at telomeres, indicating the activation of a DNA damage response at natural chromosome ends. This response was observed in cells entering G1 and had disappeared by the time cells entered S phase. The transient nature of this signal might explain why cells do not arrest upon induction of this form of telomere damage. Why does the telomere damage signal disappear? We favor the possibility that the DNA damage signal is extinguished by a process that restores the protected state of telomeres. One possibility is that POT1 is normally required to re-establish the fully protected state during or after mitosis and that the process is delayed or slow when POT1 levels are low. It is tempting to link the transient DNA damage response to the defect in the structure of the telomere termini. If POT1 generates the correct 3' overhang by recruiting or activating a specific nuclease that leaves ATC-5' ends, a DNA damage response could ensue as long as the termini have insufficient or no

3’ overhang. Early in G1, other nucleases, possibly stimulated by the DNA damage response, may also be able to generate a 3’ overhang ensuring telomere protection. These nucleases would leave the telomeres with a 3’ overhang of different length and with 5’ ends with an altered sequence. This process may be slow, inaccurate, and unregulated, but eventually could extinguish the telomere damage signal, allowing cells to progress into S phase.

4. Recent expansion of the telomeric complex in rodents: Two distinct POT1 proteins protect mouse telomeres

Introduction

Specific knock down of human POT1 using RNAi techniques revealed that POT1 functions in telomere protection and telomere length regulation. However, as these experiments involved a partial (<10-fold) reduction of POT1, the consequences of complete loss of function remained to be determined. To study the complete loss of function of POT1, we used targeted deletion in mouse cells. Mouse knockouts proved previously to be an invaluable approach to understanding the function of telomerase and shelterin components [67,80,87,119,145]. All shelterin components have been identified in mouse cells and generally share high sequence similarity with their human homologues. Embryonic lethality of conventional gene knockout mice for TRF1, TIN2 and RAP1 indicated the essential role of these shelterin components for cellular viability [80,86,87,152]. Later, Cre-mediated conditional gene disruption of TRF2 provided a molecular tool to study the consequences of shelterin dysfunction [80]. Furthermore, crosses between the TRF2 knockout mice and mice deficient for components of the NHEJ machinery confirmed previous findings on TRF2 in human cells [80,119]. This body of work indicates that mouse cells are a legitimate system to study the role of POT1 in telomere biology. Nevertheless, significant differences in telomere biology exist between mouse and human cells. Not only are mouse telomeres longer than human telomeres [25], mouse cells also constitutively express telomerase [153] while human somatic cells have no significant telomerase activity. Mouse and human cells also respond differently to can be found in

their response to telomere dysfunction [154,155]. Mouse cells arrest after telomere dysfunction predominantly through the activation of p53, while in human cells the inactivation of both p16 and p53 are necessary to suppress cellular arrest. Together, these differences between mouse and human cells can explain why cellular senescence in mouse and human cells results from different cellular events. Under optimal growth conditions human primary fibroblast enter replicative senescence as a consequence of progressive telomere shortening[19]. In contrast, mouse fibroblasts taken into culture enter senescence earlier through a process called "culture shock". Culture shock results in the activation of p53 by ambient oxygen levels and is independent of telomere length (reviewed in)[156].

An additional difference in the organization of human and mouse telomeres became apparent when we found that mouse telomeres contain two POT1 paralogs, POT1a and POT1b, while only one POT1 gene exists in the human genome. We addressed the function of POT1a and POT1b individually, using conditional gene deletion. To address the phenotypes of the complete loss of POT1 we generated POT1a/POT1b double deficient cells. The result presented in this section were in part published [157].

Results

Two Distinct POT1 Proteins at Mouse Telomeres

The human genome contains only one gene with significant homology to the ciliate telomere terminus proteins [93], and a single POT1 gene is present in the primate, dog, and cow genomes (Figures 4.1 B, and Figure 4.2). In contrast, we identified two POT1 orthologs (POT1a and POT1b) in the mouse and rat genomes (Figures 4.1A and B). Mouse POT1a and POT1b show 71%–75% amino acid identity to human POT1 and to each other (Figures 4.1C and D). The mouse POT1a locus on chromosome 6 is syntenic with the human POT1 locus on chromosome 7; POT1b is located on mouse chromosome 17. The most likely origin of the two rodent POT1 genes is a recent gene duplication (Figure 4.1).

Both POT1 mRNAs are represented in the EST databases (POT1a: AK036052; POT1b: XM_355022) and appeared ubiquitously expressed based on RT-PCR analysis (Figure 4.3A). The embryonic expression pattern of POT1a was examined using mice derived from a gene-trap ES cell line containing a β-galactosidase-neo (GEO) fusion gene inserted after the 8th coding exon in the POT1a locus (POT1a^{8GEO}; Figure 4.3C). Heterozygous POT1a$^{8GEO/+}$ E13.5 embryos had β-galactosidase activity in the developing tissues (Figure 4.3B), indicating (near) ubiquitous expression during embryonic development.

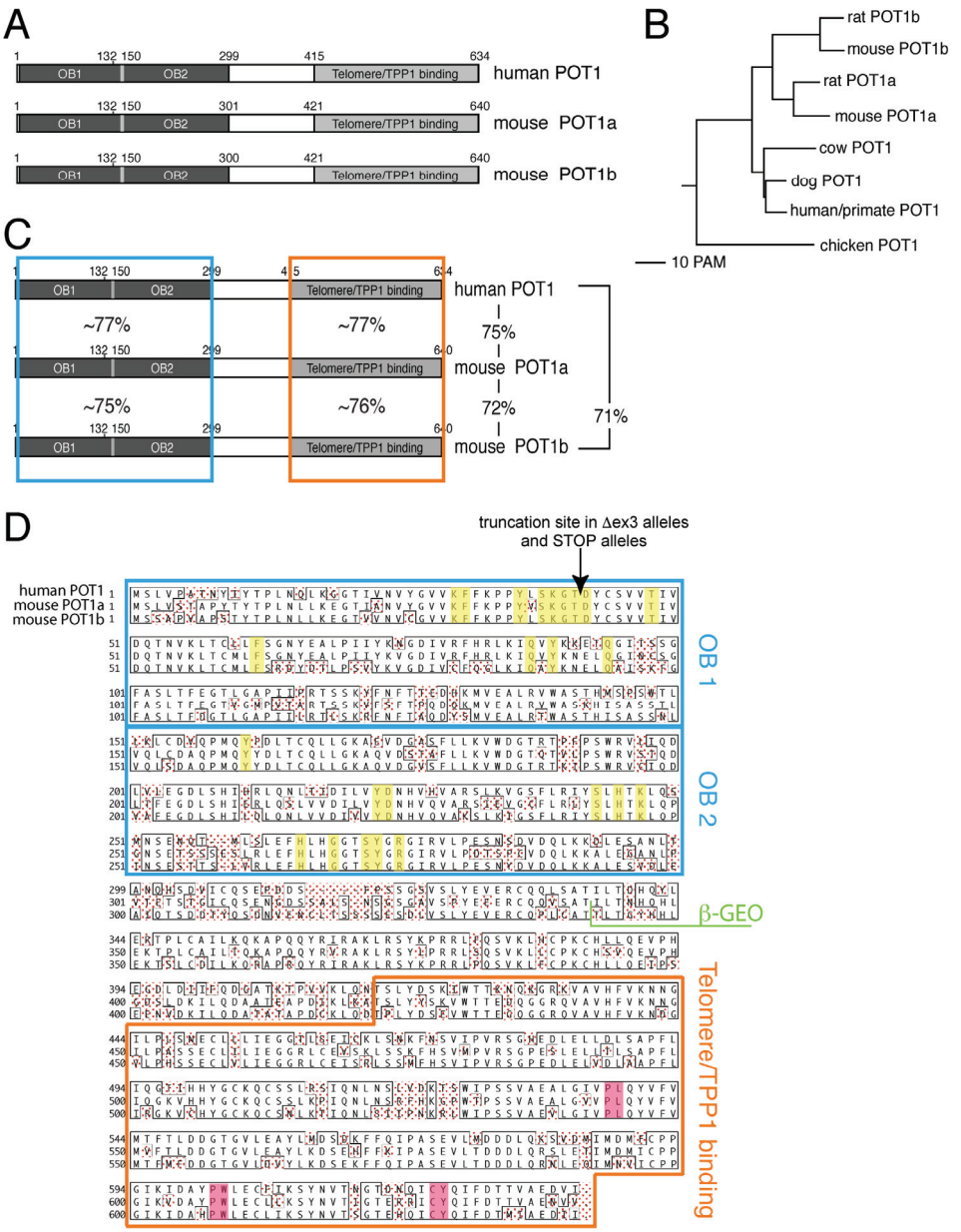

Figure 4.1 Two POT1 proteins in the mouse

(A) Schematic of the human and mouse POT1 proteins, dark fill: OB-folds, light fill: TPP1 interacting domain. (B) Phylogenetic tree of vertebrate POT1 proteins based on the sequences given in Figure 4.2 using the Multalin website and default settings (http://prodes.toulouse.inra.fr/multalin/).

(C) Alignment of mouse POT1a and POT1b with human POT1 showing sequence identifies in functional domains and landmarks relevant to the altered mouse alleles. Identical amino acids are boxed black. Inferred OB-folds are boxed blue and the putative TPP1 interaction domains are boxed in yellow. Amino acids known from the crystal structure of human POT1 essential for DNA binding [94] are shaded yellow and amino acids known in human POT1 to be essential for the interaction with TPP1 [55,98,99,111,112,147] are shaded red. Indicated are the truncation sites in POT1a and POT1b STOP alleles, POT1a and POT1b Δex3 alleles and the truncation site of POT1a in the POT1a^{8GEO} allele.

(D) Schematic overview of sequence similarity between hPOT1, POT1a and POT1b. Boxes as in (C).

Figure 4.2 Comparison of POT1 proteins

(A) Alignments of the POT1 proteins of Mus musculus (mouse), Rattus norvegicus (rat), Homo sapiens (human), Pan troglodytes (chimpanzee), Canis familiaris (dog, boxer), Gallus gallus (chicken), and Bos taurus (cow). For part of the sequences (dog POT1, rat POT1b, and cow POT1) no EST information was available. These POT1 sequences were derived from BLAST searches of genomic DNA and spliced together based on identification of exon-intron boundaries using the human POT1 sequence as a guide. Alignments were generated by CLUSTALW using the Multialin website (http://prodes.toulouse.inra.fr/multalin/) and default setting for all parameters. Identical amino acids in red; similar amino acids in blue.

Both POT1 proteins were detectable in immunoblots of extracts from mouse embryo fibroblasts (MEFs), ES cells, and NIH3T3 cells (Figure 4.4A). Two anti-sera raised against POT1a peptides detected a protein of 70 kDa apparent MW whose abundance was significantly reduced by shRNAs specific to POT1a. Similarly, two anti-

sera raised to POT1b peptides reacted with a protein of 75 kDa apparent MW, that was identified as POT1b based on shRNA knockdown. Immunoblots and immunoprecipitation experiments indicated that the POT1a and POT1b antibodies were specific to the respective POT1 proteins (Figure 4.4A). Semiquantitative immunoblotting experiments using recombinant proteins as a standard suggested that POT1a and POT1b are expressed at similar levels (Figure 4.4 B).

Indirect immunofluorescence (IF) for POT1a and POT1b revealed the punctuate nuclear pattern typical of telomeres and many of the POT1 sites coincided with TRF1

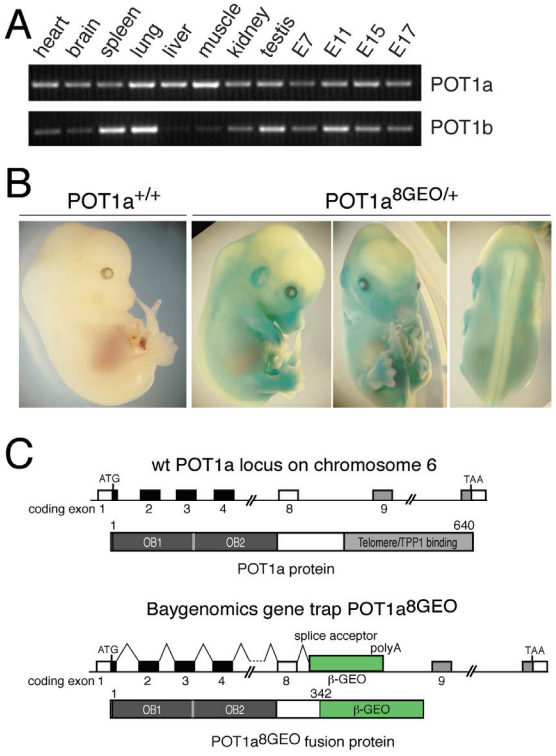

Figure 4.3 Expression analysis of POT1a and POT1b

(A) Expression of POT1a and POT1b mRNAs in the indicated tissues and embryonic stages determined by RT-PCR. (B) β-galactosidase staining of E13.5 embryos. (C) Schematic representation of the POT1a^{8GEO} allele. Shown are the wt POT1a locus on chromosome 6 and a schematic of the wt POT1a protein. Below the POT1a locus of Baygenomics clone RRA096 is shown and a schematic overview of the truncated POT1a^{8GEO} protein.

signals (Figure 4.4B). Telomeric localization was also observed for MYC-tagged POT1a and POT1b (Figure 4.4C). Furthermore, chromatin immunoprecipitation (ChIP) with POT1a and POT1b antibodies recovered approximately the same amount of telomeric DNA but no chromosome-internal sequences, confirming that both proteins are specifically associated with telomeres (Figure 4.6). RNAi-mediated partial (70%) depletion of POT1a or POT1b demonstrated the specificity of the antibodies used in these experiments (Figures 4.6A and B).

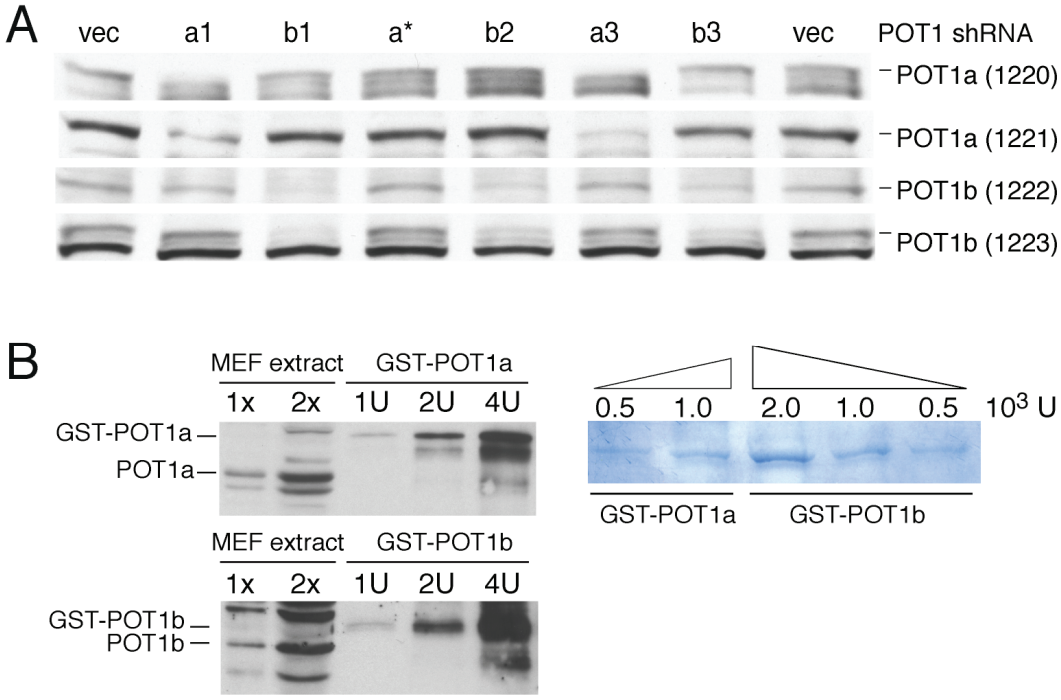

Figure 4.4 POT1a and POT1b protein levels in mouse fibroblasts

(A) Immunoblots for POT1a and POT1b on extracts from NIH3T3 cells with shRNAs to POT1a (a1 or a3) or POT1b (b1-3). vec: vector control; a*: ineffective POT1a shRNA. (B) Quantitative analysis of expression levels of POT1a and POT1b. POT1a and POT1b signals obtained in MEF extract were compared to signals obtained with identical amounts of recombinant GST-POT1a and GST-POT1b fusion protein. Loading of equal amounts ("units") for the two GST fusion proteins was based on Coomassie staining as shown on the right. The experiment in (A) was performed by Jan-Peter Daniels.

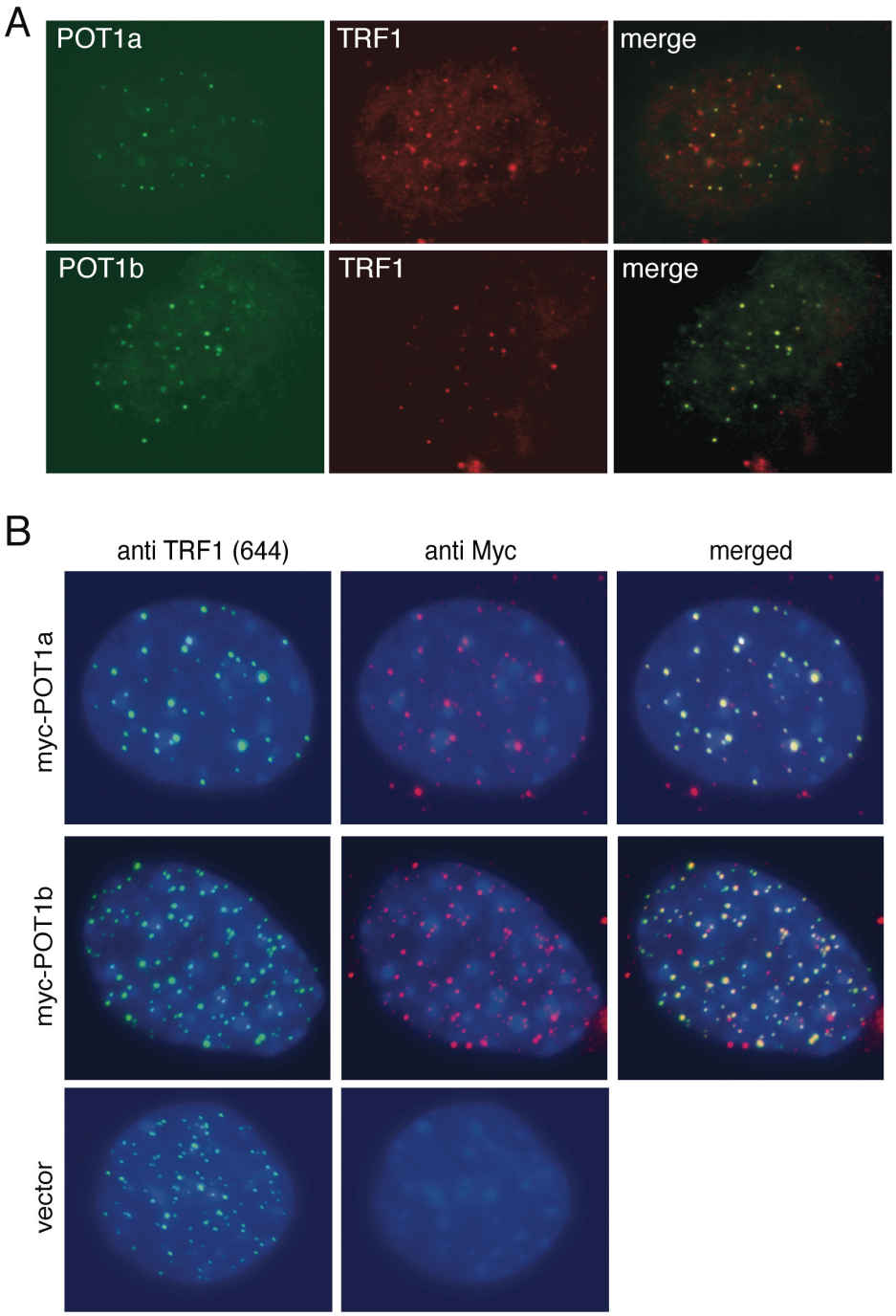

Figure 4.5 Telomere localization of POT1a and POT1b

(A) IF for POT1a and –b in NIH 3T3 cells. IF with mouse anti-POT1a and POT1b sera (green) and rabbit anti-TRF1 (644) (red). (B) MYC IF showing telomeric localization for overexpressed MYC-POT1a and MYC-POT1b. MEFs were infected with the indicated retroviruses and processed for IF (MYC, red) and TRF1 (green).

Lack of POT1a Results in Embryonic Lethality, whereas POT1b$^{STOP/STOP}$ Mice Are Viable and Fertile

Whereas ES cells and mice heterozygous for the genetrap allele POT1a^{8GEO} had no apparent phenotype, intercrosses of POT1a$^{8GEO/+}$ mice failed to yield homozygous offspring (Figure 4.10B). POT1a$^{8GEO/8GEO}$ blastocysts failed to yield ES cells and cultured E1.5–E3.5 embryos did not form an inner cell mass and died around E6.5 (Figure 4.7). According to these data, POT1a is essential in early embryonic development and ES cells, even though POT1b is expressed (Figures 4.10A and 4.3A), suggesting that POT1a and POT1b are not redundant. We therefore generated mice carrying targeted alleles allowing conditional deletion of the third coding exon of POT1a, POT1b, or both.

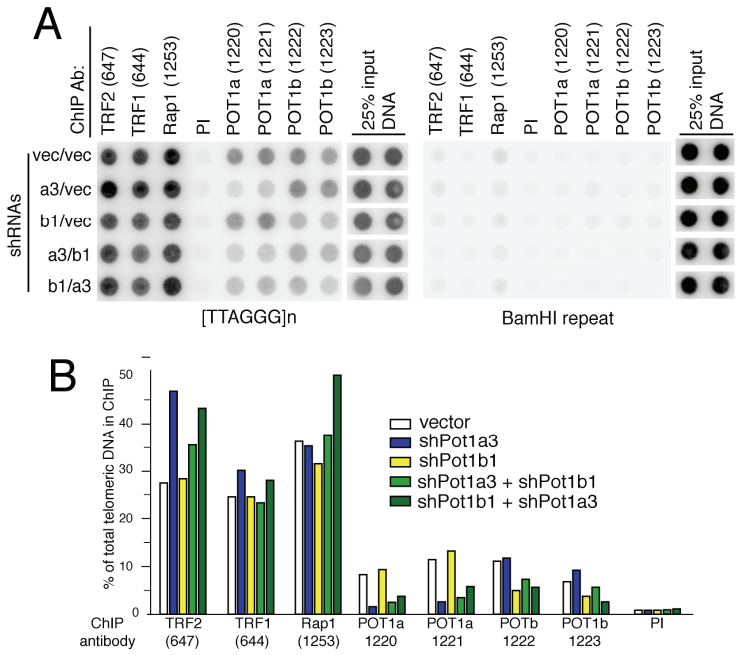

Figure 4.6 Telomere binding of POT1a and POT1b

(A) Telomeric DNA ChIP for POT1a and POT1b. ChIPs with the indicated antibodies on NIH3T3 cells infected with shRNAs described in panel E. Left: TTAGGG signal. Right: Bulk DNA detected with the BamHI repeat. (B) Bargraph of quantification of ChIP analysis show in (A). The assay was performed by Jan-Peter Daniels

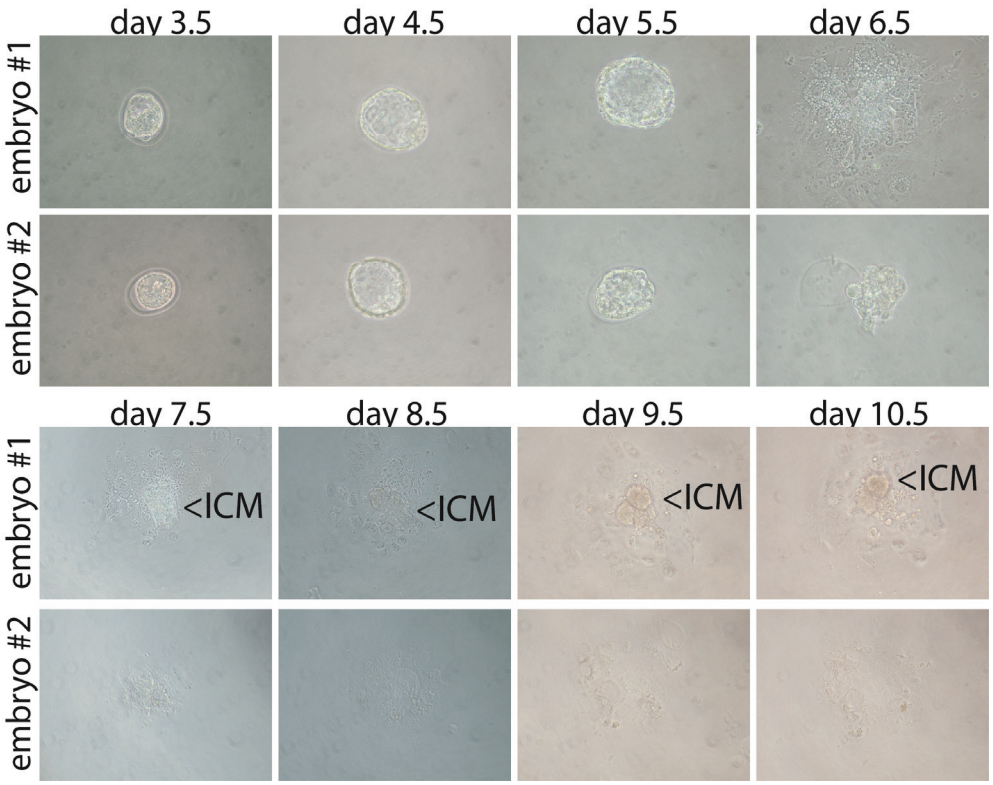

Figure 4.7 Early embryonic lethality of POT1a deficient mice

Phase-contrast microscopic images show in vitro blastocysts growth at the indicated times after fertilization. Blastocysts were isolated from POT1a8$^{GEO/+}$ heterozygous intercrosses. One fourth of isolated blasocycst failed to form an inner cell mass (ICM). This is in agreement with the mendelian distribution expected for embryonic lethality of POT1a$^{8GEO/8GEO}$. Embryo1 is a wt embryo while embryo2 is a POT1a$^{8GEO/8GEO}$ (determined by the lack of POT1a wt PRC product). The pictures of day 3.5 to 6.5 were taken with a 40x magnification and the pictures of day 6.5 to 10.5 were taken with a 10x magnification.

Analysis of the mouse POT1 loci and rationale for the targeting strategy

Analogous strategies were used for the POT1a and POT1b loci (Figures 4.9A and B). In both genes, the third coding exon was deleted based on several considerations. For simplicity, the details below only refer to POT1a. According to the NCBI modelmaker tool (http://www.ncbi.nlm.nih.gov/mapview/modelmaker.cgi?QSTR=pot1&QUERY=uid(18408376)&taxid=10090&contig=NT_039340.6&gene=Pot1), deletion of the first

\

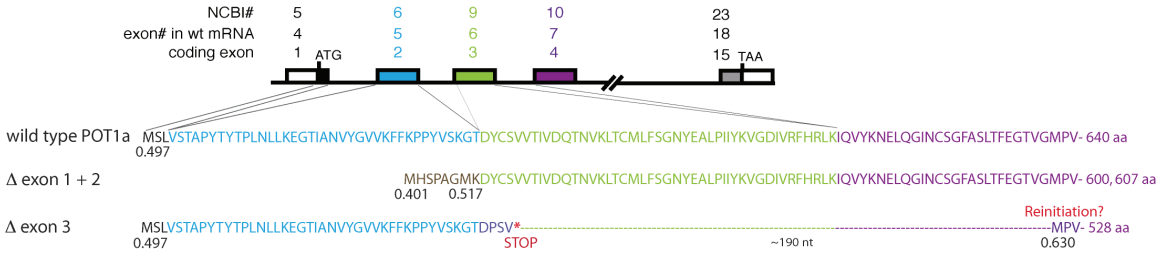

Figure 4.8 Schematic overview of targeting strategies for the mPOT1a locus deleting either exon 1 and 2 or deleting exon 3

The schematic gives the amino acid and exon information for the POT1a locus and the Kozak score values for the pertinent ATGs as well as the length of the predicted open reading frames.

two coding exons (exons 5 and 6 in the NCBI site) generates an N-terminally truncated POT1a protein lacking about one third of the first OB-fold (Figure 4.8). The truncated allele is predicted to start on an ATG in the 5'UTR, brought in frame with coding exon 3 by the normal splicing pattern of the POT1a mRNA. The Kozak score for this ATG is 0.401 (out of 1.0) and the resulting open reading frame is 607 aa. This ATG is closely followed by a second in-frame ATG with a score of 0.517, better than the natural POT1a ATG (0.497). Thus, truncation proteins of 600 and 607 aa might be generated if these ATGs are used in the context of deletion of the first two protein coding exons. These N-terminal deletions of POT1a will lack the ability to bind to single-stranded telomeric DNA but retain the ability to interact with the TPP1 component of shelterin. They are therefore expected to have a dominant negative effect, which has been documented for similar truncations of human POT1 [55]. Furthermore, an N-terminal truncation allele of POT1a might be expected to affect POT1b function and vice versa.

Given these considerations, we opted for a targeting strategy that would allow conditional deletion of the third coding exon (exon 9 in the NCBI nomenclature) while preserving the first two coding exons. Upon deletion of exon 3, the protein initiated on the first ATG of POT1a will terminate early due to a frame-shift at position 41 which generates an in-frame stop codon four amino acids downstream. After this stop codon, there is no in-frame ATG until the methionine at aa position 112 in coding exon 4. Initiation on this ATG is predicted to yield a 528 aa truncation allele lacking DNA binding activity. However, use of this ATG is rendered less likely since there is a favorable ATG upstream and therefore the generation of the 528 aa protein most likely requires reinitiation. Anticipating this possible protein product, we also employed an alternative strategy to disrupt POT1. We introduced an FRT-flanked STOP cassette [158] after the second coding exon, interrupting the first OB-fold of the DNA binding domain (Figure 4.1D) allowing us to study the complete loss of function phenotype of POT1a and POT1b independent of the exon 3 deletion. Through the expression of the FLPe recombinase the STOP cassette is removed to generate the conditional targeted allele (FLOX) (Figure 4.9 A and B). No significant differences were detected in the phenotypes observed by the disruption of the POT1 loci using these two different strategies.

Cells heterozygous for the STOP allele showed 50% less POT1a (or POT1b) protein (Figures 4.11A and C), consistent with previous data on the STOP cassette [158]. Intercrosses of POT1a$^{STOP/+}$ mice confirmed that POT1a deficiency is incompatible with mouse development (Figure 4.10B)

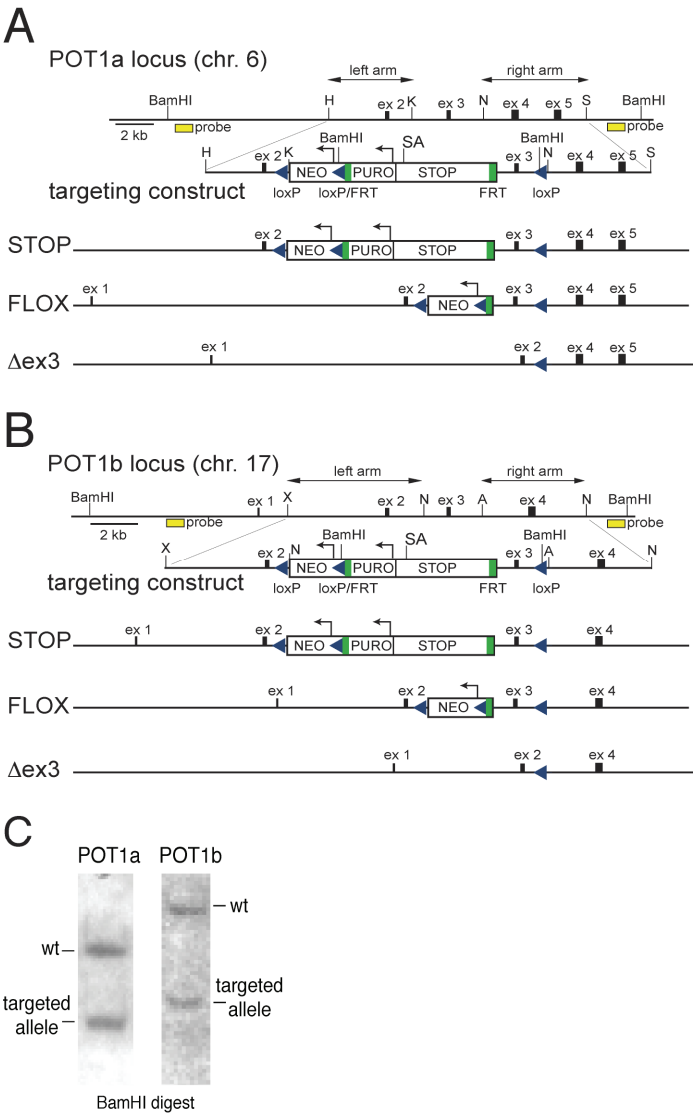

Figure 4.9 Targeting the mouse POT1a and POT1b loci

(A) Targeting strategy for POT1a. Coding exons 1-5 of the POT1a genomic locus (chromosome 6), the targeting construct, and the POT1a alleles generated are shown. Yellow: probes used for genotyping by genomic blotting of BamHI digested DNA used in panel (C); green boxes: FRT sites; blue: LoxP sites; SA: splice acceptor. (B) Conditional knockout strategy used to target the POT1b gene. Given are the genomic locus on mouse chromosome 17 containing the coding exons 1-4 of the POT1b gene, the targeting construct, and the POT1b alleles generated. Yellow boxes: probes used for genotyping by genomic blotting of BamHI digested DNA used in panel (C); green boxes: FRT sites; blue: LoxP sites; SA: splice acceptor of the STOP cassette. (C) Autoradiogram of genomic blotting analysis of BamHI digested DNA from ES-cells targeted with POT1a targeting construct (left panel) and POT1b (right panel) using the probes indicated panel A and B (above) located proximal to exon 3.

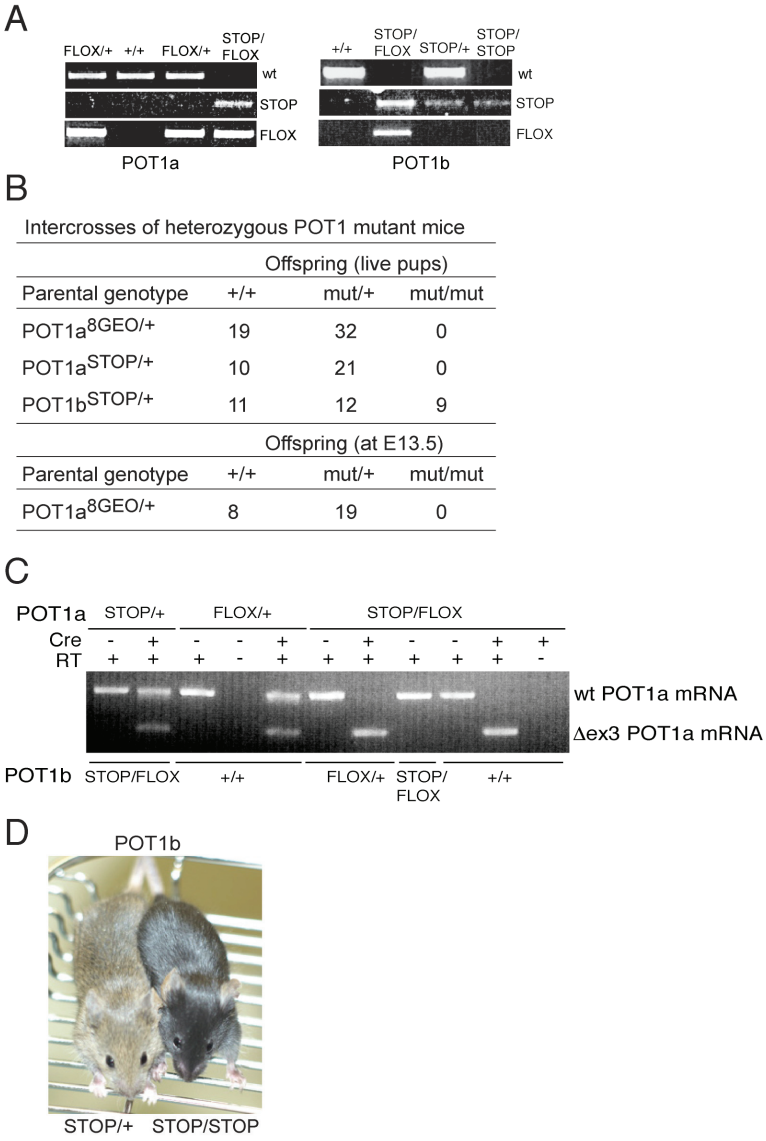

Figure 4.10 Conditional deletion of POT1a and POT1b

(A) Genotyping PCR for POT1a and -b using DNA from MEFs. (B) Table of the genotypes found in the offspring of heterozygous intercrosses of indicated POT1a or –b mutant mice at weaning (top) or at E13.5 (bottom). (C) RT-PCR analysis of POT1a mRNA isolated from MEFs with the indicated genotypes after infection with pWzl-Cre or control vector and 4 days of selection. (D) Photograph of POT1b$^{STOP/+}$ (left) and POT1b$^{STOP/STOP}$ (right) mice.

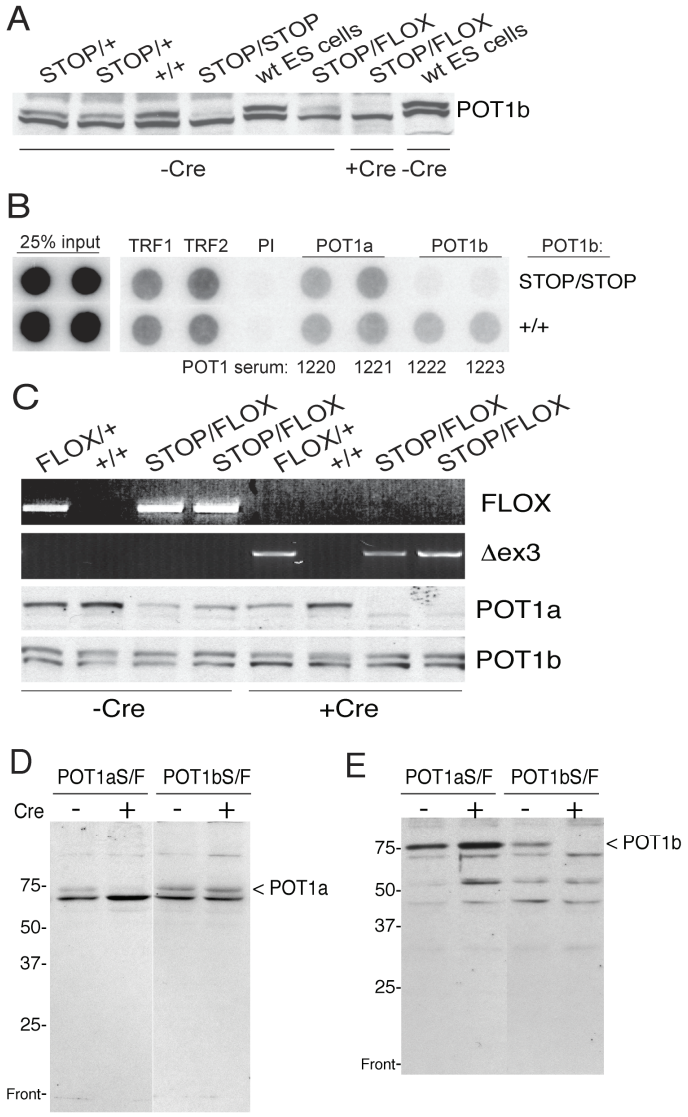

Figure 4.11 Efficient depletion of POT1a and POT1b proteins in MEFs

(A) Immunoblot POT1b extracts from MEFs of the indicated genotypes and 129SV/J ES-cells using antibody 1223 detecting POT1b (top band). For the +Cre lane, POT1bSTOP/FLOX MEFs were infected with H&R-Cre virus and analyzed 5 days later. (B) ChIP using the indicated antibodies on MEFs with the indicated genotype. (C) Genotyping PCR and immunoblot analysis of POT1a mutant MEFs of the indicated genotype. Immunoblots with POT1a antibody 1221 and POT1b antibody 1223. Cells were infected with H&R-Cre virus were analyzed 5 days post infection (+Cre). (D) Immunoblot for POT1a and POT1b (E) in control cells and after Cre-mediated deletion. Note that no new lower MW products are detected after Cre treatment.

However, POT1b$^{STOP/STOP}$ mice appeared healthy and fertile (Figures 4.10B and 4.10D). MEFs isolated from POT1b$^{STOP/STOP}$ embryos lacked POT1b (Figure 4.11A), and ChIP confirmed that POT1b was not present at telomeres whereas POT1a, TRF1, and TRF2 remained bound (Figure 4.11B). The targeting strategy was such that floxed alleles of POT1a and POT1b could be generated allowing the isolation of MEFs from which the third protein coding exon (referred to as exon 3) of either gene could be deleted with Cre recombinase. Multiple independent POT1a$^{STOP/FLOX}$ and POT1b$^{STOP/FLOX}$ MEFs were isolated and immortalized with SV40 large T antigen (SV40-LT). Cre recombinase efficiently excised exon 3 as shown by PCR and RT-PCR and resulted in the expected loss of POT1a and POT1b protein (Figures 4.10C and 4.11 A-E). It has to be noted that the RT-PCR result also indicated that the deletion of exon 3 resulted in a stable POT1a mRNA (Figure 4.11C). Upon Cre-mediated deletion of either POT1 gene, the other POT1 paralog, TRF1, TRF2, and RAP1 remained associated with telomeres (see Figures 4.13A, 4.14A,C and 4.16A).

Redundant Roles for POT1a and POT1b in Cell Proliferation

Cre-mediated deletion of either POT1a or POT1b from SV40-LT immortalized MEFs did not lead to a growth arrest (Figure 4.12A). Both cell types continued to proliferate with unaltered cellular morphology although POT1a-deficient cells grew slightly slower than the controls. Similarly, deletion of POT1a from primary MEFs did not result in a growth

arrest; POT1b deficiency is tolerated in the context of the whole animal, indicating that POT1b is also not required for proliferation of nontransformed cells. In contrast, simultaneous Cre-mediated deletion of POT1a and POT1b from $POT1a^{STOP/FLOX}POT1b^{STOP/FLOX}$ MEFs resulted in a rapid proliferative arrest (Figure 4.12A). These double-knockout (DKO) cells appeared to undergo senescence, as deduced from their enlarged and flattened morphology and their expression of SA-β-galactosidase (Figure 4.12B). The cultures were eventually overtaken by the small fraction of cells in which the Cre-mediated deletion of POT1a and/or POT1b was incomplete (Figure 4.12B), hampering long-term analysis of DKO cells. $POT1a^{STOP/FLOX}POT1b^{STOP/FLOX}$ MEFs, which contain half the normal level of POT1a and POT1b, showed no growth defect (Figure 4.12A and B), nor did NIH3T3 cells in which POT1a and POT1b were simultaneously knocked down to 30% with shRNA. Thus, immortalized cells can proliferate normally without either POT1a or POT1b or when the total POT1 level is lowered 2- to 3-fold but not in the complete absence of both POT1a and POT1b.

Repression of the Telomere DNA Damage Signal by POT1a and POT1b

The role of POT1a and POT1b in the repression of the DNA damage signal at telomeres was assayed based on the formation of telomere dysfunction-induced foci (TIFs) [109], which are cytological foci of DNA damage response factors, such as 53BP1 and γ-H2AX, at chromosome ends. When both POT1a and POT1b were deleted, 70%–80% of the nuclei contained γ-H2AX and 53BP1 foci at most of the telomeres (Figures 4.13 A-C), indicating that the majority of chromosome ends had lost protection. Cells lacking only POT1b or cells heterozygous for POT1a and POT1b did not show this phenotype (Figures 4.13A,C, and D). A TIF response was also observed upon deletion of POT1a alone but the phenotype was limited to 30% of the cells (Figures 4.13A and C), indicating

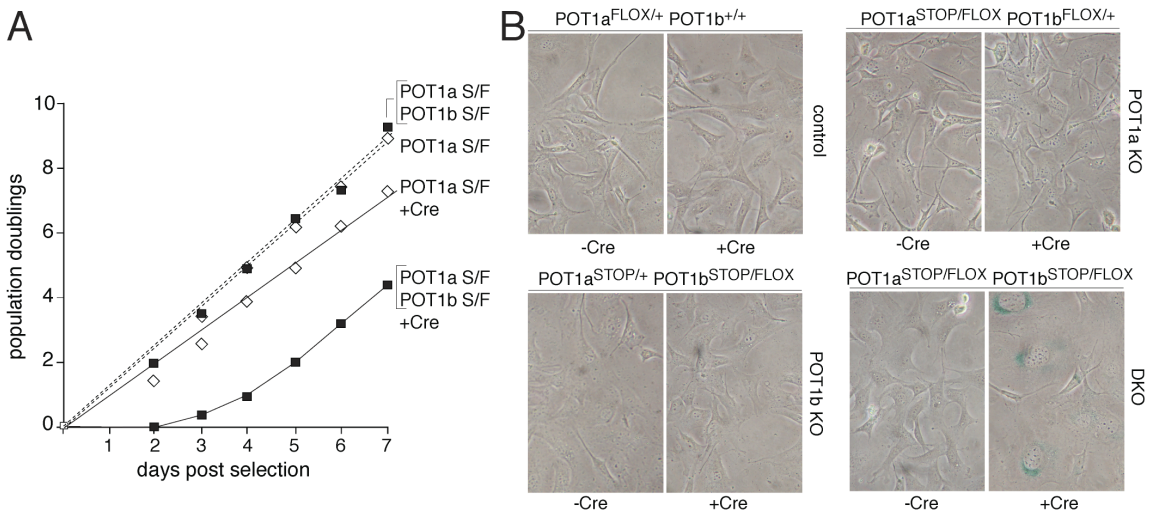

Figure 4.12 POT1a/b double deficient cells arrest and enter senescence

(A) Graph showing growth curves of SV40-LT immortalized MEFs targeted for either POT1a, or both POT1 genes after infection with pWZL-Cre or vector control viruses. Cells were selected with hygromycin for 96 hours and proliferation was monitored over the next 7 days in medium without hygromycin. (B) Phase-contrast microscopic images of MEFs with the indicated genotypes with or without the infection with Cre adenovirus 7 days after infection (stained for SA-β-galactosidase).

that POT1b contributed to the protection of telomeres. The data suggest that POT1a is sufficient to repress DNA damage signaling at telomeres even when POT1b is absent. However, POT1b contributes to telomere protection and a complete telomere DNA damage response is only observed when both proteins are removed from the telomeres. DKO cells retained TRF2 and its interacting factor RAP1 at their telomeres (Figure 4.14A). Inspection of large numbers of nuclei before and after introduction of Cre showed no obvious change in the IF patterns and intensity of TRF2 and RAP1. In addition, there was widespread colocalization of TRF2/RAP1 signals with γ- H2AX in the DKO cells (Figure 4.14A). Thus, while TRF2 contributes to the recruitment of POT1 [55], POT1a/b are not needed for the accumulation of TRF2 and RAP1 at telomeres. Furthermore, the results indicate that telomeres lacking POT1a/b have lost the ability to prevent activation of a DNA damage signal, even though TRF2 is still present. Whereas both POT1a and POT1b contribute to the repression of the DNA damage response at telomeres, the data suggested that POT1a and POT1b are not interchangeable in terms of this function.

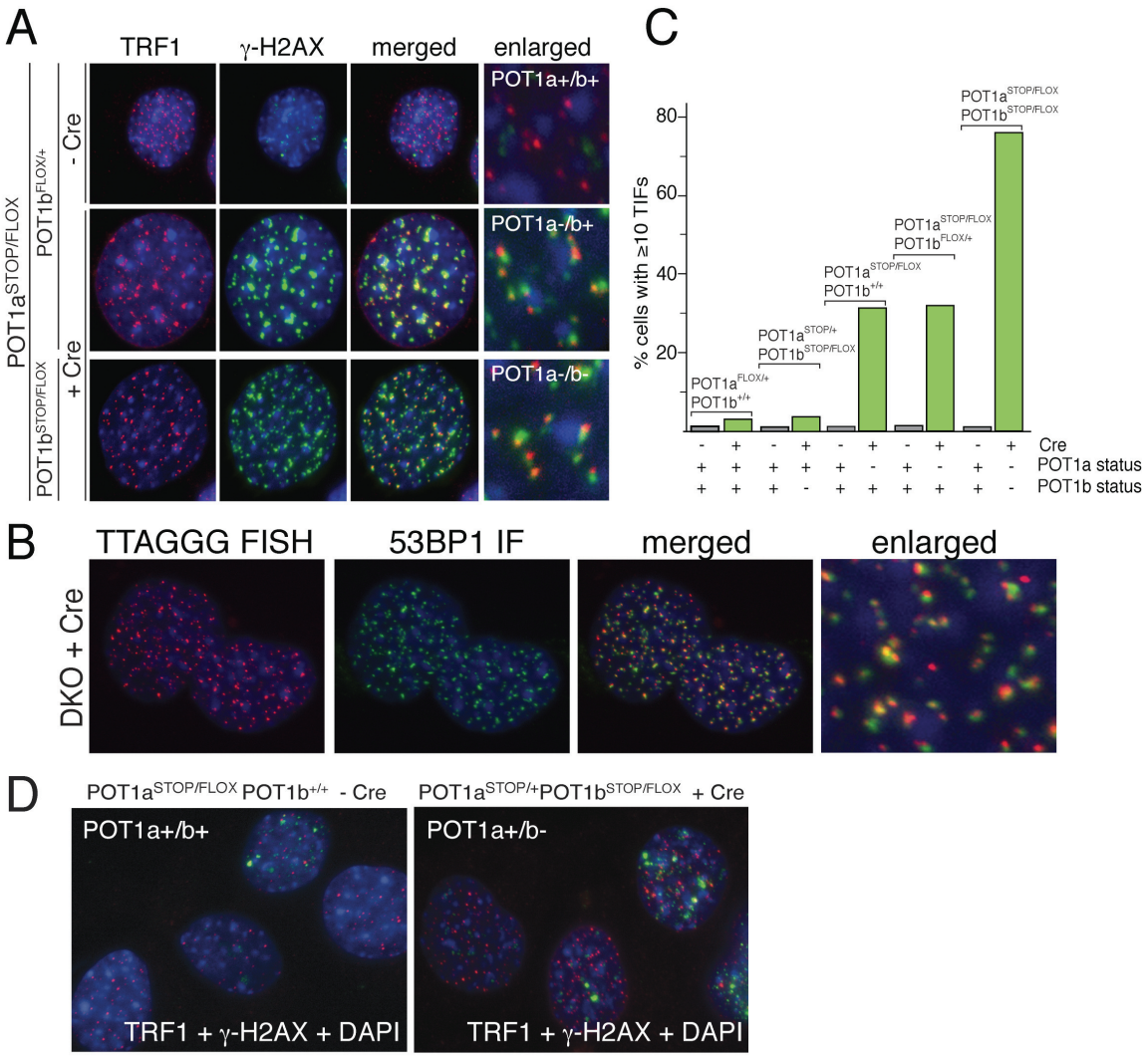

Figure 4.13 DNA damage signal at telomeres lacking POT1 function

(A) MEFs of the indicated POT1 genotypes were infected either with pWZL-Cre retroviruses or control vector, selected for 5 days with hygromycin and analyzed by IF for TRF1 (red), γ-H2AX (green) and counter stained with DAPI (blue). (B) FISH-IF analysis of POT1 DKO cells treated as in (A) stained for telomeric DNA (red) and 53BP1 (green) and DAPI (blue). (C) Quantification of TIF positive cells. Cells with 10 or more TRF1 signals co-localizing with γ-H2AX foci were scored. Grey bars: no Cre, control vector; green bars: pWZL-Cre. (D) TIF analysis as shown in Figure 3 (panel A) using MEFs with the indicated genotypes and Cre infection.

In order to further explore the possibility that POT1a and POT1b differ in their ability to repress the telomere DNA damage response, we monitored the ability of overexpressed MYC-tagged POT1a and POT1b to repress the formation of TIFs in POT1a -/- cells. Both proteins were overexpressed and localized to telomeres (Figures 4.14B and C) but differed in their ability to protect the telomeres. Overexpression of

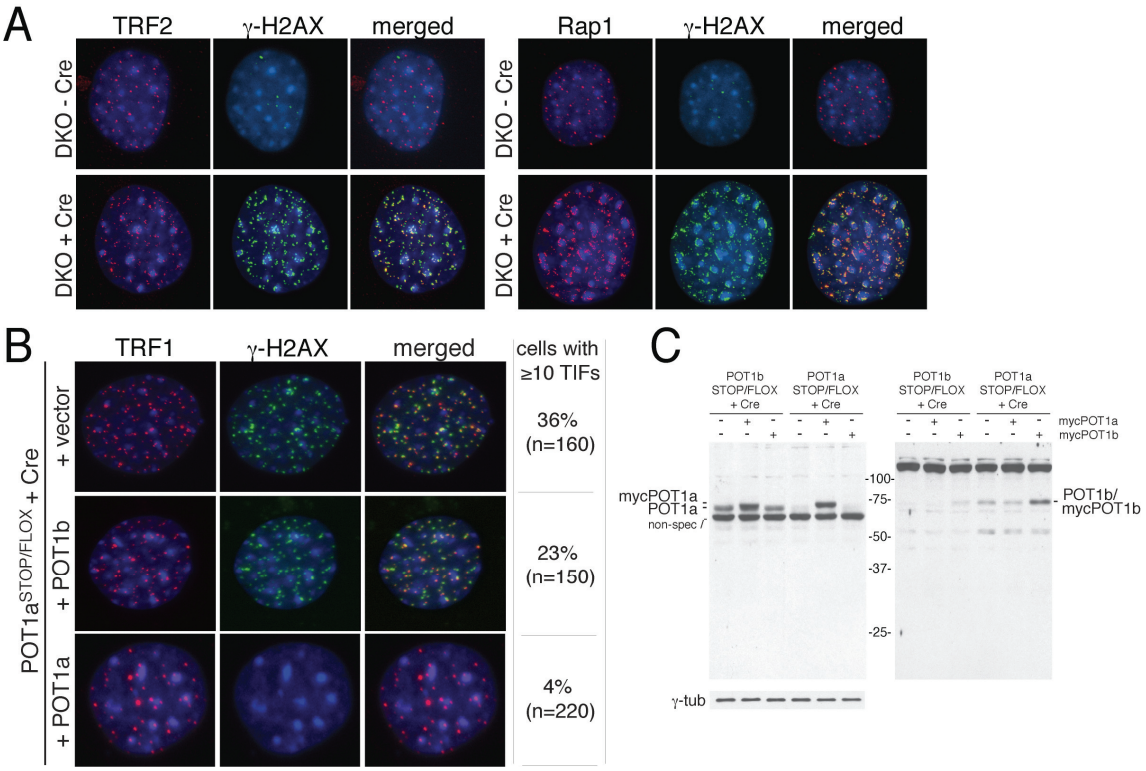

Figure 4.14 Telomere dysfunction induced foci are a phenotype of POT1a, but not of POT1b loss

(A) POT1a$^{STOP/FLOX}$ POT1b$^{STOP/FLOX}$ examined before and after Cre expression as in Figure 4.12 (A) but using antibodies to TRF2 (1254, red) or RAP1(1252, red) and γ-H2AX (green) for IF. The images of nuclei – and +Cre are not shown at the same magnification. Cre-treated nuclei are considerably larger. (B) Suppression of the DNA damage response in POT1a-/- cells by POT1a but not POT1b. POT1a$^{STOP/FLOX}$ cells were treated with Cre to delete POT1a and subsequently infected with retroviruses expressing N-terminally MYC-tagged POT1a or POT1b (or the empty pLPC-MYC vector) as indicated. TIFs were detected and scored as in panels A and C. (C) Immunoblot detection of POT1a and POT1b overexpression in POT1a or POT1b deficient cells. Genotypes and overexpression as indicated above the lane. MYC-tagged POT1a migrates slightly slower than the endogenous POT1a.

POT1a diminished the frequency of TIF positive cells by 10-fold, whereas overexpression of POT1b had only a minor effect (Figures 4.14B and C). These data point to a functional difference between POT1a and POT1b and argue against the possibility that the distinct phenotypes of POT1a and POT1b deletion are due to slight differences in the level of expression of the two genes.

Infrequent Chromosome-End Fusions in DKO Cells

Although many metaphases from the DKO cells showed no aberrations (Figure 4.15A, panel I), approximately 60% of the metaphases contained one or a few aberrant chromosomes (Figures 4.15A and B). Metaphase spreads in which telomeres were detected using FISH revealed the occurrence of chromosome-type fusions with telomeric DNA at the fusion site (Figure 4.15A, panels II–VI). These fusions affected 2% of the chromosomes, which is 30- fold more frequent than in control cells (Figure 4B). The increase in fusions in DKO cells was significant and depended on the introduction of Cre (Figure 4.15B). However, the phenotype is much less pronounced than the nearly complete fusion phenotype of cells lacking TRF2 in which each chromosome undergoes one or two fusion events [80]. Furthermore, whereas TRF2 null cells have long trains of fused chromosomes, fusions of more than two chromosomes were rare in POT1 DKO cells (Figure 4.15A, panels II, III, and VI). The chromosometype fusions occurred on both the short and long arm and in some cases clearly involved two different chromosomes (e.g., Figure 4.15A, panel IV). The fusions of two chromosomes always involved both chromatids, suggesting that most fusions occurred before DNA replication. In addition to chromosome-type telomere fusions, DKO cells contained a significant

number of chromosome fusions without detectable telomeric DNA at the fusion site (Figures 4.15A, panel IX, and 4B), which

could be a consequence of breakage-fusion-bridge cycles. Consistent with this possibility,

A

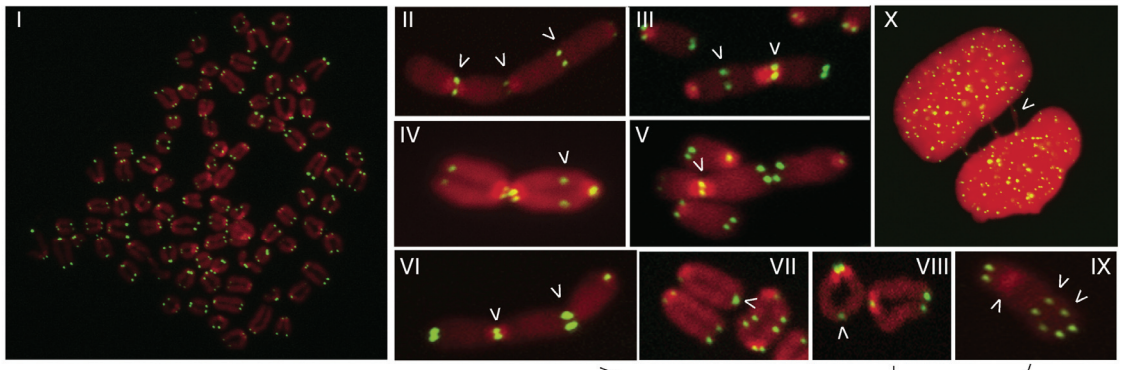

B

Genotype	Cre	POT1a status	POT1b status	Chromosomes analyzed	Chromosome fusions + tel. signal	Chromosome fusions - tel. signal	Sister fusions	Multiple tel. signals
POT1a$^{FLOX/+}$ POT1b$^{+/+}$	-	+/+	+/+	1851	2	3	0	1
	+	+/-	+/+	2171	1	4	0	0
POT1a$^{STOP/FLOX}$ POT1b$^{+/+}$	-	+/-	+/+	2023	1	2	0	0
	+	-/-	+/+	2318	6 (0.3%)	17 (0.7%)	15 (0.6%)	1
POT1a$^{STOP/+}$ POT1b$^{STOP/FLOX}$	-	+/-	+/-	2616	1	3	2	0
	+	+/-	-/-	2670	1	4	2	3
POT1a$^{STOP/FLOX}$ POT1b$^{STOP/FLOX}$	-	+/-	+/-	2773	2	5	0	0
	+	-/-	-/-	3485	69 (2%)	43 (1.2%)	49 (1.4%)	6

Figure 4.15 Mild telomere fusion phenotype associated with POT1 deficiency

(A) Metaphase spreads of SV40LT MEFs with telomeric DNA detected by FISH (green) and stained with DAPI (false-colored in red). POT1a$^{STOP/FLOX}$ POT1b$^{STOP/FLOX}$ MEFs were infected with AdCre and analyzed 78 hours later. Representative metaphase (I). Examples of the chromosomal aberrations found in the POT1 DKO: chromosome-type fusions with and without telomeric DNA at the site of fusion (II-VI), sister telomere fusions (VII-VIII), chromosomes with multiple internal TTAGGG signals (IX) and two interphase nuclei connected with multiple chromatin bridges containing with telomeric signal.
(B) Frequencies of aberrant chromosomes in metaphases (as in (A)) of POT1a and/or -b deficient MEFs. Fusions of short arm sister telomeres were not scored.

anaphase bridges were observed and occasionally, chromatin bridges containing telomeric signals persisted after reformation of the nuclear envelope (Figure 4.15A, panel X). DKO cells also contained a few complex chromosomal rearrangements as well as chromosomes with multiple TTAGGG repeat FISH signals separated by large segments of nontelomeric DNA (Figure 4.15A, panel IX). The origin of these rare abnormalities is not clear. POT1 DKO cells appeared to have an unusual propensity to fuse or associate sister telomeres (Figures 4.15A, panels VII and VIII, and 4.15B). Although sister telomere fusions have been observed in cells lacking TRF2 [81], they are rare and the vast majority of fusions involve nonsister telomeres [159]. In order to distinguish sister telomere fusion from spurious juxtaposition, we only analyzed the q arm telomeres of chromosomes with clearly separated long arms. These long-arm sister telomeres of DKO cells showed a rate of sister fusion of 1%–2% of the chromosomes per cell division which is comparable to the rate of nonsister fusions. Each of the chromosomal abnormalities observed in DKO cells were also present in POT1a-deficient cells but at significantly reduced frequency (Figure 4.15B). In contrast, POT1b-deficient cells showed no increase in telomere fusions or other chromosomal abnormalities (Figure 4.15B). Thus, POT1a appears to be sufficient for the protection of telomeres from inappropriate fusion and in its absence POT1b can partially, but not fully compensate for this function. However, the telomere fusion phenotype of DKO cells is minor compared to the phenotype of TRF2 -/- cells, indicating POT1 function is largely dispensable for the repression of NHEJ at telomeres.

Endoreduplication with Formation of Diplochromosomes

POT1a/b DKO cells displayed extensive endoreduplication (Figures 4.16A,B and 4.17). As a result, some of the DKO interphase nuclei had an increased size and contained

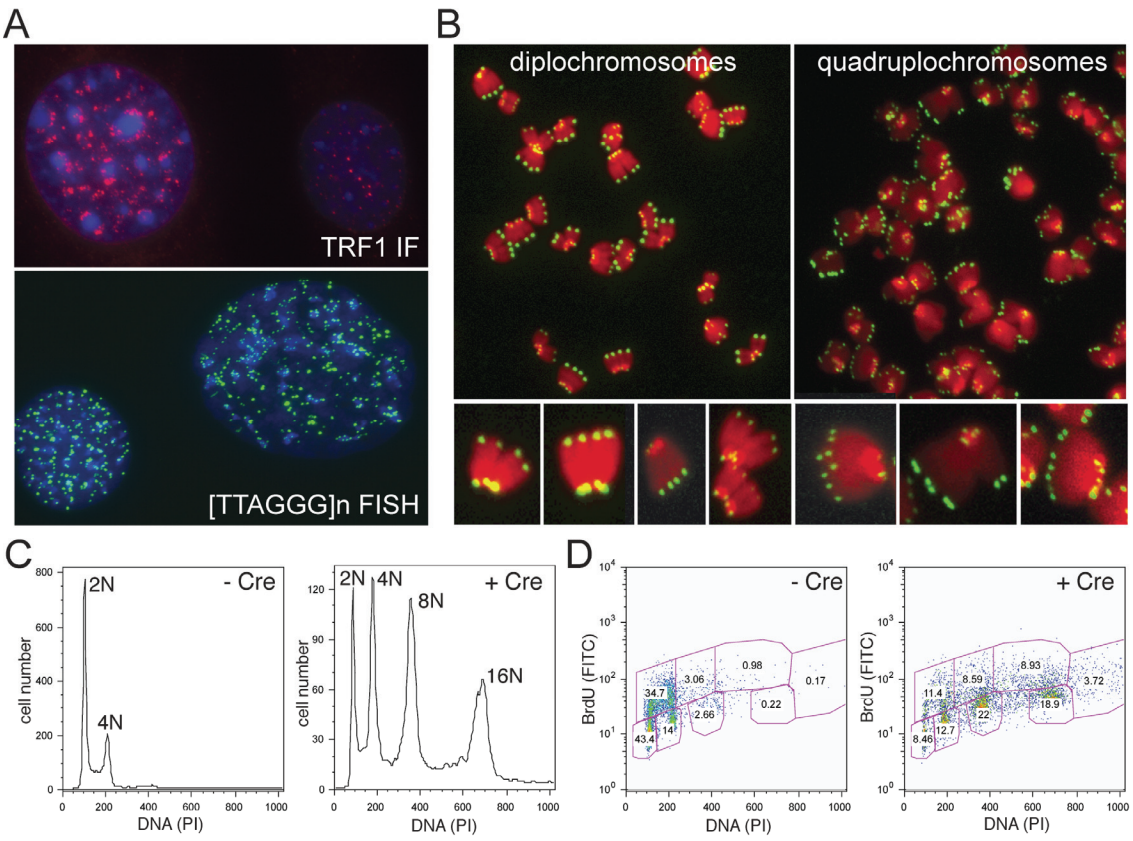

Figure 4.16 Endoreduplication with diplo- and quadruplochromosomes in DKO cells

(A) Example of enlarged DKO nuclei with supernumerary telomeres. Top panel: TRF1 IF (red) in POT1 DKO cells counter stained with DAPI (blue). The nucleus on the left is enlarged and shows increased numbers of telomeric TRF1 foci and telomere clustering around heterochromatin. The nucleus on the right is of normal size. Bottom: Telomeric FISH (green) in DKO cells counter stained with DAPI (blue). Enlarged nucleus with supernumerary telomeres on the right shown next to a nucleus of normal size. (B) Telomeric FISH on DKO metaphase chromosomes showing diplochromosomes and quadruplochromosomes. (C) FACS profiles of POT1a$^{STOP/FLOX}$ POT1b$^{STOP/FLOX}$ MEFS infected with pWZL-Cre or vector control, selected for 5 days and analyzed 2 days after selection. Sub-G1 cells are not shown. (D) MEFs were treated as in (C) and incubated in BrdU for 1 hour prior to harvesting. FACS profiles represent BrdU content and DNA content. Numbers represent % of cells in each compartment.

supernumerary telomeric signals (see for example Figure 4.16A). In these nuclei, the telomeres tended to cluster around regions of more intense DAPI staining, which is expected since half of the mouse telomeres abut the centromeric heterochromatin. Metaphase spreads revealed a high frequency (17%) of endoreduplicated karyotypes in which all chromosomes were present as diplo- or quadruplochromosomes (Figures 4.16B and 4.17). Endoreduplication with formation of diplochromosomes is rare in immortalized control MEFs (%3% of metaphases; Figures 4.17 A and B). FACS analysis showed that POT1a/b DKO induced an increase in cells with 8N and 16N DNA content (Figures 4.16 C and D), consistent with one and two rounds of endoreduplication, respectively. The repression of endoreduplication by POT1 proteins followed the pattern seen for repression of the DNA damage signal and (rare) telomere fusions. POT1a-deficient cells exhibited endoreduplication with formation of diplochromosomes in approximately 17% of the metaphase spreads (Figure 4.17B). However, FACS analysis indicated that their extent of endoreduplication was somewhat less than the DKO cells and metaphases with quadruplochromosomes were not observed (4.17A). FACS analysis and inspection of metaphase spreads showed that endoreduplication was not induced in POT1b-deficient cells (Figures 4.17A and B). Thus, also with regard to endoreduplication, POT1a is primarily responsible for repression of this phenotype. The mechanism by which loss of POT1 function induces endoreduplication is not known. Chromosome-end fusions are not a likely culprit since they are thought to impede the progression of mitosis after resolution of the centromeric cohesin and hence do not explain the occurrence of diplochromosomes which retain cohesion at the centromeres.

A

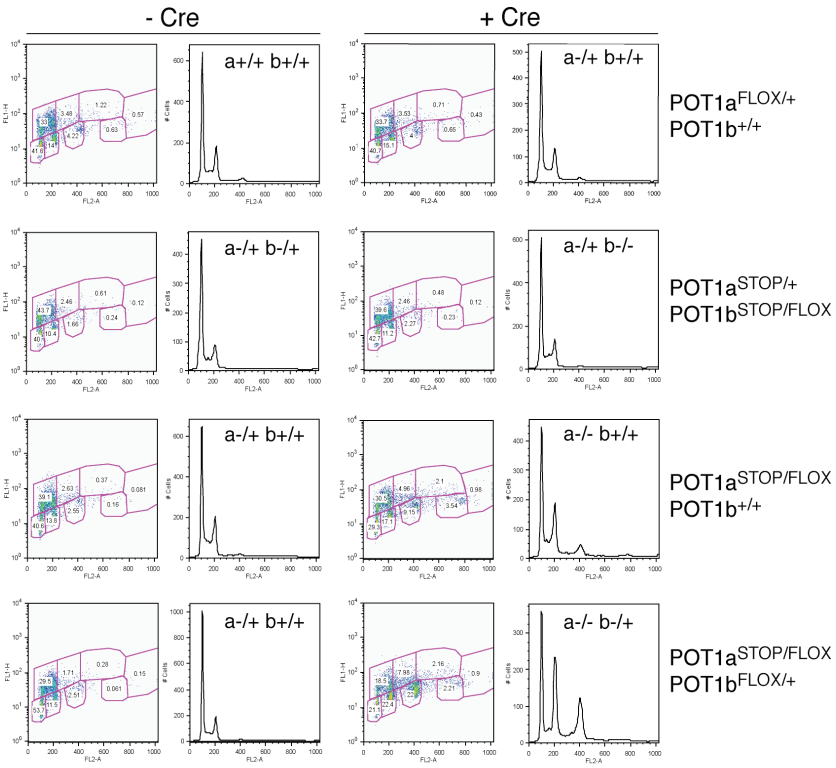

B

Genotype	Cre	POT1a status	POT1b status	Metaphases analyzed	Metaphases w/ diplo-chromosomes (%)
POT1a$^{FLOX/+}$ POT1b$^{+/+}$	-	+/+	+/+	54	2 (3.7%)
	+	-/+	+/+	50	1 (2%)
POT1a$^{STOP/+}$ POT1b$^{STOP/FLOX}$	-	-/+	-/+	59	3 (5%)
	+	-/+	-/-	51	1 (2%)
POT1a$^{STOP/FLOX}$ POT1b$^{+/+}$	-	-/+	+/+	54	2 (3.7%)
	+	-/-	+/+	63	11 (17%)
POT1a$^{STOP/FLOX}$ POT1b$^{STOP/FLOX}$	-	-/+	-/+	53	1 (1.9%)
	+	-/-	-/-	69	12 (17%)

Figure 4.17 Cell cycle profile changes after deletion of POT1a or POT1b

(A) FACS profiles MEFs with the indicated genotypes and BrdU incorporation as in Figure 5 panels C and D. (B) Frequency of diplochromosome-containing metaphases in MEFs with the indicated genotypes. Metaphases were generated as in Figure 4.15

POT1b Controls Telomerase-Independent Processing of the Telomere Terminus

The structure of the telomeres in cells lacking POT1a and/ or POT1b was examined by genomic blotting of telomeric restriction fragments (Figures 4.18-4. 21). Although each mouse embryo has a different pattern of telomeric restriction fragments, the size of the bulk telomeres can be assessed when the DNA is fractionated on CHEF gels.

This analysis indicated that deletion of POT1a or POT1b did not result in a rapid loss or elongation of telomeric DNA. Furthermore, the size of the telomeric fragments of second- generation POT1b-deficient mice was unaltered (Figure 4.18A, 4.19 and 4.20A). In addition, DKO cells had telomeres in a normal size range, consistent with the retention

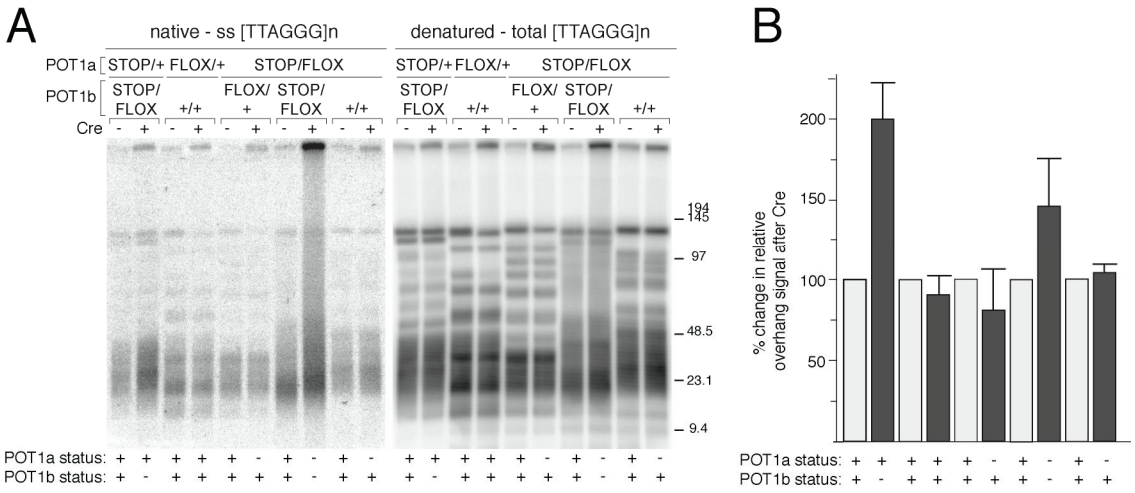

Figure 4.18 POT1b loss leads to an increase in single stranded telomeric DNA

(A) DNA from MEFs of the indicated genotypes was analyzed using the in-gel telomere overhang assay. Phenotypes were analyzed 7 days after infection with H&R-Cre or without infection at the same time point. The left image shows hybridization signal using the TelC probe ([CCCTAA]4) under native conditions detecting the telomeric 3' overhang. The right image shows the total telomeric hybridization signal obtained with the same probe after in-gel denaturation of the DNA. MEFs are derived from littermate embryos and were analyzed one week after introduction of Cre. (B) Quantification of overhang changes based on three independent experiments as shown in (A). Bar-graphs represent quantified overhang signals normalized to the total telomeric signal in the same lane. For each genotype, % overhang changes induced by Cre are depicted. Error bars represent one SD.

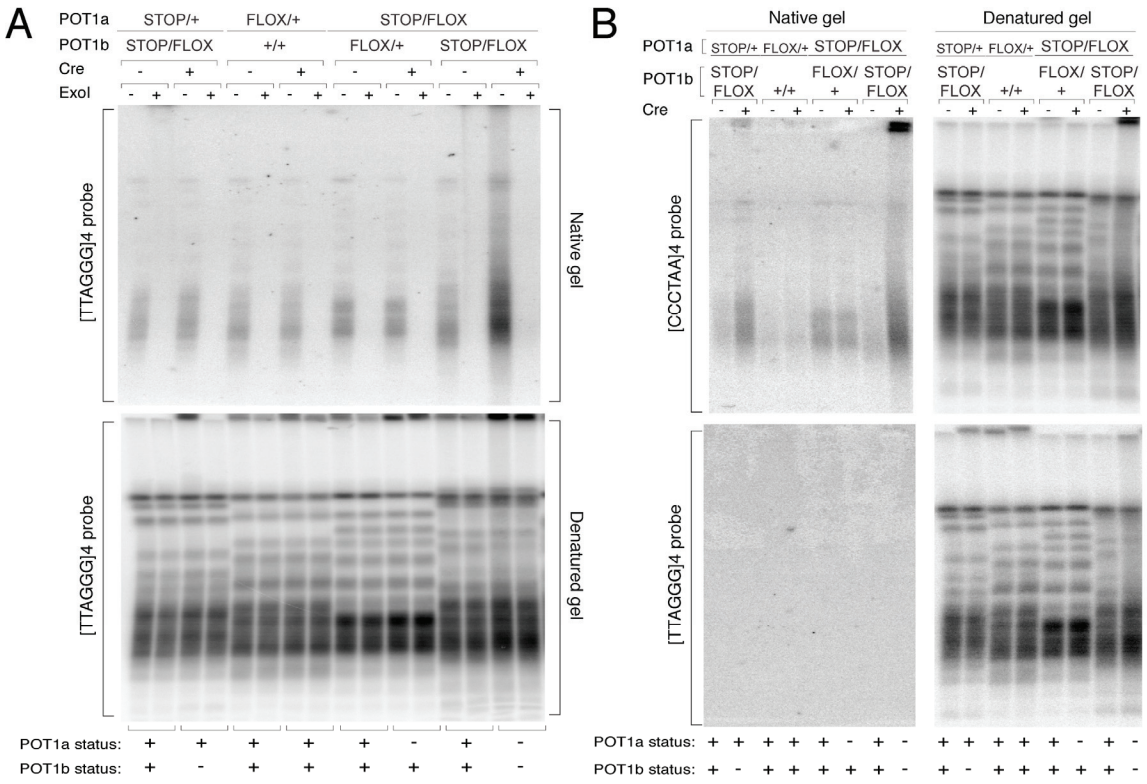

Figure 4.19 ExoI and C-strand control experiments for extended overhang phenotype of POT1b deficiency

(A) In-gel hybridization analysis on DNA from MEFs with the indicated genotypes treated as in Figure 6. Before digest of genomic DNA plugs were incubated with ExoI nuclease as indicated. Top panel shows the native overhang signal, bottom panel shows the denatured total telomeric DNA. (B) In-gel hybridization of MEFs with the indicated genotypes treated as in Figure 6. Top panel: the single-stranded and total telomeric DNA signals obtained with a [CCCTTA]4 probe. Bottom panel: the single-stranded and total telomeric DNA signals obtained with a [TTAGGG]4 probe.

of the telomeric FISH signals in interphase cells and metaphase spreads (Figures 4.13-4.16). The status of the telomere terminus was examined by quantitative analysis of the 3' telomeric overhang. The single-stranded telomeric DNA was detected in native DNA gels using a single-stranded [CCCTAA]4 probe. After quantification of the signal, the DNA was denatured in situ and the total amount of telomeric DNA was determined in the same lane by rehybridization with the [CCCTAA]4 probe. The ratios of single-stranded to total telomeric DNA signals were compared between samples in order to evaluate changes in

the single-stranded TTAGGG repeat DNA. The relative amount of single-stranded TTAGGG repeats was not altered upon deletion of POT1a (Figures 4.18A and B).

In contrast, loss of POT1b resulted in increased single-stranded telomeric DNA signals (Figures 4.18A and B). The increased signal was derived from a 3' overhang since it was sensitive to the E. coli 3' exonuclease ExoI and was specific for the telomeric overhang sequence, as no signal was detected in hybridazations using a TTAGGG single stranded probe. (Figures 4.19A and B). POT1b$^{STOP/STOP}$ mice showed a 7- to 11-fold increase in the overhang signal in liver, kidney, and spleen, and this phenotype was stable over two generations (Figures 4.20A). It appeared that the overhangs in POT1b-deficient MEFs gradually increased with proliferation, consistent with the greater amount of ss TTAGGG DNA *in vivo*. Cells lacking both POT1a and POT1b had a similar overhang extension phenotype as POT1b-deficient cells (Figures 4.18 A and B and 4.19).

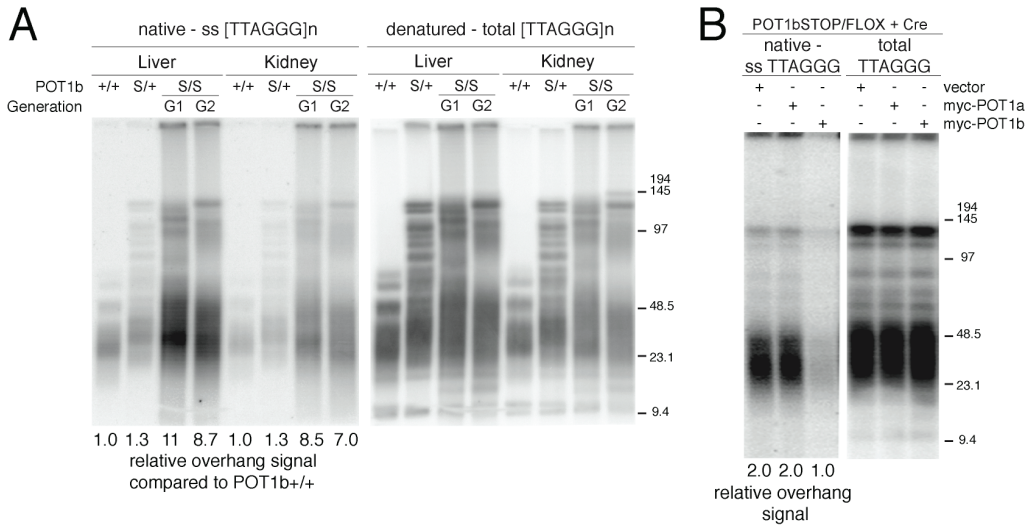

Figure 4.20 POT1b loss results in increased single stranded telomeric DNA in mice and overexpression of POT1a is not able to complement the loss of POT1b

(A) In-gel overhang assay of cells isolated from liver and kidney from mice with the indicated genotype. Left panel shows the native overhang signal, right panel shows the denatured total telomeric DNA. Relative overhang signals are indicated below the lanes. (B) Repression of the overhang phenotype by overexpression of POT1b, not POT1a. $POT1b^{STOP/+}$ or $POT1b^{STOP/FLOX}$ cells were treated with Cre and infected with retroviruses expressing MYC-tagged POT1a or POT1b as shown in Fig. 3F. Telomeric overhang signals were determined as in Figure 4.18.

Due to the rapid arrest of the DKO cells, we could not determine whether POT1a loss exacerbates the phenotype. The DKO cells contained a class of overhang-bearing telomeric restriction fragments that migrated throughout the lane, suggesting an unusual DNA structure. The smearing of the signal into the higher MW fractions and beyond was not prominent when the total telomeric DNA was examined after denaturation of the DNA, indicating that these molecules were relatively rare and only detectable due to their longer overhangs. In order to establish whether the elongation of the overhangs was a specific phenotype of loss of POT1b, we determined to what extent exogenously expressed POT1a and POT1b were able to suppress this phenotype of POT1b-deficient

cells. As shown above, both proteins were overexpressed and localized to telomeres. POT1b was able to reestablish a normal telomere terminus structure, whereas POT1a overexpression had no effect (Figure 4.20 B).

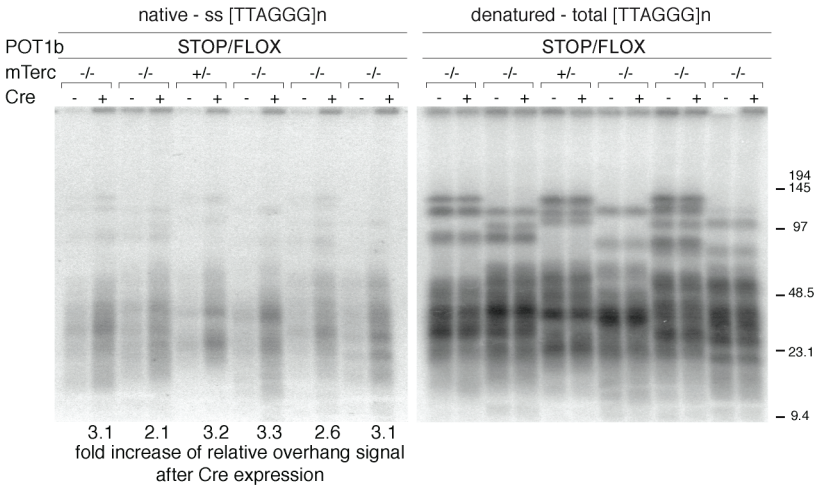

Figure 4.21 POT1b controls a telomerase-independent telomere terminus processing step

In-gel overhang assay of MEFs either heterozygous or null for mTerc and conditionally targeted for POT1b with or without H&R-Cre infection. Left panel shows the native overhang signal, right panel shows the denatured total telomeric DNA. All MEFs are derived from littermates embryos. MEFs were examined one week after introduction of Cre. MEFs in lanes (from left) 3, 4, 5, 6, 9, and 10 were POT1a$^{FLOX/+}$.

We conclude that the control of the telomeric overhang is primarily dependent on POT1b. We next asked whether the extended telomeric overhangs are due to deregulation of telomerase at the telomere terminus. POT1b mutant mice were crossed with mice that lack telomerase due to deletion of the mTERC gene encoding the RNA component of telomerase [67]. MEFs that lacked mTERC and had a conditional POT1b allele were established and immortalized with SV40-LT. Cre-mediated POT1b deletion resulted in comparable extension of the 30 overhang in both mTERC+/- and mTERC -/- cells, indicating that telomerase is not responsible for the elongation of the 30 ends (Figure

4.21). We conclude that POT1b maintains the integrity of the telomere terminus by regulating a telomerase independent processing step.

Discussion

Our results reveal an unexpected difference between human and rodent shelterin. Human shelterin contains a single POT1 protein, whereas the mouse version of this complex is more elaborate, containing roughly equal levels of two functionally distinct POT1 proteins, POT1a and POT1b. Since their duplication, the two mouse POT1 paralogs diverged to the extent that full protection of the telomeres requires both factors. For example, POT1a is necessary to fully repress a DNA damage signal at telomeres. POT1b can partially compensate for the loss of POT1a, but its ability to repress the telomere damage response is incomplete. Conversely, POT1b has a specific role in regulating the structure of the telomere terminus, leading to deregulation of the telomeric overhang in POT1b-deficient cells, despite the presence of POT1a. Thus, while POT1a and POT1b are relatively recent additions to shelterin, they have distinct functions and are both required for the protection of mouse telomeres. Within the context of fundamental aspects of mammalian chromosome biology, the rodent duplication of the POT1 gene and functional divergence of the two resulting POT1 paralogs is unprecedented. No comparable case has emerged from comparisons of human and mouse genes involved in kinetochore function, origin firing and regulation, or DNA damage detection and repair. Other genes relevant to telomere biology, such as those for telomerase components and the genes for the other shelterin proteins are present at single copy in all sequenced mammalian genomes. Previous findings revealed substantial differences between the telomeric proteins in budding yeast on the one hand and fission yeast and mammals on the other. The current results provide evidence for much more recent changes in the telomeric complex and attest to the rapid evolution of the telomere/telomerase system.

POT1a and POT1b Play a Key Role in Repressing the Telomere DNA Damage Response

POT1a/b DKO cells lack the ability to distinguish telomeres from sites of DNA damage. Most of their telomeres become associated with DNA damage response factors and the cells arrest, most likely due to a permanent DNA damage signal. The severity of this telomere damage phenotype is similar to that of mouse cells lacking TRF2 [80].Yet, TRF2 is not removed from telomeres lacking POT1a/b. This finding raises the possibility that the POT1 proteins contribute to the mechanism by which TRF2 prevents DNA damage signaling at chromosome ends (Figure 4.22). The recruitment of POT1 to telomeres is thought to depend on both TRF1 and TRF2, which bring the POT1 interacting factor TPP1 to the telomere (reviewed in) [72]. In the next chapter I will present experiments that show that this interaction is conserved in the mouse and that both POT1a and POT1b are recruited to the telomere through TPP1. Thus, the DNA damage phenotype of TRF2 null mouse cells could be solely due to insufficient POT1 at the chromosome ends but other possibilities have not been excluded.

The Repression of NHEJ at Telomeres

When TRF2 is deleted, most telomeres are processed by the NHEJ pathway, leading to nearly complete fusion of the genome [80]. In contrast, telomeres lacking POT1a and POT1b remain largely protected from this type of inappropriate repair. This result

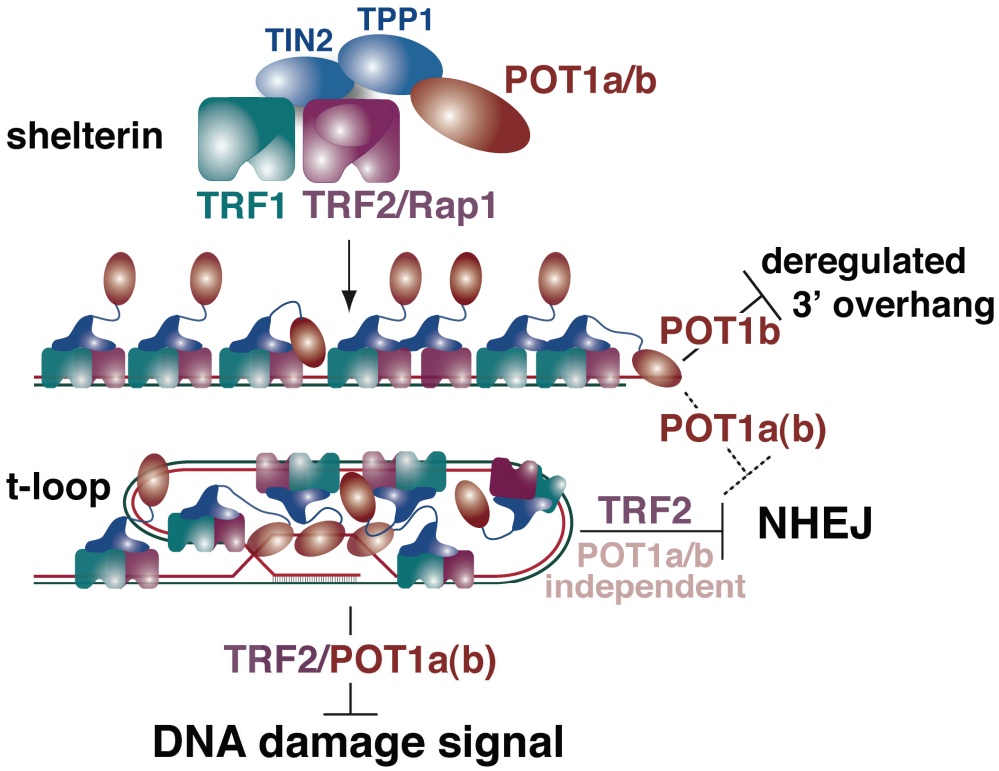

Figure 4.22 Summary of the roles of TRF2, POT1a and POT1b at mouse telomeres

Mouse shelterin is depicted as a complex of TRF1, TRF2, RAP1, TIN2, TPP1, and POT1a and –b. The details of the protein interactions are in part based on information form human shelterin. It is not known whether POT1a and –b are present in the same complex or in two different versions of shelterin. Repression of the DNA damage signal at telomeres requires TRF2, POT1a and –b. Repression of NHEJ is largely independent of POT1a and –b but requires TRF2. NHEJ is proposed to be repressed through sequestration of the telomere terminus in the t-loop. POT1a and –b are proposed to repress NHEJ at telomeres that are not in the t-loop configuration. POT1b is required to prevent generation of inappropriately long telomeric 3' overhangs.

indicates that POT1 is not required for the repression of most NHEJ events and is consistent with NHEJ being blocked by the formation of t-loops, a process ascribed to TRF2 (Figure 4.22). However, a small fraction of the chromosome ends in POT1 DKO cells do undergo fusions, pointing to an important, albeit minor role of POT1a/b in the repression of NHEJ. One possibility is that POT1a/b aids in repression of NHEJ when t-loops are resolved (Figure 4.22), for instance when the replication fork progresses through the strand-invasion site. We imagine that the presence of POT1a/b on the single-stranded overhang might interfere with efficient loading of Ku70/80 or prevent cleavage of the overhang, thereby thwarting NHEJ.

POT1b Blocks Formation of Excessive Single-Stranded Telomeric DNA

The maintenance of the normal structure of the telomere terminus is dependent on POT1b. In its absence, cells contain up to 10-fold more single-stranded TTAGGG repeat DNA. Although we do not know whether the increase in overhang sequences affects all telomere equally, if it does, the overhangs may be as long as 2 kb. The total amount of single-stranded TTAGGG repeat DNA could be in excess of 200 kb in the nuclei of liver cells lacking POT1b. This type of alteration has not previously been observed in mammalian cells, nor does it occur in fission yeast lacking POT1 (Baumann and Cech, 2001). However, in the budding yeast cdc13-1 mutant, inactivation of the POT1-like Cdc13 protein results in excessively long 3' overhangs [148]. The long single-stranded regions are thought to activate the MEC1/RAD9 pathway, explaining the lethality of cdc13-1. In contrast, the excess single-stranded DNA of POT1b-deficient cells did not appear to activate a DNA damage checkpoint and mice lacking POT1b are healthy and

fertile. In the cdc13-1 mutant, the long 3' overhangs are generated by exonucleolytic degradation of the C-rich telomeric DNA strand in an Exo1- and Rad24-dependent manner [160]. A similar mechanism may well be responsible for the excess single-stranded telomeric DNA in POT1b-deficient cells (Figure 4.22). In this context, it is possible that the randomization of the 5' end of the C-rich telomeric strand after RNAi-mediated knockdown of human POT1 could be caused by diminished control of a 5' exonuclease (see chapter 3 and Figure 3.11).

More Than One Pathway for Telomere Protection

The results argue against models in which all telomere protection is simply based on the loading of one protective protein. Rather, different shelterin components have distinct as well as overlapping roles in preventing inappropriate DNA damage signaling and repair at chromosome ends (Figure 4.22). POT1b is required for the maintenance of a normal telomere terminus structure. Neither POT1a nor TRF2 have the ability to control this pathway when POT1b is absent. On the other hand, complete repression of DNA damage signaling at telomeres requires POT1a. POT1b is insufficient to fully protect telomeres in this regard although its contribution to this pathway is inferred from the more severe telomere damage phenotype of the DKO cells. TRF2 is also required for repression of the telomere DNA damage signal although it remains to be determined whether its function is independent of POT1a/b. In contrast, the protection of telomeres from NHEJ involves a pathway that requires TRF2 but is largely independent of the POT1 paralogs. The simplest interpretation of these findings is that telomere protection is achieved through at least three distinct pathways: POT1b-dependent control of the terminus structure;

repression of a DNA damage signal involving TRF2, POT1a, and POT1b; and TRF2-dependent repression of NHEJ. In addition, telomeres are protected from inappropriate homologous recombination, but the genetic requirements for this aspect of telomere function remain largely undefined [133].

Implications

The unusual divergence of mouse shelterin has implications for the use of mouse models for human telomere related disease states. Deletion of essential telomerase components has allowed the establishment of mice with shortening telomeres that ultimately become dysfunctional and mimic aspects of telomere dysfunction in human cells [67,161]. These systems have been used to study the impact of telomere dysfunction on tumor genesis, revealing that telomere dysfunction can limit tumor progression in some settings while promoting genome instability in others [114,144,145]. Furthermore, the telomerase-knockout mouse has been used to model aspects of the human telomerase disease, dyskeratosis congenita [137], and to study interactions between shortening telomeres and genetic defects such as Ataxia Telangiectasia and Werner syndrome [162,163]. Similarly, we have used a mouse TRF2-knockout model to dissect the signaling pathway activated by dysfunctional telomeres [80]. Interpretation of these and other experiments rely on the assumption that mouse and human telomeres are structurally and functionally identical. The finding of an altered shelterin at mouse telomeres challenges this assumption. As more refined mouse models are developed, the potential pitfalls of working within the context of a different shelterin complex will have to be taken into account and the principles gleaned from work on mouse telomeres will require detailed verification in human cells.

5. Cooperative telomere protection by TPP1 and POT1 provides functional evidence for their correspondence to ciliate TEBPα/β

Introduction

The POT1 protein family was identified based on the sequence similarity between the ss DNA binding domain of POT1 and the first OB-fold in TEBPα. TEBPα and its binding partner TEBPβ form a tight complex with the short protrusion of ciliate macronuclear telomeres suggesting a protective role. Recently, crystallography showed that the telomeric protein TPP1 carries an OB-fold with structural similarity to TEBPβ and biochemical evidence indicated that, like TEBPα/β, POT1 and TPP1 bind DNA cooperatively *in vitro* [103,104]. In human cells TPP1 and POT1 are linked to the duplex telomeric DNA binding proteins through TIN2 [55,99,100]. Thus, POT1 can accumulate along the duplex telomeric repeat array. As the single-stranded DNA binding domain of POT1 is not required for its telomere association, it has been suggested that the interaction with TPP1 is the main mechanism for the telomere recruitment of POT1[95].

If POT1 and TPP1 act analogous to TEBPα and -β, it is predicted that POT1 function requires TPP1. This prediction is borne out by observations on telomere length regulation by TPP1 and POT1. The finding that reduced levels of TPP1 lead to telomere elongation is consistent with TPP1 being necessary for POT1 to inhibit telomerase. However, with regard to the protection of telomeres, it has not been excluded that POT1 acts independently of TPP1. Indeed, partial depletion of TPP1 by RNAi did not result in

the telomere deprotection phenotypes induced by POT1 knockdown. The hypothesis that TPP1 is necessary for telomere protection by POT1 is further challenged by the finding that a mouse strain with a mutation in the TPP1 gene, the acd (adrenocortical dysplasia) mouse, has a phenotype that is strikingly different from the phenotypes associated with deletion of the mouse POT1 genes [102] (see previous chapter). Although the acd mutation leads to developmental defects and the mice die postpartum on certain genetic backgrounds, it elicits neither the early embryonic lethality nor the telomere deprotection phenotypes of the POT1a/b DKO. These findings raised the possibility that POT1 might protect telomeres independent of TPP1 and the other shelterin components, which would argue against POT1 functioning as a TEBPα/β-like dimer with TPP1. In order to address this possibility we determined the role of TPP1 in telomere protection in mouse cells. The results in this chapter indicate that depletion of TPP1 from mouse cells results in a telomere deprotection phenotypes similar to the ones found in POT1 DKO cells.

Results

Discrepancy between the two POT1a knockout phenotypes

At the same time as we reported on the POT1a and POT1b knockout phenotypes, the group of Sandy Chang [164] reported their findings on POT1a deficient mouse cells. The observations by Wu et al. were significantly different from my findings on POT1a and -b. As my experiments on the function of TPP1 directly address some of these differences, I will discuss the data of Wu et al. here. Wu et al used a conditionally gene targeting approach, which deletes the first two exons of POT1a, while our targeting strategy deletes exon3 (see chapter 4). They find that POT1a deletion results in a DNA damage response at telomeres (TIFs) and a growth arrest [164], whereas we document TIFs but no inhibition of proliferation after deletion of POT1a. Furthermore Wu et al. document and an increase in overhang signal and report telomere elongation, whereas neither of these phenotypes occur in our experiments. Overall the phenotypes of Wu et al. report are reminiscent of the phenotypes we find for the simultaneous loss of POT1a and POT1b [164]. As the Wu et al. POT1a phenotype is more severe, their strategy might result in a dominant negative allele of POT1a or my strategy creates a hypomorphic POT1a allele. Below I will discuss data that argues against the possibility that my KO strategy generates a hypomorphic allele.

As discussed in detail in chapter 4 and outlined in Figure 4.8, both the deletion of exon 1 and 2 as well as the deletion of exon 3 could generate an N-terminally truncated POT1 fragment.

RNAi depletion of residual POT1 proteins in POT1 deficient cells

In order to test whether our targeting strategy generates a hypomorphic allele of POT1a and POT1b we used RNAi depletion. If the Wu et al. allele represents the null allele and our strategy creates a hypomorph, we expect that RNAi to POT1a in our POT1a KO cells would elicit the severe phenotypes reported by Wu et. al: increased overhang length,

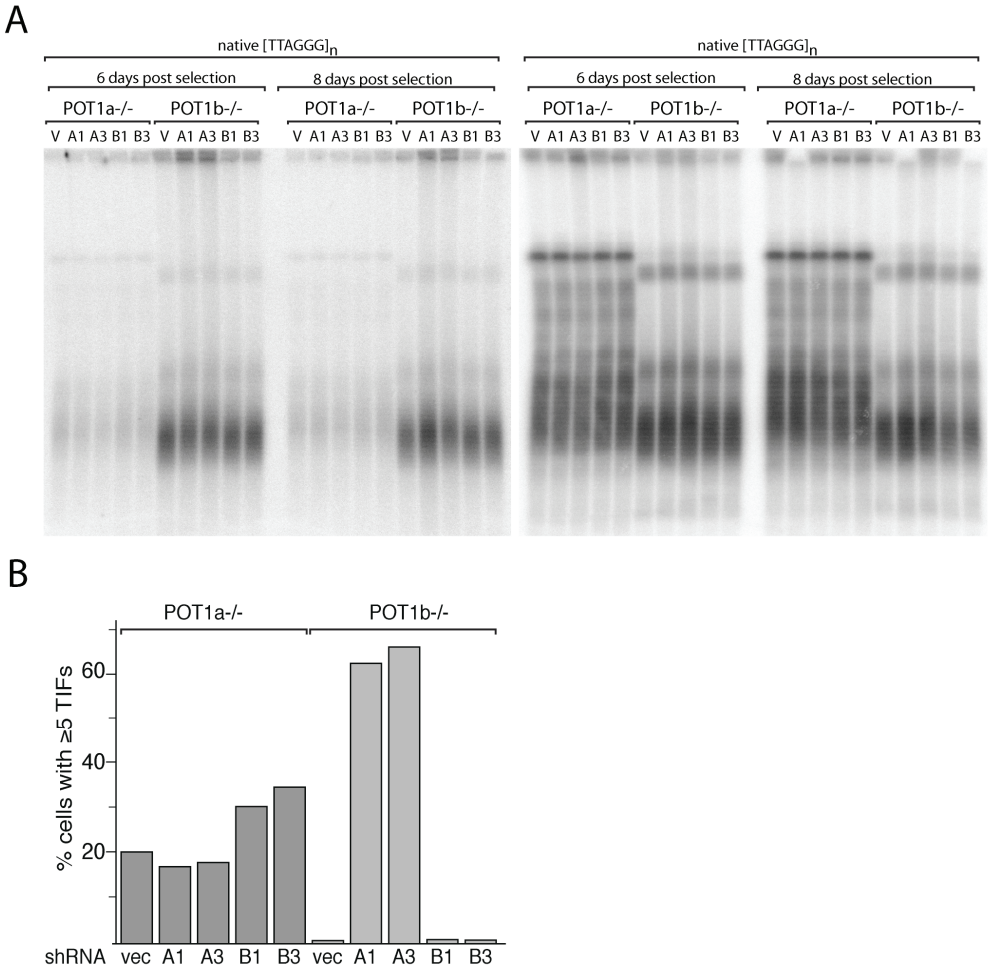

Figure 5.1 Deletion of exon 3 of POT1a and POT1b does not result in a hypomorphic allele

(A) In-gel overhang assay of POT1a-/- (Δ3/Δ3) and POT1b-/- (Δ3/Δ3) cells after the infection with POT1a shRNAs (A1 and A3), POT1b shRNAs (B1 and B3) and vector control either 6 days or 8 days after selection. Prior infection with the indicated shRNAs, POT1a S/F and POT1b F/Δ cells were infected with pWzl-Cre and selected with hygromycin to generated POT1a-/- and POT1b -/- cells. The left panel shows the single stranded telomeric signal and the right panel shows the total telomeric signal after denaturation of the same gel (B) TIF analysis of the cells described in panel (A) 5 days after selection.

growth arrest and a two-fold increase in TIFs [164]. However, reduced levels of POT1a mRNA in POT1a deficient cells did not result in an increase in overhang length (Figure 5.1A), or increase the fraction of TIF positive cells (Figure 5.1B). These data strongly argue against the possibility that deletion of exon 3 results in a hypomorphic POT1a allele.

As our POT1a and POT1b knockout strategies are essentially identical, similar arguments can be made for POT1b. If our POT1b knock out strategy created a hypomorphic allele, depletion of POT1b mRNA using RNAi would be expected to change the phenotype. However, the telomeric overhang in POT1b deficient cells remained unchanged upon the expression of POT1b shRNAs. Furthermore, POT1b shRNA did not induce other telomere dysfunction phenotypes (TIFs, telomere fusions) in POT1b KO cells. As expected, RNAi depletion of POT1a in POT1b-/- cells and the knockdown of POT1b in POT1a-/- cells resulted in phenotypes that are reminiscent of POT1a/b dKO cells. These data argue against our KO strategy generating hypomorphic alleles.

TPP1 mediates telomeric association of POT1a and POT1b

In order to address the functional dependence of POT1 on TPP1, we analyzed acd mutant mouse cells. The acd phenotype is caused by aberrant splicing of the gene encoding TPP1, which carries a G-A transition 5 nt beyond the splice donor site of exon 3 [102]. This mutation results in the use of a cryptic splice donor site and is predicted to generate a

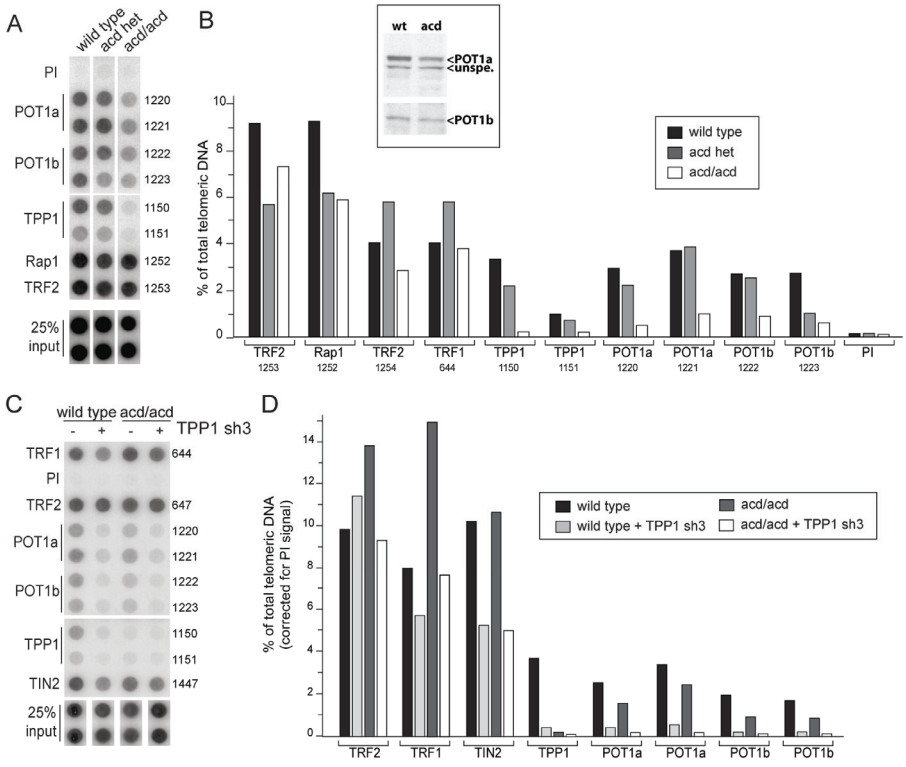

Figure 5.2 Dependence of POT1a/b telomeric localization on TPP1

(A) Telomeric DNA ChIP on MEFs that are wild type, heterozygous or homozygous for the TPP1 acd allele. The numbers next to the radiograph specifies the antibodies used. The antibodies are specific for telomeric ChIP as indicated by absence of non-specific sequences (BamHI repeat) in the ChIPs (data not shown). The cells used for the ChIP had been cultured for less than 10 PD. (B) Quantification of the % of the total telomeric DNA recovered in the ChIPs shown in (A). (C) Immunoblots for POT1a and POT1b in wild type and acd/acd cells with antibodies 1221 and 1223, respectively. The non-specific band in the POT1a blot serves as a loading control. (D) Telomeric DNA ChIP on wild type or acd/acd MEFs transduced with TPP1 sh3 as indicated. The numbers next to the radiograph specifies the antibodies used. ChIP was performed after 5 days of puromycin selection for the retroviral shRNA vector. The acd/acd cells used in this ChIP analysis had been cultured for more than 30 PD.

truncated TPP1 protein lacking part of the OB-fold, the POT1 binding domain, and TIN2 binding domain. Due to lack of appropriate antibodies we were so far unable to determine the effects of this splice mutation on the TPP1 protein level and therefore do not know if a truncated protein or other potential TPP1 fragments are expressed in acd/acd cells. To examine the effect of the acd mutation on telomere structure and function, acd/acd mouse embryo fibroblasts (MEFs) were isolated from E13.5 embryos generated by heterozygous intercrosses and immortalized with SV40 large T antigen (SV40-LT). Chromatin immunoprecipitation (ChIP) using TPP1 antibodies recovered about >10-fold less telomeric DNA in the acd/acd cells compared to wild type cells, whereas ChIPs with antibodies against TRF1, TRF2, and Rap1 showed only minor changes (Figure 5.2A and B). In acd/acd cells telomere association of POT1a and POT1b was reduced about 4 fold based on telomeric this ChIP analysis, indicating that a significant fraction of POT1a and –b remained associated with the telomeres of acd/acd cells. Consistent with this result, the acd/acd cells expressed significant levels of POT1a and –b although the protein levels were lower than in wild type cells (Figure 5.2B inset). We noted that acd/acd cells cultured for prolonged periods (>30 PD) had close to wild type levels of POT1 at the telomeres (Figure 5.2C and D). Such improved POT1 recruitment may be associated with a selective growth advantage (see below).

The residual POT1a and POT1b at acd/acd telomeres could be explained if POT1a/b has the ability to associate with telomeres in a TPP1-independent manner. Alternatively, the acd mutation might generate an unexpected hypomorphic allele that still retains the POT1 and TIN2 binding domains and can recruit POT1a/b to telomeres. We tested the latter possibility with three shRNAs that target the TPP1 mRNA at

positions downstream of the acd mutation. ChIP analysis showed that TPP1 shRNA 3 efficiently reduced the levels of telomere associated TPP1 in wild type MEFs (Figure 5.2 C and D). TPP1 knockdown in acd/acd cells that were grown for >30 PD significantly lowered the telomeric binding of POT1a and POT1b, indicating that the residual POT1a/b at telomeres of acd/acd was recruited by TPP1. In addition to its effect on POT1a/b, TPP1 knockdown reduced the association of TIN2 and TRF1 with telomeres by ~2 fold. This finding is in agreement with the previous report that TPP1 is necessary to stabilize shelterin [165]. Collectively, the TPP1 shRNA data argue that acd represents a hypomorphic allele of TPP1. The TPP1 expression in acd/acd cells is most likely due to the fact that TPP1 cells remain about 1% of the correctly spliced wild type TPP1 mRNA (Garry Hammer personal communication).

Localization of C-terminal truncation mutants of POT1b

According to a report by He et al. mouse POT1b (POT1bN aa 1-341) lacking the TPP1 binding domain accumulates at telomeres [166]. Furthermore, an analogous fragment of human POT1 (often referred to as splice variant V2 [97]) was reported to affect telomere length, a phenotype that is presumed to require the localization of V2 at telomeres [146]. These results appear in conflict with the data described in Figure 5.2, which indicate that POT1 relies primarily on TPP1 for its telomeric localization. To test the requirement for TPP1 interaction further, we generated two POT1b alleles, one representing aa 1-352 (POT1b-V2) and one lacking the last 17 aa, including amino acids implicated in TPP1 binding (POT1b-623) (Figure 5.3A). According to the genome databases, POT1b-V2 and POT1b-623 could be generated by alternative splicing. While retrovirally transduced

POT1b-V2 and POT1b-623 were detectable in immunoblots, neither protein was detectable at telomeres of wild type or POT1b KO MEFs by immunoflourescence. Furthermore, cellular fractionation experiments showed that most of POT1b-623 and all POT1b-V2 was recovered in the cytoplasmic fraction (Figure 5.3B).

As expected, full length POT1b was predominantly nuclear (Figure 5.3B). The non-telomeric localization of POT1b-V2 and POT1b-623 is consistent with the observed lack of telomeric binding of a human POT1 with a point mutation in the TPP1 binding domain. Together the data argue that the OB-fold domain of POT1 proteins does not

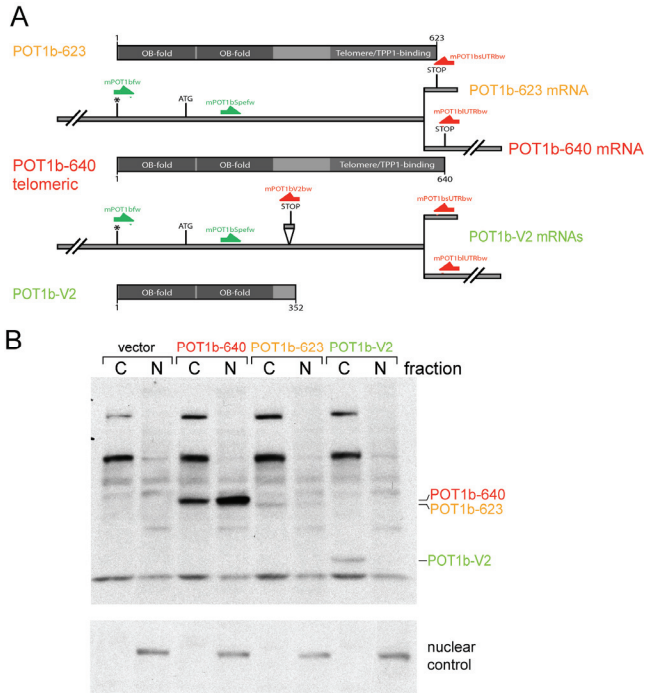

Figure 5.3 Potential products of the POT1b locus and their subcelllular localization

(A) Schematic of potential alternatively spliced mRNAs derived from the POT1b locus. Primers used for RT-PCR reactions are indicated. No products were obtained with RT-PCR for POT1b-623 or POT1b-V2 whereas POT1b-640 was readily detectable in the same RNA samples from mouse cells. (B) Subcellular localization of ectopically expressed POT1b. MYC-tagged versions of the POT1b alleles shown in (A) were expressed in POT1b KO MEFs using retroviral transduction. An antibody to the MYC tag was used to detect the POT1b alleles in immunoblots of cytoplasmic and nuclear fractions as indicated. The nuclear control represents an unknown nuclear protein of ~100 KDa detected with our Ab1252. The same result was obtained in wild type cells. Wilhelm Palm and Jan-Peter Daniels performed the experiments.

support telomeric accumulation in absence of TPP1 interaction. These findings contradict the reports by He et al.

Occasional telomere deprotection in TPP1-hypomorphic acd/acd cells

We next addressed the contribution of TPP1 to telomere protection by analyzing the telomeres of newly-derived (<10 PD) acd/acd cells. We did not observe a significant change in telomere length in these or older cells nor was there an increase in the relative abundance of the single-stranded telomeric DNA (see Figure 5.4 and 5.8B and C). The normal structure of the acd/acd telomeres contrasts with the 2-3 fold excess in ss TTAGGG repeat DNA observed in POT1b KO cells. However, acd/acd cells did show a mild telomere deprotection phenotype based on the occasional occurrence TIFs.

As expected, wild type cells and cells heterozygous for the acd mutation did not

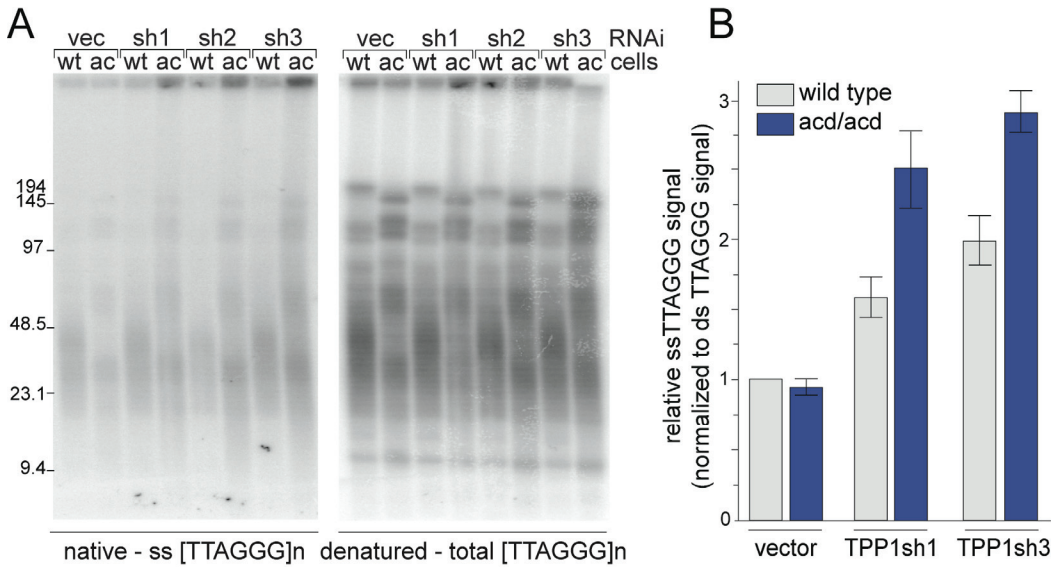

Figure 5.4 Reduced levels of TPP1 result in increased telomere overhang signals

(A) In-gel overhang assay of MEFs of the indicated TPP1 genotypes (wild type (wt) and acd/acd (ac)) infected with the indicated TPP1 shRNAs or vector control retrovirus. (B) Quantification of overhang signals from three different wild type or acd/acd cell lines infected with the indicated shRNAs. Error bars indicate the standard deviation of the mean of three experiments.

contain a significant number of TIFs (<1% of cells have ≥10 TIFs; Fig. 2a and b and data not shown). However, a small fraction (2-3%) of acd/acd MEFs contained 10 or more TIFs (Figure 5.5A and B). This level of TIFs is significant yet very minor compared to the phenotype of POT1a KO and POT1a/b DKO cells (>70% of cells with ≥10 TIFs). Similarly, acd/acd cells show a significant increase in the frequency of telomere fusions (~10 fusions/1000 chromosomes in acd cells compared to ~1 fusions/1000 chromosomes in wild type cells) but this phenotype was less pronounced than in POT1a/b DKO cells (35 fusions/1000 chromosomes) (Figure 5.6 A and B). Furthermore, the acd mutation was associated with the occasional occurrence of tetraploid metaphases with diplochromosomes, a phenotype that is prominent in POT1a KO and POT1a/b DKO cells. Tetraploid metaphase spreads composed of diplochromosomes occurred in ~5% of the acd/acd cells. Thus, acd/acd MEFs displayed a significant but relatively infrequent telomere deprotection phenotypes consistent with the diminished presence of POT1a/b at their telomeres. Despite being mild, the telomere phenotype of acd/acd cells might result in the selection for enhanced POT1 recruitment, explaining the presence of nearly wild type POT1a/b levels at telomeres of acd/acd cells cultured for >30 PD (see Figure 5.2).

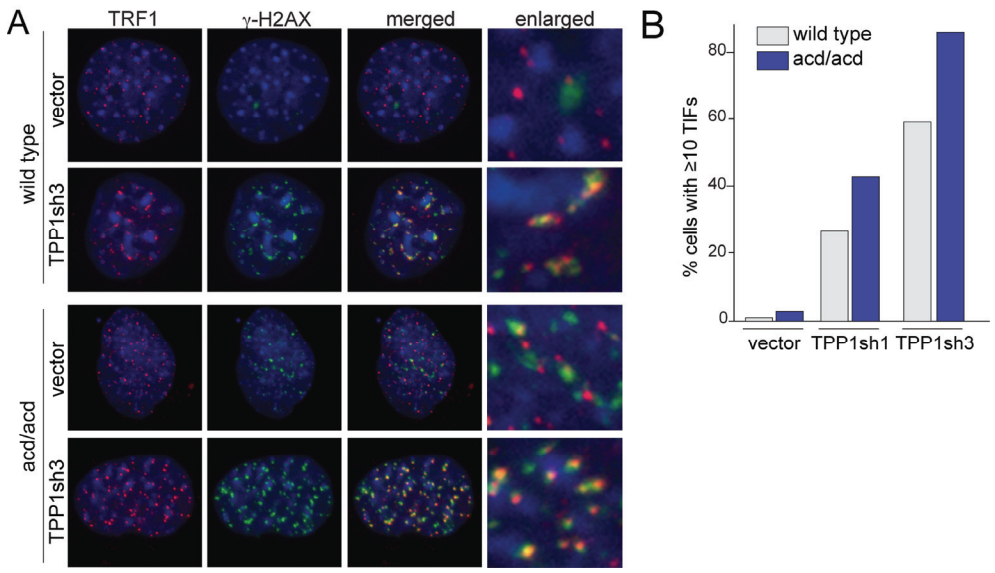

Figure 5.5 TIFs in cells with reduced TPP1 levels

(A) Occurrence of TIFs upon TPP1 knockdown. MEFs of the indicated TPP1 genotypes were infected with TPP1 sh3 or control vector (pSuperior), selected for 4 days with puromycin and analyzed by IF for TRF1 (red), γ-H2AX (green) and counterstained with DAPI (blue). In agreement with the ChIP data, TRF1 levels are reduced in some acd/acd MEFs infected with TPP1 shRNAs. (B) Quantification of TIF positive cells shown in (A). Cells with 10 or more TRF1 signals co-localizing with γ−H2AX foci were scored as TIF positive. At least 120 cells were analyzed for each experiment.

TPP1 knockdown with RNAi results in a POT1a/b DKO phenotype

RNAi was used to target TPP1 in wild type and acd/acd cells and the knockdown efficiency was determined by telomeric ChIP. Knockdown of TPP1 resulted in a very strong telomere deprotection phenotype. Cells with TIFs became very frequent (Figure 5.5), there was a higher frequency of telomere fusions (~20% of chromosomes showing a telomere fusion (Figure 5.6), and the amount of single-stranded telomeric DNA was increased 2-3 fold (Figure 5.4). All three phenotypes were most prominent in acd/acd cells treated with TPP1 shRNA 3 but also occurred when TPP1 was knocked down in wild type cells. TPP1 shRNAs 1 and 2 also resulted in TIFs, telomere fusions, and increased telomeric overhang signals (Figure 5.4-5.6). Strikingly, the frequency of

telomere fusions in acd/acd cells treated with TPP1 shRNA3 is 3-4 fold higher than in POT1a/b DKO cells. Therefore, it appears that TPP1 loss, perhaps due to concomitant changes in the shelterin complex has a more severe effect on the protection of telomeres from NHEJ than POT1a/b deficiency. This is in agreement with the *in vitro* finding that TPP1 is necessary for shelterin assembly [165].

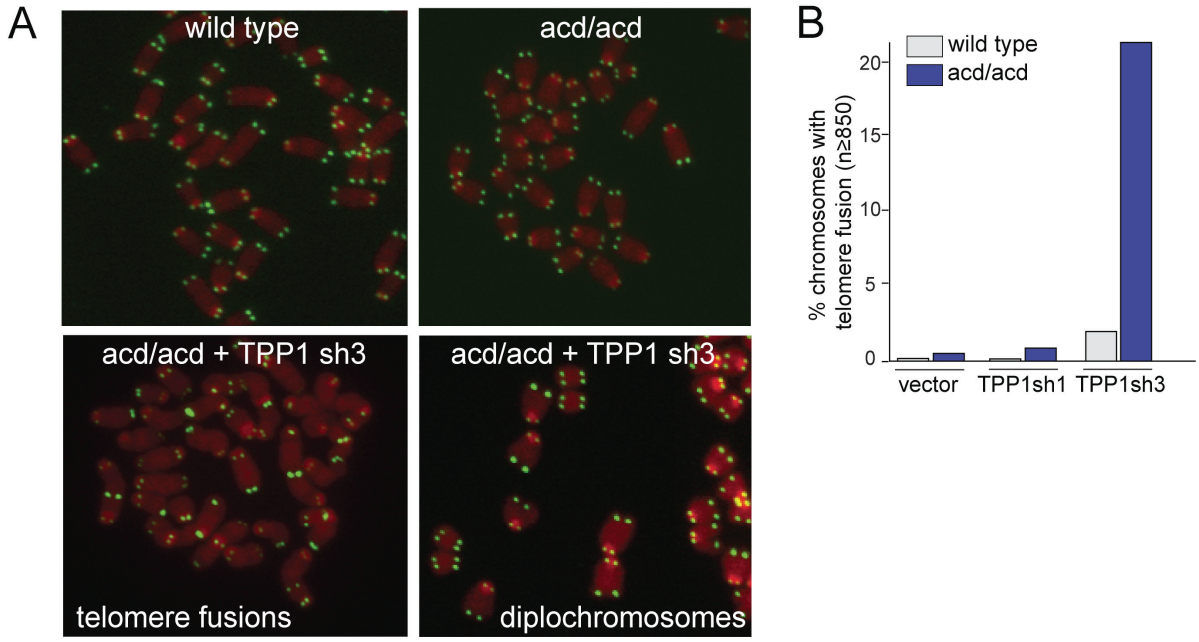

Figure 5.6 Telomere fusions in cells with reduced TPP1 levels

(A) Telomeric FISH on metaphases derived from cells of the indicated TPP1 genotypes infected with TPP1 shRNA3 or vector control. Telomeric hybridization signal is shown in green and DAPI counterstained chromosomes are false colored in red. (B) Quantification of telomere fusion frequency in MEFs of the indicated TPP1 genotypes infected with the indicated shRNAs or control vector.

N-terminal truncation mutants of POT1a and -b act as dominant negative alleles

Finding that the phenotypes of TPP1 loss closely reassemble the loss phenotypes of POT1 suggests that TPP1 and POT1 function through the same telomere protection pathway. To test to what extent the single stranded binding activity is necessary for telomere protection by POT1 we expressed N-terminal truncation mutants of POT1a and POT1b, lacking the first OB-folds. We previously generated the corresponding human mutant and found that it displaces the endogenous human POT1 form telomeres. This allele retains the TPP1 interaction domain and acts as a dominant negative allele in the context of telomere length homeostasis. However, a telomere deprotection phenotype was not observed upon overexpression of human POT1ΔOB. Analogous POT1aΔOB and

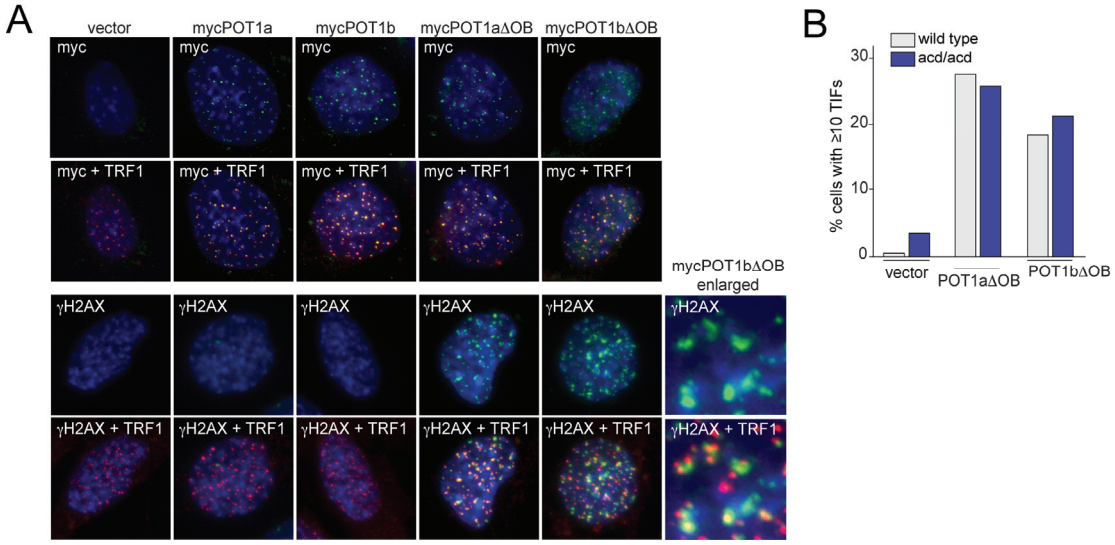

Figure 5.7 Overexpression of N-terminal truncation mutants of POT1a and -b lead to TIF formation

(A) MEFs of the indicated TPP1 genotypes were infected with pLPC N-MYC-POT1a, pLPC N-MYC-POT1b, pLPC N-MYCPOT1aΔOB, pLPC N-MYC-POT1bΔOB or vector control retrovirus (pLPC-N-MYC), selected for 4 days with puromycin and analyzed by IF for TRF1 (red), γ-H2AX (green) and counter stained with DAPI (blue). (B) Quantification of TIF positive cells shown in (A). Cells with 10 or more TRF1 signals co-localizing with γ−H2AX foci were scored as TIF positive. More that 120 cells were analyzed.

POT1bΔOB alleles were generated and found to accumulate at telomeres as predicted from the retention of their TPP1-binding domains (Fig. 5.7A).

The expression level of POT1aΔOB was somewhat higher than POT1bΔOB. Both proteins showed diminished expression in acd/acd cells, consistent with their dependence on TPP1 (Figure 5.8A). POT1bΔOB induced a strong increase in the amount of single-stranded telomeric DNA (Figure 5.8B and C) as expected if POT1b depends on TPP1 for

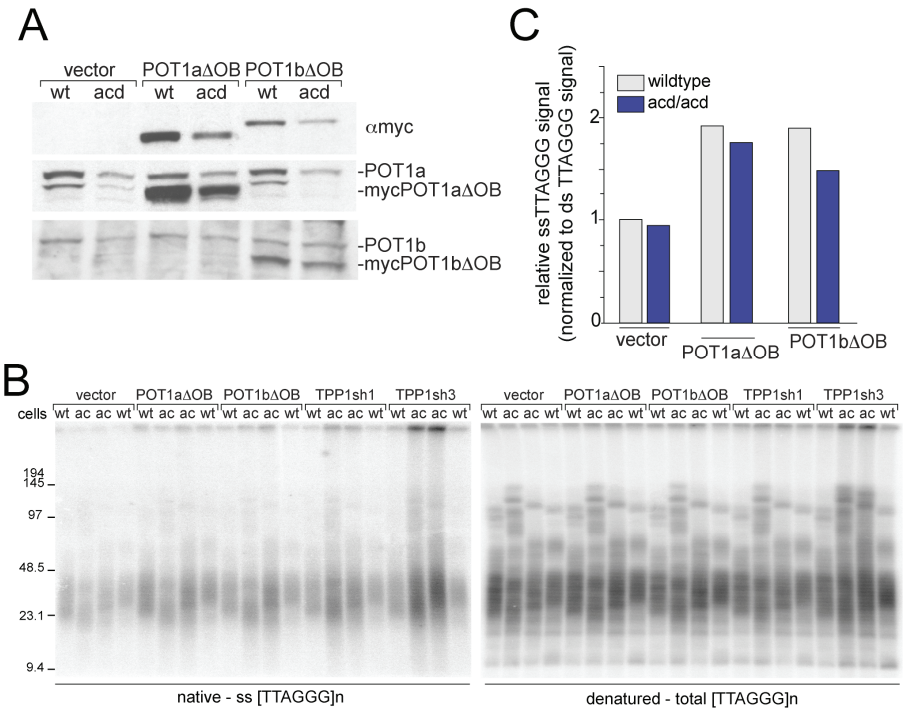

Figure 5.8 Pleiotropic effects of dominant negative alleles of POT1a and POT1b

(A) Immunoblots for MYC epitope tagged POT1aΔOB and POT1bΔOB in extracts of MEFs of the indicated TPP1 genotypes infected with pLPC POT1aΔOB, pLPC POT1bΔOB or vector control (pLPC N-MYC). Antibodies used are: MYC: 9E10, POT1a: 1221, POT1b: 1223. (B) In-gel overhang assay of MEFs of the indicated TPP1 genotypes (wild type (wt) and acd/acd (ac)) infected with pLPC N-MYC-POT1ΔOB, pLPC N-MYC-POT1bΔOB, TPP1 sh1, TPP1 sh3 or the vector control. Overhang assay was performed 5 days after selection with puromycin. (C) Quantification of the overhang signals from three different wild type or acd/acd MEF cell lines infected with pLPC N-MYC-POT1aΔOB, pLPC N-MYC-POT1bΔOB or vector control retrovirus. Error bars indicate the standard deviation of the mean of three experiments.

its ability to limit the length of the 3' overhang. The phenotype of POT1aΔOB was the induction of TIFs, suggesting that POT1aΔOB displaced POT1a from its TPP1 binding sites (Figure 5.7A and B). Interestingly, POT1bΔOB expression also elicited a TIF response (Figure 5.7A and B), which is a phenotype not observed in POT1b KO cells. Conversely, POT1aΔOB induced aberrantly high overhang signals, which is a phenotype specific for POT1b loss (Figure 5.8 B and C). The simplest interpretation of these data is that POT1a and POT1b both require TPP1 for telomere protection and that the TPP1 binding domains of POT1a and –b can displace the endogenous POT1a and –b from the telomeres.

Furthermore, these findings could explain the phenotypes observed in the POT1a KO generated by the Chang laboratory [164]. If their knockout strategy creates the predicted N-terminal truncated POT1a fragment (Figure 4.8), this protein would act as a dominant negative allele that impedes the function of POT1a and -b. This scenario is supported by the similarities between of Wu et al. the POT1a KO and our DKO phenotypes [164].

Additionally, the finding that N-terminal truncated forms of POT1b can act as a dominant negative on POT1a can explain another observation of the Chang laboratory [166]. They showed that overexpression of a POT1b allele bearing a point mutation in the DNA binding domain induces telomere fusions and the activation of a DNA damage response [166]. Contrary to our findings, they conclude that POT1b is necessary to prevent these phenotypes. Our finding that a dominant negative allele of POT1b can affect POT1a suggests that their phenotypes are primarily due to inhibition of POT1a, not POT1b.

Human POT1 requires human TPP1 to bind mouse telomeres

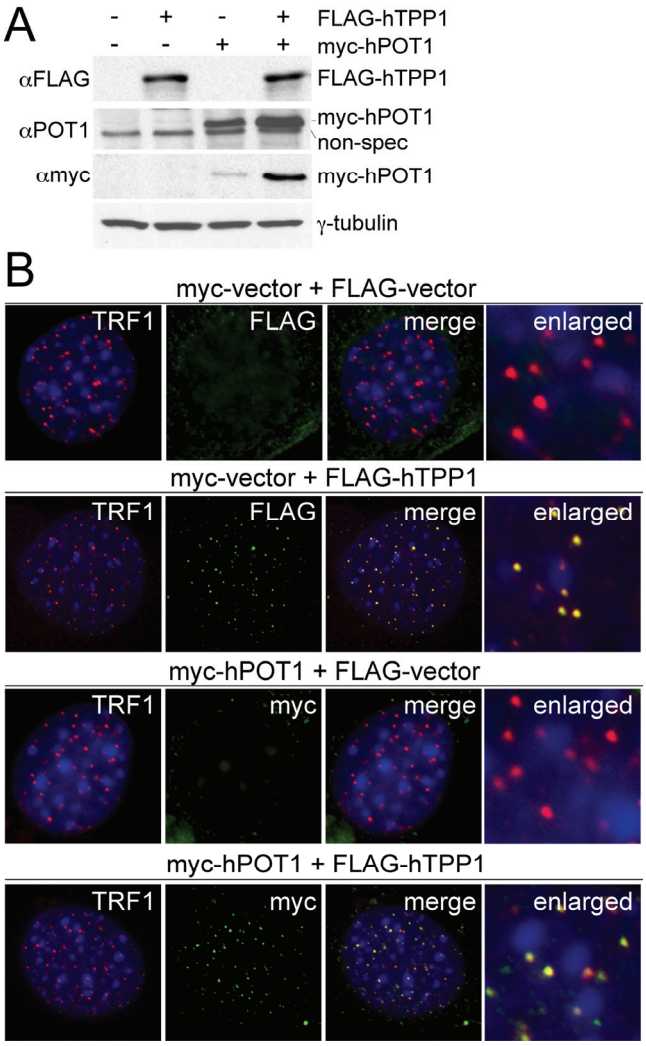

Figure 5.9 Human POT1 can be targeted to mouse telomeres by human TPP1

(A) Immunoblots for MYC epitope tagged human POT1 and Flag tagged human TPP1 on extracts from wt MEFs infected with pWzl-N-MYC-hPOT1 (hygromycin), pLPC-N-FLAGhTPP1 (puromycin), or vector control (pLPC). Antibodies used are: MYC (9E10), 1151 (TPP1) and 978 (hPOT1). Because the cells used in this experiment were already resistant to puromycin before the transduction of TPP1, TPP1 was introduced without subsequent selection. TPP1 infection efficiency was greater than 80% in all infections. (B) Immunofluorescence on cells described in (A). After selection with puromycin cells were analyzed by IF for TRF1 (Ab 644; red) and MYC and FLAG epitope tags of hPOT1 and TPP1 respectively (green) and counter stained with DAPI (blue).

As a further tool to test the dependence of POT1 on TPP1, we used the introduction of human proteins into mouse cells. Epitope tagged versions of human POT1 and TPP1 (hPOT1 and hTPP1) were expressed in wild type MEFs. Immunoblotting showed that the steady state level of hPOT1 was improved by co-expression of hTPP1 whereas the expression level of hTPP1 was independent of hPOT1 (Figure 5.9A). IF showed that hTPP1 by itself had the ability to accumulate at mouse telomeres whereas hPOT1 expressed alone did not localize to telomeres (Figure 5.9B). Presumably, the divergence in the pertinent regions of TPP1 and POT1 (approximately 30% and 10% changes among the relevant amino acid in TPP1 and POT1 respectively) has abrogated the ability of human POT1 to interact with the heterologous partner. However, hPOT1 accumulated at telomeres when it was co-expressed with hTPP1 (Figure 5.9B).

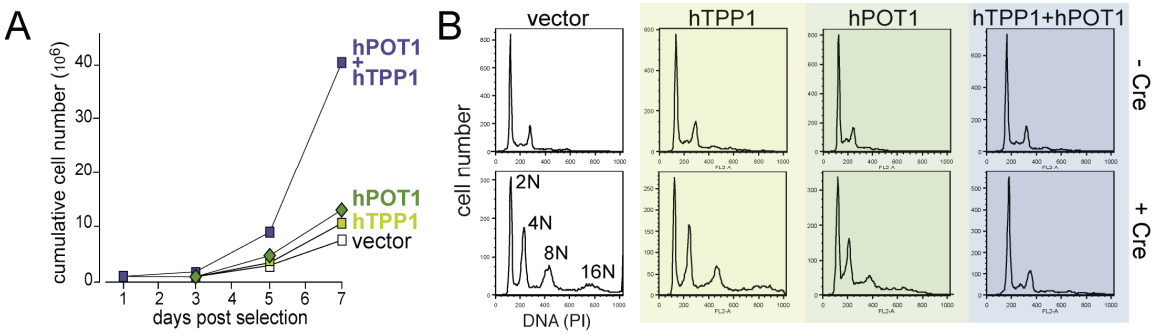

Figure 5.10 Human POT1 can suppress the growth defect and endoreduplcation of POT1 DKO cells when Co-expressed with human TPP1

(A) Growth curve of MEFs conditionally targeted for both POT1a and POT1b (POT1aSTOP/FLOX POT1bSTOP/FLOX) infected with the indicated retroviral constructs and with adenoviral Cre. The POT1 DKO cellular arrest and senescent morphology (data not shown) is rescued in cells infected with both hPOT1 and hTPP1. (B) FACS profiles of POT1aSTOP/FLOX POT1bSTOP/FLOX MEFs infected with pWzl-N-MYC-hPOT1, pLPC-N-FLAG-hTPP1, or vector control. Cells were infected with a hit-and-run Cre retrovirus to delete POT1a and POT1b. Cells were gated to remove sub-G1 peaks.

Human POT1/TPP1 can protect mouse telomeres from the DNA damage response

We next asked whether the combined expression of human POT1 and TPP1 resulted in repression of the phenotypes associated with the loss of POT1a and POT1b. SV40-LT

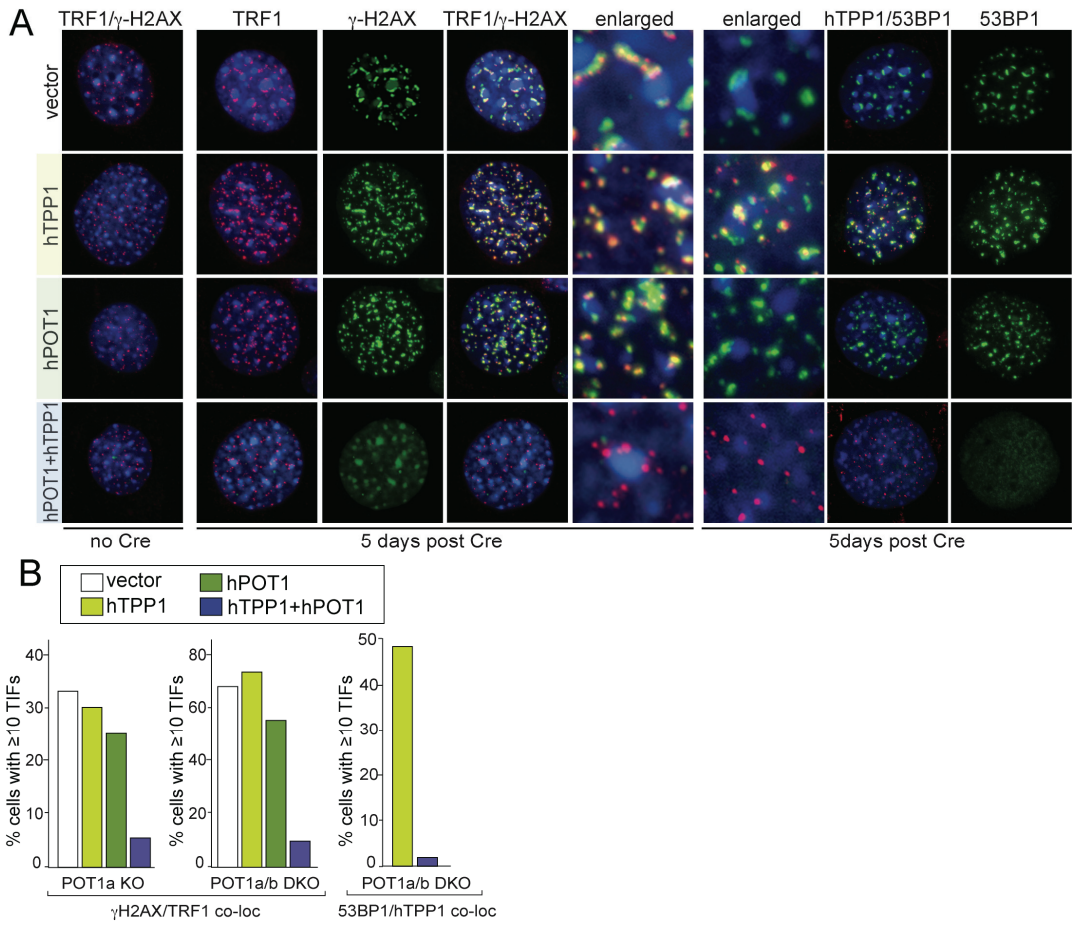

Figure 5.11 Human POT1 can suppress TIF formation in mouse POT1Ko cells when Co-expressed with human TPP1

(A) Cells from Figure 5.x-1 transduced with the indicated genes were analyzed by IF for TRF1 (red), γ-H2AX (green) and counter stained with DAPI (blue). Cells were also co-stained for the FLAG epitope tagged TPP1 (red) and γ-H2AX (green) to detect cells that were successfully transduced with TPP1 yet contained 53BP1 foci at their telomeres. (B) Quantification of TIF positive cells shown in (A). Cells with 10 or more TRF1 signals co-localizing with γ−H2AX foci were scored and more that 120 cells were analyzed. The quantification of TIF positive cells is shown in the left graph for POT1a KO cells and in the middle graph for POT1 DKO cells. The right graph shows the quantification of TPP1 foci colocalizing with 53BP1 in hTPP1 transduced DKO cells with and without the presence of hPOT1 (right graph).

immortalized mouse embryo fibroblasts carrying the conditional KO alleles of POT1a and POT1b were infected with retroviruses expressing human POT1 or human TPP1 (or both). After retroviral transduction, the cells were infected with adenoviral Cre-recombinase to delete POT1a and POT1b. The presence of human POT1 and TPP1 largely rescued the proliferation defect of the DKO cells, whereas DKO cells containing either human POT1 or TPP1 alone proliferated as poorly as the vector control (Figure 5.10A).

The combined expression of human POT1 and TPP1 also repressed the endoreduplication phenotype associated with the loss of POT1a and –b, based on FACS analysis (Figure 5.10B) and the increased total telomeric DNA signals in genomic blots loaded with equal cell equivalents (Figure 5.12A). In contrast, expression of hPOT1 or hTPP1 alone was not sufficient to suppress this phenotype (Figure 5.10B and 5.12A).

Finally, co-expression of human TPP1 and POT1 largely abrogated the formation of γ- H2AX and 53BP1 TIFs at mouse telomeres (Fig. 5.11 A and B), indicating that the presence of human TPP1/POT1 at telomeres allows mouse cells to make the distinction between DNA breaks and natural chromosome ends. In contrast to the complementation of the DNA damage response phenotypes of the POT1a/b DKO, the combined expression of human TPP1 and POT1 did not exert appropriate control over the structure of the telomere terminus. POT1a/b DKO cells expressing both human TPP1 and POT1 continued to carry an excess of single-stranded telomeric DNA (Figure 5.12 A and B). The lack of overhang control by human POT1 and by mouse POT1a indicates that the binding of POT1 to single-stranded DNA is not sufficient to execute this function. Perhaps the control of the overhang length requires a specific interaction between POT1b

and a mouse protein that can not be bound by POT1a or human POT1. These complementation analyses indicate the human POT1 can suppress phenotypes associated with the loss of POT1a, but not with the loss of POT1b. Further experiments will be necessary to determine why human POT1 fails to complement the POT1b KO and to address the relationship between human POT1 and POT1b.

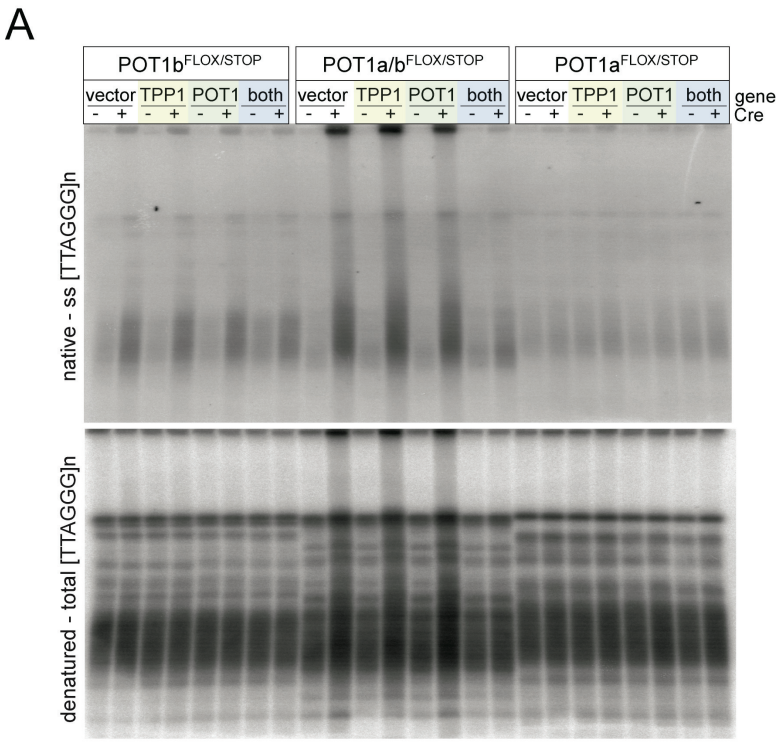

B

		vector	hTPP1	hPOT1	both
POT1a KO	-Cre	105	103	96	105
	+Cre	101	100	89	95
POT1b KO	-Cre	100	99	105	138
	+Cre	149	162	173	172
DKO	-Cre	108	123	111	132
	+Cre	166	190	150	143

Figure 5. 12 Human POT1 does not suppress the increase of single stranded telomeric DNA in POT1b KO and DKO cells

(A) In-gel overhang assay of POT1b, POT1a, and POT1a/POT1b conditionally targeted cells retrovirally transduced with pWzl-N-MYC-hPOT1, pLPC-N-FLAG-hTPP1 or vector. POT1 genes were deleted using H&R-cre and overhang length was determined 5 days after infection. The increase of telomeric DNA seen in the lanes 10,12, and 14 (from the left) are the result of endoredupliaction of POT1 DKO cells. Equal cell numbers were loaded in each lane (B) Quantification of telomeric overhang assay shown in (A).

Deletion of TRF2 results in diminished telomeric association of POT1a/b

The data presented above argue in favor of the correspondence of POT1/TPP1 to TEBPα/β. However, TEBPα/β is thought to bind telomeres by itself, whereas the proposed structure of shelterin predicts that TPP1 and POT1 are bound to the duplex part of the telomeric DNA through TIN2. As TIN2 interacts with both TRF1 and TRF2, it is expected that deletion of TRF2 would reduce the presence of TIN2, TPP1, and POT1 at telomeres but not fully remove these proteins. In human cells, inhibition of TRF2 with a dominant negative allele indeed results in partial loss of POT1 but the interpretation of the data was confounded by the fact that inhibition of TRF2 also removes part of the telomeric overhang. Therefore, it was not possible to distinguish between effects on the

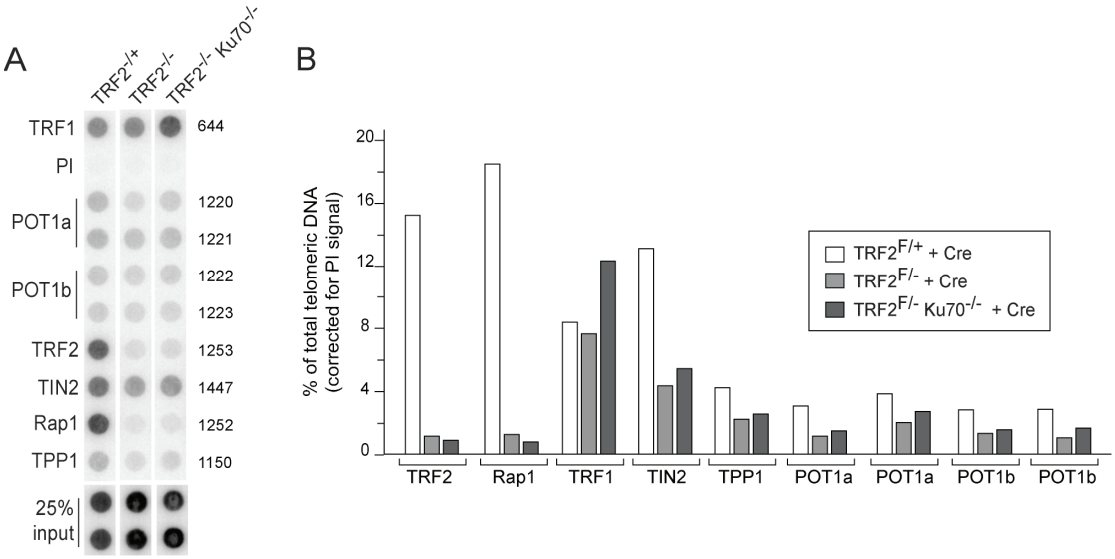

Figure 5.13 Diminished telomeric accumulation of POT1a and POT1b upon loss of TRF2

(A) Telomeric ChIP on cells lacking TRF2. The listed genotypes refer to the genotype at the time of the ChIP experiment which was done after infection with pWzl-Cre and 5 day selection with hygromycin B. The pre-recombination (floxed) genotypes were from left to right: TRF2F/+, TRF2F/-, and TRF2F/-Ku70-/-. Proteins and antibodies used in the ChIPs are indicated next to the dot-blots. (B) Quantification of the % of the total telomeric DNA recovered in the ChIPs shown in (A).

protein interactions of POT1 and its binding to the single-stranded telomeric DNA.

In order to further examine the contribution of TRF2 to the recruitment of TIN2, TPP1, and POT1 to telomeres, we used TRF2F/- MEFs from which TRF2 can be deleted with Cre. When TRF2 is deleted in Ku70-/- cells, the telomere fusion phenotype typical of TRF2 deficiency is largely abrogated and, importantly, the telomeric overhang remains intact. Therefore, in this setting, the effect of TRF2 on the telomeric recruitment of POT1 can be determined without the confounding aspects of overhang loss. ChIP on TRF2F/-Ku70-/- cells showed the expected loss of TRF2 and its interacting factor Rap1 from telomeres (Figure 5.13). TRF1 was not significantly affected but the telomeric association of TIN2, TPP1, POT1a and POT1b were reduced (Fig. 5.13). These data indicate the telomeric accumulation of the TIN2-TPP1-POT1 complex is in part dependent on TRF2. Previous data on human cells argued for a role of TRF1 in the telomeric association of POT1. Mouse cells lacking both TRF1 and TRF2 will be required to establish whether recruitment of POT1a and -b is entirely dependent on the duplex telomeric DNA binding proteins.

Discussion

Previous data argued that POT1a and POT1b have different functions at mouse telomeres. Our current work indicates that both proteins interact with shelterin and require TPP1 for their function. In addition overexpression of truncated forms of POT1a and POT1b that do not bind the telomeric overhang, result in POT1 DKO phenotypes, suggesting the function of POT1on the telomeric overhang is TPP1 dependent. Furthermore, our data suggest that POT1a and POT1b can compete for binding to TPP1. This cross-competition can explain the results that He et al. obtained with overexpression of a POT1b allele deficient in DNA binding. This allele induced end-to-end fusions and elicited a telomere DNA damage response, which are hallmarks of loss of POT1a, not POT1b. We propose that the POT1b allele used in those studies diminished the telomeric binding of POT1a, acting similar to the POT1bΔOB alleles described here. Similarly, the cross-competition of a dominant negative allele of POT1a with POT1b can explain the phenotypes of POT1a KO found by the Chang laboratory. The knockout strategy employed in that study is predicted to generate an N- terminal deletion with similar dominant effects as POT1ΔOB and may therefore elicit a phenotype similar to the POT1a/b DKO.

The data reported here argue against the view that POT1 proteins act alone to protect telomeres. Several lines of evidence indicate that POT1 requires an interaction with TPP1 to fulfill its function. Mouse POT1a and POT1b are dependent on TPP1 for recruitment to telomeres and removal of TPP1 from mouse telomeres results in telomere deprotection phenotypes similar to the POT1a/b DKO. Human POT1 by itself does not bind or protect mouse telomeres. But when co-expressed with human TPP1, human

POT1 can complement the essential functions of mouse POT1a/b. Finally, neither mouse nor human TPP1 is capable of protecting telomeres when POT1 is not present. Collectively the findings indicate that neither POT1, nor TPP1 are functional without their partner and that full telomere protection requires the interaction of both proteins at telomeres. It remains to be determined whether this cooperative telomere protection simply reflects TPP1's ability to position POT1 at telomeres or involves additional attributes of TPP1. The functional relationship of POT1 and TPP1 is consistent with the proposal that these factors are related to TEBPα/β. In vertebrates, the TEBPα/β orthologs are embedded within the shelterin complex which anchors POT1/TPP1 on the doublestranded part of the telomere. Although our data do not exclude the possibility that TPP1 and POT1 function as a heterodimer independent of the other shelterin components, we consider this unlikely because TPP1 interacts with TIN2 and its TIN2 binding domain is required for its telomeric accumulation. Furthermore, as we show here, the telomeric binding of TPP1 (and POT1a and b) is strongly diminished upon deletion of TRF2, one of the two proteins that anchor shelterin to the double-stranded telomeric DNA. Previous work showed that POT1 accumulation at telomeres is also diminished when TRF1 is removed. Therefore, we favor the view that TPP1/POT1 protects telomeres in the context of shelterin. The ciliate TEBPα/β complex appears to function without assistance of duplex telomeric DNA binding proteins.

Despite their relatedness to ciliate and fission yeast telomeric proteins, the mammalian POT1 proteins diverge rapidly. The preeminent example of this divergence is the acquisition of a second POT1 gene in rodents. The copy number difference between

rodents and other mammals is unlikely to be due to a gene deletion which would have had to occur more than once to explain the single POT1 gene of chicken, Xenopus, and most mammals. We also consider it unlikely that the sequenced nonrodent genomes contain an unrecognized second POT1 gene because the missing POT1 is expected to have at least 70% sequence identity to its homologs. Thus, the most parsimonious interpretation is that the two POT1 proteins of rodents originate from a recent (~75 My) gene duplication. In addition to the POT1 gene duplication, the divergence of human and mouse POT1 apparently prohibits a cross-species interaction with TPP1. In contrast, human TPP1 is capable of interacting with mouse TIN2. Our data also hints at a functional divergence of human and mouse POT1. Whereas human TPP1/POT1 appears to effectively complement the loss of POT1a, the human proteins fail to take on the role of POT1b in limiting the amount of single-stranded telomeric DNA. The question whether POT1b has evolved a new function not represented by human POT1 will require further analysis. Together the data illuminate recent (75 Mya) variations on a telomere theme that has played a major role at chromosome ends for at least 1.5 Gya.

6. The role of POT1b in telomere overhang generation and maintenance

Introduction

Although it has been previously shown that shelterin is necessary to maintain the telomeric overhang, the finding that POT1b loss leads to longer telomeric overhangs shows for the first time that shelterin also prevent the excessive elongation of overhangs. Since POT1b loss induces overhang extension independent of telomerase activity, we reasoned that this process could either be the result of elongation by a DNA polymerase other than telomerase, nucleolytic degradation of the C-rich telomeric strand, or incomplete C-rich-lagging-strand DNA synthesis. Degradation of the telomeric C-rich strand as well as the untimely uncoupling of leading and lagging strand synthesis is predicted to result in the overall loss of telomeric DNA. If this loss of telomeric DNA is not counteracted by telomerase, both processes would lead to telomere shortening. By contrast, if a DNA polymerase generates the extended overhangs, telomere shortening is not anticipated. These possibilities can be distinguished by determining the telomere shortening rate in cells that lack both POT1b and telomerase. If the telomere shortening of telomerase negative cells were accelerated by POT1b deficiency, we would conclude that the longer overhangs in POT1b KO cells are generated at the expense of double stranded telomeric DNA.

The hypothesis that loss of POT1b leads to C-strand resection seems possible, as a similar phenotype can be found in yeast after the loss of Cdc13, the single stranded telomeric binding protein of *S. cerevisiae* [149,167]. Cdc13 deficient cells accumulate single

stranded telomeric DNA generated by exonucleolyitc degradation of the C-strand telomeric DNA. This excess of single stranded DNA leads to the activation of a Rad9 andRad24 dependent DNA-damage checkpoint and a cell cycle arrest in G2 [148,149,168]. The generation of single stranded DNA was found to be partially dependent on the 5' to 3' exonuclease, Exo1. In addition to Exo1, at least two other nucleases are proposed be involved in this pathway. Although these other nucleases are not yet identified, it is known that their activity is controlled by Rad24, a clamp loader for the yeast homologue of the 9-1-1 complex, and by Rad9 [160].

In this chapter, I provide evidence to support the notion that POT1b controls a nuclease. I show that loss of POT1b leads to accelerated telomere shortening that is not fully counteracted by telomerase. As a consequence POT1b deficiency results in delayed phenotypes *in vitro* and *in vivo*. Finally, I report on a preliminary search for the culprit nuclease.

Results

POT1b loss results in accelerated telomere shortening regardless of the telomerase status

In order to distinguish between extension by the overhang by a polymerase or C-strand resection by a nuclease, POT1-/- MEFs were cultured for more than 100 PDs and changes in telomere length monitored. The results in Figure 6.1 show progressive telomere shortening in POT1-/- cells. The data also document the persistence of elongated overhangs in POT1b -/- cells in long-term cultures (Figure 6.1).

Based on telomere length measurements at the different time points we calculated a telomere shortening rate of about 300-500 bp/PD for POT1b deficient cells, while telomeres of control cells maintained a constant length. As telomeres of telomerase deficient cells shorten with about 60-80 base pairs per population doublings, telomere shortening in POT1b deficient cells is accelerated as the result of active telomere degradation. This telomere shortening phenotype is specific for POT1b, as the loss of POT1a does not result in any detectable telomere length changes (Figure 6.2). This finding is in contrast to the data of Wu et al. [164] that show that loss of POT1a leads to telomere elongation after only a few PDs. It remains unclear if this telomere elongation can also be explained by a dominant negative effect (see chapter 5).

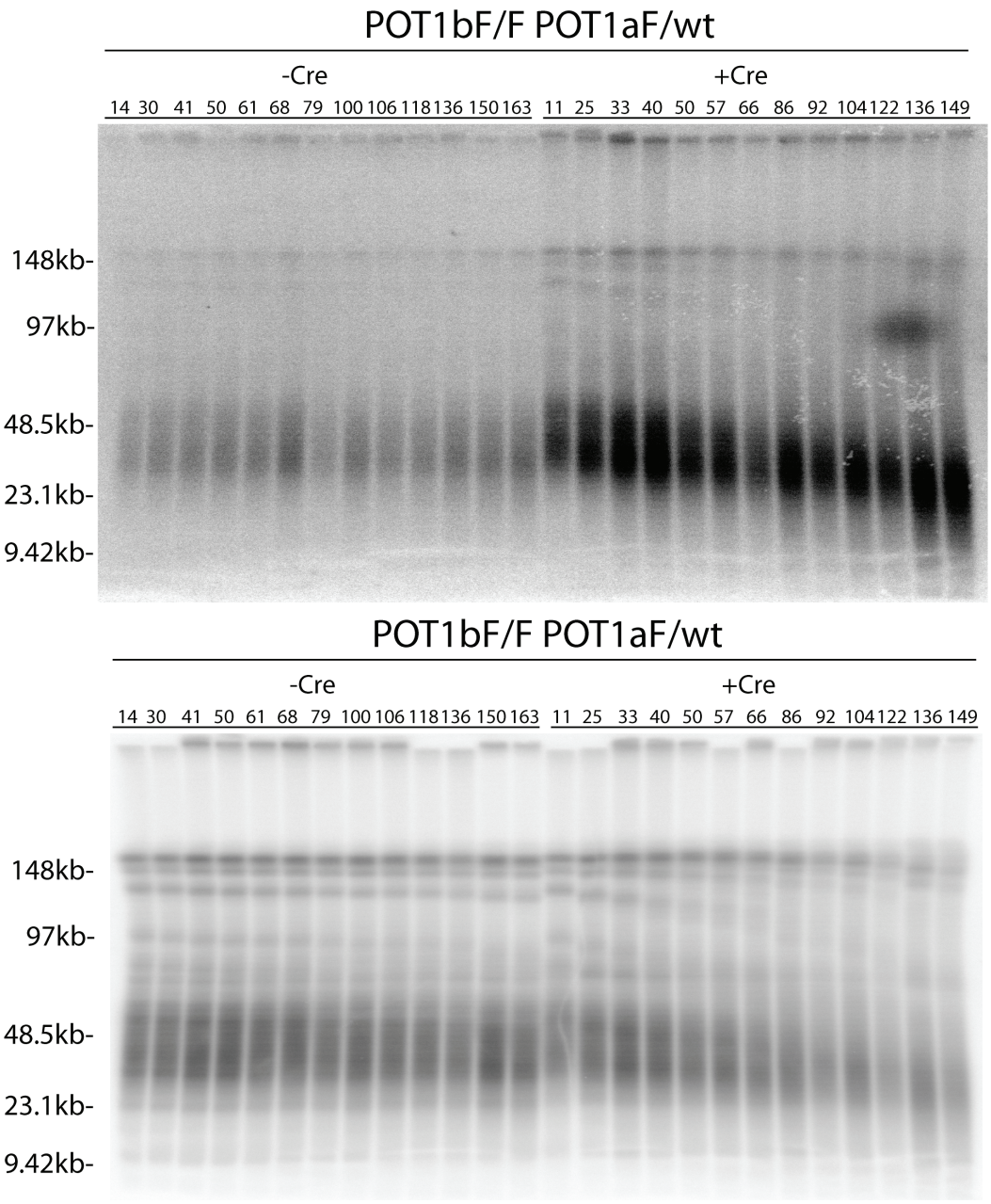

Figure 6.1 POT1b loss leads to progressive telomere shortening

Telomere overhang and telomere length analysis of POT1b S/F, POT1a F/wt MEFs infected with pWzl-Cre or the pWzl control vector. DNA from MEFs of the indicated accumulative population doublings was analyzed using the in-gel telomere overhang assay. The top image shows hybridization signal using the TelC probe ($[CCCTAA]_4$) under native conditions detecting the telomeric 3′ overhang. The bottom image shows the total telomeric hybridization signal obtained with the same probe after in-gel denaturation of the DNA.

Telomeres of MEFs are normally maintained at a constant length through the constitutive expression of telomerase. In order to address if telomerase is capable of partially counteracting the telomere shortening in cells lacking POT1b, we monitored telomere length changes in POT1b deficient MEFs that are either heterozygous or homozygous deleted for the telomerase RNA component, mTR. As heterozygosity for mTR is haploinsufficient, analysis of mTR heterozygous cells can already reveal effects caused by reduced telomerase activity. We found that telomeres in cells heterozygous (Figure 6.3) or deleted for mTR (Figure 6.2-6.4) shorten after POT1b deletion with similar rates as telomerase proficient cells. This result suggests that telomerase is not compensating for POT1b loss induced telomere erosion.

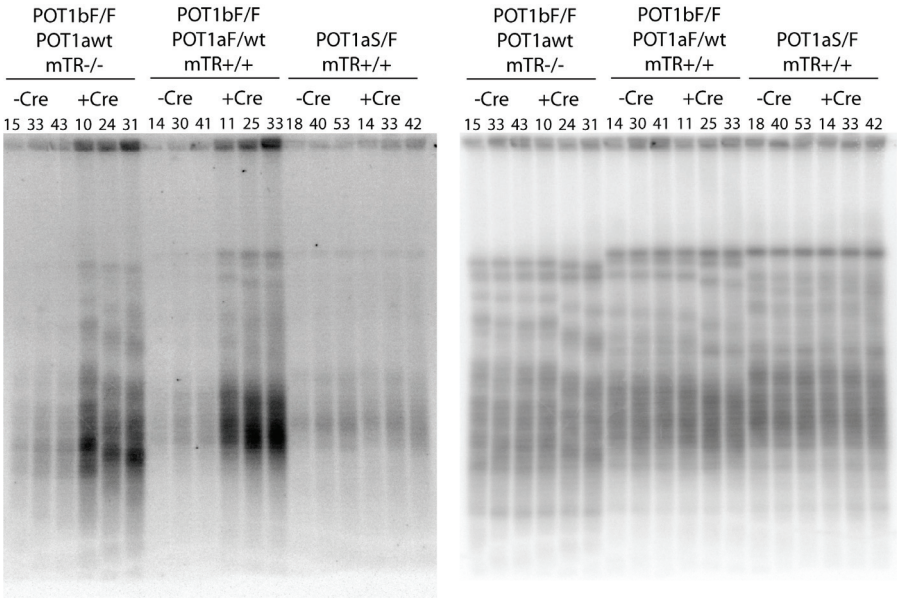

Figure 6.2 Telomere shortening in wild type and POT1b telomerase double deficient cells

Telomere overhang and telomere length analysis of MEFs with the indicated genotypes. MEFs were infected with pWlz-Cre or the pWzl control vector. DNA from MEFs of the indicated accumulative population doublings was analyzed using the in-gel telomere overhang assay. The left image shows hybridization signal using the TelC probe ([CCCTAA]4) under native conditions detecting the telomeric 3′ overhang. The right image shows the total telomeric hybridization signal obtained with the same probe after in-gel denaturation of the DNA.

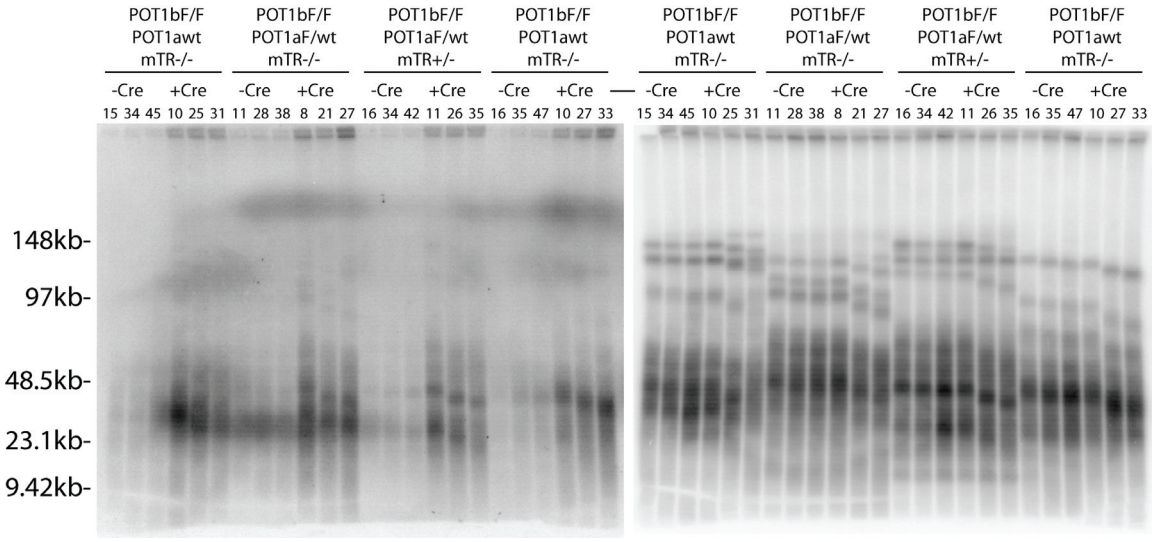

Figure 6.3 Telomere shortening in POT1b cells heterozygous or deficient for telomerase

Telomere overhang and telomere length analysis of MEFs with the indicated genotypes. MEFs were infected with pWlz-Cre or the pWzl control vector. DNA from MEFs of the indicated accumulative population doublings was analyzed using the in-gel telomere overhang assay. The left image shows hybridization signal using the TelC probe ([CCCTAA]4) under native conditions detecting the telomeric 3′ overhang. The right image shows the total telomeric hybridization signal obtained with the same probe after in-gel denaturation of the DNA.

POT1b loss accelerates telomere length induced crisis

To determine the consequences of telomere shortening after POT1b loss, we monitored the growth of telomerase negative cell clones after the deletion of POT1b. Long-term culture of these clones reveals that cells deficient for POT1b and telomerase enter crisis earlier than cells lacking only telomerase (Figure 6.5A). This growth defect is caused by the loss of POT1b, as retroviral infection with a POT1b cDNA restores the proliferation of these cells (Figure 6.5B). In-gel overhang analysis shows that the telomeric overhang of these clones is still elongated after several months in culture and that telomeres, which

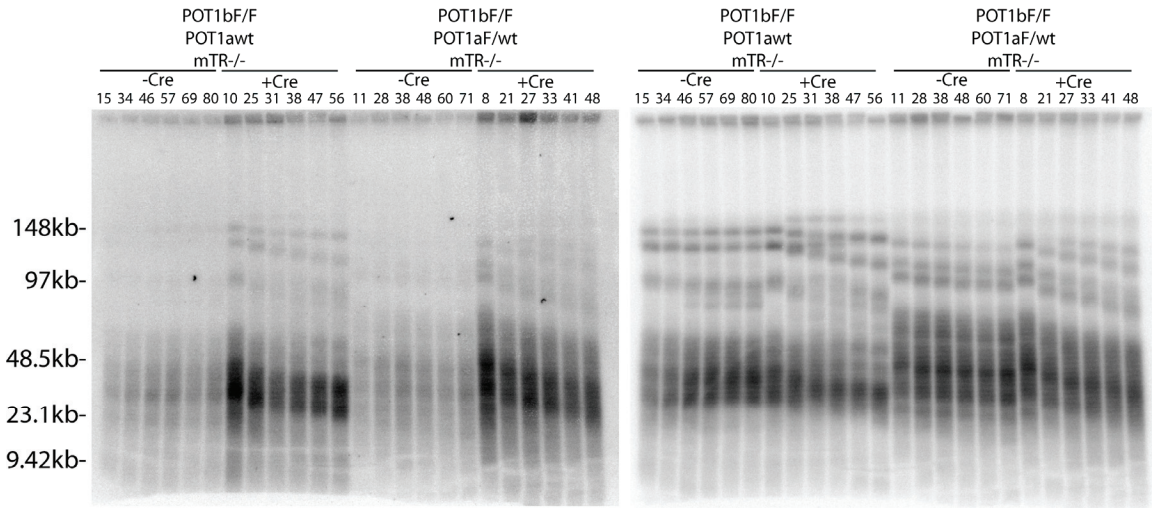

Figure 6.4 Telomere shortening in POT1b telomerase double deficient cells

Telomere overhang and telomere length analysis of MEFs with the indicated genotypes. MEFs were infected with pWlz-Cre or the pWzl control vector. DNA from MEFs of the indicated accumulative population doublings was analyzed using the in-gel telomere overhang assay. The left image shows hybridization signal using the TelC probe ([CCCTAA]4) under native conditions detecting the telomeric 3′ overhang. The right image shows the total telomeric hybridization signal obtained with the same probe after in-gel denaturation of the DNA.

are already very short, continue to shorten (Figure 6.5C). Cells that are POT1b/mTR double deficient enter crisis after approximately 40-50 days after POT1b deletion. Metaphases of these cells contain a high number of very short telomeres as indicated by the lack of hybridization of a telomere specific FISH probe (Figure 6.6A). Furthermore, cells deficient for mTR and POT1b accumulate Robertsonian fusions, which are stable in mitosis. Robertsonian fusions are indicative of critically short telomeres. POT1b deficient cells that retain telomerase activity also present Robertsonian fusions but at a lower frequency suggesting that telomerase can partially counteract the telomere shortening after POT1b loss.

Figure 6.5 POT1b deficiency exacerbates effect of telomere shortening in telomere knockout cells

(A) Growth curve of individual cell clones from POT1bF/F mTR-/- isolated either after the deletion of POT1b with pWzl-Cre (1C3, 1C5, 1C9, 1C13 and 1C14) or after the infection with pWzl vector control (1V1). The growth curve was started about 60 days after plating the cells for sub-cloning and about 120 days after the retroviral infections with pWzl or pWzl-Cre (B) Rescue of POT1b loss induced growth defect w by retroviral infections with the POT1b cDNA. Cells described in (A) were infected either with POT1b cDNA (POT1b) or an empty vector control (vector). The clones 1V1 (POT1b+/+), 1C3 (clone1) and 1C9 (clone2) shown in panel (A) were analyses. (C) Telomere overhang and telomere length analysis of the clones shown in panel (A) and panel (B). For each clone two time points are loaded in lanes next to each other. The first time point corresponds to day 30 of the growth curve shown in (A), while the second time point corresponds to day 39. The left image shows hybridization signal using the TelC probe ([CCCTAA]4) under native conditions detecting the telomeric 3′ overhang. The right image shows the total telomeric hybridization signal obtained with the same probe after in-gel denaturation of the DNA.

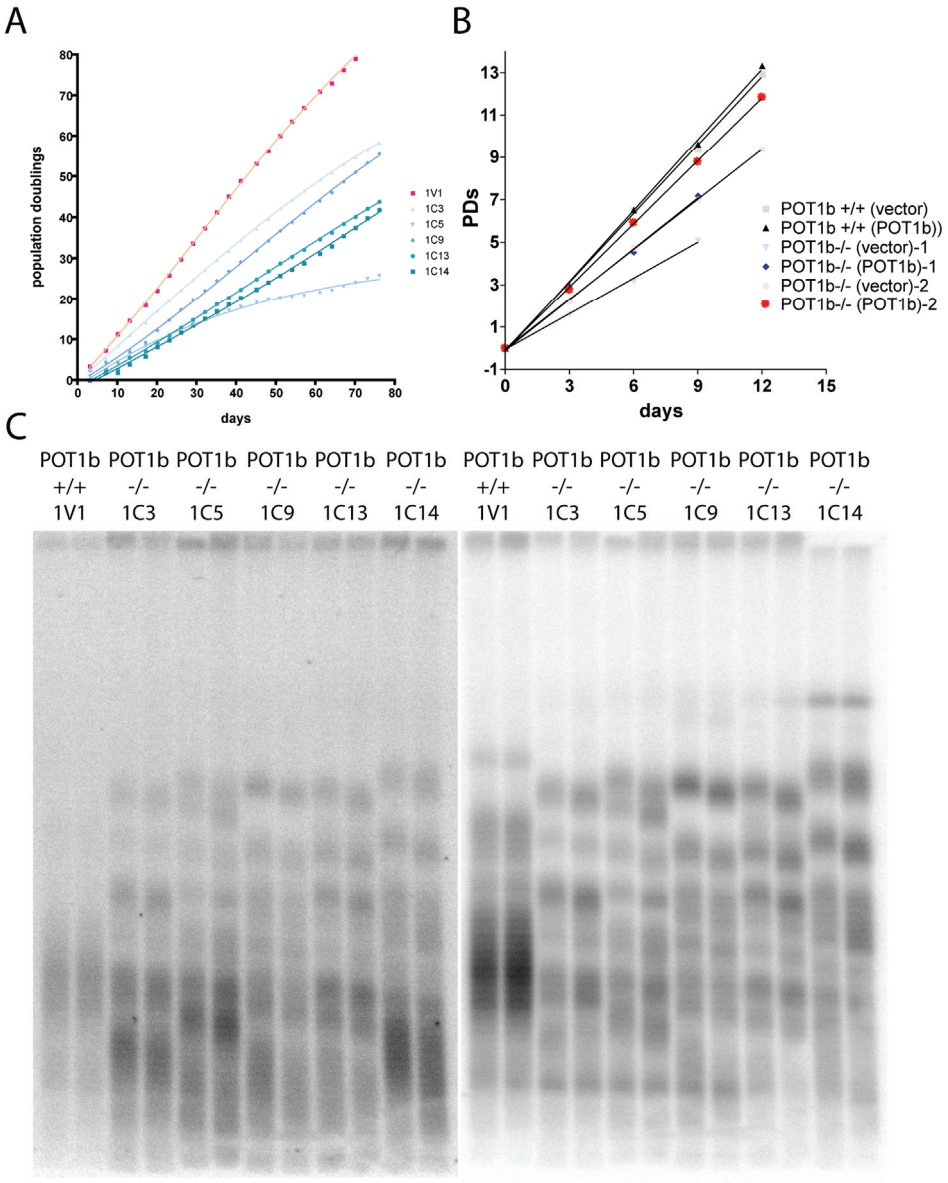
A
population doublings
days
1V1
1C3
1C5
1C9
1C13
1C14
B
PDs
days
POT1b +/+ (vector)
POT1b +/+ (POT1b))
POT1b-/- (vector)-1
POT1b-/- (POT1b)-1
POT1b-/- (vector)-2
POT1b-/- (POT1b)-2
C
POT1b +/+ 1V1
POT1b -/- 1C3
POT1b -/- 1C5
POT1b -/- 1C9
POT1b -/- 1C13
POT1b -/- 1C14

A

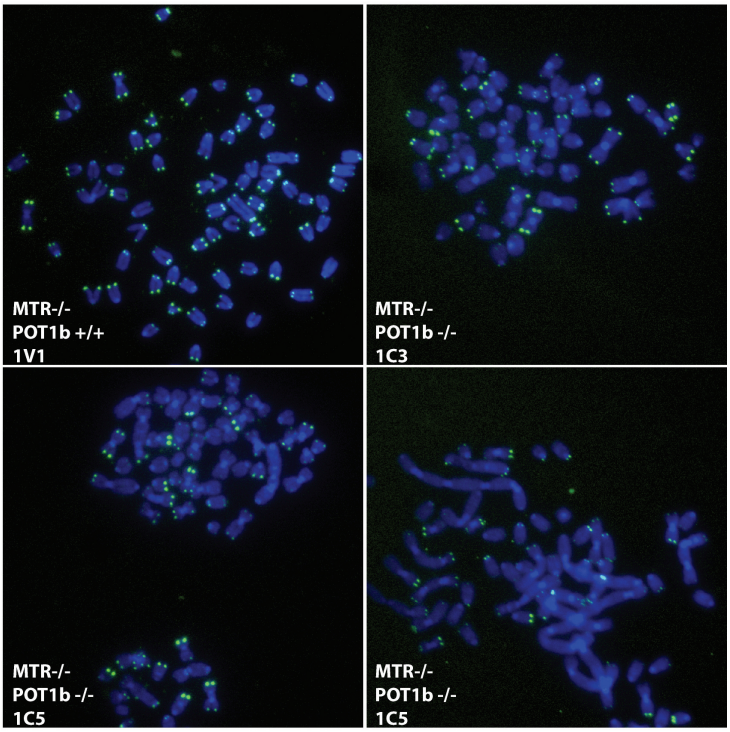

B

	1V1	1C3	1C5
POT1b	+/+	-/-	-/-
MTR	-/-	-/-	-/-
# of chromosomes analysed	1362	1283	1V1
short-arm fusions without signal	67	282	292
short-arm fusions with signal	1	0	1
long-arm fusions without signal	15	45	178
long-arm fusions with signal	0	0	0
% of chromosomes with fusion	6.09	25.49	41.96

Figure 6.6 POT1b loss leads to a increase of Robertsonian fusions in telomerase deficient cells

(A) Metaphase spreads of cell clones shown in Figure 6.5 with telomeric DNA detected by FISH (green); DNA stained with DAPI (in blue). The clones 1V1 (POT1b+/+, mTR-/-), 1C3 (POT1b-/-, mTR-/-) and 1C5 (POT1b-/-, mTR-/-) were analyzed at day 40 of the growth curve shown in panel (A) of Figure 6.5. (B) Frequencies of aberrant chromosomes in metaphases shown in (A).

POT1b deficient mice show phenotypes associated with critically short telomeres

The finding that POT1b loss in MEFs results in telomere shortening, led us to investigate the phenotypes of POT1b deficient mice in more detail. The phenotypes discussed below are found in mice in which the POT1b gene was disrupted by either homozygous deletion of exon 3 (POT1bΔ/Δ) or by the presence of a STOP cassette on both POT1b alleles (POT1bS/S). Most results presented here came from the analysis of POT1bS/S mice. Nevertheless, experiments on POT1bΔ/Δ mice MEFs suggest that the POT1b STOP allele and the POT1b Δexon 3 allele are equivalent and both represent a POT1b null allele.

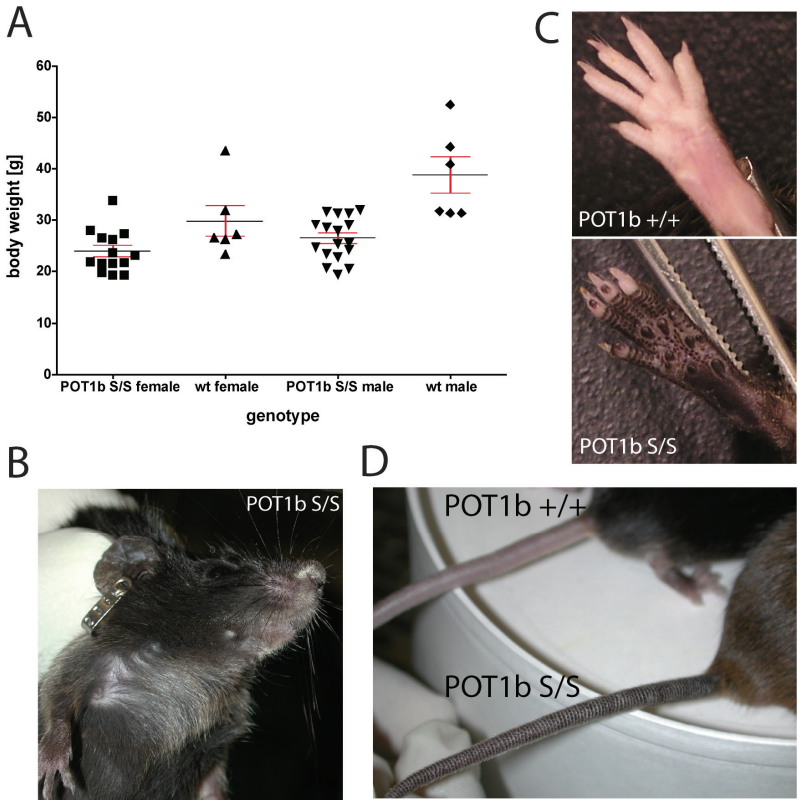

Figure 6.7 Reduced bodyweight and hyperpigmentation of POT1bS/S mice

(A) Bodyweight of POT1bS/S and control animals older than 3 month, separated by gender. (B-D) Pictures of POT1b mice and control animals showing the hyperpigmentation of the ears and snout (B) the paws (C) and the tails (D) of POT1bS/S animals.

Although POT1b KO mice are alive, we observed that POT1b deficient animals do not grow to the same size and weight as their littermates. (Figure 6.7A). Furthermore, while littermate controls have normal pigmentation, POT1b knockout animals show hyperpigmentation of the paws (Figure 6.7C), snout, ears (Figure 6.7B) and tail (Figure 6.7D). This defect is progressive and becomes prominent after three to four month of age. Interestingly, POT1bS/S mice show generational anticipation of this phenotype, as consecutive generations of homozygous intercrosses of POT1bS/S mice show hyperpigmentation at progressively earlier age. Hyperpigmentation is also a phenotype of the TPP1 mutant acd mice and can be seen in patients suffering from dyskeratosis congenita, a disease that is caused by lack of telomerase activity.

In addition to these external phenotypes of the POT1bS/S mice, we noticed that POT1bS/S mice become infertile at young age (approximately 6 month after birth). Preliminary data suggest that this phenotype also shows anticipation, as later generations of POT1bS/S mice show male sterility with an earlier time of onset. In the sixth generation (G6) of POT1bS/S intercrosses the males fail to impregnate wild type females. Gross examination shows that testis of age matched wild type control animals are about three times larger than testis of POT1bS/S males (Figure 6.8A and B). Histological analysis of testis from POT1bS/S males reveals that POT1b deficient mice suffer from testicular atrophy (Figure 6.8C). Testicular atrophy is a marked phenotype of the acd mice and of late generation telomerase KO mice.

Given the similarities between the POT1b KO and late generation telomerase KO mice, we investigated other highly proliferative organs known to be affected by loss of telomerase. We found that POT1bS/S mice have reduced numbers of peripheral white

blood cells and a pronounced lymphopenia. Moreover, we noticed a strong increase in apoptotic cells based on TUNEL in the small intestine of POT1bS/S mice compared to wild type control animals. This finding could suggest that POT1b loss results in the depletion of the stem cell compartment of highly proliferative tissues in a similar fashion as it is seen in the late generation of the telomerase KO.

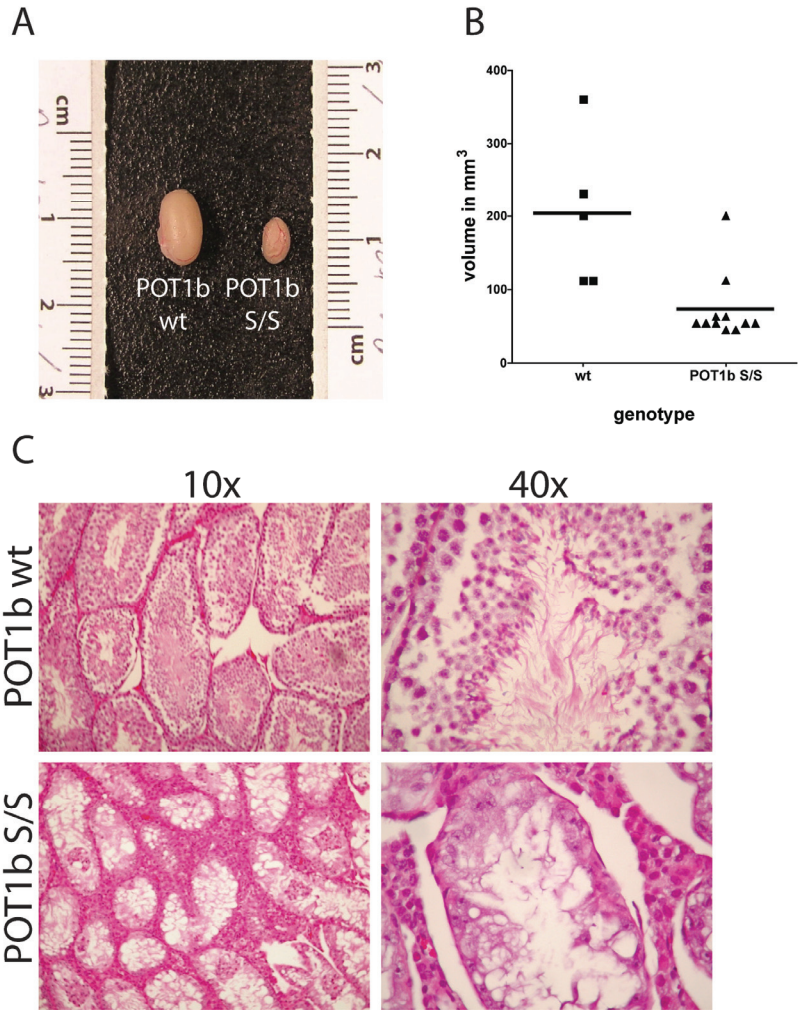

Figure 6.8 Testicular atrophy in POT1bS/S mice

(A) Photograph of testis from POT1b S/S and control animals. (B) Quantification of testis volume of POT1b S/S and control animals. Histological analysis of testis from POT1b S/S and control animals stained with Haematoxilin and eosine shown at two magnifications (10x left and 40x right)

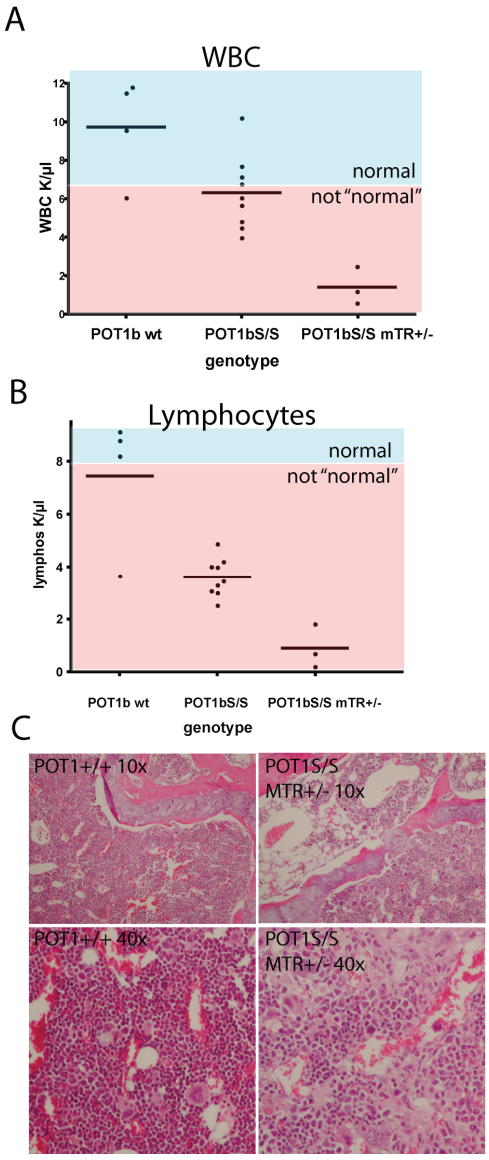

Figure 6.9 POT1b loss leads to lymphopenia

(A) Quantification of peripheral white blood cell (WBC) counts of POT1b S/S, POT1b S/S mTR+/- and control animals. Shaded in blue and labeled "normal" is the range of WBC counts that are expected in healthy animals according to the literature. "Not normal" and shaded in red is the range of WBC counts that are below the literature values. (B) Quantification of peripheral blood lymphocyte counts of POT1b S/S, POT1b S/S mTR+/- and control animals. Shaded in blue and labeled "normal" is the range of lymphocyte counts that is expected in healthy animals. "Not normal and shaded in red is the lymphocyte counts that are below the literature values expected for healthy animals. (C) Histological analysis of bone marrow section (femur) form POT1b S/S, mTR+/- and control animals stained with Haematoxilin and eosine shown at two magnifications (10x top and 40x bottom)

In order to determine the relationship between the phenotypes caused by telomerase loss and POT1b loss we crossed mTR KO mice with POT1b KO mice. Kaplan-Meyer analysis revealed the POT1b and telomerase are not epistatic (Figure 6.9A). While G5 POT1bS/S mice do not show a premature lethality, mice that are heterozygous for mTR and deficient for POT1b die untimely. These POT1bS/S mTR+/- mice are the offspring of crosses between generation 5 POT1S/S mTR+/+ mice and POT1bS/wt mTR-/- mice. The offspring of this cross is born with the expected Mendelian distribution: 50% being POT1bS/S mTR +/-, 50% being POT1b S/wt mTR+/-. We conclude that POT1b deficiency is responsible for the premature lethality of the POT1bS/S mTR+/- mice, as their POT1b S/wt mTR +/- littermates do not die early (Figure 6.9A). POT1bS/S mTR+/- mice have a white blood cell count that is lower than the POT1bS/S mice (Figure 6.8A and B). Furthermore, histological analysis shows that POT1bS/S mTR+/- mice suffer from bone marrow depletion, a phenotype that is less severe in the POT1bS/S and not found in control animals (Figure 6.8A and B). As mTR is haplo-insufficient, this result suggests that reduced telomerase activity enhances the phenotype of POT1b loss.

In order to determine the consequences of POT1b loss in telomerase null mice, we inter-crossed POT1bΔ/+ mTR+/- mice. The offspring of this cross did not show a Mendelian distribution of genotypes (Figure 6.9 B). Out of a total of 91 live offsrings, 1, rather than 6, had the POT1bΔ/Δ mTR-/- genotype. This mouse was small, nude, failed to thrive, and died at three weeks of age (Figure 6.9C-E).

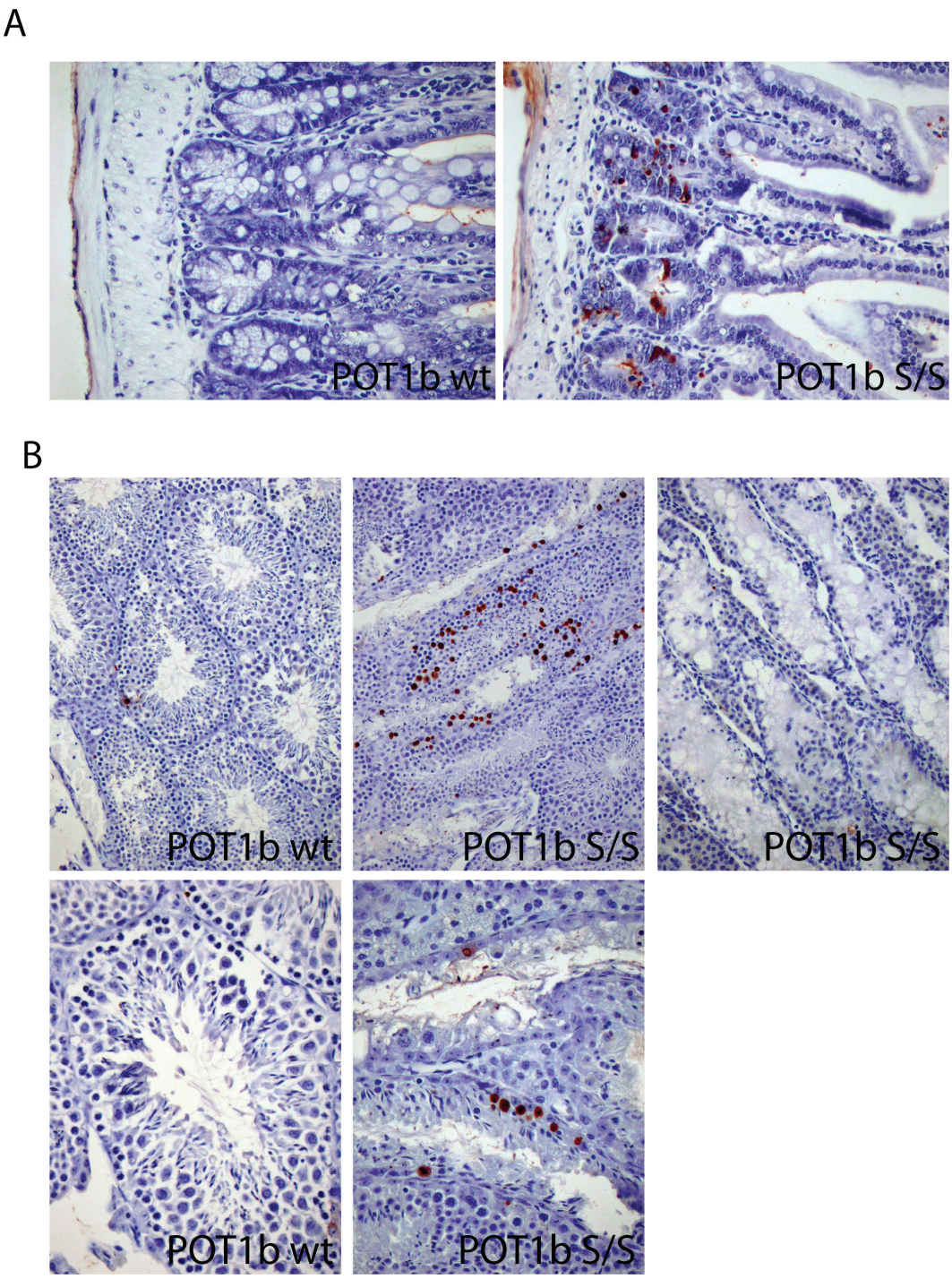

Figure 6.10 Increase apoptosis in the small intestine and testis of POT1bS/S mice

(A) Immuno-histochemical TUNEL staining of small intestine of wild type and POT1b S/S mice counterstained with Haematoxilin (B) Immuno-histochemical TUNEL staining of testis of wild type and POT1b S/S mice counterstained with Haematoxilin. The left images show staining of testis of wild type mice; the middle image shows the staining of testis from a 3 month old POT1b S/S mice, while the right image shows the staining of a 1 year old POT1b S/S mouse. The lack of apoptosis in these mice is due to the complete loss of sperm progenitor cells.

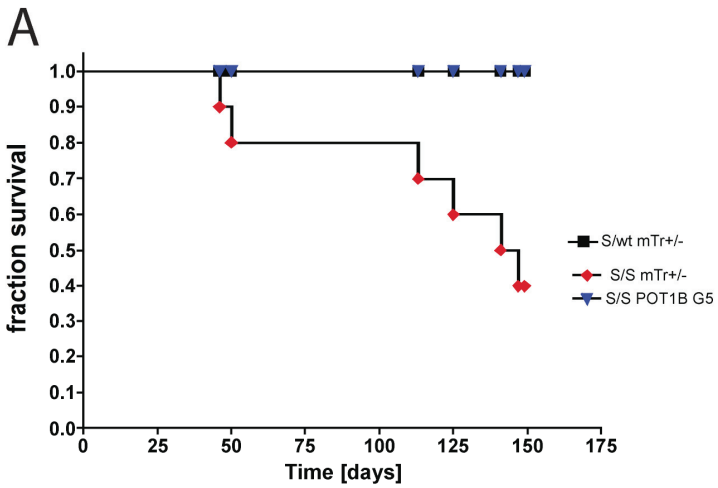

B

	mTR +/+	mTR +/-	mTR -/-
POT1b wt	10 (5.7)	12 (11.4)	8 (5.7)
POT1b +/-	14 (11.4)	17 (22.75)	8 (11.4)
POT1b -/-	3 (5.7)	18 (11.4)	1 (5.7)
	total: 26 (22.75)	total: 47 (45.5)	total: 17 (22.75)

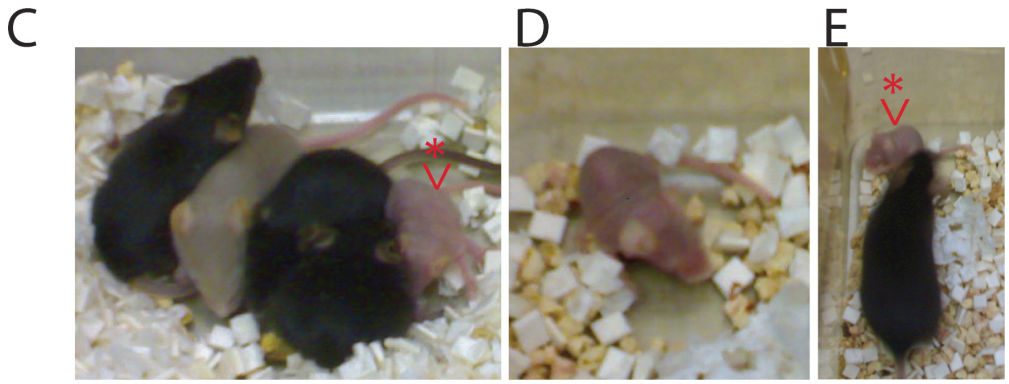

Figure 6.11 Telomerase is in POT1b mice

(A) Kaplan-Meyer analysis of generation 5 POT1bS/S mice and the offspring of intercrosses between generation 5 POT1bS/S and POT1bS/wt mTR-/- and control animals. (B) Mendelian distribution the offspring of POT1b Δ/wt mTR+/- intercrosses. Black numbers give the numbers born for each of the genotypes and the numbers in blue indicate the numbers expected for a normal Mendelian distribution (C) Photograph of the only POT1b-/- mTR-/- mouse born (D) form the cross described in panel (B) shown in size comparison to its littermates (C) and its mother (E). The POT1b-/- mTR-/- mouse is indicated with a red >*.

Exonuclease 1 is implicated in the degradation of telomeric DNA upon POT1b loss

In order to understand the process that leads to the increased overhang after POT1b loss and presumably to the telomere shortening of POT1b deficient cells, we designed a candidate screen to identify the putative nuclease that resects the telomeric C-strand after POT1b loss. In this screen, we retrovirally transduced POT1b KO cells with three independent shRNAs for each candidate gene. We reasoned that not only the knockdown of the nuclease itself but also the knockdown of proteins essential for its function would result in a decrease of overhang length in POT1b deficient cells. Therefore we not only included nucleases in this screen, but also determined the effects of candidate helicases and other genes implied in telomere DNA metabolism. Using in-gel hybridization we compared the amount of single-stranded telomeric DNA of POT1b KO cells infected with shRNAs targeting these candidate genes with cells infected with either a vector control or with a rescuing POT1b cDNA. An example of these experiments is shown in Figure 6.10.

As expected, we found that transduction of POT1b deficient cells with the POT1b cDNA restored the normal telomere overhang length (Figure 6.10 A and B). We did not note a decrease of overhang signal after the knockdown of the nucleases Mre11, Apollo, Artemis, Ercc4, Ercc5, EME1, Mus81, and Fen1. We also did not find a decrease in overhang signal in POT1b deficient cells that were depleted for the helicases Wrn, PIF1 and DNA2L or in cells with diminished protein levels for the members of the 9-1-1 complex (Rad1, Hus1a, Hus1b, Rad9a and Rad9b). Furthermore, we did not find an effect on overhang signal after inhibition of Brca2 and Brca1, genes involved in the recognition of single to double strand DNA transitions homologous recombination.

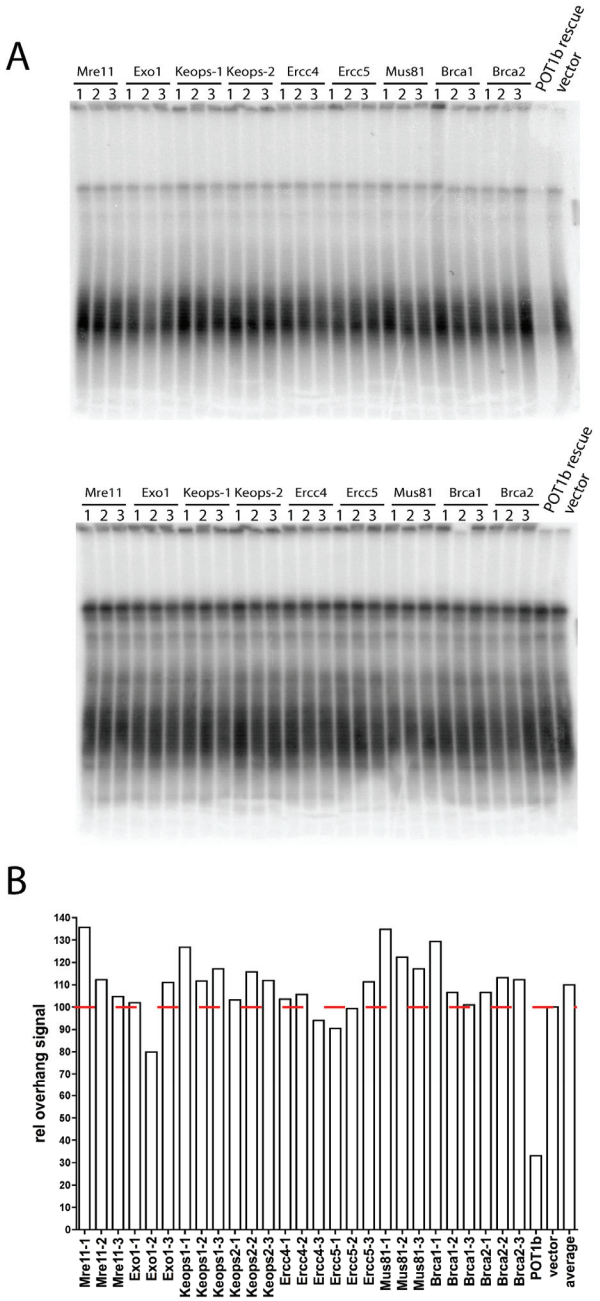

Figure 6.12 Candidate screen to identify the nuclease generating excessive single stranded telomeric DNA in POT1b KO cells

(A) Example for the overhang analysis of POT1b deficient cells after of shRNA knockdowns of candidate genes. POT1b deficient cells were infected with three independent shRNAs (1-3) targeting the indicated genes. As controls cells were infected in parallel with a POT1b cDNA or with a vector control (shown in the last two lanes). The top image shows hybridization signal using the TelC probe ([CCCTAA]4) under native conditions detecting the telomeric 3′ overhang. The bottom image shows the total telomeric hybridization signal obtained with the same probe after in-gel denaturation of the DNA. (B) Quantification of relative overhang signal of the gel shown in (A).

We did not validate the knockdown efficiency for any of these genes and therefore can not exclude the possibility that some of these genes might be involved in POT1b induced C-strand resection.

Interestingly, analysis of POT1b cells that were depleted for Exo1 showed a slight but reproducible reduction of telomeric overhang signal. While two shRNAs against Exo1 reduced the telomeric overhang signal in POT1b cells by about 10%, one shRNA resulted in an average reduction of 25% (Figure 6.10 A, B and 6.11). As the reduction of ss telomeric DNA by knockdown of Exo1 is relatively small compared to the complete rescue by POT1b, it is likely that Exo1 is not the only nuclease that is capable of resecting the telomeric C-strand after POT1b loss. It is also possible that the level of knockdown is not sufficient to completely abrogate Exo1 function. Therefore, the involvement of Exo1 in C-strand resection after POT1b loss has to be confirmed with different shRNA target sites and has to be correlated to the knockdown efficiencies of these shRNAs by western blotting analysis. Alternatively, analysis of cells from POT1bΔ/Δ Exo1Δ/Δ double knockout cells could be used to verify this result. The preliminary result that Exo1 might be responsible for overhang processing after the loss of POT1b is supported by the finding that knockdown of MutL, a protein that can stimulate the activity of Exo1, results in a similar overhang reduction (Figure 6.11). This result was reproduced with two independent shRNAs targeting MutL. In addition to Exo1 and MutL, we find that shRNA knockdown of one member of the Keops protein complex resulted in a slight reduction of telomeric overhang in POT1b KO cells (Figure 6.11). The Keops proteins were identified as a protein complex that mediates the cellular response to the loss of Cdc13 in *S. cerevisiae*.

It should be mentioned here that the average overhang signal of all knockdowns taken together is slightly lower than the one seen in cells infected with the empty vector. As knowledge of the RNAi mechanism is still limited, the significance of this potentially interesting finding remains to be determined.

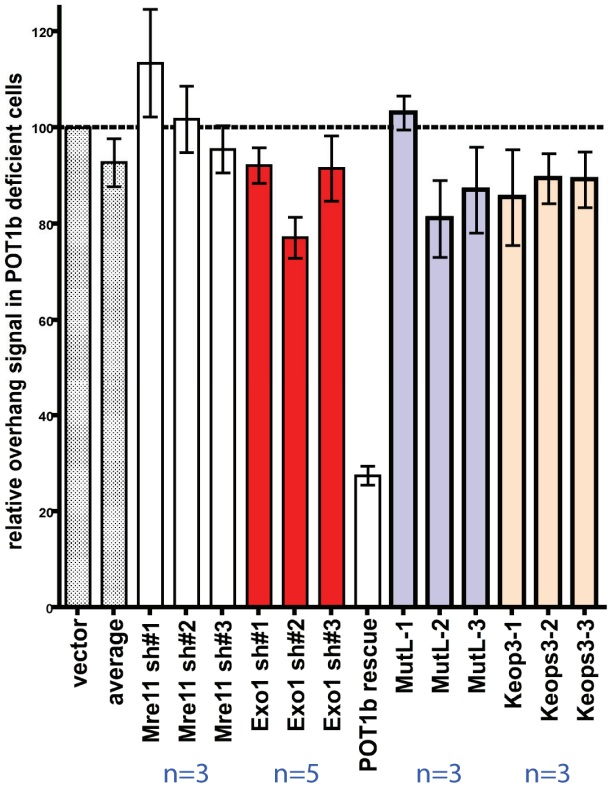

Figure 6.13 Exo1 and MUTL are implicated in the generation of increased overhang signals in POT1b KO cells

Quantification of telomere overhang changes in POT1b-/- cells after the knockdown of Mre11, Exo1, MutL and Keops3 compared to the rescue by a POT1b cDNA. The overhang signal found in the vector control infections was set to 100%. The numbers at the base of the graph indicate the number of independent experiments performed.

Discussion

Mechanism of overhang generation

We found that loss of POT1b leads to progressive telomere shortening and therefore shelterin is needed to protect against the excessive loss of telomeric DNA. As telomere shortening in POT1b deficient cells exceeds the telomere shortening in telomerase negative cells, POT1b loss either impairs the proper synthesis of telomeric DNA during replication, or results in the excessive degradation of telomeric DNA. In the first scenario telomere shortening and overhang extension could be caused by the incomplete synthesis of the lagging strand. If this were the case, it is predicted that extended overhangs in POT1b deficient cells would be found exclusively on telomeres that were generated by lagging strand synthesis. Measuring the overhang of individual telomeres by electron microscopy can test this prediction. In ongoing experiments in collaboration with the laboratory of Jack Griffith, telomeric DNA was isolated from POT1b KO liver cells and the telomeric overhang was coated *in vitro* with the *E. coli* single stranded binding protein (SSB). As the amount of SSB on the chromosome end can be measured by electron microscopy and correlated with overhang length, this technique would allow us to determine if the telomeric overhang is elongated preferentially on one chromosome end. Until this analysis is completed, we can not exclude that the POT1b overhangs are caused by the uncoupling of leading and lagging strand telomere synthesis.

Based on the results presented here we favor the view that POT1b loss causes the degradation of the C-strand by affecting a nuclease rather than by misregulating telomere replication. C-strand degradation is a phenotype that is caused by the loss of Cdc13 in *S. cerevisiae* as well as after the knockdown of human POT1. Depletion of human POT1

leads to the randomization of the otherwise precise ATC-5' ending of the telomeric C-strand, a process that requires the action of a nuclease. Furthermore, we find that depletion of the Exo1 nuclease, which is partially responsible for elongated overhangs in *S. cerevisiae*, reduces overhang signal in POT1b deficient MEFs. This result is supported by the finding that knockdown of MutL, an endonuclease that that is known to stimulate the activity of Exo1, results in a similar reduction of overhang length as the knockdown of Exo1.

Interestingly, we find that the knockdown of one member of the mouse Keops protein complex results in reduced overhang length in POT1b deficient cells. Both the Keops proteins and Exo1 are implicated in processing after the loss of Cdc13 function in *S. cerevisiae*; it is therefore possible that the mechanism by which Cdc13 and POT1b protect the telomere against degradation is conserved between *S. cerevisiae* and mice.

Our screen to find genes that regulate overhang length in POT1b KO cells does not discriminate between a nonspecific and a specific process that generates the overhang. It is possible that the extended overhangs after loss of POT1b do not simply reflect unspecific degradation by nucleases but are the result of a deregulation of a process that generates the telomeric overhang in normal cells. If POT1b loss resulted in the enhancement of this natural telomere processing step, it would be predicted that genes found in the screen would also have a telomere overhang phenotype in POT1b proficient cells. Therefore, it will be of interest to determine the function of Exo1 in a POT1b wild type setting. As we screened only a limited number of genes, a genome-wide screen could be used to identify other genes that are involved in overhang generation.

The consequences of telomere shortening in POT1b deficient cells

Loss of POT1b leads to telomere shortening regardless of the presence of telomerase. While telomeres in telomerase KO cells shorten, telomeres of wild type cells are maintained at a constant telomere length, showing that telomere length homeostasis in wild type cells is established through the constitutive action of telomerase. Therefore, the short telomeres found in POT1b deficient cells would be elongated by telomerase in a POT1b proficient setting. Several possibilities could explain why telomerase does not efficiently compensate for the telomere sequence loss in POT1b KO MEFs. Either POT1b is directly involved in the recruitment of telomerase to telomeres, or the elongated overhangs in POT1b KO cells are not a suitable substrate for telomerase elongation, or telomerase activity is limited and not sufficient to counteract shortening in POT1b KO cells. The option that POT1b might be involved in the recruitment of telomerase is attractive, because of recent reports that imply TPP1 in telomerase recruitment. TPP1 lacks DNA binding affinity, and its interaction with POT1 is thought to be necessary for overhang binding. As telomeres in POT1b knockout cells shorten with a rate comparable to telomeres of POT1b and telomerase double deficient cells, telomerase recruitment by POT1b is not excluded.

Furthermore, we find that POT1b loss leads to phenotypes in the mouse that are characteristic for late generation telomerase KO mice indicating that POT1b deficient mice are impaired in their telomere maintenance. However, crosses between the telomerase and POT1b knockout excluded that POT1b is the exclusive telomerase recruiter, as the outcome of telomere shortening in POT1b-/- cells and POT1b-/- mTR-/- cells is different. Cells that lack both genes enter telomere length induced crisis and

accumulate significantly more fusions than POT1b knockout alone. Furthermore, telomerase deficiency exacerbates the phenotypes found in POT1b KO mice. Both findings suggest that under conditions where telomeres become very short telomerase can maintain telomeres in a POT1b independent manner. Although we did not find any telomere length changes in POT1a knockout cells, it is possible that POT1a has the ability to partially compensate for POT1b in telomerase recruitment once telomere become very short. In future experiments it has to be determined if overexpression of telomerase in POT1b deficient cells can counteract telomere shortening. If we were to find that increased telomerase activity maintains the telomeres of POT1b knockout cells, it would suggest that telomerase could use elongated overhangs as a substrate.

7. Conclusion

Telomere length regulation by human POT1

Telomere shortening limits proliferation of most human somatic cells and can thereby function as a tumor suppressor mechanism. The indefinite propagation of the human germline requires telomere length maintenance by telomerase. This differential regulation of telomere maintenance is achieved by restricting expression of telomerase. A second level of regulation is required in the germline to ensure that the telomeres of the zygote are, on one hand, long enough to allow sufficient cellular proliferation for the development and life-span of the organism, but on the other hand, not too long to circumvent the tumor suppressor function of telomere shortening. Studies of telomere length regulation in tumor cells, in which telomerase is reactivated, suggest that telomere length homeostasis is based on a cis-acting mechanism that links the length of an individual telomere to the likelihood of this telomere being elongated by telomerase. This cis-regulation is mediated by shelterin through the quantitative binding of TRF1 and TRF2, and their ability to recruit the telomerase inhibitor POT1. The molecular details of POT1's effect on telomerase have not been fully established

A major unresolved issue is how telomerase is actively recruited to the 3' end of the overhang. One candidate for this function appears to be the POT1/TPP1 complex that bears similarity to the TEBPα/β complex of *Oxytricha*. Our finding that both proteins are essential for telomere protection calls for further detailed structure-function analysis of these proteins to dissect their possible role in telomerase recruitment and telomere protection. Our results showed that POT1b could be involved in the recruitment of

telomerase, as telomerase fails to fully compensate telomere shortening in POT1b KO cells. However, our data also argue against POT1b being the only telomerase recruiter, as telomerase deficiency exacerbates the loss of POT1b phenotypes in the mouse. One obvious possibility is that POT1a partially compensates for the loss of POT1b.

Telomere protection by POT1

Our understanding of the function of mammalian telomeres is based largely on studies that addressed the consequences of loss of either the telomeric DNA or the proteins that bind to the double stranded part of the telomere. Both approaches revealed the essential function of telomeres for genomic integrity and cellular survival. Nevertheless, the molecular mechanisms that underlie the coordinated interplay between the telomeric DNA and its binding proteins are not completely understood. Ultimately, it is the terminus that is modified by telomerase, or by DNA repair activities when telomeres lose their protected status. Therefore, studying the function of POT1, given its ability to bind both to the telomeric overhang as well as along the double stranded part of the telomere, seemed a promising approach to obtain an understanding of telomere function as a whole. It was tempting to speculate that proteins that bind to the double stranded part of the telomere, in particular TRF2, would ultimately protect the telomere end through a pathway that involves POT1. However, our finding that the loss of POT1 confers some phenotypes that are quite different from the loss of TRF2 suggests that the mechanism of telomere protection is more complex and involves several pathways. TRF2, for example, is essential in preventing telomere fusions, while POT1 protects both the 5' and the 3' end of the chromosome against degradation. Now, the task is to understand the relationship between the various mechanisms of telomere protection, to find the sensors

that detect telomere dysfunction, and to determine the role of these pathways in human disease.

Genesis of the telomeric overhang

Normal telomere shortening in telomerase deficient human and mouse cells exceeds the telomere sequence loss that is predicted from the end replication problem. It has been proposed that the C-strand resection needed to generate the telomeric overhang is responsible for the shortening rate detected in telomerase deficient cells.

Several observations suggest that C-strand resection is a regulated process. The telomeric overhang is established shortly after or during DNA replication on both chromosome ends and has a constant length throughout the cell cycle. Furthermore, C-strand resection results in a precise product, with the 5' end of the telomere terminating in the sequence ATC. Our finding that reduced levels of human POT1 results in the randomization of the 5' chromosome end as well as the finding that loss of mouse POT1b leads to excessive resection of the telomeric C-strand, suggest that POT1 is essential for the proper generation of telomeric overhangs. Once the nuclease that degrades the telomeric C-strand in POT1b deficient cells has been identified, it will be possible to determine whether this nuclease is normally responsible for overhang generation. So far, we identified Exo1 in an shRNA knockdown screen as a candidate nuclease that could be partially responsible for the extended overhangs in POT1b KO cells and therefore might contribute to overhang generation in normal cells. In future experiments, we will determine the role of Exo1 in telomere processing. Ultimately, identification of the nuclease(s) that generate the overhang will provide insights into the process of telomere

shortening in human cells and more importantly, into the mechanism responsible for the tumor suppressing capacity of telomeres.

Two POT1 genes in the mouse

My results suggest that a gene duplication event gave rise to two functionally distinct POT1 proteins in mice whereas humans have only one POT1 gene. This kind of divergence is unprecedented in chromosome biology and has implications for modeling telomere biology and telomere-related disease states in the mouse.

The two functionally distinct mouse POT1 proteins can be used to experimentally dissect different aspects of telomere function. In the first place, the finding that human POT1 is able to complement several of the mouse POT1 KO phenotypes shows that our study of mouse POT1 will be beneficial for understanding the function of human POT1. Secondly, by generating mutants of human and mouse POT1 through domain swapping/chimeric protein designs, we will be able to address specific structure-function questions. Did the DNA binding domains of the two mouse POT1 proteins diverge to fulfill separate roles? Alternatively, are the different functions of the two mouse POT1 proteins based on their differential binding affinity for known or unknown telomeric proteins? The POT1 knockout model that we generated could facilitate the identification and characterization of these potential POT1 interacting proteins.

POT1b deficient mice: an alternative model to study the consequences of telomere shortening

The finding that POT1b loss induces telomere shortening that is not fully counteracted by telomerase shows that shelterin is necessary to maintain telomere length through a telomerase independent pathway. Loss of POT1b leads to phenotypes that are reminiscent of the ones found in the late generation telomerase KO and reminiscent of the symptoms found in patients suffering from DC. These findings could have clinical relevance as in about 50% of all cases of DC the disease causing mutation has not been identified. It seems possible that mutations in POT1 could result in accelerated telomere shortening that exceeds the counteracting capacity of telomerase.

Inhibition of telomerase has been proposed to be a viable approach to inhibit tumor progression, as tumor cells require telomerase for long-term growth. The efficacy and specificity of telomerase-targeting drugs may be increased by the fact that telomeres of tumor cells are generally shorter than telomeres of the neighboring normal tissue. Our finding that POT1 suppresses a pathway that can enhance telomere shortening after telomerase inhibition might lead to approaches that can complement and enhance the therapeutic opportunities of telomerase drugs.

Materials and Methods

Mammalian cell culture

Transformed human mouse cells were grown in DMEM supplemented with 10% bovine calf serum, 100 U/ml penicillin (Sigma), 0.1 μg/ml streptomycin (Sigma), 2.0 mM L-glutamine (Invitrogen), and 0.1 mM non-essential amino acids (Invitrogen). If not indicated otherwise, primary human cells were cultured in DMEM supplemented with 15% fetal bovine serum, 100 U/ml penicillin, 0.1 μg/ml streptomycin, 2.0 mM L-glutamine, 0.1 mM non-essential amino acids. Primary mouse embryonic fibroblasts (MEFs) were obtained from E13.5 embryos using standard techniques and grown in DMEM containing 15% heat-inactivated fetal bovine serum, 100 U/ml penicillin, 0.1 μg/ml streptomycin, 2.0 mM L-glutamine, 0.1 mM non-essential amino acids, 1 mM sodium pyruvate and 50 μM β- mercaptoethanol. SV40 large T antigen immortalized MEFs were cultured in the same media without pyruvate and β-mercaptoethanol. MEFs were immortalized at passage 2 with pBabeSV40LT (a gift from G. Hannon) using the retroviral infection protocol given below. BJ and BJ/Tert cells were cultured in 4:1 DMEM/199medium supplemented with 15% fetal bovine serum 0.1 μg/ml streptomycin, 2.0 mM L-glutamine, 0.1 mM non-essential amino acids, and 1 mM sodium pyruvate. All Cells were passaged using 0.25% trypsin, 0.1 M EDTA and standard tissue culture techniques and grown at 37°C, 5% CO2 and 95% relative humidity.

Growth curve and long-term culture for telomere length experiments

$0.5x10^6$ cells were plated on a 10 cm cell culture dish and grown for 72 hrs. Cells were recovered in 6 ml medium and the total cell number was determined. $0.5x10^6$ cells were plated in a new culture dish. Cumulative population doublings were calculated using these cell counts. The remaining cells were used to isolate genomic DNA for analysis of telomere length in human cells or to generate plugs used in pulsfield gel electrophorsis (PFGE) to analysis telomere length in mouse cells.

RNAi

Double-stranded siRNA was generated to target human POT1 or luciferase (purchased from Darmacon). HeLa cells were transfected using Oligofectamine (Invitrogen) using a protocol supplied by the manufacturer. Specifically, 16-24 hrs before transfection, 3.5-$5x10^6$ cells were seeded into 6-well plates. On the day of transfection, 10 µl oligofectamine were mixed with 28 µl Opti-MEM by vortexing and incubated for 10 min at RT. During this time, 25 µl of 20 µM siRNA and 440 µl Opti-MEM were combined and mixed. Next, 38 µl of the oligofectamine/Opti-MEM were added to the siRNA solution. The tube was vortexed and incubated for 20 min at room temperature (RT). The target cells were rinsed with 3 ml DMEM without additives and afterwards the cells were provided with 2 ml of DMEM. The siRNA solution was added dropwise to the cells, and incubated for 4 hrs, after which 1 ml of 30% FBS in DMEM without additives was added. 24 hrs later, the transfection was repeated. 48-72 hrs after the first transfection, cells were harvested for immunoblot lysate.

Calcium phosphate transfection of mammalian cells

16-24 hours before transfection, 4-6x10^6 cells (PhoenixE/A: 4.3x10^6, 293T: 6x10^6) were plated on a 10 cm cell culture dish. Right before transfection, 2X DNA mix was prepared in a 1.5 ml Eppendorf reaction tube: ddH2O (500µl final volume), 62 µl 2 M CaCl2, 15 µg of plasmid DNA. The samples were mixed and the 2X DNA mix was added drop wise to 500 µl 2X HBSS (50 mM HEPES, pH 7.05, 10 mM KCl, 12 mM dextrose, 280 mM NaCl, 1.5 mM Na2PO4) in a 15 ml conical tube while bubbling the mixture with a 2 ml pipette. The resulting 1 ml was added dropwise onto the cells. The medium was changed 5-12 hours after transfection.

Retroviral infection of mammalian cells

The day before the infection, cells were seeded on a 10 cm cell culture dish. The number of cells that were plated was dependent on the cell type. Generally, cells were plated so that they reached confluence about three days after plating. PhoenixE/A cells were transfected with a retroviral vector, following the calcium phosphate transfection protocol. 48 hrs after transfection, the virus-containing medium was collected in a 50 ml conical tube. Cells were given fresh pre-warmed medium and used for consecutive rounds of infections. The virus was passed through a 0.45 µm filter into a fresh 50 ml conical tube. Next, polybrene was added to a final concentration of 4 µg/ml and mixed by inverting the tube. This solution was then used to replace the medium of the cells to be infected. Cells were infected with this protocol four times in 12-hour intervals. 12 hrs after the last infection, the infected cells were provided with fresh medium. 12 hrs later, the cells were split into selection marker containing medium. As a control for successful

infection and selection, uninfected cells were included with the same medium. If not indicated otherwise, cells were selected for 4-5 days with 4μg/ml puromycin, 5-6 days with 90μg/ml hygromycine or 8-10 days with 300μg/ml neomycin and 8μg/ml blastocidine, respectively.

Lentiviral infection of mammalian cells

Three days before the infection, 293T cells were transfected with 3.5 μg of each helper plasmid (pMDLg/RRE, pRSV-rev and pCMV-VSVG) and 7 μg of lentiviral vector per 10 cm cell culture dish by calcium phosphate transfection. Cells were plated the day before the infection. The number of cells plated and lentiviral titiers were determined beforehand in separate experiments. 72 hrs after changing the medium on the transfected cells, the virus-containing medium was collected in a 50 ml conical tube. The tubes were centrifuged for 5 min at $1x10^3$ rpm at 4°C in a clinical centrifuge. The virus was passed through a 0.45 μm filter and a final concentration of 4 μg/ml of polybrene was added. Half of the virus-containing medium was used for infections. The remaining virus was kept on ice and used for a second infection 3 hrs later. 3 hrs after this second infection, the virus-containing medium was replaced with fresh medium.

Expression of Cre recombinase

Cre was introduced into immortalized MEFs using pMMPHit&Run Cre-GFP (Silver and Livingston, 2001), pWzl-Cre (containing the hygromycin resistance gene), or Ad5 CMV Cre (Resource center, The University of Iowa Carver College of Medicine GTVC, Iowa City, USA). For all experiments, Cre-mediated gene deletion was monitored by PCR. For

retroviral gene delivery, $4x10^6$ PhoenixE cells were transfected with 15 μg of retroviral construct DNA using a standard calcium phosphate transfection protocol, and the medium was changed 6 hrs after transfection. Virus containing medium was collected at 48, 60, 72 and 84 hours post-transfection and used in 4 sequential infections of MEFs. For adenoviral Cre delivery, $0.5x10^6$ SV40 transformed MEFs were infected in suspension with adenovirus at 0.8-1pfu/cell. The effective adenoviral titer was determined in GFP-LacZ 293T reporter cells ((Brown and Baltimore, 2003); a gift from E. Brown). The infection was repeated after 6 hours and 12 hours later the medium was replaced with virus-free medium. Using this protocol, re-adherence of the cells was efficient (>95%) and cell death was minimal prior to Cre-mediated deletion. Deletion efficiency was >80% at 78 hours post infection.

Adenoviral expression of TRF2DBDM

HeLa cells ($2x10^6$) were infected in suspension with adenovirus at 20 pfu/cell. Medium was changed 12 hours later and 48 hours post-infection the cells were treated with demecolcine (100 ng/ml; Sigma) for 1 hour. Cells were harvested and prepared for metaphase spreads and FISH analysis as described below.

Synchronization of Hela cells

HeLa cells ($0.5x10^6$) were plated in a 10 cm culture dish and treated with 2 mM thymidine 24 hours later. After 14 hrs, cells were washed 3 times with pre-warmed PBS and given fresh medium for 11 hours before adding 2 mM final concentration of thymidine. After 14 hrs, cells were washed with pre-warmed PBS and again provided

with fresh medium. Cells were fixed at the indicated time points for immunoflourescence staining using 2% formaldehyde in PBS, or in cold 70% ethanol for FACS analysis.

FACS analysis

For FACS analysis, $1*10^6$ cells were plated on 10 cm cell culture dishes and grown for 24 hrs. BrdU was added directly to the culture medium to a final concentration of 10 μM 60 min prior harvesting. Cells were collected, washed in PBS, and fixed in ice cold 70% ethanol for 30 min while mixing on ice. Cells were recovered by centrifugation and the DNA was denatured in 1 ml of 2N HCl in 0.5% Triton X-100 (v/v) added dropwise while mixing. After 30 min at RT, cells were recovered by centrifugation and samples were neutralized with 1 ml of 0.1 M sodium-tetraborate, pH 8.5. Cells were washed once with 0.5% BSA in PBS and re-suspended in 100 μl of 0.5% BSA in PBS. 10 μl of FITC-conjugated α-BrdU antibody (Becton Dickinson) was added and samples were incubated for 30 min at RT in the dark. Cells were washed twice with 0.5% BSA in PBS and re-suspended in 0.4 ml of 0.5% BSA in PBS containing 5 μg propidium-iodide and 100 μg RNAseA per ml. The samples were analyzed on a FACScalibur flow cytometer (Becton Dickinson). Data analysis was performed using FlowJo software.

Senescence associated β-galactosidase staining

For the SA-β-galactosidase assay (Dimri et al., 1995), $1*10^5$ cells were plated on a 6-well cell culture dish and 48 hrs later, the cells were washed twice in PBS for 5 min. The cells were fixed for 3 min in 2% formaldehyde and 0.2% glutaraldehyde in PBS and washed twice in PBS for 5 min. The staining reaction was performed with 3 ml staining

solution (1 mg/ml 5-bromo-4-chloro-3-indolyl β-D-galactoside (X-Gal), 40 mM citric acid/sodium phosphate, pH 6.0, 5 mM potassium ferrocyanide, 5 mM potassium ferricyanide, 150 mM NaCl, 2 mM MgCl2) at 37°C for 8 to 14 hrs in the dark. Cells were washed twice with PBS and photographed

Indirect immunofluorescence (IF)

Cell were grown on glass coverslips, fixed for 10 min at room temperature with PBS containing 2% paraformaldehyde and permeabilized for 10 min in PBS containing 0.5% Nonidet P-40. Non-specific interactions were blocked by incubation for 30 min in PBS with 0.2% coldwater fish gelatin and 0.5% BSA (PBG). Thereafter cells were incubated with primary antibody for 2 h at room temperature. Cells were washed 3 times for 5 minutes using PBG and incubated 45min with rhodamine- or fluorescein-conjugated secondary antibodies in PBG (The Jackson Laboratory, Bar Harbor, Maine 04609 USA). After two washes in PBG, one wash in 100 ng/ml DAPI in PBS, and one wash in PBS for 5 min each, cover slips were mounted on microscope slides and analyzed using a Zeiss Axioplan II (Thornwood, CA, USA) fluorescence microscope in combination with a Hamamatsu digital camera (C474295) (Bridgewater, MA, USA). Cells were randomly chosen by screening the slides with a ZEISS Plan Apochroma 63X/1.40 Oil DIC objective in the DAPI channel of the fluorescence microscope. For all dual IF experiments, bleed-through controls were performed by leaving out one of the two primary antibodies.

Telomeric FISH (fluorescence in situ hybridization)

Metaphase spreads:

Cells were grown to 50 -70% confluence and incubated for 60-75 min in medium containing colcemide (human cells: 0.1 mg/ml colcemide, mouse cells: 0.2 mg/ml colcemide). The medium was collected and cells were trypsinized and combined with the supernatant culture medium. Cells were pelleted by centrifugation in a clinical centrifuge at $1x10^3$ rpm at 4°C. The cell pellet was gently resuspended in 2 ml of 75 mM KCl and incubated for 7 min in a 37°C waterbath. Cells were then spun down in a clinical centrifuge. The cell pellet was loosened by tapping and , 1 ml of 4°C cold fixative (75% v/v methanol, 25% v/v glacial acetic acid) was added dropwise while vortexing. Afterwards, an additional 4 ml of cold fixative were added and the tubes were stored at 4°C overnight (o/n) or longer. Fixed cells were centrifuged for 5 min at $1x10^3$ rpm and 4°C and most of the supernatant was removed. Cells were resuspended in the remaining 1 ml of fixative by tapping. 150 µl of the cell suspension were dropped from approximately 30 cm onto a tilted microscope slide pre-wetted in cold water. Next, the slide was rinsed twice with 1 ml of cold fixative and then placed on a humidified 80°C heating block for 1 minute.

Hybridazation:

Metaphase spreads slides were aged overnight and rehydrated for 5 min in PBS. Samples were fixed in 4% formaldehyde in PBS for 2 min. Slides were then washed 3 times for 5 min in PBS. The spreads were treated with freshly prepared 1 mg/ml pepsin in 10 mM glycine, pH 2.0, at 37°C for 10 min. The slides were then washed twice for 2 min in PBS. Next, the samples were fixed again in 4% formaldehyde in PBS for 2 min and washed 3

times in PBS for 5 min. The slides were then sequentially dehydrated for 5 min each in 70%, 95% and 100% ethanol. After air-drying the slides, 85 µl of hybridization mix (10 mM Tris-Cl, pH 7.2, 70% formamide, 0.5% blocking reagent for nucleic acid hybridization, 0.1 µM FITC-TelC) was placed onto each slide. The samples were then immediately denatured for 3 min on a 75°C humidified heating block. For hybridization, the slides were incubated for 2-3 hours in a dark, humid atmosphere at RT. Subsequently, the samples were washed twice for 15 min in 10 mM Tris-Cl, pH 7.2, 0.1% BSA, 70% formamide, and the washed for 5 min in 0.1 M Tris-Cl, pH 7.5, 0.15 NaCl, 0.08% Tween at RT in the dark with agitation. DAPI was added to the second to the last wash at a final concentration of 0.5 µg/ml. Slides were then dehydrated as above and air-dried. The slides were mounted with 80 µl embedding medium, coverslipped, and sealed with nail polish. Microscope slides were stored at -20°C in the dark.

Preparation of total RNA from mammalian cells

RNA was isolated using the RNeasy Mini kit (QIAGEN). In order to remove possible DNA contaminants, 12 µg of RNA were incubated 30 min at 37°C with 500 U RNase-free DNaseI in a total volume of 20 µl (including 2 µl 10X DNaseI buffer, adjusted with RNase-free water). The DNase was heat-inactivated for 20 min at 65°C and RNA was quick-frozen in liquid nitrogen and stored at -80°C.

Immunoblotting

Preparation of cell lysates for POT1 immunoblotting:

Cells were harvested, spun down for 5 min at $1x10^3$ rpm at 4°C in a clinical centrifuge. Cells were washed in 500 µl PBS and transferred into a 1.5 ml Eppendorf reaction tube. Next, cells were recovered by centrifugation, resuspended in immunoblot lysis buffer (50 mM Tris-Cl pH 7.4, 1% TritonX-100, 0.1% SDS, 150 mM NaCl, 1 mM EDTA, 1 mM PMSF and protease inhibitor tablets (Boehringer)) (50 µl/ $2x10^6$ cells) and briefly vortexed. After incubation on ice for 5 min, 2.5 µl of 5 M NaCl were added per $2x10^6$ cells and the tubes were briefly vortexed. The lysate was incubated on ice for at 10 min. For every $2x10^6$ cells, 50 ul of cold water were added to each sample followed by vortexing and centrifugation at $13.2x10^3$ rpm for 10 min at 4°C in a tabletop centrifuge. Next, 90% of the supernatant was mixed with 2X Laemmli buffer (100 mM Tris-HCl pH 6.8, 200 mM DTT, 3% SDS, 20% glycerol), and the cell lysates were stored at -20°C.

Immunoblotting:

Protein samples in Laemmli buffer were denatured at 100°C for 5 min and briefly centrifuged. An equivalent of $0.15x10^6$ to $0.2x10^6$ cells and 7.5 µl of Precision Plus protein standard size marker (Bio-Rad) were loaded on a 10% SDS polyacrylamide gel. Proteins were separated for 20 min at 40 V and subsequently at 90 V. The proteins were transferred onto a nitrocellulose membrane in cold transfer buffer for 2 hrs at 90 V by wet blotting at 4°C. Immunoblots detecting POT1 were processed following the guanidine protocol.

Guanidine protocol:

The membrane was incubated at RT in 25 ml 6 M guanidine-Cl solution for 30 min, followed by incubation in 50 ml 3 M guanidine-Cl solution for 30 min. Next, the membrane was incubated at 4°C for 30 min in 50 ml of each of the following buffers: 1 M guanidine-Cl, 0.1 M guanidine-Cl, and 2% M. P. solution. Unless stated otherwise, only blots probed for POT1 were treated with this guanidine protocol.

guanidine-Cl	**6 M**	**3 M**	**1 M**	**0.1 M**	**2% M.P.**
glycerol 50%	2.5 ml (100%)	5 ml	5 ml	5 ml	5 ml
NaCl 5 M	0.5 ml	0.5 ml	0.5 ml	0.5 ml	0.5 ml
Tris 1 M pH7.5	0.5 ml	0.5 ml	0.5 ml	0.5 ml	0.5 ml
EDTA 0.5 M	50 µl	50 µl	50 µl	50 µl	50 µl
Tween 20 10%	250 µl	250 µl	250 µl	250 µl	250 µl
Guanidine-Cl 8M	18.75 ml	9.30 ml	3.13 ml	0.31 ml	0
milk powder	0.5 g	0.5 g	0.5 g	0.5 g	0.5 g
DTT 1 M	25 µl	25 µl	25 µl	25 µl	25 µl
H_2O dd	2.45 ml	10.32 ml	15.57 ml	18.39 ml	18.70 ml
total	25 ml	25 ml	25 ml	25 ml	25 ml

Membranes were blocked with 5% milk in PBS with 0.1% Tween-20 (PBS-T) for 30 min. at RT. Membranes were then incubated with primary antibody in 5% milk in PBST overnight at 8°C. The following day, membranes were washed 4 times in PBST for 10 min at RT and then incubated in $1:5x10^3$ diluted horseradish peroxidase-conjugated α-rabbit or α-mouse IgG antibody in 5% milk/PBS-T for 45 min at RT. Again, the membrane was washed 4 times in PBS-T for 10 min at RT. Antibody binding was visualized by incubation with ECL solution and exposured to a film for 30 sec, 2 min, 10 min and 1 hr.

Human telomere length analysis and overhang in-gel assay

Telomere Length Analysis:

Genomic DNA was isolated from HTC75 cultures grown as described previously (van Steensel and de Lange 1997) except that Phase Lock Gel tubes (Eppendorf) were used for phenol extraction. DNA was digested with AluI and MboI, quantified using Hoechst fluorimetry, separated on a 0.7% agarose gel, and transferred to a Hybond-N membrane for hybridization using an [α-32P]dCTP Klenow-labeled 800-bp telomeric DNA probe from pSP73Sty11 (de Lange et al. 1990; de Lange 1992). Blots were exposed to PhosphorImager screens, and mean telomeric restriction fragment lengths were determined using ImageQuant software. Rates of telomere length changes were determined by linear regression.

In-Gel G-Overhang Assay:

The In-gel G-overhang assay was done essentially the same as described in Hemann and Greider, 1999. Following electrophoresis, gels were dried at RT and prehybridized at 50°C for 1 hr in Church mix (0.5 M Na_2HPO_4 [pH 7.2], 1 mM EDTA, 7% SDS, and 1% BSA), followed by hybridization at 50°C overnight with an end-labeled $(CCCTAA)_4$ oligonucleotide. After hybridization, gels were washed three times with 4x SSC (20X SSC :3 M NaCl, 0.3 M sodium citrate) for 30 min and once with 4x SSC/0.1% SDS. Gels were exposed on Phosphoimager screens. Following the G-overhang assay, gels were alkali denatured (0.5 M NaOH and 1.5 M NaCl), neutralized (3 M NaCl and 0.5 M Tris-HCl [pH 7.0]), rinsed with dH2O, and reprobed with the (CCCTAA)4 oligonucleotide at 55°C and processed as described previously. To determine the relative overhang, the

signal intensity for each lane was determined before denaturing and after denaturing using ImageQuant software. The ratio of these intensities is the overhang intensity. The relative overhang intensity was determined relative to the vector control.

Mouse telomeric overhang/telomere length assay

Preparation of plugs for mouse telomeric overhang/telomere length assay:

Cells were washed with 1 ml PBS, taken up in 50 µl PBS and pre-warmed at 50°C. An equal volume of melted 2% agarose in PBS was added at 50°C and the suspension was mixed carefully with a cut pipette tip. 100 µl of the cell-agarose suspension were transferred into a well of a labeled Biorad CHEF disposable PFGE (pulsed-field gel electrophoresis) plug mold (Catalog Number 1703706). The plug was left for 10 min at RT to solidify. Each plug was then incubated in 500 µl of proteinase K digest buffer (100 mM EDTA, pH 8.0, 0.2% sodium desoxycholate, 1% sodium lauryl sarcosine and 1 mg/ml proteinase K) at 50°C overnight. The next day, the plugs were washed 4 times in T10E1 pH 8.0 for 1 hr at RT. In the last wash, PMSF was added to a final concentration of 1 mM in order to inactivate residual proteinase K activity and plugs were stored at 4°C in this solution. If not indicated otherwise each plug contained $0.5x10^6$ cells.

Pulse field-gel-electrophoresis PFGE:

The PFGE plugs were washed at RT with T10E1 pH 8.0 for 1 hr, with sterile water for 20 min., and with 500 µl MboI enzyme restriction buffer (NEB 3) for 1 hour. Genomic DNA was digested with 60 U MboI in NEB3 buffer o/n at 37 °C. The plugs were washed for 1 hr in T10E1 pH 8.0 at RT and then equilibrated in 0.5X TBE for 20 min. The plugs were loaded into the wells of a 1% 0.5X TBE agarose gel. One well was loaded with high

molecular weight marker. The gel was run in a Biorad CHEF-DR pulsed-field gel electrophoresis apparatus in 0.5X TBE (initial pulse 5 sec, final pulse 5 sec, voltage 6 V/cm, 14°C, for 24 hours). The DNA in the gel was stained with ethidium bromide in ddH2O, destained in ddH2O and photographed. The gel was dried with a vacuum pump at 30°C and then pre-hybridized in 25 ml Church Mix for 30 min at 50°C. The gel was hybridized with 25 ml probe in Church Mix at 50°C overnight. The hybridization mix was recovered and stored at RT. The gel was then washed three times for 30 min 4X SSC at 50°C, once for 30 min in 4X SSC/0.1% SDS at 50°C and subsequently exposed on a phosphoimager screen. Next, the DNA in the gel was denatured for 30 min in denaturing solution (1.5 M NaCl, 0.5 M NaOH) and washed twice for 15 min in neutralizing solution (3 M NaCl, 0.5 M Tris-Cl, pH 7.0). The gel was pre-hybridized for one hour at 55°C and then hybridized with the same probe at 55°C overnight. The gel was then washed as above and exposed for 2 hrs on a phosphoimager screen. Screens were scanned on a Molecular Dynamics Storm 880 Scanner. The relative overhang length was determined by dividing the native signal of one lane (ss stranded telomeric DNA) by its signal in the denaturing gel (total telomeric DNA).

Chromatin Immunoprecipitation (ChIP)

Preparation of cell lysates for ChIP:

Cells were grown on a 15 cm cell culture dish under optimal conditions and processed before reaching confluence. Cells were recovered in a 50 ml conical tube, counted, spun down for 5 min at $1x10^3$ rpm at 4°C in a clinical centrifuge and washed once in 20 ml PBS. The cells were then resuspended in 36 ml PBS. 1 ml of 37% formaldehyde was

added dropwise to the cell suspension, inverting the tube after each few drops. Cells were fixed for 1 hr at RT and the tube was inverted a few times during incubation. Cells were washed in 10 ml PBS, transferred into a 15 ml conical tube, and recovered by centrifugation. Cells were then resuspended in ChIP lysis buffer (50 mM Tris-Cl, pH 8.0, 10 mM EDTA, 1% SDS (w/v), 1 mM PMSF and protease inhibitors tablets (Boehringer)) to achieve a final cell concentration of $20x10^6$ cells/ml. The cell lysate was kept on ice for 15 min and afterwards the lysate was sonicated on ice (10 cycles of 20 sec each, 50% duty, 0.5 sec on/off, power 5). After sonication, the tube was centrifuged for 5 min at $3x10^3$ rpm at 4°C in a clinical centrifuge. The supernatant was then divided into 1.2 ml aliquots in 1.5 ml Eppendorf reaction tubes and spun down in tabletop centrifuge for 10 min at $13.2x10^3$ rpm at 4°C. Supernatants were pooled into a 15 ml conical tube.

Immunoprecipitation (IP):

200 µl of lysate were used per IP and 1.2 ml of IP dilution buffer (16.7 mM Tris-Cl pH 8.0, 150 mM NaCl, 1.2 mM EDTA, 0.01% SDS (w/v),1 mM PMSF and prtease inhibitors tablets) were added. A 50ul aliquot of the lysate from each cell population was taken at this step to be used later in the analysis as the total fraction. The tubes were gently inverted a few times and incubated on ice for 10 min. Specific antibodies or pre-immune serum was then added to the IPs. The pre-immune serum served as a control for the specificity of the antibody and was obtained from rabbits before they were injected with an immunogenic peptide. 4 µl of purified antibody or 20 µl of crude serum were used for the IP's. The lysate/antibody mixture was incubated overnight at 8°C on a spinning wheel. The following day protein G Sepharose beads were prepared the following way: 30 µl of Protein G Sepharose beads, 5 µg sonicated E. coli DNA and 30

µg BSA per IP were mixed with a cut pipette tip. The lysate, antibodies, and beads were incubated another 45 min at 4°C on a spinning wheel. The beads were washed once with 1 ml of ChIP buffer A (20 mM Tris-Cl, pH 8.0, 150 mM NaCl, 2 mM EDTA, pH 8.0, 1% Triton X-100 (v/v), 0.1% SDS (w/v) and protease inhibitor tablets) on ice and sequentially with ChIP buffers B (20 mM Tris-Cl, pH 8.0, 500 mM NaCl, 2 mM EDTA, pH 8.0, 1% Triton X-100 (v/v), 0.1% SDS (w/v)), C (10 mM Tris-Cl, pH 8.0, 0.25 M LiCl, 1 mM EDTA, pH 8.0, 1% NP-40 (v/v), 1% sodium deoxycholate (w/v)) and D (10 mM Tris-Cl, pH 8.0, 1 mM EDTA, pH 8.0) at RT. Between the washes, beads were vortexed and placed on ice. They were spun down in a tabletop centrifuge for 1 min at $5x10^3$ rpm. After the last wash, beads were resuspended by vortexing in 250 µl of freshly made 1% SDS/0.1 M NaHCO3 and incubated at RT for 10 min. The beads were centrifuged and the eluate was transferred into a fresh tube. The beads were eluted again with 250 µl of 1% SDS/0.1 M $NaHCO_3$ and the eluates were combined. In order to reverse the crosslinking, 20 µl of 5 M NaCl were added to each eluate and the samples were incubated o/n at 65°C. The saved total fractions were brought up to 500 µl by adding 450 µl of 1% SDS/0.1 M $NaHCO_3$ and 20 µl of 5 M NaCl. The total fractions were also incubated o/n at 65°C and from this step on processed like the IP samples. Next, 10 µl of 0.5 M EDTA, 20 µl 1 M Tris-Cl, pH 6.5, and 20 µg RNase A, DNase-free, were added and mixed without vortexing. The samples were then incubated for 30 min at 37°C. After further addition of 40 µg Proteinase K, the mixtures were kept at 37°C for 1 hr. The samples were placed into Phase Lock Gel tubes and were thoroughly mixed with 0.5 ml of phenol/chloroform/isoamylalcohol (25:24:1 v/v). The tubes were then centrifuged in a tabletop centrifuge at RT for 5 min at $13.2x10^3$ rpm. The upper phase

was transferred into a fresh 1.5 ml Eppendorf tube and mixed with 20 µg of glycogen by vortexing at $1.4x10^3$ rpm. 1 ml of ethanol was added to precipitate the DNA. The tubes were then inverted and stored o/n at -20°C. The precipitated DNA was pelleted the next day in a tabletop centrifuge for 10 min at $1^3.2*10^3$??? rpm at 4°C. The final pellet was resuspended in 100 µl of ddH2O. DNA was stored at -20°C.

Hybridazation:

The DNA was thawed and boiled in a sandbath for 1 min, then incubated on ice for 5 min and briefly spun down in a tabletop centrifuge. 200 µl 2X SSC were loaded into a well of the assembled S&S Minifold I dot blot apparatus. 30 µl of DNA were mixed with the 200 µl 2X SSC for the TTAGGG membrane and the vacuum was applied. For the BamHI repeat control membrane, 10 µl DNA were used. The membranes were denatured by floating them on lab bench paper wetted with 1.5 M NaCl, 0.5 M NaOH for 10 min. Next, the membranes were neutralized with 1 M NaCl, 0.5 M Tris-Cl, pH 7.0, for 10 min. DNA was cross-linked to the dried membranes in the Stratagene UV cross-linker ($0.12x10^6$ µJ/cm2). After rinsing the membranes in 2X SSC, the membranes were pre-hybridized in a medium-sized Hybaid-bottle with 7 ml Church Mix for 30 min at 65°C. . It was heated in a 100°C sandbath and spun down briefly. 200 µl of the denatured probe were added to the membrane in the Hybaid-bottle. Hybridization was performed o/n at 65°C in the Hybaid incubator. The next day, the membrane was washed 3 times for 5 min in 2X SSC at RT. The membrane was then exposed for a few hours to a phosphoimager screen. The signals were developed on a Molecular Dynamics Storm 880 Scanner and counts for each sample were determined by Imagequant software.

Altered POT1 alleles

POT1a$^{8GEO/+}$ mice were generated from the Baygenomics clone RRA096 using protocols supplied by Baygenomics website (http://baygenomics.ucsf.edu/). Chimeras were generated by blastocyst injections of C57BL/6J blastocysts and founder chimeras were backcrossed to female C57BL/6J mice obtained from Jackson laboratory, USA. SA-β-galactosidase staining of E13.5 mouse embryos was performed as described on the Baygenomics website. For gene-targeting of POT1a and POT1b, BAC clones of genomic DNA were isolated form the CT7 male CJ7/129SV BAC library (Research Genetics) using the first coding exons of POT1a and POT1b as probes. Appropriate restriction fragments (POT1a: HindIII/SacI fragment; POT1b XhoI/NheI fragment) were subcloned into pSL301 (Invitrogen) next to the negative selection (DTA) cassette. A STOP cassette (Jackson et al., 2001) flanked by FRT sites was introduced into the KpnI and NdeI sites for POT1a and –b, respectively. The constructs contained a puromycin resistance gene next to the STOP cassette and a neomycin resistance gene flanked by LoxP sites. A third LoxP site was introduced by inserting an oligonucleotide into an NheI site for POT1a and an ApaI site for POT1b. This oligonucleotide introduced a BamHI restriction site used for the analysis of targeting in ES cells. The vector was linearized with SalI, and gene targeting was performed following standard techniques using the E14 ES cell line derived from 129P2/Ola. Genomic blotting with probes positioned outside of the targeting constructs were used to identify the diagnostic BamHI restriction fragment in correctly targeted ES cells. A probe specific for neo showed that there was only one integration event and confirmed the presence of the STOP cassette. ES cell clones that fulfilled these criteria were selected for C57BL/6J blastocyst injection and resulting chimeric founders

were crossed to C57BL/6J females. Mice were kept in a mixed 129/ C57BL/6J mixed background. FLOXed alleles were generated by removing the STOP cassette using the 129S4/SvJaeSor-Gt(ROSA)26Sortm1(FLP1)Dym/J FLPe deleter mouse stain (Jackson Labs). mTERC deficient mice (Blasco et al., 1997) were obtained form R.A. DePinho and C.W. Greider. MEFs were isolated from a cross of a male POT1bSTOP/FLOX mTERC-/- mice and a female POT1bFLOX/FLOXmTERC+/- mice.

Genotyping PCRs

Genotyping PCRs were preformed using standard DNA isolation techniques and Takara Taq polymerase (Madison, WI, USA).

POT1a wt PCR: 6-wtfw-1 CCAGCCTCCCCTCCACCAAGTC; 6-FRTbw-1 ACAAACCCACCCCGTCAGAGTAAG.

POT1a FLOX PCR: 6-FRTfw-2 TGAGCCCAGAAAGCGAAGGAG; 6-FRTbw1 ACAAACCCACCCCGTCAGAGTAAG.

POT1a Δex3 PCR: 6-allfw-2 CTTCCCTGTTTGCCCTCCTTTACT; 6-allbw-2 TTCCCCCTTTCATTTTCTTTTCTC.

POT1b wt PCR: 17-wtfw-1 CGCTGGGGAGGGTATCGTAG; 17wtbw-1TCCCTGCCCTGACTTCCATC.

POT1b FLOX PCR: 17wtfw-1 CGCTGGGGAGGGTATCGTAG; 6-FRTfw-2 TGAGCCCAGAAAGCGAAGGAG.

POT1b Δex3 PCR: 17-allfw-1 GTTGCCCCTATCATCCTACACG; 17-FRTbw-2 TGTGTTGGGAGAGGAAGTGAAAGA.

These PCRs were performed for 32 cycles (94°C for 45 s, 60°C for 45 s, 72°C for 60 s). POT1a and POT1b STOP PCR: 6-FRTfw-2 TGAGCCCAGAAAGCGAAGGAG and 6-Neobw-1 CCCCCTTCCCTGTTTGCCCTCCTT at 32 cycles (94°C for 30 s, 58°C for 30 s, 72°C for 60 s). Restriction endonuclease digestion and/or DNA sequencing confirmed identity of the PCR products.

Purification of PCR products

QIAquick PCR Purification Kit was used to purify PCR-products

DNA sequencing

The GENEWIZ sequencing service (http://lims-genewiz.com) was used for DNA sequencing

Restriction digest of plasmid DNA and PCR products with endonucleases

Restriction digests were performed using New England Biolabs restriction enzymes and the protocol recommended by this company.

Agarose gel electrophoresis

DNA fragments were separated in 0.7 to 2% agarose gels in 1X TAE (40 mM Tris-acetate, 1 mM EDTA), depending on the expected sizes of the fragments. For UV-detection of DNA, ethidium bromide was added to a final concentration of 0.4 μg/ml into the gel. Samples were loaded with 4x loading buffer (50% glycerol (v/v), 0.5% orange G (w/v)). As a molecular weight marker 0.5 to 2 μg of a mixture of equal volumes of NEB

Lambda DNA-HindIII digest and fX174 DNA-HaeIII digest was used. Gels were run in 1X TAE with approximately 10 V/cm unless indicated otherwise.

Gel extraction of DNA fragments

DNA fragments were purified from agarose gels using the QIAquick Gel Extraction Kit.

DNA ligation

DNA ligation reactions were performed using T4 DNA ligase from New England Biolabs with a protocol recommended by this company.

Mini and Maxi preparation (QIAprep Spin Miniprep Kit Protocol)

Plasmid purifications were performed using the QIAprep Spin Miniprep Kit and QIAGEN Plasmid Maxi kit using protocols provided by the manufacturer. Bacmids were purified using the QIAGEN Plasmid Maxi kit and a protocol for large DNAs provided by Qiagen.

Transformation of competent E. coli cells

50 µl of competent TOP10 were transformed with 1 ng of DNA by heat shock of 42°C for 70 sec followed by incubation on ice for 10 min. Cells were plated on selective LB plates and incubated at 37°C o/n. After the heat shock, large constructs, bacmids and kanamycin containing plasmids were incubated for 60 min in non-selective LB Medium at 37°C prior to plating.

RT-PCR

For expression analysis of mouse POT1a and POT1b, RT-PCR was performed using a mouse cDNA panel form Research Genetics. cDNA was amplified using standard PCR techniques. POT1a primers: fw: TGGTTTCAACAGCTCCCTATA, bw:CCCTACAGTCCCTTCAAATG; POT1b primers: fw:CGGCCCCAGTAGCACCTTCTAC, bw:TCTCTTGCTTAAAGTACGCAG. RT-PCR was performed using the oligo-dT ThermoScript RT-PCR system, (Invitrogen). RNA was isolated from approximately 10^6 cells using Qiagene RNAeasy kit. 1 µg RNA was reverse transcribed using the thermoScript RT-PCR system (Invitrogen,USA) using oligo dT priming and the protocol provided by the manufacturer. To detect the recombined POT1a locus, fw: TGGTTTCAACAGCTCCCTATA and bw: CTTAGAAAGCATCCAACCTCG were used as primers.

Generation of [^{32}P] labeled oligonucleotides with Klenow polymerase

20-100 ng of double stranded DNA fragments were mixed with 5 µl of 1 ng/µl oligo (specific priming) or random hexamers and 29 µl ddH_2O. DNA was boiled in a 100°C sandbath for 5 min, centrifuged very briefly in a tabletop centrifuge and cooled down on ice. Next, 5 µl OLB-C (0.5 M Tris-Cl, 0.1 M MgOAc, 1 mM DTT, 0.5 mg/ml BSA, 0.18 µM dNTPs (dATP, dTTP, dGTP)), 5 µl 3x10^3 Ci/mmol [^{32}Pα]dCTP and 1 µl 2 U/µl Klenow polymerase were added, mixed, and the tubes were incubated for at least 90 min at RT. 50 µl TNES (10 mM Tris-Cl, pH 7.4, 10 mM EDTA, 100 mM NaCl, 1% SDS) were added and the mixture was loaded onto a 3.5 ml G50 column, equilibrated with 1 ml TNES. The column was washed with 1 ml TNES and eluted with 800 µl TNES.

[γ-^{32}P] labeling of oligonucleotides with T4 polynucleotide kinase (PNK)

2 µl ddH2O, 1 µl 10X NEB T4 DNA PNK buffer, 1 µl 10 U/µl NEB T4 DNA PNK, 1 µl of 50 ng/µl oligonucleotide and 5 µl 10.0 mCi/ml [γ-^{32}P]ATP were mixed in a 1.5 ml Eppendorf reaction tube by pipetting and incubated for 45 min at 37°C. 80 µl of TES (10 mM Tris-Cl, pH 8.0, 10 mM EDTA, pH 8.0, 0.1% SDS) were then added to the tube to stop the reaction. The probe was loaded onto a 3 ml G25 Sephadex column that had previously been equilibrated with 1 ml TNES. The column was washed with 700 µl TNES and then eluted with 600 µl TNES.

siRNA/shRNA design

siRNA/shRNAs were designed by utilizing the software provided on http://jura.wi.mit.edu/siRNAext/. The mRNA sequence of the targeted gene was screened for possible target sites using the algorithm: NNSANNNNNNNDNANNAWNN (personal communication with Markus Landthaler, Tuschl laboratory, Rockefeller University, New York City). Target sequences were used for a UNIGene BLAST analysis through the mouse genome in order to detect possible off-targets. Off-targets were identified according to Jackson et al. 2003. Target sites in the 5' or 3' UTR were preferentially chosen, because they provide the opportunity to rescue their effects by overexpressing the unmutated ORF of the gene.

shRNAs were designed in the following format:

sense 5'-GATC4(19mer)T2CA2GAGA(19mer reverse complement)T5G2A4-3'

antisense 5'-AGCT4C2A5(19mer)TCTCT2GA2(19mer reverse complement)G2-3'.

Target sequences were:

Luciferase: 5'- CGTACGCGGAATACTTCGA-3' (Dharmacon).

human POT1:

Ex7: 5’-GGGTGGTACAATTGTCAAT-3’

Ex7/8: 5’-GGAACTGATTATTGCTCAG-3’

Ex7/9a: 5’-GGAACTGATTCAAGTATAT-3’

Ex7/9b: 5’-CAAAGGAACTGATTCAAGT-3’

Ex8a: 5’-GATATTGTTCGCTTTCACA-3’

Ex8b: 5’-GCCCTTCCAATAATTTATA-3’

Ex18: 5’-GTACTAGAAGCCTATCTCA-3’

mouse POT1:

POT1a-1: 5’- GCATCACTATGGATGTAAA-3’

POT1a-3: 5’- GCATTTCTCTACAACATTA-3’

POT1b-1: 5’- GCAGCTGCTTTGAAGATTA-3’

POT1b-3: 5’- GGAGAAGGGTGATCCTGTA-3’

mouse TPP1

mTPP1-1: 5’- GTAGCTTGGGCCTTGAATA-3’

mTPP1-2: 5’- GAACCGGGCAGCTGCTCAA-3’

mTPP1- 3: 5’- GGACACATGGGCTGACGGA-3’

shRNA target used in nuclease screen (all against mouse proteins):

mMre11-1: 5’- GGACCAGAAGGGTCTTATA-3’

mMre11-2: 5’- GCACCCTGCTTGTTATCAA-3’

mMre11-: 5’- GCAGTTAGAGGAAATGATA-3’

mEXO1-1: 5’- GGAGACGGGACTAAGTTAA-3’

mEXO1-2: 5’- GCATTTGGCACAAGAATTA-3’

mEXO1-3: 5’- GGAAGCTGGTCCCTCTGAA-3’

mSnm1-a-1: 5’- GCAGCTTTCGGTCTAGGAA-3’

mSnm1-a-2: 5’-GCACTTACTGCATCGGAAA-3’

mSnm1-a-3: 5’- GGAGACTGGAAGCCGGATA-3’

mSnm1-b-1: 5’- GGAGACACTACTTTGTTAA-3’

mSnm1-a-2: 5’-GCACATGGCAAATTGTTTA-3’

mSnm1-b-3: 5’-GGATGTAACTACATGTTAA-3’

mSnm1-c-1: 5’- GGATCACATGAAAGGATTA-3’

mSnm1-c-2: 5’- GGAAATACAGGAAGAGAAA-3’

mSnm1-c-3: 5’- GGAGACTTCAGACTGGCAA-3’

mWrn-1: 5’- GGAACAGCAAGCTAAAGAA-3’

mWrn-2: 5’- GCAAGAGGAGGTTGATGTA-3’

mWrn-3: 5’- GCACTCTCCGCTACTGCAA-3’

mRad17-1: 5’- GCACGACCGGGACACTTTA-3’

mRad17-2: 5’- GGAGTTACTTAGTTTAGAA-3’

mRad17-3: 5’- GGAAAGACAACTACTATAA-3’

mPIF1-1 NM_172453: 5’- GGAGCAGCCTGTCTTATTA-3’

mPIF1-2 NM_172453: 5’- GGAGCGCAGGGACAGGAAA-3’

mPIF1-3 NM_172453: 5’- GCACGCACAGCATATTGTA-3’

mRAD9-1: 5’- GTAGCTGCTGGGACTCATA-3’

mRAD9-2: 5’- GGACTCATAATATGTCCTA-3’

mRAD9-3: 5’- GAAGGACGGGCTCTCCCTA-3’

mRAD9b-1NM_144912: 5’- GGACAGAGCTGGCAGCATA-3’

mRAD9b-2NM_144912: 5’- GAAGTCACCTTCTCTGTTA-3’

mRAD9b-3NM_144912: 5’- GAAAGCAGTACAAACGCTA-3’

mRAD1-1: 5’- GCACCAATGTTATGAATAA-3’

mRAD1-2: 5’- GCAGCACCAATGTTATGAA-3’

mRAD1-3: 5’- GCACTAGCTTTATCCTGTA-3’

mHUS1-1: 5’- GGAGCTGCCTCACCCTAAA-3’

mHUS1-2: 5’- GCAGGCACTGTGTGCCAAA-3’

mHUS1-3: 5’- GCAGTGATGTAATATCATA-3’

mHUS1b-1: 5’- GCAGTCATGTGCTGGTGGA-3’

mHUS1b-2: 5’- GTAGAAACTGATAGAGTGA-3’

mHUS1b-3: 5’- GCATGGAGGGTGCCTCGCA-3’

mMUTL-1: 5’- GGAGCACATTATCTATAAA-3’

mMUTL-2: 5’- GGAGGACTCTGATGTGGAA-3’

mMUTL-3: 5’- GCATTAGTATCTCAGTTAA-3’

mDNA2L-1: 5’- GGAGATCAGAGGACTATTA-3’

mDNA2L-2: 5’- GGAGCTGAAGACCGGCAAA-3’

mDNA2L-3: 5’- GGAGTCAGGTGGTCCTGTA-3’

mKeops1-1 (BC091757.1 Mosgep): 5’- GCACAGGACTCCTCTCAAA

mKeops1-2 (BC091757.1 Mosgep): 5’- GGACCCTATATAAGGCTTA

mKeops1-3 (BC091757.1 Mosgep): 5’- GGAGGGACTAACACCATCA

mKeops2-1 (BC024858.1 mTP53rkbp): 5’- GGACATAGTGACAGTCAAA

mKeops2-2 (BC024858.1 mTP53rkbp): 5’- GGAGGGCAGAGAAACCTAA

mKeops2-3 (BC024858.1 mTP53rkbp): 5’- GGAAAGTCTTCCAGAAATA

mKeops3-1 (BC017155.1 mTP53rk-1): 5’- GCAAAGCATGGGTTGTTAA

mKeops3-2 (BC017155.1 mTP53rk-1): 5’- GTAGAATCTGCCATATGGA

mKeops3-3 (BC017155.1 mTP53rk-1): 5’- GGATTAAAGGTGTATGTCA

mERCC4-1 (NM_015769.1): 5’- GGAGCGTGCTTCCGCCAAA

mERCC4-2 (NM_015769.1): 5’- GCACCTCCATGTTTGTGAA

mERCC4-3 (NM_015769.1): 5’- GCACCGACCGGCTCCTCTA

mERCC5-1 (NM_011729.1): 5’- GCACCTCCGACGACAAGAA

mERCC5-2 (NM_011729.1): 5’- GCATCCATTGACTCGAGAA

mERCC5-3 (NM_011729.1): 5’- GCAATGAGTAACTTAGAAA

mFEN1-1(NM_007999.3): 5’- GGAGGAGAGGTGACTAGAA

mFEN1-2(NM_007999.3): 5’- GGACTCCAAACCACTGCTA

mFEN1-3(NM_007999.3): 5’- GCATTAAGTGTGCCACTGA

mMus81-1 (NM_027877.2): 5’- GCAGGACACAGGCCAGAAA

mMus81-2 (NM_027877.2): 5’- GGACCCTGTACCAGTTGTA

mMus81-3 (NM_027877.2): 5’- GCACCCATCTTCATCTCTA

mEME1-1(NM_177752.2): 5’- GGAGCTGGCAGTCTCCAAA

mEME1-2(NM_177752.2): 5’- GCAACCAGATCTCATCTTA

mEME1-3(NM_177752.2): 5’- GCAGCACCGAGAAAGGGAA

mBRCA1-1 (NM_009764.2): 5’- GCAGGAGCCAAATCTATAA

mBRCA1-2 (NM_009764.2): 5’- GGAGACCTGATTATATAAA

mBRCA1-3 (NM_009764.2): 5’- GCAGCGTTCAGAAAGTTAA

mBRCA2-1(NM_009765.1): 5'- GGAGCTGTGGCACGAAATA

mBRCA2-2(NM_009765.1): 5'- GGACCCTTCTGCTCAAGTA

mBRCA2-3(NM_009765.1): 5'- GCAGCATCCTGAATATGAA

Cloning of shRNAs into pSUPER/pSUPERIOR vectors

59-64mer oligos were obtained from FISHER oligos, annealed, phosphorylated and cloned into pSUPERIOR-Puro. Plasmids were sequenced with 5'-GGAAGCCTTGGCTTTTG-3' and 5-'CGAACGCTGACGTCATC-3' to confirm integrity of the plasmid and shRNA target-sequence.

POT1 expression constructs

POT1-55 was cloned into the pLPC retroviral vector by PCR using POT1 variant 4 mRNA (EST Id aa66fo8.s1). This construct retained the Kozak sequence and the first POT1 ATG in exon 6. The POT1* construct was generated by PCR mutagenesis of POT1 cDNA and expressed from pBabeNeo expression vector. The silent change was at position: +1660 to 1678 to generate the sequence: GTACTAGAAGCTTACTTGA, conferring resistance to ex18 shRNA. pBabeSV40Tag was a gift from G.Hannon. The human POT1 cDNA was also subcloned using BamHI and XhoI restrictions sites ligated to BamHI/ SalI digested pWzl-Myc retroviral vector.. The ΔOB versions of POT1a and –b were cloned into pLPC-N-Myc using the following PCR primers: POT1aΔOB fw: ACCTGGATCCCCTCAGGACCAAAAAATGGTAG, POT1aΔOB rev: ACCTCTCGAGCTAGACAACATTTTCTGCAACTG, POT1bΔOB fw:

ACCTGGATCCGCTCAGGACTACAGTATGGTAG, POT1bΔOB rev: ATGCGTCGACATCATAGTTACTTTCTGGTAAG.

Lentiviral shRNA constructs

POT1 proteins were stably knocked down in NIH3T3 cells using pSicoR-GFP vector technology ((Ventura et al., 2004); a gift from T. Jacks). The following target sequences were cloned into pSico and confirmed by DNA sequencing: a1: GCATCACTATGGATGTAAA; a* (inactive): GGAACTCCCAAATAAAGTA; a3: GCATTTCTCTACAACATTA; b1: GCAGCTGCTTTGAAGATTA; b2: GGAGTGTCATTTCTCCTAA; b3: GGAGAAGGGTGATCCTGTA. Three days before the infection, 293T cells were transfected with 3.5 μg of each helper plasmid pMDLg/RRE, pRSV-rev and pCMV-VSVG and 7 μg of lentiviral vector per 10 cm dish using calcium phosphate transfection. 72 hrs after changing the medium on the transfected cells, half of the virus-containing medium supplemented with 4 μg/ml polybrene was used to infect 75,000 NIH3T3 cells. After 3 hrs, the infection was repeated and 3 hrs later, the virus containing medium was replaced by pre-warmed fresh medium. The infection efficiency was >90% as determined using lentiviral vectors carrying the GFP gene (pSicoR-GFP and derivates) and quantification of cells that exhibited GFP fluorescence 48 hrs after infection. Cells used in ChIP analysis were generated by two rounds of infection with the indicated lenti-viruses separated by approximately one week of culture.

Immunological reagents

ID	antigen	source/type	dilution	origin
644	mTRF1 (peptide)	rabbit polyclonal	IF 1:2000 ChIP 1:350	J. Karlseder/de Lange lab
647	hTRF2 (baculoviral full-length)	rabbit polyclonal	ChIP 1:70 (serum)	X. Zhu/de Lange lab
1253/4	mRAP1 (GST full-length)	rabbit polyclonal	ChIP 1:70 (serum)	G. Celli/de Lange lab
978	hPOT1 (peptide)	rabbit polyclonal	Immunoblot 1:1000	D. Loayza/de Lange lab
1220	mPOT1a (peptide)	rabbit polyclonal	Immunoblot 1:1000 ChIP 1:350	D. Hockemeyer/de Lange lab
1221	mPOT1a (peptide)	rabbit polyclonal	Immunoblot 1:1000 ChIP 1:350	D. Hockemeyer/de Lange lab
1222	mPOT1b (peptide)	rabbit polyclonal	Immunoblot 1:1000 ChIP 1:350	D. Hockemeyer/de Lange lab
1223	mPOT1b (peptide)	rabbit polyclonal	Immunoblot 1:1000 ChIP 1:350	D. Hockemeyer/de Lange lab
αmPOT1a	mPOT1a (GST full-length)	mouse polyclonal	IF 1:1000	D. Hockemeyer/de Lange lab
αmPOT1b	mPOT1b-V2 (GST full-length)	mouse polyclonal	IF 1:1000	D. Hockemeyer/de Lange lab
αγH2AX	hγH2AX (Ser139 phospho)	mouse monoclonal	IF 1:1000	upstate (05-636)
16	MRE11	rabbit polyclonal	ChIP 1:140 (serum)	J. Petrini lab, Memorial Sloan Kettering Cancer Centre, New York City
95	NBS1	rabbit polyclonal	ChIP 1:140 (serum)	J. Petrini lab
9E10	human c-Myc (peptide)	mouse monoclonal	IF 1:1000 Immunoblot 1:1000	oncogene (OP10)
GTU88	γ-Tubulin (peptide)	rabbit polyclonal	Immunoblot 1:1000	Sigma (T3559)
hTRF1	human TRF1	rabbit polyclonal	IF 1:2000	de Lange Lab
h53BP1	human 53BP1	mouse monoclonal	IF 1:50	generously provided by T. Halazonetis, The Wistar Institute, Philadelphia, Pennsylvania);
864	h-Mre11	rabbit	ChIP	hMRE11

		polyclonal		de Lange Lab
M2	Flag-epitope-tag	mouse monoclonal	IF 1:5000 Immunoblot 1:10000	Sigma
53BP1	γ-Tubulin (peptide)	rabbit polyclonal	Immunoblot 1:1000	(Novus, (NB 100-304)
978	hPOT1 (peptide)	rabbit polyclonal	Immunoblot 1:1000	D. Loayza/de Lange lab

POT1a antibodies 1220 and 1221 were raised in rabbits against a POT1a peptide representing amino acids 395-421. POT1b antibodies 1222 and 1223 were raised against a POT1b peptide representing amino acids 285-307. POT1a IF was performed using an antibody raised in mice against recombinant GST-tagged full-length POT1a protein. POT1b IF was performed using an antibody raised in mice against GST-tagged POT1b protein from amino acid 1 to 342 (the C-terminus contained the additional amino acids SKPFSSVVTDT). TRF1 IF was performed with Ab 644 (Karlseder et al., 2003).

Secondary antibodies

Rhodamine (TRITC)-conjugated Donkey Anti-Rabbit IgG (Jackson ImmunoResearch 711-025-152)

Fluorescein (FITC)-conjugated Donkey Anti-Rabbit IgG (Jackson ImmunoResearch 711-095-152)

Rhodamine (TRITC)-conjugated Donkey Anti-Mouse IgG (Jackson ImmunoResearch 715-025-150)

Fluorescein (FITC)-conjugated Donkey Anti-Mouse IgG (Jackson ImmunoResearch 715-095-150)

Horseradish Peroxidase-conjugated Sheep Anti-Mouse IgG (Amersham NA931V)

Horseradish Peroxidase-conjugated Donkey Anti-Rabbit IgG (Amersham NA934V)

References

1. Cawthon, R. M., Smith, K. R., O'Brien, E., Sivatchenko, A. & Kerber, R. A. Association between telomere length in blood and mortality in people aged 60 years or older. *The Lancet* **361**, 393-395 (2003).
2. Vulliamy, T., Marrone, A., Dokal, I. & Mason, P. J. Association between aplastic anaemia and mutations in telomerase RNA. *Lancet* **359**, 2168-2170 (2002).
3. Vulliamy, T. et al. The RNA component of telomerase is mutated in autosomal dominant dyskeratosis congenita. *Nature* **413**, 432-435 (2001).
4. de Lange, T. Protection of mammalian telomeres. *Oncogene* **21**, 532-540 (2002).
5. de Lange, T. in *Telomeres* (eds de Lange, T., Lundblad, V. & Blackburn, E.) 387-432 (Cold Spring Harbor Laboratory Press, Cold Spring Harbor, New York, 2005).
6. Muller, H. J. The remaking of chromosomes. *The Collecting Net, Woods Hole* **8**, 182-195 (1938).
7. McClintock, B. The stability of broken ends of chromosomes in Zea mays. *Genetics* **26**, 234-282 (1941).
8. Olovnikov, A. M. A theory of marginotomy. The incomplete copying of template margin in enzymic synthesis of polynucleotides and biological significance of the phenomenon. *J Theor Biol* **41**, 181-190 (1973).
9. Watson, J. D. Origin of concatemeric T7 DNA. *Nat New Biol* **239**, 197-201 (1972).
10. Greider, C. W. & Blackburn, E. H. Identification of a specific telomere terminal transferase activity in Tetrahymena extracts. *Cell* **43**, 405-413 (1985).

11. Greider, C. W. & Blackburn, E. H. The telomere terminal transferase of Tetrahymena is a ribonucleoprotein enzyme with two kinds of primer specificity. *Cell* **51**, 887-898 (1987).

12. Ancelin, K. et al. Targeting assay to study the cis functions of human telomeric proteins: evidence for inhibition of telomerase by TRF1 and for activation of telomere degradation by TRF2. *Mol Cell Biol* **22**, 3474-3487 (2002).

13. Kim, N. W. et al. Specific association of human telomerase activity with immortal cells and cancer. *Science* **266**, 2011-205. (1994).

14. Meyerson, M. et al. hEST2, the putative human telomerase catalytic subunit gene, is up- regulated in tumor cells and during immortalization. *Cell* **90**, 785-95. (1997).

15. Nakamura, T. M. et al. Telomerase catalytic subunit homologs from fission yeast and human. *Science* **277**, 955-959 (1997).

16. Steinert, S., White, D. M., Zou, Y., Shay, J. W. & Wright, W. E. Telomere biology and cellular aging in nonhuman primate cells. *Exp Cell Res* **272**, 146-152 (2002).

17. Harley, C. B., Futcher, A. B. & Greider, C. W. Telomeres shorten during ageing of human fibroblasts. *Nature* **345**, 458-460 (1990).

18. Hayflick, L. The limited in vitro lifetime of human diploid cell strains. *Exp Cell Res* **37**, 614-636 (1965).

19. Bodnar, A. G. et al. Extension of life-span by introduction of telomerase into normal human cells. *Science* **279**, 349-352 (1998).

20. Counter, C. M., Botelho, F. M., Wang, P., Harley, C. B. & Bacchetti, S. Stabilization of short telomeres and telomerase activity accompany immortalization

of Epstein-Barr virus-transformed human B lymphocytes. *J Virol* **68**, 3410-3414 (1994).

21. Shay, J. W. & Bacchetti, S. A survey of telomerase activity in human cancer. *Eur J Cancer* **33**, 787-791 (1997).
22. Vaziri, H. & Benchimol, S. Reconstitution of telomerase activity in normal human cells leads to elongation of telomeres and extended replicative life span. *Curr Biol* **8**, 279-282 (1998).
23. Meyne, J., Ratliff, R. L. & Moyzis, R. K. Conservation of the human telomere sequence (TTAGGG)n among vertebrates. *Proc Natl Acad Sci USA* **86**, 7049-7053 (1989).
24. Moyzis, R. K. et al. A highly conserved repetitive DNA sequence, (TTAGGG)n, present at the telomeres of human chromosomes. *Proc Natl Acad Sci USA* **85**, 6622-6626 (1988).
25. Kipling, D. & Cooke, H. J. Hypervariable ultra-long telomeres in mice. *Nature* **347**, 400-402 (1990).
26. Huffman, K. E., Levene, S. D., Tesmer, V. M., Shay, J. W. & Wright, W. E. Telomere shortening is proportional to the size of the G-rich telomeric 3'-overhang. *J Biol Chem* **275**, 19719-19722 (2000).
27. Makarov, V. L., Hirose, Y. & Langmore, J. P. Long G tails at both ends of human chromosomes suggest a C strand degradation mechanism for telomere shortening. *Cell* **88**, 657-666 (1997).
28. Sfeir, A. J., Chai, W., Shay, J. W. & Wright, W. E. Telomere-end processing the terminal nucleotides of human chromosomes. *Mol Cell* **18**, 131-138 (2005).

29. Riethman, H. et al. Mapping and initial analysis of human subtelomeric sequence assemblies. *Genome Res* **14**, 18-28 (2004).

30. Williamson, J. R., Raghuraman, M. K. & Cech, T. R. Monovalent cation-induced structure of telomeric DNA: the G-quartet model. *Cell* **59**, 871-880 (1989).

31. Fang, G. & Cech, T. R. The beta subunit of Oxytricha telomere-binding protein promotes G- quartet formation by telomeric DNA. *Cell* **74**, 875-885 (1993).

32. Zahler, A. M., Williamson, J. R., Cech, T. R. & Prescott, D. M. Inhibition of telomerase by G-quartet DNA structures. *Nature* **350**, 718-720 (1991).

33. Zaug, A. J., Podell, E. R. & Cech, T. R. Human POT1 disrupts telomeric G-quadruplexes allowing telomerase extension in vitro. *Proc Natl Acad Sci USA* **102**, 10864-10869 (2005).

34. Cesare, A. J., Quinney, N., Willcox, S., Subramanian, D. & Griffith, J. D. Telomere looping in P. sativum (common garden pea). *Plant J* **36**, 271-279 (2003).

35. Griffith, J. D. et al. Mammalian telomeres end in a large duplex loop. *Cell* **97**, 503-14. (1999).

36. Munoz-Jordan, J. L., Cross, G. A., de Lange, T. & Griffith, J. D. t-loops at trypanosome telomeres. *Embo J* **20**, 579-88. (2001).

37. Nikitina, T. & Woodcock, C. L. Closed chromatin loops at the ends of chromosomes. *J Cell Biol* **166**, 161-165 (2004).

38. Lingner, J. et al. Reverse transcriptase motifs in the catalytic subunit of telomerase. *Science* **276**, 561-567 (1997).

39. Greider, C. W. & Blackburn, E. H. A telomeric sequence in the RNA of Tetrahymena telomerase required for telomere repeat synthesis. *Nature* **337**, 331-337 (1989).

40. Nakamura, T. M. & Cech, T. R. Reversing time: origin of telomerase. *Cell* **92**, 587-590 (1998).

41. Chen, J. L., Blasco, M. A. & Greider, C. W. Secondary structure of vertebrate telomerase RNA. *Cell* **100**, 503-514 (2000).

42. Romero, D. P. & Blackburn, E. H. A conserved secondary structure for telomerase RNA. *Cell* **67**, 343-353 (1991).

43. Cohn, M. & Blackburn, E. H. Telomerase in yeast. *Science* **269**, 396-400 (1995).

44. Chai, W., Ford, L. P., Lenertz, L., Wright, W. E. & Shay, J. W. Human Ku70/80 physically associates with telomerase through interaction with hTERT. *J Biol Chem* **107**, (2002).

45. Reichenbach, P. et al. A human homolog of yeast est1 associates with telomerase and uncaps chromosome ends when overexpressed. *Curr Biol* **13**, 568-574 (2003).

46. Snow, B. E. et al. Functional conservation of the telomerase protein est1p in humans. *Curr Biol* **13**, 698-704 (2003).

47. Mitchell, J. R., Wood, E. & Collins, K. A telomerase component is defective in the human disease dyskeratosis congenita. *Nature* **402**, 551-55. (1999).

48. Beattie, T. L., Zhou, W., Robinson, M. O. & Harrington, L. Functional multimerization of the human telomerase reverse transcriptase. *Mol Cell Biol* **21**, 6151-6160 (2001).

49. Prescott, J. & Blackburn, E. H. Functionally interacting telomerase RNAs in the yeast telomerase complex. *Genes Dev* **11**, 2790-2800 (1997).

50. Wenz, C. et al. Human telomerase contains two cooperating telomerase RNA molecules. *Embo J* **20**, 3526-3534 (2001).

51. Ray, S., Karamysheva, Z., Wang, L., Shippen, D. E. & Price, C. M. Interactions between telomerase and primase physically link the telomere and chromosome replication machinery. *Mol Cell Biol* **22**, 5859-5868 (2002).

52. Vermeesch, J. R. & Price, C. M. Telomeric DNA sequence and structure following de novo telomere synthesis in Euplotes crassus. *Mol Cell Biol* **14**, 554-566 (1994).

53. Vermeesch, J. R., Williams, D. & Price, C. M. Telomere processing in Euplotes. *Nucleic Acids Res* **21**, 5366-5371 (1993).

54. Ten Hagen, K. G., Gilbert, D. M., Willard, H. F. & Cohen, S. N. Replication timing of DNA sequences associated with human centromeres and telomeres. *Mol Cell Biol* **10**, 6348-6355 (1990).

55. Loayza, D. & de Lange, T. POT1 as a terminal transducer of TRF1 telomere length control. *Nature* **424**, 1013-1018 (2003).

56. Pardue, M. L. & DeBaryshe, P. G. Telomeres and telomerase: more than the end of the line. *Chromosoma* **108**, 73-82 (1999).

57. Biessmann, H. et al. Addition of telomere-associated HeT DNA sequences "heals" broken chromosome ends in Drosophila. *Cell* **61**, 663-673 (1990).

58. Young, B. S., Pession, A., Traverse, K. L., French, C. & Pardue, M. L. Telomere regions in Drosophila share complex DNA sequences with pericentric heterochromatin. *Cell* **34**, 85-94 (1983).

59. Lundblad, V. Telomere maintenance without telomerase. *Oncogene* **21**, 522-531 (2002).

60. Reddel, R. R. Alternative lengthening of telomeres, telomerase, and cancer. *Cancer Lett* **194**, 155-162 (2003).

61. Hemann, M. T. & Greider, C. W. G-strand overhangs on telomeres in telomerase-deficient mouse cells. *Nucleic Acids Res* **27**, 3964-3969 (1999).

62. Dreesen, O. & Cross, G. A. Telomerase-independent stabilization of short telomeres in Trypanosoma brucei. *Mol Cell Biol* **26**, 4911-4919 (2006).

63. Johnson, F. B. et al. The Saccharomyces cerevisiae WRN homolog Sgs1p participates in telomere maintenance in cells lacking telomerase. *Embo J* **20**, 905-13. (2001).

64. Levis, R. W. Viable deletions of a telomere from a Drosophila chromosome. *Cell* **58**, 791-801 (1989).

65. Lundblad, V. & Szostak, J. W. A mutant with a defect in telomere elongation leads to senescence in yeast. *Cell* **57**, 633-643 (1989).

66. Walter, M. F., Bozorgnia, L., Maheshwari, A. & Biessmann, H. The rate of terminal nucleotide loss from a telomere of the mosquito Anopheles gambiae. *Insect Mol Biol* **10**, 105-110 (2001).

67. Blasco, M. A. et al. Telomere shortening and tumor formation by mouse cells lacking telomerase RNA. *Cell* **91**, 25-34. (1997).

68. Niida, H. et al. Severe growth defect in mouse cells lacking the telomerase RNA component. *Nat Genet* **19**, 203-26. (1998).

69. Fan, X. & Price, C. M. Coordinate regulation of G- and C strand length during new telomere synthesis. *Mol Biol Cell* **8**, 2145-2155 (1997).

70. Wellinger, R. J., Wolf, A. J. & Zakian, V. A. Origin activation and formation of single-strand TG1-3 tails occur sequentially in late S phase on a yeast linear plasmid. *Mol Cell Biol* **13**, 4057-4065 (1993).

71. Chai, W., Du, Q., Shay, J. W. & Wright, W. E. Human telomeres have different overhang sizes at leading versus lagging strands. *Mol Cell* **21**, 427-435 (2006).

72. de Lange, T. Shelterin: the protein complex that shapes and safeguards human telomeres. *Genes Dev* **19**, 2100-2110 (2005).

73. Bianchi, A., Smith, S., Chong, L., Elias, P. & de Lange, T. TRF1 is a dimer and bends telomeric DNA. *Embo J* **16**, 1785-1794 (1997).

74. Bianchi, A. et al. TRF1 binds a bipartite telomeric site with extreme spatial flexibility. *Embo J* **18**, 5735-5744 (1999).

75. Stansel, R. M., de Lange, T. & Griffith, J. D. T-loop assembly in vitro involves binding of TRF2 near the 3' telomeric overhang. *EMBO J* **20**, 5532-5540 (2001).

76. van Steensel, B., Smogorzewska, A. & de Lange, T. TRF2 protects human telomeres from end-to-end fusions. *Cell* **92**, 401-413 (1998).

77. Liu, D., O'Connor, M. S., Qin, J. & Songyang, Z. Telosome, a mammalian telomere-associated complex formed by multiple telomeric proteins. *J Biol Chem* **279**, 51338-51342 (2004).

78. Ye, J. Z. et al. TIN2 binds TRF1 and TRF2 simultaneously and stabilizes the TRF2 complex on telomeres. *J Biol Chem* **279**, 47264-47271 (2004).

79. Smogorzewska, A. et al. Control of human telomere length by TRF1 and TRF2. *Mol Cell Biol* **20**, 1659-1668 (2000).

80. Celli, G. & de Lange, T. DNA processing not required for ATM-mediated telomere damage response after TRF2 deletion. *Nat Cell Biol* **7**, 712-718 (2005).

81. Smogorzewska, A., Karlseder, J., Holtgreve-Grez, H., Jauch, A. & de Lange, T. DNA Ligase IV-Dependent NHEJ of Deprotected Mammalian Telomeres in G1 and G2. *Curr Biol* **12**, 1635 (2002).

82. Chong, L. et al. A human telomeric protein. *Science* **270**, 1663-1667 (1995).

83. Zhong, Z., Shiue, L., Kaplan, S. & de Lange, T. A mammalian factor that binds telomeric TTAGGG repeats in vitro. *Mol Cell Biol* **12**, 4834-4843 (1992).

84. Kim, S. H., Kaminker, P. & Campisi, J. TIN2, a new regulator of telomere length in human cells. *Nat Genet* **23**, 405-412 (1999).

85. Griffith, J., Bianchi, A. & de Lange, T. TRF1 promotes parallel pairing of telomeric tracts in vitro. *J Mol Biol* **278**, 79-88 (1998).

86. Iwano, T., Tachibana, M., Reth, M. & Shinkai, Y. Importance of TRF1 for functional telomere structure. *J Biol Chem* **279**, 1442-1448 (2004).

87. Karlseder, J. et al. Targeted deletion reveals an essential function for the telomere length regulator Trf1. *Mol Cell Biol* **23**, 6533-6541 (2003).

88. Bilaud, T. et al. Telomeric localization of TRF2, a novel human telobox protein. *Nat Genet* **17**, 236-239 (1997).

89. Broccoli, D., Smogorzewska, A., Chong, L. & de Lange, T. Human telomeres contain two distinct Myb-related proteins, TRF1 and TRF2. *Nat Genet* **17**, 231-235 (1997).

90. Amiard, S. et al. A topological mechanism for TRF2-enhanced strand invasion. *Nat Struct Mol Biol* **14**, 147-154 (2007).

91. Li, B., Oestreich, S. & de Lange, T. Identification of human Rap1: implications for telomere evolution. *Cell* **101**, 471-483 (2000).

92. Zhu, X. D., Kuster, B., Mann, M., Petrini, J. H. & de Lange, T. Cell-cycle-regulated association of RAD50/MRE11/NBS1 with TRF2 and human telomeres. *Nat Genet* **25**, 347-352 (2000).

93. Baumann, P. & Cech, T. R. Pot1, the putative telomere end-binding protein in fission yeast and humans. *Science* **292**, 1171-115. (2001).

94. Lei, M., Podell, E. R. & Cech, T. R. Structure of human POT1 bound to telomeric single-stranded DNA provides a model for chromosome end-protection. *Nat Struct Mol Biol* **11**, 1223-1229 (2004).

95. Loayza, D., Parsons, H., Donigian, J., Hoke, K. & de Lange, T. DNA binding features of human POT1: A nonamer 5'-TAGGGTTAG-3' minimal binding site, sequence specificity, and internal binding to multimeric sites. *J Biol Chem* **279**, 13241-13248 (2004).

96. Lei, M., Zaug, A. J., Podell, E. R. & Cech, T. R. Switching human telomerase on and off with hPOT1 protein in vitro. *J Biol Chem* **280**, 20449-20456 (2005).

97. Baumann, P., Podell, E. & Cech, T. R. Human pot1 (protection of telomeres) protein: cytolocalization, gene structure, and alternative splicing. *Mol Cell Biol* **22**, 8079-8087 (2002).

98. Liu, D. et al. PTOP interacts with POT1 and regulates its localization to telomeres. *Nat Cell Biol* **6**, 673-680 (2004).

99. Ye, J. Z. et al. POT1-interacting protein PIP1: a telomere length regulator that recruits POT1 to the TIN2/TRF1 complex. *Genes Dev* **18**, 1649-1654 (2004).

100. Houghtaling, B. R., Cuttonaro, L., Chang, W. & Smith, S. A dynamic molecular link between the telomere length regulator TRF1 and the chromosome end protector TRF2. *Curr Biol* **14**, 1621-1631 (2004).

101. Kim, S. H. et al. TIN2 mediates functions of TRF2 at human telomeres. *J Biol Chem* **279**, 43799-43804 (2004).

102. Keegan, C. E. et al. Urogenital and caudal dysgenesis in adrenocortical dysplasia (acd) mice is caused by a splicing mutation in a novel telomeric regulator. *Hum Mol Genet* **14**, 113-123 (2005).

103. Wang, F. et al. The POT1-TPP1 telomere complex is a telomerase processivity factor. *Nature* **445**, 506-510 (2007).

104. Xin, H. et al. TPP1 is a homologue of ciliate TEBP-beta and interacts with POT1 to recruit telomerase. *Nature* **445**, 559-562 (2007).

105. van Steensel, B. & de Lange, T. Control of telomere length by the human telomeric protein TRF1. *Nature* **385**, 740-743 (1997).

106. Kelleher, C., Teixeira, M. T., Forstemann, K. & Lingner, J. Telomerase: biochemical considerations for enzyme and substrate. *Trends Biochem Sci* **27**, 572-579 (2002).

107. Karlseder, J., Broccoli, D., Dai, Y., Hardy, S. & de Lange, T. p53- and ATM-dependent apoptosis induced by telomeres lacking TRF2. *Science* **283**, 1321-1325 (1999).

108. Bakkenist, C. J. & Kastan, M. B. DNA damage activates ATM through intermolecular autophosphorylation and dimer dissociation. *Nature* **421**, 499-506 (2003).

109. Takai, H., Smogorzewska, A. & de Lange, T. DNA damage foci at dysfunctional telomeres. *Curr Biol* **13**, 1549-1556 (2003).

110. d'Adda di Fagagna, F. et al. A DNA damage checkpoint response in telomere-initiated senescence. *Nature* **426**, 194-198 (2003).

111. Veldman, T., Etheridge, K. T. & Counter, C. M. Loss of hPot1 function leads to telomere instability and a cut-like phenotype. *Curr Biol* **14**, 2264-2270 (2004).

112. Yang, Q., Zheng, Y. L. & Harris, C. C. POT1 and TRF2 cooperate to maintain telomeric integrity. *Mol Cell Biol* **25**, 1070-1080 (2005).

113. DE Lange, T. Telomere-related Genome Instability in Cancer. *Cold Spring Harb Symp Quant Biol* **70**, 197-204 (2005).

114. Maser, R. S. & DePinho, R. A. Connecting chromosomes, crisis, and cancer. *Science* **297**, 565-569 (2002).

115. Zhu, X. D. et al. ERCC1/XPF Removes the 3' Overhang from Uncapped Telomeres and Represses Formation of Telomeric DNA-Containing Double Minute Chromosomes. *Mol Cell* **12**, 1489-1498 (2003).

116. de Lange, T. & Petrini, J. A new connection at human telomeres: association of the Mre11 complex with TRF2. *Cold Spring Harb Symp Quant Biol* **LXV**, 265-273 (2000).

117. Verdun, R. E., Crabbe, L., Haggblom, C. & Karlseder, J. Functional human telomeres are recognized as DNA damage in G2 of the cell cycle. *Mol Cell* **20**, 551-561 (2005).

118. Verdun, R. E. & Karlseder, J. The DNA damage machinery and homologous recombination pathway act consecutively to protect human telomeres. *Cell* **127**, 709-720 (2006).

119. Celli, G. B., Lazzerini Denchi, E. & de Lange, T. Ku70 stimulates fusion of dysfunctional telomeres yet protects chromosome ends from homologous recombination. *Nat Cell Biol* **8**, 885-890 (2006).

120. d'Adda di Fagagna, F. et al. Effects of DNA nonhomologous end-joining factors on telomere length and chromosomal stability in mammalian cells. *Curr Biol* **11**, 1192-116. (2001).

121. Ozgenc, A. & Loeb, L. A. Current advances in unraveling the function of the Werner syndrome protein. *Mutat Res* **577**, 237-251 (2005).

122. Crabbe, L., Verdun, R. E., Haggblom, C. I. & Karlseder, J. Defective telomere lagging strand synthesis in cells lacking WRN helicase activity. *Science* **306**, 1951-1953 (2004).

123. Opresko, P. L. et al. The Werner Syndrome Helicase and Exonuclease Cooperate to Resolve Telomeric D Loops in a Manner Regulated by TRF1 and TRF2. *Mol Cell* **14**, 763-774 (2004).

124. Opresko, P. L. et al. Telomere binding protein TRF2 binds to and stimulates the Werner and Bloom syndrome helicases. *J Biol Chem* **277**, 41110-41119 (2002).

125. Francia, S., Weiss, R. S., Hande, M. P., Freire, R. & d'Adda di Fagagna, F. Telomere and telomerase modulation by the mammalian Rad9/Rad1/Hus1 DNA-damage-checkpoint complex. *Curr Biol* **16**, 1551-1558 (2006).

126. Kaminker, P. G. et al. TANK2, a new TRF1-associated PARP, causes rapid induction of cell death upon overexpression. *J Biol Chem* **276**, 35891-35899 (2001).

127. Lillard-Wetherell, K. et al. Association and regulation of the BLM helicase by the telomere proteins TRF1 and TRF2. *Hum Mol Genet* **13**, 1919-1932 (2004).

128. Smith, S., Giriat, I., Schmitt, A. & de Lange, T. Tankyrase, a poly(ADP-ribose) polymerase at human telomeres. *Science* **282**, 1484-1487 (1998).

129. Stavropoulos, D. J. et al. The Bloom syndrome helicase BLM interacts with TRF2 in ALT cells and promotes telomeric DNA synthesis. *Hum Mol Genet* **11**, 3135-3144 (2002).

130. Tarsounas, M. et al. Telomere maintenance requires the RAD51D recombination/repair protein. *Cell* **117**, 337-347 (2004).

131. van Overbeek, M. & de Lange, T. Apollo, an Artemis-related nuclease, interacts with TRF2 and protects human telomeres in S phase. *Curr Biol* **16**, 1295-1302 (2006).

132. Karlseder, J. et al. The telomeric protein TRF2 binds the ATM kinase and can inhibit the ATM-dependent DNA damage response. *PLoS Biol* **2**, E240 (2004).

133. Wang, R. C., Smogorzewska, A. & de Lange, T. Homologous recombination generates T-loop-sized deletions at human telomeres. *Cell* **119**, 355-368 (2004).

134. Dokal, I. & Vulliamy, T. Dyskeratosis congenita: its link to telomerase and aplastic anaemia. *Blood Rev* **17**, 217-225 (2003).

135. Dokal, I. & Vulliamy, T. in *Telomeres* (eds de Lange, T., Lundblad, V. & Blackburn, E.) 139-162 (Cold Spring Harbor Laboratory Press, Cold Spring Harbor, New York, 2005).

136. Liu, Y. et al. The telomerase reverse transcriptase is limiting and necessary for telomerase function in vivo. *Curr Biol* **10**, 1459-162. (2000).

137. Armanios, M. et al. Haploinsufficiency of telomerase reverse transcriptase leads to anticipation in autosomal dominant dyskeratosis congenita. *Proc Natl Acad Sci USA* **102**, 15960-15964 (2005).

138. Hathcock, K. S. et al. Haploinsufficiency of mTR results in defects in telomere elongation. *Proc Natl Acad Sci USA* **99**, 3591-3596 (2002).

139. Hemann, M. T., Strong, M. A., Hao, L. Y. & Greider, C. W. The shortest telomere, not average telomere length, is critical for cell viability and chromosome stability. *Cell* **107**, 67-77. (2001).

140. Lee, H. W. et al. Essential role of mouse telomerase in highly proliferative organs. *Nature* **392**, 569-574 (1998).

141. Rudolph, K. L. et al. Longevity, stress response, and cancer in aging telomerase-deficient mice. *Cell* **96**, 701-712 (1999).

142. Chin, L. et al. p53 deficiency rescues the adverse effects of telomere loss and cooperates with telomere dysfunction to accelerate carcinogenesis. *Cell* **97**, 527-538 (1999).

143. Gonzalez-Suarez, E., Samper, E., Flores, J. M. & Blasco, M. A. Telomerase-deficient mice with short telomeres are resistant to skin tumorigenesis. *Nat Genet* **26**, 114-117 (2000).

144. Greenberg, R. A. et al. Short dysfunctional telomeres impair tumorigenesis in the INK4a(delta2/3) cancer-prone mouse. *Cell* **97**, 515-525 (1999).

145. Artandi, S. E. et al. Telomere dysfunction promotes non-reciprocal translocations and epithelial cancers in mice. *Nature* **406**, 641-65. (2000).

146. Colgin, L. M., Baran, K., Baumann, P., Cech, T. R. & Reddel, R. R. Human POT1 Facilitates Telomere Elongation by Telomerase. *Curr Biol* **13**, 942-946 (2003).

147. Hockemeyer, D., Sfeir, A. J., Shay, J. W., Wright, W. E. & de Lange, T. POT1 protects telomeres from a transient DNA damage response and determines how human chromosomes end. *EMBO J.* **24**, 2667-2678 (2005).

148. Garvik, B., Carson, M. & Hartwell, L. Single-stranded DNA arising at telomeres in cdc13 mutants may constitute a specific signal for the RAD9 checkpoint. *Mol Cell Biol* **15**, 6128-6138 (1995).

149. Nugent, C. I., Hughes, T. R., Lue, N. F. & Lundblad, V. Cdc13p: a single-strand telomeric DNA-binding protein with a dual role in yeast telomere maintenance. *Science* **274**, 249-252 (1996).

150. Wellinger, R. J., Wolf, A. J. & Zakian, V. A. Use of non-denaturing Southern hybridization and two dimensional agarose gels to detect putative intermediates in

telomere replication in Saccharomyces cerevisiae. *Chromosoma* **102**, S150-6 (1992).

151. de Laat, W. L. et al. DNA-binding polarity of human replication protein A positions nucleases in nucleotide excision repair. *Genes Dev* **12**, 2598-2609 (1998).
152. Chiang, Y. J., Kim, S. H., Tessarollo, L., Campisi, J. & Hodes, R. J. Telomere-associated protein TIN2 is essential for early embryonic development through a telomerase-independent pathway. *Mol Cell Biol* **24**, 6631-6634 (2004).
153. Prowse, K. R. & Greider, C. W. Developmental and tissue-specific regulation of mouse telomerase and telomere length. *Proc Natl Acad Sci USA* **92**, 4818-4822 (1995).
154. Jacobs, J. J. & de Lange, T. Significant Role for p16(INK4a) in p53-Independent Telomere-Directed Senescence. *Curr Biol* **14**, 2302-2308 (2004).
155. Smogorzewska, A. & de Lange, T. Different telomere damage signaling pathways in human and mouse cells. *Embo J* **21**, 4338-4348 (2002).
156. Sherr, C. J. & DePinho, R. A. Cellular senescence: mitotic clock or culture shock? *Cell* **102**, 407-10. (2000).
157. Hockemeyer, D., Daniels, J. P., Takai, H. & de Lange, T. Recent expansion of the telomeric complex in rodents: Two distinct POT1 proteins protect mouse telomeres. *Cell* **126**, 63-77 (2006).
158. Jackson, E. L. et al. Analysis of lung tumor initiation and progression using conditional expression of oncogenic K-ras. *Genes Dev* **15**, 3243-3248 (2001).

159. Bailey, S. M., Cornforth, M. N., Kurimasa, A., Chen, D. J. & Goodwin, E. H. Strand-specific Postreplicative Processing of Mammalian Telomeres. *Science* **293**, 2462-2465 (2001).

160. Zubko, M. K., Guillard, S. & Lydall, D. Exo1 and Rad24 differentially regulate generation of ssDNA at telomeres of Saccharomyces cerevisiae cdc13-1 mutants. *Genetics* **168**, 103-115 (2004).

161. Erdmann, N., Liu, Y. & Harrington, L. Distinct dosage requirements for the maintenance of long and short telomeres in mTert heterozygous mice. *Proc Natl Acad Sci USA* **101**, 6080-6085 (2004).

162. Laud, P. R. et al. Elevated telomere-telomere recombination in WRN-deficient, telomere dysfunctional cells promotes escape from senescence and engagement of the ALT pathway. *Genes Dev* **19**, 2560-2570 (2005).

163. Wong, K. K. et al. Telomere dysfunction and Atm deficiency compromises organ homeostasis and accelerates ageing. *Nature* **421**, 643-648 (2003).

164. Wu, L. et al. Pot1 deficiency initiates DNA damage checkpoint activation and aberrant homologous recombination at telomeres. *Cell* **126**, 49-62 (2006).

165. O'Connor, M. S., Safari, A., Xin, H., Liu, D. & Songyang, Z. A critical role for TPP1 and TIN2 interaction in high-order telomeric complex assembly. *Proc Natl Acad Sci USA* **103**, 11874-11879 (2006).

166. He, H. et al. POT1b protects telomeres from end-to-end chromosomal fusions and aberrant homologous recombination. *Embo J* **25**, 5180-5190 (2006).

167. Lin, J. J. & Zakian, V. A. The Saccharomyces CDC13 protein is a single-strand TG1-3 telomeric DNA- binding protein in vitro that affects telomere behavior in vivo. *Proc Natl Acad Sci USA* **93**, 13760-13765 (1996).

168. Lendvay, T. S., Morris, D. K., Sah, J., Balasubramanian, B. & Lundblad, V. Senescence mutants of Saccharomyces cerevisiae with a defect in telomere replication identify three additional EST genes. *Genetics* **144**, 1399-1412 (1996).